ISSN 1818-1112
№ 3(126)
Scientific journal
Научный журнал

VESTNIK
of Brest State Technical University

ВЕСТНИК
Брестского государственного технического университета

WWW.BSTU.BY

DOI 10.36773/1818-1112-2021-126-3

EDITORIAL TEAM

Chief Editor

Doctor of Technical Sciences, Associate Professor, Rector of BrSTU BAKHANOVICH ALEXANDER GENNADEVICH

Deputy editor-in-chief

Ph.D in Engineering, Associate Professor, Vice Rector for Scientific Affairs of BrSTU SHALOBYTA NIKOLAY NIKOLAEVICH

TECHNICAL SCIENCE

Section «Civil and Environmental Engineering»

*Doctor of Technical Sciences, Professor TUR VIKTOR VLADIMIROVICH (*Responsible editor*)*
*Doctor of Technical Sciences, Professor POITA PETR STEPANOVICH (*Deputy executive editor*)*

Doctor of Technical Sciences, Professor BATYANOVSKY EDUARD IVANOVICH
Doctor of Technical Sciences, Professor BOLTRYK MIKHAIL
Academician RAACS, Doctor of Technical Sciences, Professor KOLCHUNOV VITALY IVANOVICH
Corresponding Member of BACIAA, Doctor of Architecture, Professor MOROZOVA ELENA BORISOVNA
Doctor of Technical Sciences, Associate Professor NAYCHUK ANATOLY YAKOVLEVICH
Doctor of Technical Sciences, Professor LAZOVSKY DMITRY NIKOLAEVICH
Doctor of Technical Sciences, Professor LEONOVICH SERGEI NIKOLAEVICH

Section «Mechanical Engineering»

*First Vice-Rector of BrSTU, Ph.D in Engineering, Associate Professor NERODA MIKHAIL VLADIMIROVICH (*Responsible editor*)*
*Ph.D in Engineering, Associate Professor PODDUBKO SERGEI NIKOLAEVICH (*Deputy executive editor*)*

Doctor of Technical Sciences, Professor DEVOINO OLEG GEORGIEVICH
Doctor of Technical Sciences, Professor POBOL IGOR LEONIDOVICH
Academician of NASB, Doctor of Technical Sciences, Professor VITYAZ PETR ALEXANDROVICH
Corresponding Member of NASB, Doctor of Technical Sciences, Professor SHELEG VALERY KONSTANTINOVICH
Ph.D in Engineering, Associate Professor HVISEVICH VITALY MIKHAILOVICH

Section «Information Technology»

*Doctor of Technical Sciences, Professor GOLOVKO VLADIMIR ADAMOVICH (*Responsible editor*)*
*Ph.D in Phys.-Math. Sciences, Associate Professor LEBED SVETLANA FYODOROVNA (*Deputy executive editor*)*

Doctor of Technical Sciences, Professor GOLENKOV VLADIMIR VASILIEVICH
Doctor of Technical Sciences, Professor DUDKIN ALEXANDER ARSENTIEVICH
Doctor of Technical Sciences, Professor KRASNOPROSHIN VICTOR VLADIMIROVICH
Doctor of Physics and Mathematics, Associate Professor ORLOV VIKTOR NIKOLAEVICH
Doctor of Physics and Mathematics, Professor CHICHURIN ALEXANDER VYACHESLAVOVICH

Section «Geoecology»

*Doctor of Geographical Sciences, Professor VOLCHAK ALEXANDER ALEXANDROVICH (*Responsible editor*)*
*Ph.D in Engineering, Associate Professor MESHYK OLEG PAVLOVICH (*Deputy executive editor*)*

Corresponding Member of NASB, Doctor of Geological and Mineralogical Sciences, Professor BOGDASAROV MAXIM ALBERTOVICH
Doctor of Technical Sciences, Professor GAVARDASHVILI GIVI VALERIANOVICH
Corresponding Member of NASB, Doctor of Technical Sciences, Professor LIKHATSEVICH ANATOLY PAVLOVICH
Corresponding Member of NASB, Doctor of Geographical Sciences, Professor LOGINOV VLADIMIR FYODOROVICH
Doctor of Agricultural Sciences, Professor MAZHAYSKY YURI ANATOLIEVICH

ECONOMICS

*Ph.D in Economics, Associate Professor ZAZERSKAYA VICTORIA VASILIEVNA (*Responsible editor*)*
*Ph.D in Economics, Associate Professor MEDVEDEVA GULNARA BARANGALIEVNA (*Deputy executive editor*)*

Doctor of Economics Sciences, Professor VYSOTSKY OLEG ARSENTIEVICH
Doctor of Economics Sciences, Associate Professor BELYATSKAYA TATIANA NIKOLAEVNA
Doctor of Economics Sciences, Professor TARASOV VLADIMIR IVANOVICH
Doctor of Economics Sciences, Professor KHATSKEVICH GENNADY ALEKSEEVICH
Doctor of Economics Sciences, Professor IVUT ROMAN BOLESLAVOVICH

Registration number 144

By the decision of the board of the Higher Attestation Commission of the Republic of Belarus, the scientific and theoretical journal "Vestnik of Brest State Technical University" is included in the List of Scientific Publications of the Republic Belarus to publish the results of dissertation research of technical (civil and environmental engineering, mechanical engineering, geoecology, information technology) branches of science and economic branches of science.

The journal is included in the Russian Science Citation Index (RSCI)

© «Vestnik of Brest State Technical University», 2021

VESTNIK
OF BREST STATE TECHNICAL UNIVERSITY

TECHNICAL SCIENCE (CIVIL AND ENVIRONMENTAL ENGINEERING, MECHANICAL ENGINEERING, GEOECOLOGY); ECONOMICS

Scientific-theoretical journal
Published since January 2000
Circulation — 3 times a year

3(126)'2021

CONTENTS

CIVIL AND ENVIRONMENTAL ENGINEERING

UDC 692.21

THE STRENGTH AND DEFORMABILITY OF THE LARGE-FORMAT POROUS CERAMIC BLOCKS MASONRY UNDER SHEAR

V. N. Derkatch

Doctor of Technical Sciences, Director of the branch of the RUE "Institute BelNIIS" – "Scientific and Technical Center", Brest, Belarus

Abstract

The article presents the results of experimental studies of shear strength, shear modulus and the limit value of the angle of shear deformations of masonry made of porous ceramic blocks with groove connection system of vertical joints. Studies of these parameters were carried out by the method of diagonal compression of masonry specimens, the vertical joints of which were made without filling and with filling with mortar. It is established that when filling vertical joints of masonry with a mortar on a mineral binding material, its shear strength and shear modulus significantly increase. It is indicated that it is necessary to take these factors into account when designing wall-stiffening diaphragms, multi-loaded load-bearing walls, floor-by-floor supported walls and partitions constructing using masonry from porous ceramic blocks.

Keywords: masonry, ceramic porous blocks, diagonal compression, shear strength, shear modulus.

ПРОЧНОСТЬ И ДЕФОРМАТИВНОСТЬ ПРИ СДВИГЕ КАМЕННОЙ КЛАДКИ ИЗ КРУПНОФОРМАТНЫХ ПОРИЗОВАННЫХ КЕРАМИЧЕСКИХ БЛОКОВ

В. Н. Деркач

Реферат

В статье приведены результаты экспериментальных исследований прочности при сдвиге, модуля сдвига и предельного угла сдвиговых деформаций каменных кладок из поризованных керамических блоков с пазогребневым соединением вертикальных швов. Исследования данных параметров осуществлялись методом диагонального сжатия образцов каменной кладки, вертикальные швы которой были выполнены без заполнения и с заполнением раствором. Установлено, что при заполнении вертикальных швов каменной кладки клеевым раствором на минеральном вяжущем существенно возрастает ее прочность на сдвиг и модуль сдвига. Указано на необходимость учета данных факторов при проектировании стен-диафрагм жесткости, разнонагруженных несущих стен, поэтажно опертых стен и перегородок, возводимых с применением каменной кладки из поризованных керамических блоков.

Ключевые слова: каменная кладка, керамические поризованные блоки, диагональное сжатие, прочность при сдвиге, модуль сдвига.

Introduction

Recently, during the construction of walls, masonry from large-format porous ceramic blocks with a width equal to the thickness of the wall has become widespread. These masonry products have profiled side faces that form a groove connection system in the joint during the construction of masonry. At the same time, vertical joints of masonry are allowed not to be filled with mortar, which significantly increases labor productivity and reduces the consumption of masonry mortar. However, as practice has shown, the walls made with the use of masonry with groove connection system of masonry units have disadvantages. The absence of mortar in vertical joints leads to a violation of the continuity of masonry and, as a consequence, an increase in the degree of anisotropy of its strength and deformation characteristics [1-5]. This circumstance negatively affects the shear and bending strength of masonry, as well as the crack resistance of masonry structures under force and temperature and humidity influences.

It should be noted that the studies of the mechanical characteristics of masonry with groove connection system without filling of vertical joints have been performed significantly less than traditional masonry, which to a certain extent constrains their use in construction practice.

Experimental research methodology

The main mechanical characteristics of masonry, which determine the stiffness and crack resistance of walls during shear, are the shear modulus, the strength of masonry during shear, as well as the limit value of the angle of shear deformations (skewness) of masonry. In order to obtain these characteristics, two series of specimens of masonry from porous hollow ceramic blocks with groove connection system with dimensions of 250x250x138 mm on standard mortar joints were manufactured and tested. Each series included three specimens of masonry. The DC-1 series specimens were manufactured with ceramic blocks with groove connection system without filling of vertical joints by the mortar. The DC-2 series specimens were manufactured with ceramic blocks with groove connection system with filling of vertical joints by the mortar for thin-layer joints of masonry. The normalized value of the compressive strength of ceramic blocks, established in accordance with STB EN 772-1, was 13.0 MPa, and the average value of the compressive strength of the masonry mortar according to STB EN 1015-11 was 15.3 MPa. After manufacturing, a vertical uniformly distributed compressive load was applied to each test specimen, so that the compressive stresses in the specimen cross section were about $2.5 \cdot 10^{-3}$ MPa. In the loaded state, the specimens covered with polyethylene film were cured for 28 days before the test at a temperature of +15...20 ° C and an air humidity of 60...70 %.

The mechanical characteristics of masonry under shear were determined by the method of diagonal compression of experimental masonry specimens in accordance with RILEM TC [6]. A general view of the masonry specimen with installed measuring devices is shown in Figure 1.

Figure 1 – A general view of the masonry specimen

doi.org/10.36773/1818-1112-2021-126-3-2-4

The masonry specimens were loaded using an installation equipped with a hydraulic jack with a load capacity of 250 kN and a force measuring device. The force was transferred uniformly to the specimen, while the loading speed was chosen so as to achieve the failure of the specimen within 15-30 minutes from the appying of the load. The masonry deformations in the vertical and horizontal directions were determined using clock-type displacement indicators with a graduation of 0.001 mm.

Based on the tests of the specimens, the shear strength of the masonry f_{vvo} was determined according to the equation (1):

$$f_{vvo} = \frac{0,707 \cdot F_{max}}{A_n} \quad (1),$$

where F_{max} – failure load;

A_n – specimen area (net).

$$A_n = \left(\frac{w+h}{2}\right) \cdot t \cdot n \quad (2),$$

where w – specimen width;

h – specimen height;

t – specimen thickness;

n – coefficient that takes into account the void ratio of masonry products (for porous ceramic blocks n = 0.48);

The value of the angle of shear deformations γ_{obs} (мм/м) was determined by the equation (3):

$$\gamma_{obs} = \frac{\Delta V + \Delta H}{g} \quad (3),$$

where ΔV – vertical compression deformations (mm);

ΔH – horizontal tensile deformations (mm);

g – distance between displacement indicators (m).

The shear module of masonry G_{obs} was determined according to the equation (4) at a load of 30% of the failure load and before the failure of the specimen.

$$G_{obs} = \frac{f_{vvo}}{\gamma_{obs}} \quad (4).$$

Results of experimental studies

The failure of the DC-1 series masonry specimens was plastic and occurred as a result of their cracking along a zigzag trajectory passing along vertical and horizontal mortar joints at loads F_{max} = 49.28-59.96 kN, which corresponded to the value of shear stresses τ_{max} = 0.39-0.47 MPa. The type of the failure of the specimens and the graphs of the dependence "shear stresses τ_{obs} – strains in the horizontal $\varepsilon_{x.obs}$ and vertical directions $\varepsilon_{y.obs}$ " are shown in Figure 2.

a)

b)

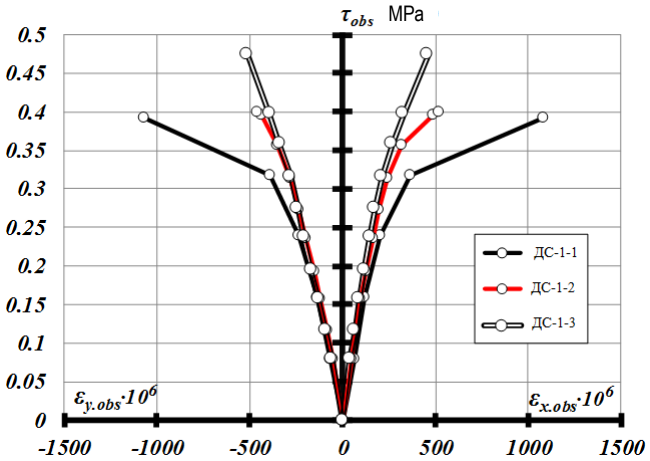

a) – the general view of the failure of the specimens;

b) – the relationship «τ_{obs} - ε_{obs}»

Figure 2 – Test results of DC-1 series specimens

Analysis of masonry deformation diagrams (Figure 2b) shows that with an increase in shear stresses τ_{obs} to a level of about 0,7τ_{max}, the masonry worked almost elastically, both in the direction along of action of the compressive load and in the orthogonal direction to it. At the same time, the limit value of the angle of shear deformations γ_{max} was about 1 mm/m. The average value of the shear modulus G_{obs} at τ_{obs} = 0,3τ_{max} was equal to 620 MPa, and at the stage close to failure – 360 MPa.

The values of the mechanical characteristics of masonry obtained from the test results of the DC-1 series specimens are shown in Table 1.

Table 1 – Mechanical characteristics of masonry specimens of the DC-1 series

Series No.	Specimen No.	Failure load $F_{i,max}$ (N)	Shear strength f_{vvoi} (MPa)	Limit value of the angle of shear deformations, γ_{obsi}(mm/m)	Shear modulus at τ_{obs}=0,3 τ_{max}, $G_{obs,i}$ (MPa)	Shear modulus at τ_{max}, $G_{obs,i}$ (MPa)
DC-1	DC-1-1	49280	0,39	-	543	182
	DC-1-2	50910	0,40	0, 98	650	408
	DC-1-2	59960	0,47	0, 97	656	488
Average value			**0,42**	**0, 975**	**620**	**360**

The failure mode of the DC-2 series masonry specimens was brittle because of their cracking along a diagonal trajectory at loads F_{max} from 114 to130 kN, which was more than 2 times higher than the failure load for specimens of the DC-1 series. At the same time, until the failure of the specimens, the proportionality between the increment of shear stresses and strains in the masonry remained. The type of the failure and deformation diagrams of DC-2 series masonry specimens are shown in Figure 3.

As was shown above the average value of the shear modulus G_{obs} at τ_{obs} = 0,3τ_{max} of the DC-2 series specimens was more than 2 times higher than the DC-1 series specimens. At the same time, the average value of the limit value of the angle of shear deformations of masonry specimens of the DC-2 series γ_{max} was 0.83 mm/m, which is 15 % lower than for specimens of the DC-1 series.

The values of the mechanical characteristics of masonry obtained from the test results of the DC-2 series specimens are shown in Table 2.

a)

b)

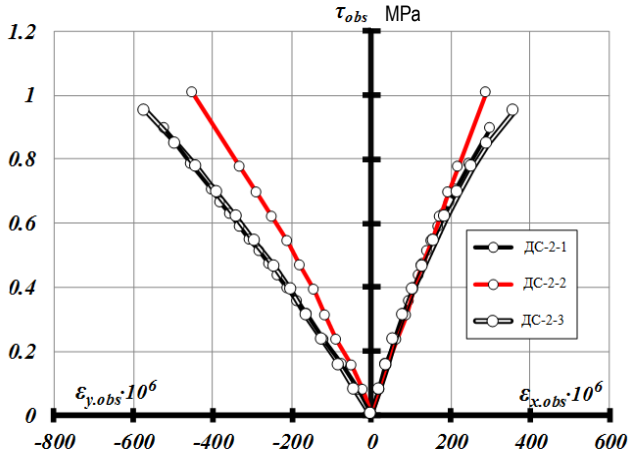

a) – the general view of the failure of the specimens;

b) – the graphs of the dependence «τ_{obs} - ε_{obs}»

Figure 3 – Test results of DC-2 series specimens

Table 2 – Mechanical characteristics of masonry specimens of the DC-1 Series

Series No.	Specimen No.	Failure load $F_{i,max}$ (N)	Shear strength f_{vvoi} (MPa)	Limit value of the angle of shear deformations, γ_{obsi} (mm/m)	Shear modulus at τ_{obs}=0,3 τ_{max}, $G_{obs,i}$ (MPa)	Shear modulus at τ_{max}, $G_{obs,i}$ (MPa)
DC-2	DC-2-1	114000	0,89	0,82	1194	1090
	DC-2-2	130000	1,01	0,74	1475	1362
	DC-2-2	123110	0,95	0,93	1184	1023
Average value			**0,95**	**0,83**	**1280**	**1160**

Conclusion

Based on the above, the following conclusion can be made:

1. The technology of performing vertical joints of masonry from porous ceramic blocks has a significant impact on the strength and deformation characteristics of masonry under shear. According to the results of experimental studies, it was found that when filling the joint with groove connection system of blocks with the mortar, the shear strength of masonry and its shear modulus increase by more than two times
2. The results obtained are recommended to be taken into account when designing wall-stiffening diaphragms, multi-loaded load-bearing wall, floor-by-floor supported walls and partitions constructing using masonry from porous ceramic blocks. It is recommended to revise the provisions of the building regulations governing the requirements for the design of foundations in terms of the limit values of the difference in the foundation settlement of masonry walls, which are made of masonry units with groove connection system.

References

1. Demchuk, I. Strength and deformability during shear of masonry from ceramic masonry elements: abstract for dissertation of Candidate of Technical Sciences / I. Demchuk; Research Republican Unitary Enterprise for Construction "Institute BelNIIS". – Brest, 2018. – 31 p.
2. Kubica, J. Mechanics of a wall loaded in its plane. Monographs of the Silesian University Of Technology / J. Kubica. – Gliwice, 2011. – 382 p.
3. Derkatch, V. Deformation characteristics of masonry in conditions of flat stress state / V. Derkatch // Construction and reconstruction. – Orel : OrelGTU. − 2012. − №2 (40). − P. 3–11.
4. Drobiec, L. Influence of the type of mortar on the mechanical parameters of walls of cellular concrete subjected to shear / L. Drobiec, R. Jasiński // Building Materials. − 2015. − № 5. – P. 106–109.
5. Identification of shear parameters of masonry panels through the in-situ diagonal compression test / A. Brignola [et al.] // International Journal of Architectural Heritage: Conservation, Analysis, and Restoration. − 2008. − № 3. − P. 52–73.
6. Diagonal tensile strength tests of small walls specimens. TC76-LUM: RILEM LUMB6 1991. – Bruxelles : TC76-LUM, 1991. – 5 p.

Accepted 03.11.2021

UDC 691

ANALYSIS OF THE STRAIN-STRESS STATE OF THE BENDING CONTINUOUS RC-BEAMS WITH HYBRID REINFORCEMENT IN THE TENSILE ZONE UNDER INTERMEDIATE SUPPORT

A. I. Hil[1], Y. D. Lazouski[2]

[1] Master of Technical Sciences, Assistant of the Department of Building Structures, Polotsk State University, Novopolotsk, Belarus, e-mail: a.hil@psu.by
[2] Ph.D in Engineering, Associate Professor, Head of the Department of Building Structures, Polotsk State University, Novopolotsk, Belarus, e-mail: y.lazouski@psu.by

Abstract

The article considers the proposed model describing the stress-strain state of bent statically indeterminate reinforced concrete beams with combined reinforcement (the joint arrangement of metal and composite rods) of the stretched zone of the central support section, based on the positions of the general deformation model of cross-sections with normal separation cracks between concrete subelements formed by two adjacent cracks and the block model of the resistance of the bent element. The prerequisites and assumptions for applying the proposed model are presented. The stress-strain state of the central reference section of the considered elements is analyzed according to the proposed model. The criterion of destruction of statically indeterminate reinforced concrete beams with hybrid reinforcement of the stretched zone of the central support section is revealed, which fully allows taking into account the redistribution of internal forces between the support and span sections of the element.

Keywords: statically indeterminate beams, reinforced concrete, composite reinforcement, block model, combined reinforcement, bending.

АНАЛИЗ НАПРЯЖЕННО-ДЕФОРМИРОВАННОГО СОСТОЯНИЯ ИЗГИБАЕМЫХ СТАТИЧЕСКИ НЕОПРЕДЕЛИМЫХ ЖЕЛЕЗОБЕТОННЫХ БАЛОК С КОМБИНИРОВАННЫМ АРМИРОВАНИЕМ НАД ЦЕНТРАЛЬНОЙ ОПОРНОЙ РАСТЯНУТОЙ ЗОНОЙ

А. И. Гиль, Е. Д. Лазовский

Реферат

В статье рассматривается модель, описывающая напряженно-деформированное состояние изгибаемых статически-неопределимых железобетонных балок с комбинированным армированием (совместное расположение металлических и композитных стержней) растянутой зоны центрального опорного сечения, основанная на положениях общей деформационной модели поперечных сечений с трещинами нормального отрыва между бетонными подэлементами, образованными двумя соседними трещинами и блочной модели сопротивления изгибаемого элемента. Представлены предпосылки и допущения при применении предлагаемой модели. Выполнен анализ напряженно-деформированного состояния центрального опорного сечения рассматриваемых элементов по предлагаемой модели. Выявлен критерий разрушения статически неопределимых железобетонных балок с комбинированным армированием растянутой зоны центрального опорного сечения, который в полной мере позволяет учитывать перераспределение внутренних усилий между опорными и пролетными сечениями элемента.

Ключевые слова: статически неопределимые балки, железобетон, композитная арматура, блочная модель, комбинированное армирование, изгиб.

Introduction

To date, there is an increase in the use of composite reinforcement in construction (in international practice, FRP – fiber reinforced polymer composite), which is a polymer element reinforced with high-strength fibers (glass, carbon, basalt or aramid) [1–3]. The main application of this type of reinforcement is found in the production of reinforced concrete structures, the exploitation of which takes place in highly aggressive environments, where it is difficult to provide reliable corrosion protection to metal fittings, or in structures in which it is necessary to ensure neutral magnetic and dielectric properties.

The main factor that does not allow directly replacing all tension steel reinforcement with FRP is its low modulus of elasticity. Numerous studies [4-6] show that it is the modulus of elasticity of the composite reinforcement used that is the dominant factor in the operation of flexure reinforced concrete elements reinforced with composite bars without prestressing.

One of the possible solutions to expand the scope of application of composite reinforcement without prestressing will be the introduction of a reinforced concrete element reinforced with composite reinforcement into the tension zone of a certain percentage of metal reinforcement (combined or hybrid reinforcement), thereby achieving a more rational and safe operation of the structure as a whole [7]. The greatest effect from the use of combined reinforcement is expected from its application in statically indeterminate bending elements, primarily due to the rational redistribution of actions effects (mainly moments) between the support sections with combined reinforcement and span sections with tension indeterminate steel reinforcement.

To describe the stress-strain state of statically undetectable bent reinforced concrete beams with combined reinforcement, a model is proposed based on the provisions of the general deformation model for cross sections with cracks of normal separation between concrete sub elements and a block model of the resistance of the bending element.

Assumptions of the general deformation model

The general deformation model of a reinforced concrete element [8, 9] makes it possible to take into account the nonlinear properties of materials in the cross section under consideration, using nonlinear relationships «stress-strain» of concrete and reinforcement deformation.

In accordance with the provisions of the general deformation model, the cross-section of the bending reinforced concrete element is represented as a set of elementary areas (layers) and longitudinal reinforcing tars. Within these sites, normal stresses are considered to be uniformly distributed and equal to their average values.

Relative deformations along the section height are distributed according to the hypothesis of plain sections [10, 11], i.e. for relative strains averaged along the length of the element section with cracks of normal separation. The distribution of normal stresses over the height of the

element, which correspond to the averaged strains, correspond to the cross section with a crack of normal separation.

Each elementary area of concrete beams, bars of steel reinforcement and composite reinforcement under the influence of forces from the applied load experience uniaxial tension or compression in accordance with the «stress-strain» diagrams used $\sigma = f(\varepsilon)$ (Fig. 1).

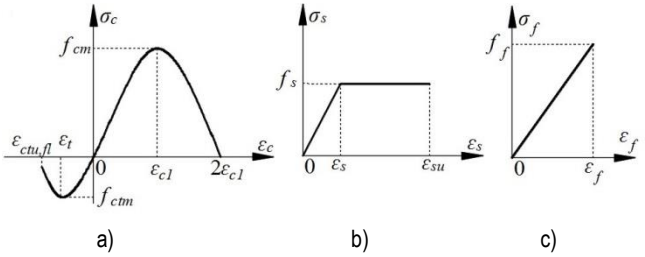

a) b) c)

Figure 1 – Relationship «σ – ε» for concrete (a), steel reinforcement (b) and composite reinforcement (c)

As an approximation of the diagrams of concrete «σ_c – ε_c» under compression (1) and tension on the ascending (3a) and descending (3b) branches, a nonlinear relationships according to Model Code 2010 and [12] with a descending branch are used:

$$\sigma_c = \frac{k\eta - \eta^2}{1+(k-2)\eta} f_{cm}, \quad (1)$$

where $k = \frac{1{,}1E_{cm,n}/\varepsilon_{c1}/}{f_{cm}}$; $\eta = \frac{\varepsilon_{c0}}{\varepsilon_{c1}}$; (2)

$$\sigma_{c_t} = 1{,}2\left(\frac{\varepsilon_{ct}}{\varepsilon_{ct1}}\right) - 0{,}2\left(\frac{\varepsilon_{ct}}{\varepsilon_{ct1}}\right)^6; \quad (3a)$$

$$\sigma_{c_t} = \frac{\left(\frac{\varepsilon_{ct}}{\varepsilon_{ct1}}\right)}{\alpha_{ct}\left[\left(\frac{\varepsilon_{ct}}{\varepsilon_{ct1}}\right) - 1\right]^{1,7} + \left(\frac{\varepsilon_{ct}}{\varepsilon_{ct1}}\right)} f_{ctm}; \quad (3b)$$

Where ε_{ct1} – strains corresponding to the peak point of the deformation diagram (Fig. 1 a), equal to $\varepsilon_{ct1} = (44f_{cm})\cdot 10^{-6}$ MPa;

$\alpha_{ct} = 0{,}312(f_{ctm})^2$ – correction factor depending on the tensile strength of concrete $f_{ctm} = 0{,}3f_{cm}^{2/3}$ (calculated based on the average compressive strength of concrete f_{cm} [13].

The ultimate strains of concrete, which according to [15] are equal to:

$$\varepsilon_{ctu,fl} = \frac{K\cdot\varepsilon_{ct1}}{2}; \quad (4)$$

where $K = 6{,}4 + 0{,}1223f_{cm}$.

The maximum strains of concrete under compression, in accordance with the current code [15], are accepted depending on the concrete class within $\varepsilon_{cu1} = (-3{,}5\ldots-2{,}8)\cdot 10^{-3}$. Based on the fact that in the sections of statically indeterminate reinforced concrete elements at the stage close to the ultimate (the appearance of plastic hinges with the opening of cracks of normal separation), there is a redistribution of forces along the section with the achievement of significant strains exceeding the ultimate values, a diagram of concrete deformation under compression without limiting the length of the descending branch is adopted in the general deformation model.

To approximate the deformation diagrams of the longitudinal steel and composite reinforcement of the tensile zone under the support section of the beams under tension/compression uses piecewise linear functions passing through the base points(f_{ym}; $\varepsilon_{ym} = f_{ym}/E_s$),ultimate yield strength yield strains respectively and corresponding strains (E_s – the initial modulus of elasticity of the steel reinforcement) and f_{fm}; $\varepsilon_{fm} = f_{fm}/E_f$ – the ultimate strength of composite reinforcement and its corresponding value of the strains (E_f – modulus of elasticity of composite reinforcement).

Assumptions of the proposed model

To analyze the stress-strain state of flexural reinforced concrete elements with combined reinforcement, a model for continuous beams with metal reinforcement by G.Manfredi was used as a base [16].

The proposed model, which describes the stress-strain state of statically indeterminate reinforced concrete beams with combined reinforcement of the tensile zone under the support section, is based on the following assumptions of the basic block model [16], taking into account their design features: - a statically indeterminate flexural reinforced concrete element is an element with a length of L, divided into subelements of finite length ΔL (Fig. 2) formed by two adjacent cracks of normal separation, which occur in sections where tensile stresses in concrete reach the limit values. The sub-elements are interconnected by tensioned steel and composite reinforcement and compressed concrete;

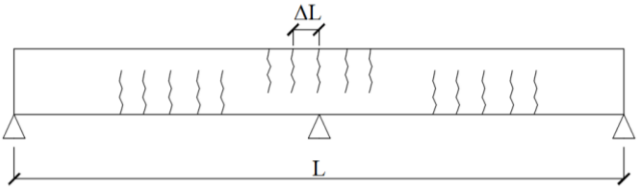

Figure 2 – Diagram of the division of a reinforced concrete element into subelements according to [16]

– concrete, composite and metal fittings work together in accordance with the accepted laws of adhesion according to ModelCode 2010 (MC2010). The laws of adhesion relate tangential stresses over the contact area of reinforcing bars with concrete and their mutual displacement $\tau_b = f(s)$, $\tau_{fb} = f_f(s_f)$ (Fig.3 a,b);

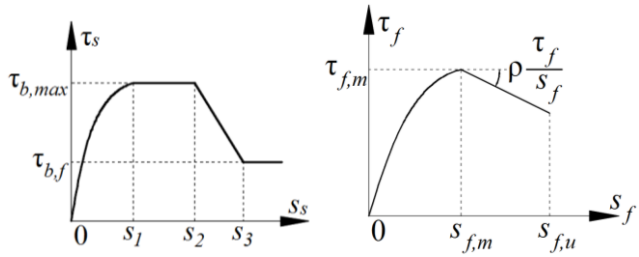

a) b)

Figure 3 – Graph of the dependence of tangential stresses of stretched metal reinforcement (a) and composite reinforcement (b) with concrete depending on the amount of slippage s in accordance with MC2010

Graph of tangential stress dependence τ_b according to the contract of stretched metal reinforcement with concrete, depending on the amount of slippage s according to MC2010 it includes the following parametric points:

$$\begin{aligned}
&\tau_b = \tau_{bmax}(s/s_1)^{\alpha} && \text{for } 0 \le s \le s_1;\\
&\tau_b = \tau_{bmax} && \text{for } s_1 \le s \le s_2; \quad (4a)\\
&\tau_b = \tau_{bmax}(\tau_{bmax} - \tau_{b,f})(s - s_2)(s_3 - s_2) && \text{for } s_2 \le s \le s_3;\\
&\tau_b = \tau_{b,f} && \text{for } s_3 < s,
\end{aligned}$$

where, τ_{bmax} – the maximum coupling voltage, which, depending on the coupling conditions and is equal to $2{,}5\sqrt{f_{cm}}$ or $1{,}25\sqrt{f_{cm}}$;

α – the coefficient that models the shape of the coupling law curve is from 0 to 1;

$\tau_{b,f} = 0{,}4\tau_{b,max}$ – resistance to slippage on the last horizontal section of the curve.

Resistance to slippage on the last horizontal section of the curve.

doi.org/10.36773/1818-1112-2021-126-3-5-8

$$\tau_{fb} = \tau_{fm}\left(\frac{s_f}{s_{fm}}\right)^{\alpha} \quad \text{for } 0 \le s_f \le s_{fm} \qquad (46)$$

$$\tau_{fb} = \tau_{fm} - \frac{\tau_{fm}\rho(s_f - s_{fm})}{s_{fm}} \quad \text{for } s_{fm} \le s_f \le s_{fu}$$

τ_{fm} – maximum clutch tension;

α – a coefficient that models the shape of the coupling law curve.

The values of parametric points are determined empirically for a specific type of composite reinforcement:

– tensile stresses in concrete are distributed evenly from steel and composite reinforcement over the effective area around the tars. The depth of the effective area of concrete is taken according to BR 5.03.01-2020 and is equal to the lesser of the values $2{,}5(h-d)$, $(h-x)/3$, $h/3$ (where h – full beam cross-section height; d – working height of the beam section; x – the height of the compressed concrete zone in cross-section with a crack of normal separation) (Fig. 4). According to studies of concrete strains under tension [10, 11], it is assumed that concrete strains under tension are assumed to be constant over the entire area;

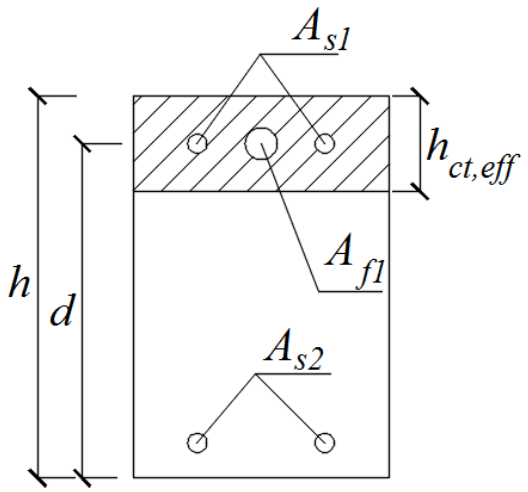

Figure 4 – Effective height $h_{ct,eff}$ stretched concrete of the support section of beams with combined reinforcement

– cracking the normal margin of the tensile zone of the reference section with a combined reinforcement occurs at a strains of concrete at the level of the centre of gravity tensile combination of rebar values that match the value of the limit of elasticity of the concrete cross-section in bending [18];

– in the process of deformation under applied load there are two stages of cracking: cracking transient, i.e., the appearance of new cracks might and established the emergence of new cracks is impossible, i.e., the number of cracks does not change;

– at the first stage of cracking, characteristic zones are identified in each concrete sub element: length $l_{f,j}$ at the edges of cracks, where there is a redistribution of tensile stresses between metal and composite reinforcement and concrete $(\varepsilon_s > \varepsilon_{ct}),(\varepsilon_f > \varepsilon_{ct})$ and length $\left(L_{m,i} - l_{f,j} - l_{f,j+1}\right)$ in the middle of the subelement where concrete and reinforcement are deformed together $(\varepsilon_s = \varepsilon_{ct})$, $(\varepsilon_f = \varepsilon_{ct})$.

– at the second stage of cracking along the entire length of the beam sub element, there is a redistribution of tensile forces between concrete, steel and composite reinforcement $(\varepsilon_s > \varepsilon_{ct}),(\varepsilon_f > \varepsilon_{ct})$;

– the opening width of cracks of normal separation in the tensile zone of the central support section of a statically indeterminate beam is due to the mutual displacement of reinforcing metal and composite rods relative to concrete at the level of its center of gravity on both sides of the crack edges along the length of the stretch stress redistribution section $l_{f,j}$.

Analysis of the stress-strain state of the sections under central support

The stress-deformable state of the central support section of a statically indeterminate reinforced concrete beam with a combined reinforcement of the tensile zone is described by the equilibrium equations of bending moments and longitudinal forces, equilibrium equations for individual steel and composite bar «bond-slip»s, equations of individual rods, the condition for the distribution of relative deformations along the cross-section height in accordance with the hypothesis of flat sections of Bernoulli and diagrams for materials of individual elementary areas, which are formed by dividing the beam section into elementary platforms-layers, while each longitudinal bar of the working steel and composite reinforcement is considered as a separate elementary area. The equations of the stress-strain state:

$$\begin{cases} \sum_{i=1}^{k}\sigma_{c,i}A_{c,i}(y_0 - y_{c,i}) - \sum_{i=k+1}^{m}\sigma_{s,i}A_{s,i}(y_0 - y_{s,i}) - \\ - \sum_{i=k+1}^{m}\sigma_{f,i}A_{f,i}(y_0 - y_{f,i}) - \sum_{j=1}^{n}\sigma_{ct,j}A_{ct,j}(y_0 - y_{ct,j}) - M = 0 \\ \sum_{i=1}^{k}\sigma_{c,i}A_{c,i} - \sum_{i=k+1}^{m}\sigma_{s,i}A_{s,i} - \sum_{i=k+1}^{m}\sigma_{f,i}A_{f,i} - \sum_{j=1}^{n}\sigma_{ct,j}A_{ct,j} = 0 \\ \frac{d\sigma_s(x)}{dx} - \frac{4}{\emptyset}\tau_s(x) = 0; \qquad \frac{d\sigma_f(x)}{dx} - \frac{4}{\emptyset}\tau_f(x) = 0; \\ \frac{ds_s(x)}{dx} - \varepsilon_s(x) + \varepsilon_{ct}(x) = 0; \qquad \frac{ds_f(x)}{dx} - \varepsilon_f(x) + \varepsilon_{ct}(x) = 0; \\ \varepsilon_{c,i} = \frac{1}{r_c}\left(y_0 - y_{c,i}\right); \quad \varepsilon_{s,i} = \frac{1}{r_c}\left(y_0 - y_{s,i}\right); \quad \varepsilon_{f,i} = \frac{1}{r_c}(y_0 - y_{f,i}); \\ \sigma_{c,i} = f(\varepsilon_{c,i}); \quad \sigma_{s,i} = f(\varepsilon_{s,i}); \quad \sigma_{f,i} = f(\varepsilon_{f,i}); \end{cases} \qquad (5)$$

where $\sigma_{c,i},\varepsilon_{c,i}$ – accordingly, normal stresses and strains in the i-th elementary site of compressed concrete;

$\sigma_{ct,j},\varepsilon_{ct,j}$ – accordingly, normal stresses and strains in the j-th elementary site of stretched concrete;

$\sigma_{s,i},\varepsilon_{s,i}$ – accordingly, normal stresses and strains in the i-th elementary area of tensil steel reinforcement;

$\sigma_{f,i},\varepsilon_{f,i}$ – accordingly, normal stresses and strains in the i-th elementary area of tensile composite reinforcement;

$A_{c,i},y_{c,i}$ – accordingly, the cross-sectional area and the distance from the selected axis to the center of gravity of the i-th elementary area of compressed concrete;

$A_{ct,j},y_{ct,j}$ – accordingly, the cross-sectional area and the distance from the selected axis to the center of gravity of the j-th elementary area of tensile concrete;

$A_{s,i},y_{s,i}$ – accordingly, the cross-sectional area and the distance from the selected axis to the center of gravity of the i-th elementary area of the tensile steel reinforcement;

$A_{f,i},y_{f,i}$ – accordingly, the cross-sectional area and the distance from the selected axis to the center of gravity of the i-th elementary area of the tensile composite reinforcement;

$\frac{1}{r_c}$ – the curvature of the beam in the section under the bending moment;

τ_s,τ_f – accordingly, the bond stresses of the longitudinal steel and composite bars.

In the first iteration in the zone under the central support with combined reinforcement under the bending moment $\Delta M = M_{sup}$, equal to the moment of cracking separation M_{crc}, the position of a subelement (or two subelements) formed on the left or right at a distance l is considered from the central crack. The value of the bending moment in the cross section along the central crack on the support from the action of load is determined by known methods of structural mechanics.

From the solution of the system of equations (5) at each stage of loading, implementing an iterative process of sequentially calculating the position of the center of gravity of the reference section under consideration y_0, the curvature of the element in this section $\frac{1}{r_c}$, strains in the reinforcement, normal stresses, secant deformation modules in elementary concrete and reinforcement pads, we obtain the parameters of the stress-strain state of the bending elements with combined reinforcement. The end of the process of successive approximations at each stage of loading is determined by the specified accuracy of solving the initial equations.

If the tensile strains in the elementary area of the concrete beam $\varepsilon_{ct,i}$ tensile of the beam exceed the ultimate values $\varepsilon_{ctu,fl}$, then this indicates the formation of a new crack of normal separation and, consequently, in further calculations, the axial stiffness of this elementary area will be zero, i.e. $E_{c,i}A_{ct,i} = 0$, and the bending moment, at which the strains reach values $\varepsilon_{ctu,fl}$, corresponds to the moment of cracking M_{crc}.

As a result of the calculation, at a given bending moment, we obtain the stress-strain state of the reference section under consideration by combined reinforcement of the tensile zone: stresses in steel and composite reinforcement in the section with a crack, the height of the compressed zone *x*, bending stiffness *EI* and the curvature of the beam $\frac{1}{r_c}$, which are used in further calculations.

For example, deflection of a beam by a span l_{eff} in a cross section with the *x* coordinate under the action of an external bending moment *M(x)* can be defined by the equation:

$$a = \int_0^{l_{eff}} \bar{M}(x)\frac{1}{r_c}(x)\,dx \qquad (6)$$

where $\bar{M}(x)$ – the moment in the cross section from the point force applied in the direction of the determined displacement;

$\frac{1}{r_c}(x)$ – the curvature of the beam with combined reinforcement from the action of the bending moment from the external load.

Substituting into equation (6), instead of the total curvature of the beam with combined reinforcement, the curvature of the beam $\frac{1}{r_c}(x)$ under load, we get an additional deflection of the beam from the increment of the load.

The failure of statically indeterminate reinforced concrete beams with combined reinforcement along the normal cross-section is applied to the longitudinal axis, at which the conditions of equilibrium of internal forces of the system of equations (5) will be observed. This failure criterion allows to fully taking into account the redistribution of internal forces in statically indeterminate reinforced concrete beams with combined reinforcement of the tensile zone under central support section.

Conclusion

To analyze the stress-strain state of bent statically indeterminate reinforced concrete beams with combined reinforcement of the tensile zone of the central support, a model is proposed based on the positions of the general deformation model of cross-sections with cracks of normal separation between concrete subelements formed by two adjacent cracks and a block model of the resistance of the flexural element. The analysis of the stress-strain state of the central support section of the elements under consideration according to the proposed model fully allows us to take into account the redistribution of internal forces between the support and span sections of the element, taking into account the influence of the difference in the characteristics of steel and composite reinforcement.

References

1. ***fib*** 2005. "FRP Reinforcement for reinforced concrete structures", Task Group 9.3 (Fiber-Reinforced Polymer) Reinforcement for Concrete Structures. – Lausanne, Switzerland, 2005. –173 p.
2. ACI 440.1R-03. "Guide for the Design and Construction of Concrete Reinforced with FRP Bars", American Concrete Institute, Farmington Hills, MI, USA. – 2003. – 81 p.
3. Guide for the Design and Construction of Concrete Structures Reinforced with Fiber Reinforced Polymer Bars – CNR–DT 203/206, Rome, June 2007. – 35 p.
4. Myasnikov, A. L. Bending structures with fiberglass reinforcement / A. L. Myasnikov, E. P. Teleshman, A. A. Varlamov // Actual problems of modern science, technology and education: materials of the 72nd international scientific and technical conference / ed. V.M. Kolokoltseva. – Magnitogorsk : Magnitogorsk State Technical University G.I. Nosova, 2014. – Volume 2. – P. 70–74.
5. Polskoy, P. P. On the effect of fiberglass reinforcement on the strength of normal sections of bent elements made of heavy concrete / P. P. Polskoy, Mervat Khishmakh, Mihub Ahmad // Electronic journal "Engineering Bulletin of the Don". – 2012. – № 4.
6. Mayilyan, D. R. Influence of steel and composite reinforcement on the width of the opening of normal cracks / P. P. Polskoy, D. R. Mayilyan // [Electronic resource]. – Access mode: http://cyberleninka.ru/article/n/vliyanie-stalnogo-i-kompozitnogo-armirovaniya-na-shirinu-raskrytiya-normalnyh-treschin/. – Access date: 24.03.2015.
7. Tur, V. V. Experimental studies of flexible concrete elements with combined reinforcement with steel and fiberglass rods / V. V. Tur, V. V. Malykha // Bulletin of the Polotsk State University. Series F Construction. Applied Sciences. – 2013. – № 8. – P. 58–65.
8. Calculation of the strength of reinforced concrete structures under the action of bending moments and longitudinal forces according to new regulatory documents / A. I. Zalesov [et al.] // Concrete and reinforced concrete. – 2002. – № 2. – P. 21–25.
9. Zalesov, A. S. Calculation of deformations of reinforced concrete structures according to new regulatory documents / A. S. Zalesov, T. A. Mukhamediev, E. A. Chistyakov // Concrete and reinforced concrete. – 2002. – № 6. – P. 12–16.
10. Murashov, V. I. Crack resistance, stiffness and strength of reinforced concrete / V. I. Murashov. – M. : Mashstroyizdat, 1950. – 268 p.
11. Nemirovsky, Ya. M. Rigidity of bending reinforced concrete elements during short-term and long-term loading / Ya. M. Nemirovsky // Concrete and reinforced concrete. – 1955. – № 5. – P. 172–176.
12. Reinforced concrete structures. Fundamentals of theory, calculation and design : textbook : a manual for students construction specialties / ed. T. M. Pezolda, V. V. Tura. – Brest : BrSTU, 2003. – 380 p.
13. Zhukyan, A. P. Strength and deformability of concrete of the compressed seam zone / A. P. Zhukyan // Vestnik Polotsk State University. Series B. Industry. Applied Sciences. – 2002. – P. 87–90.
14. Guidelines for the design of structures for large-panel residential buildings : SN-321-65 / ed. E. N. Rudkovsky. – M. : Gosstroyizdat, 1966. – 161 p.
15. Eurocode 2. Design of reinforced concrete structures: TKP EN 1992-1-1: 2009 / Ministry of Architecture and Construction of the Republic of Belarus. – Minsk, 2010. – Part 1-1: General rules and regulations for buildings. – 207 p.
16. Mantredi, G. A refined R.C. beams elements including bond-slip relationships for the analysis of continuous beams / G. Mantredi, M. Pecce // Computer and Structures. – 1998. – Volume 69, Issue 1. – P. 53–62.
17. Experimental and Analytical Evaluation of Bond Properties of GFRP Bars / G. Mantredi [et al.] // Journal of Materials in Civil Engineering. – July-August, 2001. – P. 282–290.
18. Tur, V. V. Strength and deformation of concrete in calculations of reinforced concrete structures / V. V. Tur, N. A. Rak. – Brest : BSTU, 2003. – 252 p.

Accepted 03.11.2021

UDC 624.131.534

ON THE ISSUE OF INCREASING THE RELIABILITY OF DETERMINING THE MODULUS OF THE GENERAL SOIL DEFORMATION

I. D. Huts[1], M. I. Nikitenko[2]

[1] Senior Lecturer of the Department of Agricultural Construction and Land Development of the Belarusian State Agricultural Academy, Gorki, Belarus, e-mail: gr_un@mail.ru
[2] Doctor of Technical Sciences, Professor, e-mail: michnikit@gmail.com

Abstract

The reliability of determining the modulus of general soil deformation directly affects the forecast of the final foundation settlement. Since the calculation of the 2-group ultimate conditions of the foundation bases is crucial in determining the size of the foundations, the solution of this issue is very relevant.

In this article, based on the analysis of the conditions of interaction of the system "soil base-foundation", the ways of increasing the reliability of determining the modulus of the general deformation of soil layers in the depth of the compressible thickness are considered.

Keywords: soil, deformation, tests, method, modulus, settlement, base, layer, summation, compressibility, thickness, foundation, stamp.

О ПОВЫШЕНИИ ДОСТОВЕРНОСТИ ОПРЕДЕЛЕНИЯ МОДУЛЯ ОБЩЕЙ ДЕФОРМАЦИИ ГРУНТА

И. Д. Гуц, М. И. Никитенко

Реферат

Достоверность определения модуля общей деформации грунта непосредственно влияет на прогноз конечной осадки фундамента. Поскольку расчет по 2-группе предельных состояний оснований является решающим при назначении размеров фундаментов, решение данного вопроса является весьма актуальным.

В данной статье исходя из анализа условий взаимодействия системы «грунт основания-фундамент» рассматриваются пути повышения достоверности определения модуля общей деформации слоев грунтов по глубине сжимаемой толщи.

Ключевые слова: грунт, деформация, испытания, метод, модуль, осадка, основание, слой, суммирование, сжимаемость, толща, фундамент, штамп.

Introduction

In the practice of designing foundation bases and foundations, their calculations are performed according to two ultimate conditions [1-4]: the 1st in terms of bearing capacity (stability), the 2nd in terms of deformations. For assigning the dimensions of shallow foundations [1, 4], the calculation of deformations (settlement) is crucial, and the main characteristic for each soil is its general deformation modulus, which is determined by the results of laboratory (compression) or field tests (stamp, probing, pressiometry).

During compression tests, a soil sample is subjected to uniaxial compression without the possibility of lateral expansion, leading it to compression due to a denser packing of particles, which can characterize the behavior of soils under foundations only at low pressures, and with their increase does not reflect their real compression.

The results of probing (more reliably static) of soils allow us to evaluate their properties in specific engineering and geological conditions in the form of resistances along the lateral surface of the friction sleeve and under the tip of the submerged probe along the depth of the base. Since at the same time the soil moves apart and is already in the final phase of strength loss, its compressibility is estimated indirectly based on the correlation between deformation and strength characteristics. In this case, the dependence between pressures and deformations is not reflected, which negatively affects the reliability of determining the values of E_o.

Pressiometric tests in specific soil conditions with their actual properties allow us to reflect the relationship between compressive pressures on the soil and its deformations, but in a horizontal direction when the pressiometer chamber expands in the well at appropriate depths. This does not fully reflect the process of vertical compression of the soil, introducing errors in the estimation of values E_o.

A more reliable determination of the soil deformation modulus E_o is provided by field stamp tests in specific soil conditions with their actual properties. When the stamp is pressed into the ground with its compression in the vertical direction, similar to foundations, it is possible to displace the soil to the sides due to all the stress components that arise in the base (compressive and shear).

Below we will focus on the analysis of the stress-strain state in the soil base as the pressure transmitted by the pressed stamp increases, with the interpretation of the obtained dependence of its settlement S on the values of these pressures P when determining the value of the deformation modulus E_o of the tested soil.

The essence of determining the modulus of soil deformation by stamp tests

As it is known, in the regulatory documents of the CIS, including the Republic of Belarus [1, 2, 4], the so-called **layer-by-layer summation method** is mainly used when calculating the settlement of foundations. It is based on the condition of a simple uniaxial compaction of the soil layers in the compressible thickness of the base due to vertical compressive stresses from the transfer of pressing loads by the foundation. For simplicity of calculations, horizontal compressive and tangential (shear) stresses arising in the soil are not considered, and their influence is considered by the correction coefficient β in the formula of simple uniaxial compression of each layer:

$$S_i = \beta \cdot \sum \frac{Pi \cdot h_i}{E_o} \quad (1)$$

where: S – the settlement of the foundation (stamp); P_i – the compressive pressure on the soil layer, kPa; h_i – the thickness of the soil layer, m; E_o – the modulus of the general deformation of the soil, kPa; β – the coefficient assumed for all soils to be equal to 0.8, although it was previously considered different depending on the lateral expansion coefficient (Poisson) v of the corresponding soil.

As we can see, in the formula (1), the settlement during compression of the soil layer is proportional to the compressive pressure acting on it. This ratio is characteristic of Hooke's law in the theory of elasticity, used in soil mechanics to estimate the stress-strain state in the base.

At a known value of the stamp settlement, according to the results of the indentation test, according to the formula (1), the value of E_o s

determined by reverse recalculation when interpreting the results obtained experimentally.

The method of layer-by-layer summation is based on the presence within the compressed zone of the base below the bottom of the foundation of different soil strata with their own values of E_o at varying compressive stresses σ_z in depth and width.

An example of such a distribution for a uniform band load at the ground surface is shown in Fig. 1 [3]. In the solutions of the theory of elasticity, when assessing the **stress-strain state**, the assumption is made about the uniformity (isotropy) of the properties of the soil in the base in all directions.

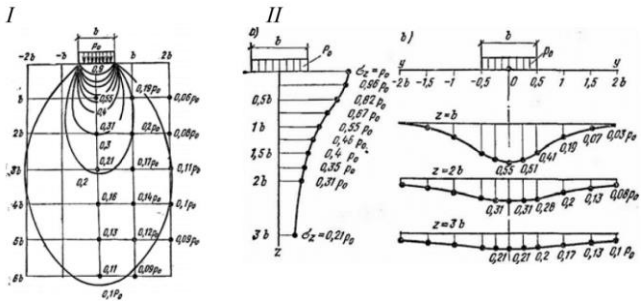

I – lines of identical values σ_z (isobars) along the depth and width of the base;
II – distribution diagrams σ_z:
a – on the vertical axis, b – on the horizontal levels

Figure 1 – Distribution of vertical compressive stresses σ_z in the ground

The method of layer-by-layer summation is based on the presence of different soil strata with their own values of E_o within the zone of the base below the bottom of the foundation, subject to compression, in the presence of varying compressive stresses σ_z along the depth and width of this zone.

In addition, the condition is accepted that at each horizontal level, the values of σ_z are the same in width and correspond to the values along the vertical axis (diagrams of position II) (see Fig. 1). Such their actual difference (see Fig. 1, II b), as well as ignoring the values of σ_x , σ_y and τ is leveled by the coefficient β.

When determining the values of σ_z by the depth of the base, the soil strata within the compressed zone are divided into elementary layers with capacities of 0.2 of the width b of the foundation (stamp). The power of the compressible zone h_c below the bottom of the foundation in domestic and foreign geotechnical practice is traditionally assumed to correspond to the level in the bottom of the foundation, where the stresses from the additional pressure transmitted by the foundation (in excess of the natural σ_{zg} from the own weight of the soil thickness) are up to: at E_o > 5 MPa – 0,2 σ_{zg}, and at E_o < 5 MPa – 0,1 σ_{zg}. [3]

In the domestic practice of engineering and geological surveys, when testing soils, hard round stamps with areas of 5000 cm^2, 2500 cm^2 are used in pits, and in wells at great depths – 600 cm^2. In this case, the dependence (Fig. 2) of the soil precipitation S under the stamp on the pressure applied by it, i.e. $S = f(P)$, is obtained.

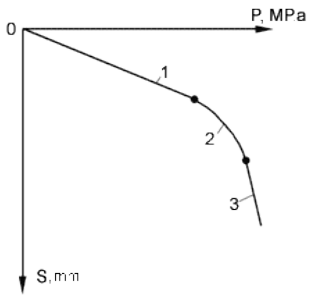

1 – the compaction phase,
2 – the shear phase, 3 – the rise phase

Figure 2 – The dependence of the settlement S of the soil under the stamp on the pressure transmitted by it P

Then, on an approximately linear initial segment of the graph, the pressure range ΔP is selected with the corresponding change in settlement ΔS and for this range, the deformation modulus E_o is calculated using the formula:

$$Eo = (1 - v^2) \cdot \frac{\pi \cdot d}{4} \cdot \frac{\Delta P}{\Delta S} \quad , \qquad (2)$$

where v – the Poisson's ratio of the soil; d – the diameter of the stamp, m;

With a strong decrease in the compressive stresses occurring in the ground σ_z (see Fig. 1), determined by multiplying the pressure transmitted by the bottom of the foundation p_o by the dispersion coefficient α, there is a need for each level of the compressible thickness to take into account its calculated (piecewise linear on a factually curved graph) pressure range ΔP and for it to calculate the modulus of deformation of the soil E_o.

It is also important not to forget that the stresses on the depth and the power of the compressible thickness in the base linearly increase in proportion to the width (Fig. 3) of the foundation (stamp) b, which inevitably affects the value of the determined modulus of the total deformation of each layer of soil at the appropriate level of such a thickness.

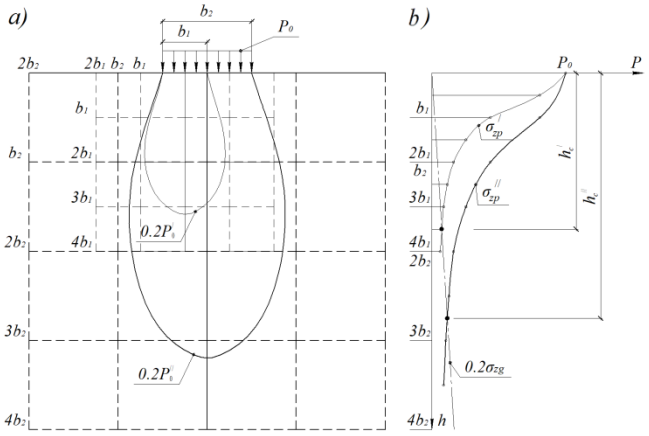

a) – lines equal stress intensity $\sigma_{zp} = 0{,}2P_o$; b) – change in the depth of the stress centers under the soles of foundations σ_{zp} from the pressure of P_o and a share of $0{,}2\sigma_{zg}$ by weight of homogeneous soil (conditional) if the definition of the boundaries of compressible zones h_c;
1 – when the width b_2, 2 – when $b_2 = 2b_1$

Figure 3 – The distribution of the vertical compressive stress σ_{zp} depth uniform base under the soles of foundations with different widths b when passing them same pressure intensity P_o

Traditionally, when assessing the distribution of compressive stresses in a soil mass (usually only vertical compressive stresses are taken into account when determining its settlement under the foundation), an assumption is made about the uniformity (isotropy) of the soil, although it actually has anisotropy or a difference in properties in different directions (Fig. 4).

Note that in the practice of engineering surveys and design, these features are not yet taken into account (ignored), and the determined values of the E_o are actually become erroneous. In this regard, it is very relevant to increase the reliability of determining the values of the deformation modules of the soil by means of field stamp tests in specific engineering and geological conditions, taking into account the above-mentioned features of interaction with the soil of stamps and conducting the necessary studies for this purpose*.

*the author aimed at the main directions of such research in the process of working on a Master's thesis under the scientific supervision of Professor, Doctor of Technical Sciences [Ph.D.] M. I. Nikitenko with their continuation in the framework of a Ph.D. candidate's dissertation under the scientific supervision of professor, Doctor of Technical Sciences [Ph.D.] P. S. Poyta.

doi.org/10.36773/1818-1112-2021-126-3-9-12

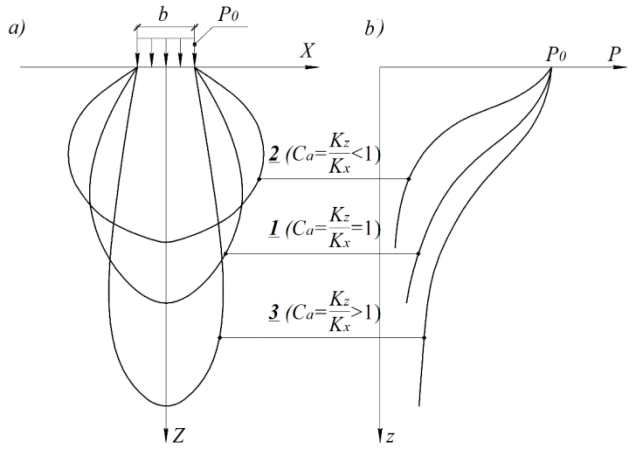

a) – lines of equal stresses $\sigma_{zp} = 0{,}2P_o$;
b) – changes in the depth of stresses under the centers of the soles of the foundations σ_{zp} from the pressure of P_o;

1 – for homogeneous (isotropic – $C_a = 1$) soil; 2 – for soil with horizontal anisotropy (ribbon clays – $C_a < 1$); 3 – the same with vertical (loess – $C_a > 1$): $Ca = K_z / K_x$ – the anisotropy coefficient, i.e. the ratio of the filtration coefficients along the vertical K_z and horizontal K_x

Figure 4 – The nature of the distribution of vertical compressive stresses σ_{zp} over the depth of anisotropic filtration bases under the soles of foundations with their identical widths b and the transmitted pressure intensity P_o:

An example of determining the modulus of total soil deformation in different ranges of ΔP

Since the natural (common) pressure σ_{zg} increases with depth, and the additional σ_{zp} weakens during dispersion in the soil thickness, it can be assumed that the modulus of total deformation E_o for each underlying elementary layer tends to increase in depth due to a sharp decrease in the ranges of ΔP.

As the initial data for the recalculation of the E_o module, we will use the results of the left stamp tests (see Table 1 and Figure 5) performed by the "Engineering Surveys" LLC in December 2020 in Minsk [5]. At the base there was a sandy soil (γ = 16 kN/m^3, v = 0,3), a round stamp (foundation) with an area of A = 2500 cm^2 (d = 0.564 m = 56.4 cm), its depth of laying h = 0.3 m, pressure P = 250 kPa.

Table 1 – Data of field stamp tests

Stamp depth, m	Stamp area, cm^2	Stamp settlement S (cm), at a pressure of P (kPa)											
		0,00	25	50	75	100	125	150	175	200	225	250	275
0,3	2500	0,00	0,10	0,22	0,36	0,52	0,69	0,89	1,06	1,26	1,47	1,69	2,22

Taking into account the data in Table. 1 and Fig. 5, we determine the E_o module by the formula (2) in the tension range from P_n = 25 kPa до P = 250 kPa:

$$E_o = (1 - 0.3^2) \cdot \frac{\pi \cdot 56.4}{4} \cdot \frac{250 - 25}{1.69 - 0.1} =$$

$$= 40.29 \cdot 141.5 = 5700 \text{ kPa};$$

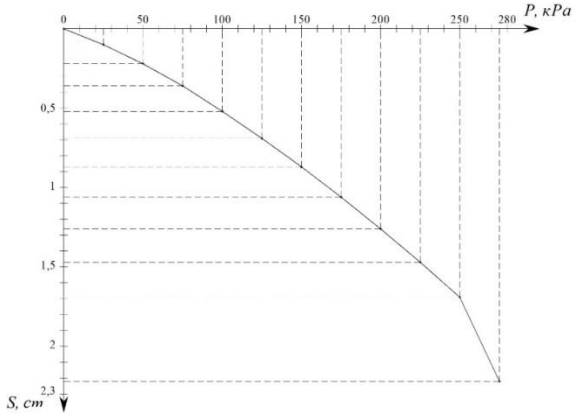

Figure 5 – Graph dependence of $S_i = f(P_i)$

We will determine the common and additional stresses in the base under the stamp. The calculations are summarized in the table. 2 and we build charts of their distribution in depth (Fig. 6) to determine the power of the compressible zone h_c. To do this, we will divide the soil under the foundation into elementary layers with the thickness of $0.2d$ (h_i = 0.2x56.4 = 11.28 cm). The additional vertical pressure on the base at the level of the foundation sole was $P_o = P - \sigma_{zg,o}$ = 245.3 kPa. We will also determine the tension from a half and a quarter of the test pressure.

Table 2 – Calculation of common and additional stresses in the base under the stamp

№ layer	h_i layer, cm	The depth z_i of the top layer, cm	$\xi = 2z/b$	α	σ_{zgi}, kPa	$0{,}2\sigma_{zgi}$, kPa	σ_{zpi}, kPa	$0{,}5\sigma_{zpi}$, kPa	$0{,}25\sigma_{zpi}$, kPa
1	11,28	0,00	0	1	4,7	0, 94	245,3	122,6	66,3
2	11,28	11,28	0,4	0,949	6,5	1,30	232,8	116,4	58,2
3	11,28	22,56	0,8	0,756	8,3	1,63	185,4	92,7	46,4
4	11,28	33,84	1,2	0,547	10,0	2,00	134,2	67,1	33,6
5	11,28	45,12	1,6	0,39	11,8	2,36	95,7	47,8	23,9
6	11,28	56,40	2	0,285	13,6	2,72	69,9	35,0	17,5
7	11,28	67,68	2,4	0,214	15,3	3,06	52,5	26,3	13,1
8	11,28	78,96	2,8	0,165	17,1	3,42	40,5	20,3	10,1
9	11,28	90,24	3,2	0,13	18,9	3,78	31,9	16,0	8,0
10	11,28	101,52	3,6	0,106	20,6	4,12	26,0	13,0	6,5
11	11,28	112,80	4	0,087	22,4	4,48	21,3	10,7	5,4
11a		**h_c = 118,0**				**4,8**			**4,8**
12	11,28	124,08	4,4	0,073	24,2	4,84	17,9	9,0	4,5
13	11,28	135,36	4,8	0,062	26,0	5,20	15,2	7,6	3,8
14	11,28	146,64	5,2	0,053	27,7	5,54	13,0	6,5	3,2
14a		**h_c = 156,0**				**5,7**		**5,7**	
15	11,28	157,92	5,6	0,046	29,5	5,90	11,3	5,6	2,3
16	11,28	169,20	6	0,04	31,3	6,26	9,8	4,9	2,4
17	11,28	180,48	6,4	0,036	33,0	6,60	8,8	4,4	2,2
18	11,28	191,76	6,8	0,031	34,8	6,96	7,6	3,8	1,9
18a		**h_c = 197,0**				**7,1**	**7,1**		
19	11,28	203,04	7,2	0,028	36,6	7,32	6,7	3,4	1,7

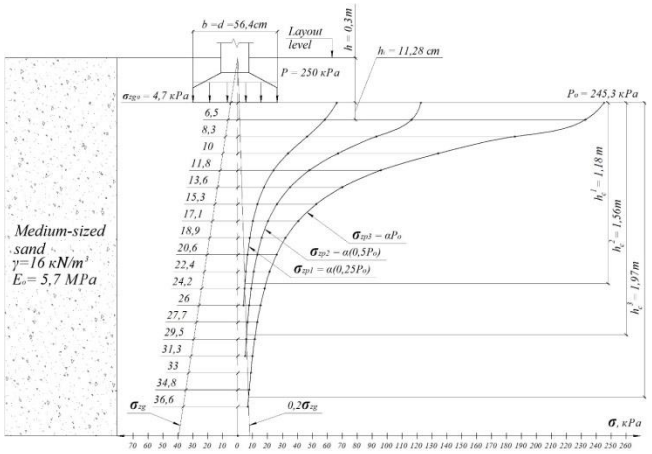

Figure 6 – Graphs of natural and additional stresses along the depth of the base for the given initial data.

It can be seen from Table 2 and Fig. 6 that the boundary of the compressible thickness below the stamp sole (taking into account the condition $\sigma_{zpi} = 0.2\ \sigma_{zgi}$) at a pressure below it of 61.3 кPa was 1.18 m, at a pressure of 122.6 кPa it increased to 1.56 m, and at 245.3 кPa it reached about 2.0 m.

As we can see, the depths of the compressible zones at the base of the stamp or foundation increase non-linearly with the increase in the pressures transmitted by them to the ground.

According to Hooke's law, the compression of elementary soil layers within the deformable h_c zones occurs proportionally to the average compressive stresses acting in each of these layers, which decline non-linearly in depth.

In this regard, we can also assume a nonlinear change in the general deformation modules of the E_o for a homogeneous soil as the thickness of the compressible h_c increases.

Below we will determine the values of E_o for different calculated depths h_c, and the values of the test pressure stages under a stamp with a diameter of 56.4 cm, which amounted to $0.25P_o$ = 61.3 кPa, $0.5P_o$ = 122.6 кPa, P_o = 245.3 кPa and caused, according to Table 1, settlements S_i respectively 0.29 cm, 0.69 cm and 1.69 cm:

$$E_{01} = (1 - 0.3^2)\cdot\frac{\pi\cdot 56.4}{4}\cdot\frac{61.3}{0.29} = 40.29 \cdot 214.4 = 8516\ \text{кPa};$$

$$E_{02} = (1 - 0.3^2)\cdot\frac{\pi\cdot 56.4}{4}\cdot\frac{122.6}{0.69} = 40.29 \cdot 177.7 = 7159\ \text{кPa};$$

$$E_{03} = (1 - 0.3^2)\cdot\frac{\pi\cdot 56.4}{4}\cdot\frac{245.3}{1.69} = 40.29 \cdot 145.1 = 5848\ \text{кPa};$$

These calculations show that the values of E_o, as the pressure levels of P_{oi} increase, decrease non-linearly in proportion to the increase in the compressible h_c thickness in the soil.

However, the fact of reducing the pressure P_{oi} and the compression deformations S_i of the soil layers at a depth h_c below the stamp has not yet been taken into account here, which undoubtedly should affect an adequate change in the values E_o.

As is known, in the existing research practice, the noted features of the nonlinear variability of the values of E_o are actually not taken into account.

In our case, it is not possible to determine the differences in the compression deformations S_i of the elementary soil layers within each of the compressible thicknesses h_i , since such measurements were not made.

An attempt to estimate analytically by dividing the total compression deformations S within all compression depths h_{ci} into fractions S_i, proportional to the average compressive stresses in each elementary layer or their groups will be incorrect, as evidenced by the analysis of formula (2).

It takes into account the diameter of the stamp (foundation) in the numerator instead of the width of the compressible soil layer at the corresponding level (see Fig. 1, pos. I and II, b – isobar graphs). At the same time, the values of ΔS and E_i included in this formula are unknown. If we take settlements in proportion to the pressures, then the ratio $\frac{\Delta P}{\Delta S}$ becomes constant, and all the values of E_i for all pressure stages are also the same.

This contradiction is due to the incorrectness of formula (2), since it gives a difference in the values of E_i only by changing the diameter of the stamp, and increasing proportionally with its increase, but does not reflect the role of increasing its area and its shape, which will differ from the existing non-circular one of the foundations.

It can be noted that in the practice of surveys, although different diameters of stamps are used, but the dependences of the values of the deformation modules of various soils on the size and area of the stamps with the depths of their immersion have not yet been investigated. When interpreting the test results, a rough assumption is made about the constancy of the E_o values in a wide range of pressures transmitted by the stamp, without taking into account the influence of differences in the volumes of the compressible array below it, i.e. not only their varying sizes in depth, but also in width in two directions.

Conclusion

When designing foundation bases and foundations using the method of layer-by-layer summation, the issue of increasing the reliability of determining the value of the soil deformation modulus E_o is relevant. The above example of taking into account one of the above features of interaction with the soil of the pressed stamp allowed us to clarify the determined value of this important parameter of the deformation properties of the soil due to its differences in depth depending on the change in the ranges of ΔP in proportion to the values of the stages of compressive pressures transmitted to the soil and the depths of h_c compressible zones in the base.

References

1. Technical Code of Practice. Slab foundations. Design rules. TCP 45-5.01-67-2007 (02250). – Introduction. 04.02.2007. – Minsk : Ministry of Architecture and Construction of the Republic of Belarus, 2007. – 140 p.
2. State Standard of the Republic of Belarus. Soils. Methods for field determination of strength and deformability characteristics. GOST 20276–2012. – Introduction. 01.01.2016. – Minsk : State Committee for Standardization of the Republic of Belarus, 2014. – 52 p.
3. Soil mechanics, foundation bases and foundations: a workshop on the discipline "Engineering geology, hydrogeology, soil mechanics, foundation bases and foundations" for students of the specialty 1-70 04 03 "Water supply, drainage and protection of water resources" / compiled: S. V. Ignatov [et al.] ; editor: M. I. Nikitenko. – Minsk, BNTU, 2014. – 184 p.
4. Poyta, P. S. Foundation bases and foundations / P. S. Poyta, P. V. Shvedovsky, D. N. Klebanyuk. – Minsk : Higher School, 2020. – 400 p.
5. Results of soil testing with a stamp at the object "Multi-apartment residential building with built-in and attached commercial and public facilities on the Kuprevich street". – Minsk : Engineering Survey, 2020.

Accepted 03.11.2021

UDC 624.15:692.115

ANALYSIS OF THE NON-LINEAR METHODS FOR FOUNDATION SETTLEMENT ANESSMENT

T. P. Shalobyta[1], P. S. Poita[2], P. V. Shvedovsky[3], D. N. Klebanyuk[4]

[1] Ph.D in Engineering, Associate Professor of the Department of Concrete Technology and Building Materials, Brest State Technical University, Brest, Belarus, e-mail: t_shalobyta@mail.ru
[2] Doctor of Technical Sciences, Professor, Professor of the Department of Geotechnics and Transport Communications, Brest State Technical University, Brest, Belarus, e-mail: ppsbrest@mail.ru
[3] Ph.D in Engineering, Professor, Professor of the Department of Geotechnics and Transport Communications, Brest State Technical University, Brest, Belarus, e-mail: ofig@bstu.by
[4] M.Sc, Senior Lecturer of the Department of Geotechnics and Transport Communications, Brest State Technical University, Brest, Belarus, e-mail: klebanyuk.dmitri@gmail.com

Abstract

The article discusses methods for calculating foundation settlement based on various approaches to solutions of the theory of limit equilibrium. The analysis of foundation settlement calculations in the linear and nonlinear stages of the subsoil reaction according to the Belarusian and Russian regulatory documents. It has been found that with a critical load equal to 0,85P_u, the calculated draft most fully corresponds to the experimental one. Thus, when calculating settlement beyond the linearity limit, it is recommended to take into account not the limit load, but 0,85 of its value.

Keywords: foundations, soils, foundation settlement, nonlinear calculation methods, foundation depth.

АНАЛИЗ РАСЧЕТА ОСАДОК ФУНДАМЕНТОВ НЕЛИНЕЙНЫМИ МЕТОДАМИ

Т. П. Шалобыта, П. С. Пойта, П. В. Шведовский, Д. Н. Клебанюк

Реферат

В статье рассмотрены методы расчета осадок фундаментов, основанные на различных подходах к решениям теории предельного равновесия. Проведен анализ расчетов осадок фундаментов в линейной и нелинейной стадии работы грунтового основания по действующим в Республике Беларусь и Российской Федерации нормативным документам. Установлено, что при критической нагрузке равной 0,85P_u, расчетная осадка наиболее полно соответствует экспериментальной. Таким образом, при расчете осадок за пределом линейности рекомендуется принимать во внимание не предельную нагрузку, а 0,85 от ее значения.

Ключевые слова: фундаменты, грунты, осадки фундаментов, нелинейные методы расчета, глубина заложения.

Introduction

The methods used in practice for determining the foundation settlement, in the linear stage of the use of the foundation soil, are considered quite reliable today, because they guarantee the overall normal facilities management without reducing their durability. However, this does not mean that they do not contain some contradictions that reduce the reliability of the obtained results, and in this regard, they continue to be discussed and improved today.

The assessment of calculation methods

In accordance with [1] in the Republic of Belarus, the following methods for calculating the final absolute compaction settlement of the foundation should be used in the engineering:

- the method of layer-by-layer summation using the calculation scheme of a linearly deformed half-space;
- the method of a linearly deformed layer of finite thickness;
- the equivalent layer method.

At the same time, the scope of each of the above methods is clearly limited, since the total final settlement S of the foundation depends on a number of factors, such as: stresses in the foundation; the distributing ability of the foundation soil; the contact plane of the foundation and the soil conditions; the size of the foundation, its shape, stiffness and depth; the structure and texture of the soil; rate of loading and it's condition; manufacturing environment, etc. and all of them to a certain extent have an impact on the value of S. Nevertheless, the actual values of the foundation deformations in many cases are significantly less than the theoretically estimated settlement values. That is why, according to the current regulations of the Russian Federation [2, 3], the calculated soil resistance R, that limits the linear relationship between the pressure along the base of the foundation P and its settlement S, is recommended to be increased to R_n with the ratio of the calculated settlement of the base S (pressure $P = R$) and the maximum settlement S_u:

- if $S \le 0{,}4S_u$ $R_n = 1{,}2R$;
- if $S \ge 0{,}7S_u$ $R_n = R$;
- if $0{,}7S_u > S > 0{,}4S_u$ R_n is determined by interpolation.

With appropriate justification, it is allowed to take $S < 0{,}4S_u$, and, accordingly, $R_n = 1{,}3R$.

The specified increase in pressure should not cause an increase in deformations of the foundation over 80% of the limit and exceed the bearing test ultimate pressure value.

Obviously, this approach provides a more economical solution of foundation structures in the building design. According to the regulations [4] of the Republic of Belarus, the calculation of the foundations is based on any known models of foundations (linear and nonlinear) and methods (direct, indirect, empirical), including simplified ones that guarantee, with the necessary reliability, protection against the leading to destruction or ultimate limit states for foundations and safety requirements; ensure suitability for normal operation, durability and economic feasibility of the decisions taken.

The use of nonlinear methods for calculating the settlement of the foundations, which is actually a move beyond of the proportionality $S = f(P)$, i.e. in the region $R < P < P_u$ (P_u is the ultimate or maximum pressure on the foundation) clearly indicates an increase in the efficiency of the foundations design solution, but their reliability, normal operation and durability must be ensured.

The analysis of approaches to calculating the foundation settlement by nonlinear methods allows us to note that in almost any proposed method, it is necessary to know R and P_u to determine the final settlement.

As for R, for its determination the necessary coefficients are introduced into the formula: the operating conditions of the soil base γ_1, the building or structure service conditions within interaction with the foundation γ_2, the reliability k, which allow us to get a better reflect of the distribution capacity of the foundation soils, the influence of the structural features of the building and its three-dimensional rigidity on composite action with the foundation and the reliability of the calculated soil characteristics used. In addition, the calculated dependence also takes into account the depth of the foundation base, the average (by layers) calculated value of the specific weight of the soil lying above and below the base of foundation, the weighing effect of groundwater if the groundwater is located above the base of foundation, etc. All this contributed to a significant increase in R.

At the same time, the average pressure under the base of the foundation is limited by the value R according to [11] (linear phase of deformation), which means that the calculation of the zones of limit equilibrium is not taken into account, i.e. the calculation of settlement is based on the linearly deformable array model. Thus, the restriction $P \le R$ indicates the absence of sufficiently developed calculation methods that take into account the presence of plastic zones in the foundation, i.e. methods based on the use of nonlinear models.

It should also be noted that there are some contradictions among the methods of calculating the settlement of foundations, in one form or another using the theory of a linearly deformable medium. For example, the calculation method proposed in [8], which allows taking into account the effect of horizontal stresses and approximately the stiffness of the foundation associated with deformations of compaction and shaping, is more accurate than the method of layer-by-layer summation, due to the fact that most of the foundation settlement (64 % or more), even at the initial stage of its loading, is associated with shear deformations of the soil.

The condition for achieving the maximum deformations of buildings is not fully used, since the determining factor is the inadmissibility of exceeding the pressure P of the value R or 1,2R. But if the value of R allows for the partial development of plastic deformation zones, then at a pressure P_1, these zones are only beginning to emerge under the edges of the foundation (Fig.1).

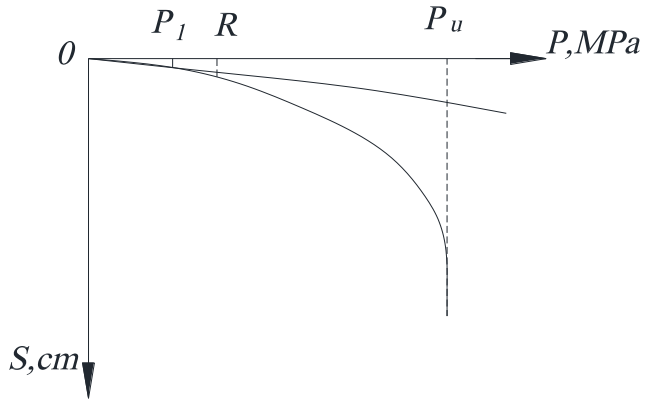

Figure 1 – Dependence of settlement S on pressure P

It is this load that is the critical initial, the value of which is determined by the formula of N. P. Puzyrevsky, N. M. Gersevanov [9, 10]. However, as M. N. Goldstein suggests [11], the methods do not take into account the actual distribution of stresses along the foundation base, at which their concentration occurs along its edges already at the lowest pressures, and, apparently, the limit equilibrium regions start to appear at these points, even when the pressure is far below than P_1.

As for the load capacity of the foundation, the most common methods are so-called rigorous methods, in which the sliding curve shape is found as a result of calculation (solutions of Sokolovsky V. V., Berezantsev V. G., Malyshev M. V., Golushkevich S. S., etc.) and methods in which the outlines of the sliding surface are given approximate, but quite well consistent with experience and theories (solutions of Berezantsev V. G., Terzaghi K., Meyergof G. G., TCP 45-5.01-67-2007).

Table 1 shows the results of calculations based on the methods for solving the theory of limit equilibrium to various degrees, performed by V. G. Berezantsev [5] and supplemented by the authors.

The calculations were performed for a non-buried foundation with a central load (plane problem case) using the values of a dimensionless coefficient equal to $P_u/\gamma b^2$ (γ – specific weight; b – width of the foundation), calculated by various methods for two values of the internal friction angle of the soil: φ = 30° and φ = 40°.

Table 1 – Values of dimensionless coefficients

The author of the method; a reference to a literary source; the formula given in [5]	$P_u/\gamma b^2$	
	φ = 30°	φ = 40°
Gorbunov-Posadov M. I., Mintskovsky M. I., formula (77)	6,1	62,3
Terzaghi K., formula (79)	20,0	50,0
Caquot and Kérisel, formula (80)	11,4	57,0
Meyerhof G. G. formula (79/)	12,5	60,0
Malyshev M. V., formula (75)	23,1	104,5
Zaharescu E., formula (78)	8,3	47,5
Gorbunov-Posadov M. I., [7]	-	95,5
Berezantsev V. G., formula (111)	10,8	50,1
TCP 45-5.01-254-2012 (02250)	12,39	66,01

Analysis of the calculation results shows that most of the methods, with the exception of the values obtained by M. I. Gorbunov-Posadov [7], M. V. Malyshev [6], and according to TCP 45-5.01-254-2012 [4], give solutions with a significant difference. $P_u/\gamma b^2$ at φ=30° variability is from 6,1 to 12,5, i.e. more than 2,0 times. In comparison with the solution of M. V. Malyshev, the coefficient increased almost 3,8 times. At φ=40°, the coefficient increases, and the difference is almost 2,2 times.

Thus, the smaller the value φ, the bigger coefficient $P_u / \gamma b^2$ variability is. The data obtained by M. I. Gorbunov-Posadov and M. V. Malyshev show that modern calculation methods P_u based on solving a mixed problem give results that provide a certain reserve of strength, but the issue of determining reliable values P_u requires detailed study.

While using nonlinear methods of calculating settlement there is a condition $R < P < P_u$. As shown by M. V. Malyshev [6], the load which is relevant to the plastic zone emergence under the edge of the foundation and its dimensions depend on the lateral pressure of the soil coefficient ξ_K. The value ξ_K = 1 corresponds to the maximum load. If ξ_K < 1,0 or ξ_K >1,0, then the load is lower and in the second case – significantly, and the strength characteristics of the ground play a decisive influence. They also revealed that the size of plastic zones depends on the depth of the foundation, the size of the foundation base, and the stiffness. If there is no loading, or if it is negligible, then zones of plastic deformations are formed even at low loads. At the same time, as noted by Elizarov S. A. and Malyshev M. V. [12], in the entire range of loads transmitted to the sandy foundation through a stiffened bandpass rugged stamp until the ultimate limited state is exhausted, the regions with the limiting state begin to emerge already at P > 0,25P_u and, despite their presence at the loading stage up to P = 0,5P_u, the dependence between the settlement and the load remains linear.

At the loading stage up to P = 0,7P_u, a new area was observed under the center of the stamp at a depth of about 0.6b (b is the width of the stamp). The reason for its occurrence is the presence of a compacted core under the stamp, at the top of which local destruction occurs [13].

The formed compacted core under the stamp digs into the foundation, and as a result the ground is destroyed along its entire surface. When loading P > 0,85P_u, the limiting state regions develop from under the edges of the foundation and merge at a depth, skirting both the elastic and plastic parts of the resilient core. With a further increase in the load, the base loses stability.

Thus, the destruction of the base occurs at loads exceeding (0,7…0,8)P_u.

The determination of settlement beyond the limit of the linear relationship between stresses and deformations $R < P < P_U$ based on the solution of M. V. Malyshev [14] is performed according to the formula:

doi.org/10.36773/1818-1112-2021-126-3-13-16

$$S_P = S_R\left[1+\frac{(P_u - R)(P - R)}{(R - \sigma_{zq,0})(P_u - P)}\right], \quad (1)$$

where S_R – is the foundation settlement at a pressure of $P = R$ or P =1,2·R;

$\sigma_{zq,0}$ – vertical stress from the soil own weight at the level of the foundation base;

P_u – the maximum resistance of the ground.

Therefore, if in (1) the value P_u is limited to 70...80% of the limit value, then the reliability of determining the value S_p increases due to the prevention of the foundation ground destruction, namely, limiting the appearance of plastic areas under the entire foundation and reducing the ground discharge to the sides from the edge of the stamp.

To a certain extent, the justification of this approach is confirmed by the studies of V. V. Lushnikov and A. S. Yardyakov [15], who came to the conclusion that the method of M. V. Malyshev allows us to obtain a fairly reliable forecast of settlement at pressures approximately corresponding to half of the interval $P_1 - P_u$, where P_1 is the critical initial load on the ground. In this case the accuracy in determining the values of settlement is estimated at 30-40%.

Figure 2 shows the graphs of the settlement of foundations on a sandy base, obtained from the results of calculations according to formula (1) and according to the test data of real foundations. Information about the soils and tested foundations is given in Table 2.

Table 2 – Value P_1, R, P_u and for various soils

Soil, dimensions of foundations	The value P_1, R, P_u, кPa and their ratio, values S_R, cm						
	P_1	R	S_R	R/P_1	P_u	P_u/P_1	P_u/R
1	2	3	4	5	6	7	8
Sand: E = 14,0 MPa; ν = 0,2; γ = 17,0 кN/m³; C = 2,0 кPa; φ = 30°; bxl = 0,8x4,8m; d = 1,5m	162	174	1,3	1,07	702	4,33	4,03
					597	3,69	3,43
Sand: E = 27,5 MPa; ν = 0,2; γ = 18,0 кN/m³; C = 1,0 кPa; φ = 32°; bxl = 1,0x4,8m; d = 1,5m	180	204	1,0	1,13	962	5,34	4,72
					818	4,54	4,01

The table and figure show that the calculated resistance differs by 14,7 %; P_1 – by 10 %, and the settlement obtained by layer-by-layer summation within the linear dependence $S = f(P)$ – by 23,1 %. The limiting pressures in medium-sized fractioned sand are 1,37 times higher than for small-sized fractioned sands and more than 4,0 times higher than the calculated soil resistance. If we take P = 0,85P_u, then this difference decreases from 3,4 to 4,0 times.

The graphs in Fig. 2 should be considered as linked to the actual loading of foundations with bxl =0,8x4,8 m and bxl = 1,0x4,8 m dimensions and a foundation depth d =1,5 m. Their analysis (curves 1, 2, 3) shows that the dependences $S = f(P)$ obtained from the test results and constructed according to the formula (1) at P = 0,85P_u, practically coincide within the entire range of operating pressures. The settlement determined for this case, at P_u = 962 kPa according to the formula (1), is considerably higher than the experimental ones. Approximately, up to P = 0,4 MPa, the experimental and calculated results are almost the same.

Moreover, the $S=f(P)$ relationship, while P in the pressure range from 0,0 to 0,4 MPa can be considered linear, since the settlement at P = 0,4 MPa is only 2,1 cm, which, however, is more than 2 times higher than S at $P = R$, but is only 26,3% of the maximum permissible settlement, assumed to be equal to 8,0 cm. And this indicates the presence of a major reserve in determining the size of the foundations in the plan. It should be noted that the pressure P = 0,4 MPa is 41,6 % of P_u.

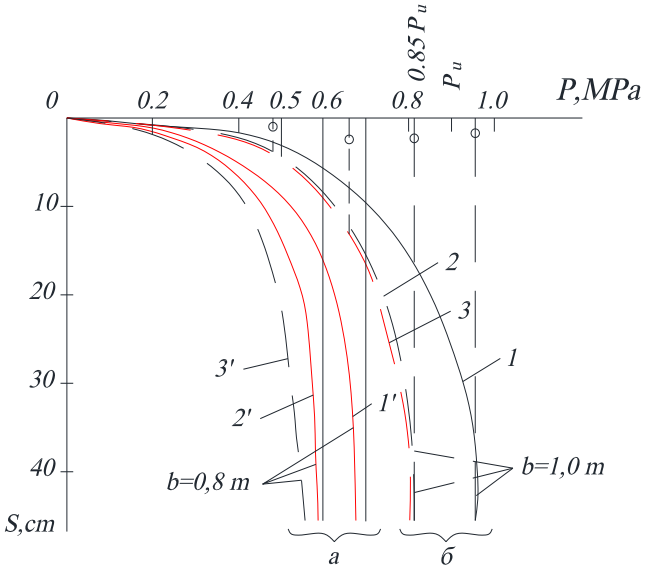

a) with the width of the foundation b = 0,8 m;
b) with the width of the foundation b = 1,0 m;

1; 1' – according to the formula of M.V. Malyshev;
2; 2' – according to the formula of M.V. Malyshev, at P = 0,85P_u;
3; 3' – results of full-scale tests of foundations

Figure 2 – Graphs of the settlement of foundations on a sandy base

With an increase in P, settlement increases markedly in different ways: at P = 0,5P_u, the difference in settlement is 1,52 times; at P = 0,7P_u, this difference is already equal to 1,56; at P = 0,85P_u, it is more than 10,0 times. Curves 1', 2', 3' complies with the calculated data and test results of foundations with a width of 0,8 m on a sandy base.

The analysis of the curves $S=f(P)$ shows that the linear section here is shorter and can be taken at a pressure of P = 0,3 MPa. The difference in settlement for all three considered cases varies in the range of 2,53...3,92 cm, which is on average 40% of the maximum permissible settlement. The settlement at $P=R$ is 1,3 cm, which is equal to 51,4...33,2%. With an increase of the foundations external load, the settlement difference is intensifying. At P = 0,5P_u, the settlement determined by the formula (1) is 3,52 cm, and the settlement according to the test results is 5,98 cm.

The settlement determined by the formula (1), but at a limit pressure of 0,85P_u is equal to 4,28 cm, i.e. it is equal to the intermediate value between the S determined by the formula (1) and the results of full-scale tests. At P = 0,7P_u, respectively, S = 8,52 cm, S =24,56 cm, S = 13,54 cm, i.e., the growth of settlement at a pressure of 0,7P_u, in comparison with the previous interval, was 2,42, 4,1 and 3,16 times, respectively. A similar character of settlement development persists at P = 0.85P_u.

This allows us to conclude that during the actual tests, the largest settlement increase is bigger than the foreseeable calculated one. If, according to the calculation, the maximum value of the settlement S is reached at $P = P_u$, then during the tests – at P = 0,85P_u, since the test results didn't reach the limit load.

Conclusion

1. The analysis of the existing methods for calculating the foundations settlement during the linear stage of the ground base work, regulated by the current normative documents, both in the Republic of Belarus and in the Russian Federation, shows the presence of a certain reserve, even if we allow an increase in the calculated resistance of the ground.
2. The use of nonlinear methods for the settlement calculating allows us to obtain fairly reliable results for determining settlement at pressures not exceeding 50% of the limit.
3. The results of the settlement calculations according to the method of M. V. Malyshev corresponded well with the experimental data, while the limiting pressure value being 85% of the maximum.
4. Theoretical solutions for the development or modernization of existing methods for calculating the settlement of foundations require clarification based on the experimental research data.

References

1. TCP 45-5.01-67-2007 (02250). Slab foundations. Design rules / Ministry of Architecture and Construction of the Republic of Belarus. – Minsk : Minarhstroy RB, 2008. – 138 p.
2. SP 50-101-2004. Design and construction of foundations and foundations of buildings and structures. – M., 2005. – 106 p.
3. SP 22.13330.2011. Foundations of buildings and structures (updated edition of SNiP 2.02.01-83). – M., 2011. – 262 p.
4. TCP 45-5.01-254-2012 (02250). Foundations and foundations of buildings and structures. Basic provisions. / Ministry of Architecture and Construction of the Republic of Belarus. – Minsk : Minarhstroy RB, 2012. – 104 p.
5. Berezantsev, V. G. Calculation of the foundations of structures / V. G. Berezantsev // Publishing house of literature on construction. – Leningrad, 1970. – 208 p.
6. Malyshev, M. V. The strength of soils and the stability of the foundations of structures. / M. V. Malyshev. – M. : Stroyizdat, 1980. – 137 p.
7. Gorbunov-Posadov, M. I. Stability of foundations on a sandy base / M. I. Gorbunov-Posadov. – M. : Gosstroyizdat, 1962. – 96 p.
8. Bronin, V. N. On the account of horizontal stresses at the base when determining the settlement of the foundation / V. N. Bronin, S. V. Tatarinov // Foundations, foundations and soil mechanics. – 1993. – Vol. 4. – P. 19–21.
9. Gersevanov, N. M. Collected works (T. 1 and 3) / N. M. Gersevanov. – M., 1958. – 516 p.
10. Puzyrevsky, N. P. The theory of tension in earthy soils / N. P. Puzyrevsky // Collection of works of LIPS. – 1929. – Vol. 99. –108 p.
11. Goldstein, M. N. Calculation of the settlement and strength of the foundations of buildings and structures / M. N. Goldstein, S. G. Kushner, M. N. Shevchenko. – Kiev : Budivelnik, 1977. – 208 p.
12. Elizarov, S. A. Carrying capacity criteria and different phases deformation of the base / S. A. Elizarov, M. V. Malyshev // Foundations, foundations and soil mechanics. – 1993. – Vol. 4. – P. 2–5.
13. Localization of deformations and destruction of sandy soil at the base of a strip stamp / S. A. Elizarov [et al.] // Interuniversity collection. – Yoshkar-Ola, 1989. – № 54. – P. 50–54.
14. Malyshev, M. V. Calculation of the settlement of foundations with a nonlinear relationship between stresses and deformations in soils / M. V. Malyshev, N. S. Nikitina // Foundations, foundations and soil mechanics. – 1982. – № 2. – P. 21–25.
15. Lushnikov, V. V. Analysis of sediment calculations in the nonlinear stage of soil work / V. V. Lushnikov, A. S. Yardyakov // Bulletin of the Perm National Research Polytechnic University. Construction and architecture. – 2014. – № 2 – P. 44–55.

Accepted 04.11.2021

UDC 624.012.45.046

SERVICE LIFE PREDICTION'S ALGORITHM: LOADING, CARBONIZATION, CHLORIDE AGRESSION

E. E. Shalyi[1], S. N. Leonivich[2], N. A. Budrevich[3]

[1] Engineer, LLC "PrimorProjectBuro", Vladivostok, Primorsky Territory, Russian Federation
[2] Doctor of Technical Sciences, Professor, Dean of the Faculty of Civil Engineering, Belarusian National Technical University, Minsk, Belarus. Foreign academician of RAASN. Qingdao University of Technology China, Qingdao, e-mail: snleonovich@yandex.ru, CEF@bntu.by
[3] Engineer, Belarusian National Technical University, Minsk, Belarus

Abstract

Corrosion reinforcement marine hydraulic structures due to chloride aggression and carbonization of concrete leads to a sharp decrease in the safety of the structure. The steel reinforcement will be subjected to a so-called depassivation process, once the chloride concentration on surface exceeds a certain threshold concentration, or the pH value in the protective layer of concrete decreases to a threshold value due to carbonation. Electrochemical reactions begin to occur with the formation of corrosion products with the penetration of oxygen on the steel reinforcement surface. This leads to cracking of the protective layer of concrete. It should also be taken into account that, due to corrosion mechanisms, the cross-sectional area of the reinforcement also decreases. The article suggests a method for predicting the complex degradation of reinforced concrete structures, taking into account various mechanisms of corrosion wear, which will allow developing effective ways to improve the durability and maintainability of structures operated in the marine environment.

Keywords: structure, concrete, corrosion, carbonation, chloride aggression.

АЛГОРИТМ ПРОГНОЗИРОВАНИЯ СРОКА СЛУЖБЫ: НАГРУЗКА, КАРБОНИЗАЦИЯ, ХЛОРИДНАЯ АГРЕССИЯ

Е. Е. Шалый, С. Н. Леонович, Н. А. Будревич

Реферат

Коррозионное армирование морских гидротехнических сооружений из-за хлоридной агрессии и карбонизации бетона приводит к резкому снижению сохранности конструкции. Стальная арматура подвергнется так называемому процессу депассивации, когда концентрация хлоридов на поверхности превысит определенную пороговую концентрацию или значение pH в защитном слое бетона снизится до порогового значения из-за карбонизации. Электрохимические реакции начинают протекать с образованием продуктов коррозии с проникновением кислорода на поверхность стальной арматуры. Это приводит к растрескиванию защитного слоя бетона. Также следует учитывать, что из-за механизмов коррозии площадь поперечного сечения арматуры также уменьшается. В статье предложен метод прогнозирования комплексной деградации железобетонных конструкций с учетом различных механизмов коррозионного износа, который позволит разработать эффективные способы повышения долговечности и ремонтопригодности конструкций, эксплуатируемых в морской среде.

Ключевые слова: структура, бетон, коррозия, карбонизация, хлоридная агрессия.

1. Research overview

The influence of the marine environment on the intensity of corrosion requires additional research, because chloride aggression and concrete carbonization significantly accelerate the degradation process [21]. Reinforcement corrosion due to chloride alone is well understood and a number of models are available to simulate this process. Some models study the transport mechanism of chloride ions from the surface of reinforced concrete elements, others [4, 5-9] study the effect of initial cracks in concrete [10-12] and the effect of loading on the transport mechanism of chlorides [18, 19].

In [16], a numerical simulation of the process of corrosion damage to concrete was proposed, in which the physical and electrochemical models are associated with a mechanical model of crack formation. There are known works on the study of joint environmental factors: chloride aggression and carbonization [13-15]. It is noted that the effect of carbonization on the diffusion coefficient of chloride ions depends on the types and proportions of the concrete mixture. In [14-15], a variable test with chloride exposure and carbonation is described, where the concentration of chloride ions was maximum near the carbonization front.

Despite the fact that carbonization and chloride aggression occur simultaneously in the marine environment, it should be noted that the diffusion of chloride ions is much faster than the carbonization process. Before carbonation, concrete usually contains Friedel's salt due to the chloride ion bound within the concrete. When Friedel's salt reacts with carbon dioxide, chloride ions are released into pore water [23]:

$$3CaO \cdot Al_2O_3 \cdot CaCl_2 \cdot 10H_2O + 3CO_2 \rightarrow 3CaCO_3 + 2Al(OH)_3 + CaCl_2 + 7H_2O \quad (1)$$

The released ions increase the concentration of free chloride, significantly exceeding the concentration of chloride ions, which are transported from the surface to the internal environment. Therefore, to analyze and predict the combined effect of carbonation and chloride penetration, it is necessary to model how carbonation interacts with chloride transport without carbonation. The authors proposed a complex model of the combined action of carbonation and chloride aggression, which is compared with chloride transfer without carbonization and is verified experimentally.

2. Carbonization model

The effect of carbonization is to reduce the alkalinity of the porous medium in concrete, which allows the passive film on the reinforcement to be destroyed and thereby initiate corrosion, leading to chipping of the concrete protective layer and a decrease in strength. Thus, concrete carbonization is a complex physicochemical process. The description of this process is based on the differential equation of the first law of A. Fick [4]:

$$J = -D\frac{dc}{dx} \quad (1)$$

If we consider carbonization as a stable constant process described by this law, then the deterministic model of the depth of passage of the carbonization front for a structure is written as follows [4]:

$$x_c(t) = \sqrt{\frac{2D(t)}{a}\int_1^t f_T(t)\cdot f_W(t)\cdot k\cdot C_{CO2}(t)\,dt}\cdot\left(\frac{t_0}{t}\right)^n \quad (2)$$

where t is the operating time in years; t_0 – 1 year; n is the age factor; k is a coefficient that takes into account the increased content of carbon dioxide in large cities; $f_T(t)$ and $f_W(t)$ are functions of temperature and humidity changes in time, respectively; $C_{CO2}(t)$ – function of changing the concentration CO_2 in time; $D(t)$ – diffusion coefficient of carbon

dioxide in concrete, as a function of time; a – the amount of CO_2 required for the conversion of all hydration products capable of carbonization, is determined by the formula [1]:

$$a = 0.75 \cdot CaO \cdot b \cdot a_H \cdot \frac{M_{CO2}}{M_{CaO}} \quad (3)$$

where CaO is the content of calcium oxide in the cement; b is the amount of cement; M_{CO2} – molar mass of carbon dioxide; M_{CaO} – molar mass of calcium oxide; a_H – degree of cement hydration.

The proposed model was used to calculate the depth of carbonization of the protective layer of concrete of a reinforced concrete shelf structure located at a distance of 10 m from the coastline and flooded only during storms. The structure is operated in the south of Sakhalin Island and is made of reinforced concrete. Concrete class B22.5 with a cement consumption of 350 kg/m^3 and a water-binding ratio of 0.4. The design service life of the structure is 50 years.

The initial data of the model are shown in Table 1.

Table 1 – Initial data

Parameter	Value
Average temperature of the warmest month T_max T_{max}	17,7 °C
Average temperature of the coldest month T_{min}	2,4 °C
Average humidity of the wettest month W_{max}	0,85
Average humidity of the driest month W_{min}	0,71
Water-binder ratio *w/b*	0,4
Cement consumption *b*	350 kg/m^3

Model (2) was calculated using the Mathcad program. The simulation results are shown in Fig. 1.

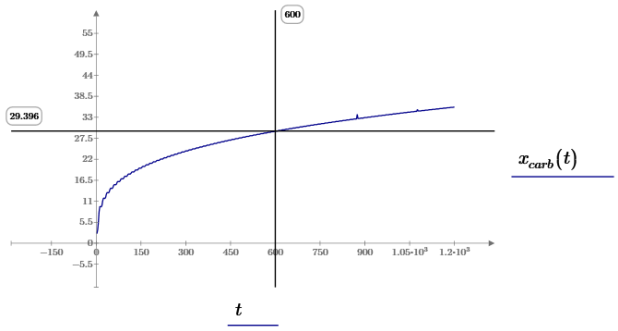

T – время, мес., $x_{carb}(t)$ – глубина карбонизации

Figure 1 – Graph of changes in the depth of carbonization of concrete of the cover over time

The graph shows that over 50 years (600 months) of operation, the depth of concrete carbonization will be 30 mm or 60 %. The degree of carbonation in this case a_c = 0.6.

3. Chloride diffusion model

The description of the diffusion of chlorides into the protective layer of concrete is based on the equation of Fick's second law [4]:

$$\frac{dc}{dt} = D\frac{d^2c}{dx^2} \quad (4)$$

Taking into account the binding capacity, the diffusion equation (4) takes the form [4]:

$$\frac{dCf}{dt} = \frac{D_{Cl}}{1+(\frac{1}{w_e})\cdot(\frac{\partial C_b}{\partial C_f})}\frac{d^2C_f}{dx^2} \quad (5)$$

where C_f is the concentration of free chlorides in concrete; C_b – concentration of bound chlorides in concrete; D_{Cl} – effective diffusion coefficient of chlorides in concrete; w_e – free pore moisture; $(\partial C_b)/(\partial C_f)$ – binding capacity of concrete.

The bonding capacity of still concrete is often determined by the slope of the bonding isotherm. This study uses the Langmuir isotherm model [4]:

$$\frac{\partial C_b}{\partial C_f} = \frac{\propto_L}{(1+\beta_L\cdot\frac{C_f}{b})^2} \quad (6)$$

The effective diffusion coefficient of chlorides is calculated as [23]:

$$D_{Cl} = D_{cl.0} \cdot f_T(t) \cdot f_W(t) \cdot f_t(t) \quad (7)$$

where $f_T(t)$, $f_W(t)$, $f_t(t)$ – respectively, the function of the influence of temperature, humidity and time on the diffusion coefficient; $D_{cl.0}$ – initial diffusion coefficient of chlorides.

Substituting equations (6) and (7) into equation (5), defining the diffusion equation is modified as follows [4]:

$$\frac{d}{dt}C_{Cl} = \frac{D_{cl.0}\cdot f_T(t)\cdot f_W(t)\cdot f_t(t)}{1+(\frac{1}{w_e})\cdot(\frac{\propto_L}{(1+\beta_L\cdot\frac{C_{Cl}}{b})^2})}\frac{d^2}{dx^2}C_{Cl} \quad (8)$$

The proposed model is used to calculate the concentration of chlorides at the depth of the protective layer of concrete of a reinforced concrete shelf structure, located at a distance of 10 m from the coastline. and flooded only during storms. The structure is operated in the south of Sakhalin Island and is made of reinforced concrete. Concrete class B22.5 with a cement consumption of 350 kg/m^3 and a water-binding ratio of 0.4. The design service life of the structure is 50 years. The initial data are presented in table 1.

Model (8) was also calculated in the Mathcad program (Fig. 2)

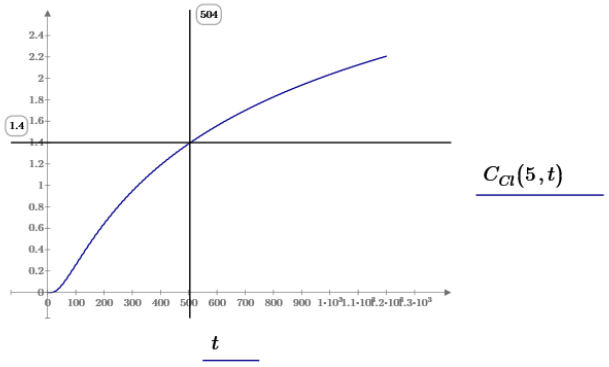

$C_{Cl}(x; t)$ – концентрация ионов хлорида на глубине защитного слоя X см. в зависимости от времени t, кг/м^3. Критическая концентрация хлоридов принята 0,4% или 1.4 кг/м^3 по массе вяжущего

Figure 2 – Graph of the change in chlorides over time (months) without taking into account carbonization at a depth of the protective layer of 5 cm

From the graph in Fig. 2, it can be seen that the level of chloride content in the near-armature zone will reach a critical concentration after 504 months of operation, or approximately 42 years.

4. Model of the combined effects of carbonation and chloride aggression

It is assumed that the transport equation for chloride ions after carbonization still corresponds to Fick's second law of diffusion (5). The total amount of chloride per unit volume of concrete consists of free chloride in the pore solution and bound chloride (Friedel's salt) [23]:

$$C_{Cl,carb} = w_e C_{fc} + C_{bc} \quad (9)$$

where $C_{Cl,carb}$ is the total chloride concentration, taking into account carbonation; C_{fc} – content of free chlorides in concrete; C_{bc} – content of bound chlorides in concrete, w_e – pore moisture.

Since in a specific case the interaction of concrete with the environment is accompanied not only by the penetration of chloride ions but also by carbonization, the residual binding capacity of concrete after carbonization is reduced.

doi.org/10.36773/1818-1112-2021-126-3-17-20

Based on experimental studies [23], the amount of bound chloride depends not only on the concentration of free chloride in the pore solution, but also on the degree of carbonization, as shown in Fig. 3, therefore it is proposed to replace $\propto_L$ with $\propto_{Lc}$ for concrete after complete carbonization [23]:

$$\propto_{Lc} = \propto_L (1 - d \cdot a_c) \quad (10)$$

where d is the coefficient of the decrease in the binding capacity of chloride ions due to carbonization, taken equal to 0.88 on the basis of research [23].

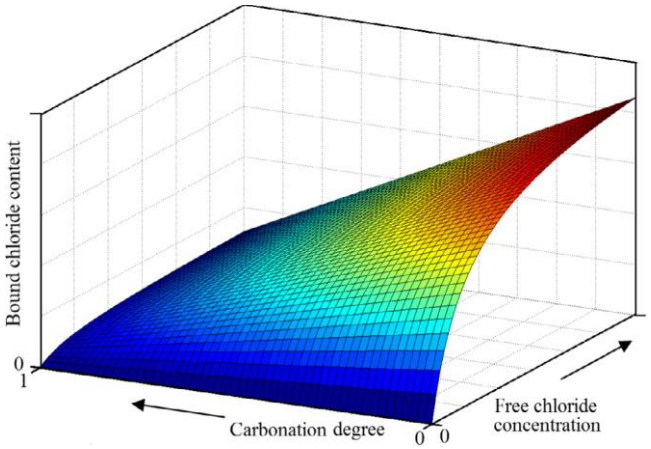

Figure 3 – Changes in the content of bound chloride depending on the concentration of free chloride and the degree of carbonation [23]

Taking into account equation (10), Langmuir's law (6) taking into account carbonation is as follows:

$$\frac{\partial C_b}{\partial C_f} = \frac{\propto_L (1 - d \cdot a_c)}{(1 + \beta_L \cdot \frac{C_f}{b})^2} \quad (11)$$

Then the governing diffusion equation is modified as follows:

$$\frac{d}{dt} C_{Cl} = \frac{D_{cl.0} \cdot f_T(t) \cdot f_W(t) \cdot f_t(t)}{1 + (\frac{1}{w_e}) \cdot (\frac{\propto_L (1 - d \cdot a_c)}{(1 + \beta_L \cdot \frac{C_{Cl}}{b})^2})} \frac{d^2}{dx^2} C_{Cl} \quad (12)$$

As in the previous case, using the Mathcad program, according to the proposed model, the chloride concentration is calculated at the depth of the protective layer of concrete of a reinforced concrete shelf structure at a distance of 10 m from the coastline. and flooded only during storms. The structure is operated in the south of Sakhalin Island and is made of reinforced concrete. Concrete class B22.5 with a cement consumption of 350 kg/m^3 and a water-binding ratio of 0.4. The design service life of the structure is 50 years. The initial data are presented in Table 1. The simulation results are shown in Figure 4.

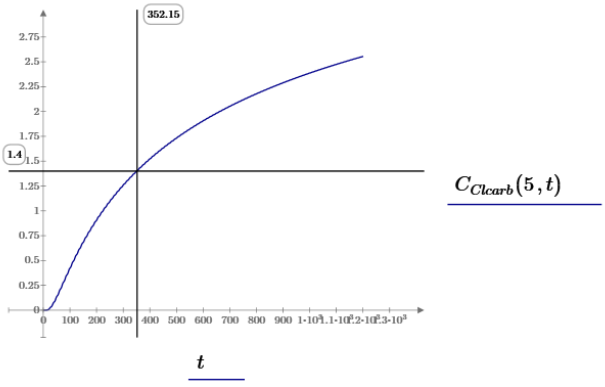

t – время (месяцы). C_{Clcarb} $(x; t)$ – концентрация ионов хлорида на глубине защитного слоя X см. в зависимости от времени t, кг/м^3. Критическая концентрация хлоридов принята 0,4% или 1.4 кг/м^3 по массе вяжущего

Figure 4 – Graph of the change in chlorides over time (months), taking into account carbonization at a depth of the protective layer of 5 cm

As can be seen from the graph in Fig. 4, the level of chloride content in the near-armature zone will reach a critical concentration after 352 months of operation or after about 29 years, which is strikingly different from the case without taking into account carbonation, where the critical concentration was reached after 42 years.

5. Verification of the model of combined action of carbonization and chloride aggression

To assess the results of the model of the combined action of carbonization and chloride aggression, in 2016 a full-scale survey of port facilities in the south of the island was carried out. Sakhalin. The combined effect of chlorides and carbon dioxide was most clearly traced in the construction of the pedestrian bridge of the Kholmsk sea trade port (Fig. 5). On the basis of the construction passport, the pedestrian bridge was put into operation in 1984. at the time of the survey, its service life was 32 years. The structure is located 10 meters from the coastline, is in the spray zone and is periodically flooded during storms.

Figure 5 – Span of the pedestrian bridge of the Kholmsk sea trade port

The results of measuring the depth of carbonation by phenolphthalein test showed that the depth of carbonation is approximately 25 mm. The level of chloride concentration at the depth of the protective layer of concrete in this case was 1.57 kg/m^3 by weight of the binder.

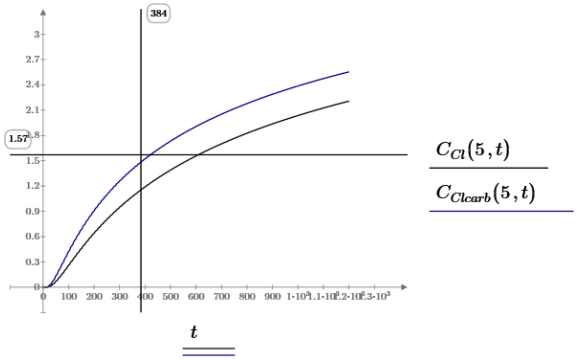

t – время (месяцы). C_{Cl} $(x; t)$ – концентрация ионов хлорида на глубине защитного слоя X см. в зависимости от времени t без учета карбонизации, кг/м^3. C_{Clcarb} $(x; t)$ – концентрация ионов хлорида на глубине защитного слоя X см. в зависимости от времени t для бетона в следствии комбинированного действия карбонизации и хлоридной агрессии, кг/м^3. Критическая концентрация хлоридов принята 0,4% или 1.4 кг/м^3 по массе вяжущего

Figure 6 – Comparison of the change in chlorides over time (months) with and without carbonization at a protective layer depth of 5 cm

Figure 6 shows a comparison of the results of modeling the change in chlorides over time with and without taking into account carbonation with field tests. As can be seen from the graph, for the construction of a pedestrian bridge with a service life of 384 months (or 32 years), the curve of joint action is the closest, which confirms the adequacy of the proposed model.

6. Influence of the operational load on the degradation of structures under the combined action of carbonization and chloride aggression

Since 2011, RILEM TC 246-TDC (which includes five laboratories from different parts of the world) has developed a method for determining the strength of concrete [24] subjected to the combined effects of chloride penetration and mechanical stress.

In the course of this work, the scientists concluded that the diffusion coefficients tend to decrease with time of exposure, while the calculated surface concentrations increase. Thus, the data they obtained are in part consistent with the literature, which states that chloride diffusion occurs more slowly under moderate compressive loading, but increases if the applied load exceeds half of the ultimate load. The chloride content at the depth of the protective layer increases significantly when tensile stress is applied. This result was expected because the pore space or microcracks expand under tensile stress. Thus, the diffusion coefficient is calculated as follows:

$$D_{cl}(t) = k_e k_l D_{cl.0} \cdot \left(\frac{t_0}{t}\right)^{ncl}$$

k_l – coefficient that takes into account the actual stress state of the structural element.

For various loading conditions, the stress coefficients k_l were calculated [24], in which k_l = 1 for the standard, k_l = 0.80 for loading (compression) 30 % of the ultimate breaking load, k_l = 1.17 for loading (compression) 60 %, k_l = 1.25 for loading (compression / tension) 50% and k_l = 1.53 for loading (tension) 80 %.

The service life of the elements loaded at 60 % of the compressive strength decreased by an average of 0.82 times in comparison with the unloaded elements. It should be noted that at a compressive stress ratio of 60 %, only two out of five laboratories found a noticeable increase in the diffusion coefficient (which is associated with a shortened service life), while others found a slight decrease in the diffusion coefficient. From the data presented by them [24], it can be concluded that further tests will be required in order to obtain more accurate information on the effect of operational loads on the service life of reinforced concrete elements. More research will be required to investigate the effect of operational loads on carbonation rate, however, some conclusions and adjustments to the cooperative model can be made now.

6. Conclusions

1. The analysis of the mechanism of corrosion destruction of shelf structures is carried out, the limiting state for the chemical reaction of chloride in the protective layer of concrete of shelf structures is formulated.
2. A model of degradation of the protective layer of concrete of coastal structures from the combined action of carbonization and chloride aggression is proposed.
3. The model was verified at the port facilities of the island. Sakhalin. The carried out field measurements of chloride penetration into concrete showed that at a depth of 50 mm, in the spray zone, the chloride concentration exceeds 0.4% of the cement weight (corrosion threshold) at a structure age of about 30 years.
4. The survey in the port of Kholmsk confirmed that locally, in certain cases, in the protective layer of concrete there are areas where the simultaneous action of both carbonization and chloride aggression is observed. In these local areas, the maximum concentration of chlorides is reached and reinforcement corrosion occurs. The service life of the surveyed structures did not reach the design service life.
5. Modeling the concentration of chlorine ions in the concrete of the protective layer in accordance with the accepted models, depending on the service life, climatic conditions and depth of reinforcement, made it possible to compare the chloride content at a certain depth when calculating with and without taking into account the combined effects of carbonization and chloride aggression.
6. The simulation results correlate well with field studies, which in the future will make it possible to develop effective ways to increase the durability and maintainability of structures operated in the marine environment.
7. The analysis of the influence of the operating load on the degradation of structures under the combined action of carbonization and chloride aggression is carried out, recommendations are given for changing the diffusion coefficient of chlorides.

References

1. Durability of reinforced concrete in aggressive environments / S. N. Alekseev [et al.]. – M. : Stroyizdat, 1990. – 320 p.
2. Alekseev, S. N. Corrosion resistance of reinforced concrete structures in an aggressive industrial environment / S. N. Alekseev, N. K. Rosenthal. – M. : Stroyizdat, 1976. – 205 p.
3. Chernyakevich, O. Yu. Calculation of the service life of reinforced concrete structures in conditions of carbonization corrosion / O. Yu. Chernyakevich, S. N. Leonovich // Prospects for the development of new technologies in construction and training of engineering personnel: collection of scientific articles / Grodno State University named after I. Kupala; editorial board: T. M. Petsold [et al.]. – Grodno : GrSU, 2010. – P. 369–375.
4. Bazant, Z. P. Physical model for steel corrosion in concrete sea structurestheory / Z. P. Bazant // Journal of Structural Division, ASCE, 105 (ST6). – 1979. – P. 1137–1153.
5. Testing and modelling chloride penetration into concrete / C. Andrade [et al.] // Construction and Building Materials. – 2011. – № 39. – P. 9–18.
6. Apostolopoulos, C. Consequences of steel corrosion on the ductility properties of reinforcement bar / C. Apostolopoulos, V. Papadakis // Construction and Building Materials. – 2008. – № 22 (12). – P. 2316–2324.
7. Yuan, C. Effect of carbonation on chloride diffusion in fly ash concrete / C. Yuan, D. Niu, D. Luo // Computers and Concrete. – 2012. – № 5 (4). – P. 312–316.
8. Caims, J. State of the art report on bond of corroded reinforcement / J. Caims // Technical report ceb-tg-2/5. – 1998.
9. Cao, C. Non-uniform rust expansion for chloride-induced pitting corrosion in RC structures / C. Cao, M. Cheung // Construction and Building Materials. – 2014. – № 51. – P. 75–81.
10. Ho, D.W.S. Carbonation of concrete and its prediction / David Wai Sum Ho, R. K. Lewis // Cement and Concrete Research. – 1987. – № 17. – P. 489–504.
11. Glass, G. K. The Influence of Chloride Binding on the Chloride Induced Corrosion Risk in Reinforced Concrete / G. K. Glass, N. R. Buenfeld // Corrosion Science. – 2000. – № 42. – P. 329–344. – DOI: http://dx.doi.org/10.1016/S0010-938X(99)00083-9
12. Corrosion in Reinforced Concrete Structures / ed.: H. Böhni. – 1st Edition. – Sawston, England : Woodhead Publishing Limited, 2005. – 264 p.
13. Yoon, I. Deterioration of concrete due to combined reaction of carbonation and chloride penetration: experimental study / I. Yoon // Key Engineering Materials. – 2007. – Vol. 348–349. – P. 729–732.
14. Yoon, I. Simple approach to calculate chloride diffusivity of concrete considering carbonation / I. Yoon // Computers and Concrete. – 2009. – Vol. 6 (1). – P. 1–18.
15. Exposure of mortars to cyclic chloride ingress and carbonation / J. Backus [et al.] // Advances in Cement Research. – 2013. – Vol. 25 (1). – P. 3–11.
16. Ozbolt, J. 3D numerical modeling of steel corrosion in concrete structures / J. Ozbolt, G. Balabanic, M. Kuster // Corrosion Science. – 2011. – Vol. 53 (12). – P. 4166–4177.
17. Lee, M. Effects of carbonation on chloride penetration in concrete / M. Lee, S. Jung, B. Oh // Aci Materials Journal. – 2013. – Vol. 110 (5). – P. 559–566.
18. Chindaprasirt, P. Effect of carbon dioxide on chloride penetration and chloride ion diffusion coefficient of blended portland cement mortar / P. Chindaprasirt, S. Rukzon, V. Sirivivatnanon // Construction and Building Materials. – 2008. – Vol. 22 (7). – P. 1701–1707.
19. Simulation of chloride migration in compression-induced damage in concrete / M. Rahman [et al.] // Journal of Materials in Civil Engineering. ASCE. – 2012. – Vol. 24 (7). – P. 789–796.
20. Aveldano, R. Behavior of concrete elements subjected to corrosion in their compressed or tensed reinforcement / R. Aveldano, N. Ortega // Construction and Building Materials. – 2013. – Vol. 38. – P. 822–828.
21. Huang, T. The experimental research on the interaction between concrete carbonation and chloride ingress under loading / T. Huang // MSc thesis. – Zhejiang : Zhejiang University, 2013.
22. Chloride content and pH value in the pore solution of concrete under carbonation / X. Wan [et al.] // Journal of Zhejiang University SCIENCE. – 2013. – Vol. 4 (1). – P. 71–78.
23. Combined effect of carbonation and chloride ingress in concrete / X. Zhu [et al.] // Construction and Building Materials. – 2016. – Vol. 110. – P. 369–380. – DOI: http://dx.doi.org/10.1016/-j.conbuildmat.2016.02.034.

Accepted 27.10.2021

UDK 624.012

SOME REMARKS ABOUT CHEMICAL PRESTRESSING OF FRP REINFORCEMENT

V. V. Tur

Doctor of Technical Sciences, Professor, Head the Department of Concrete Technology and Building Materials, Brest State Technical University, Brest, Belarus, e-mail: profturvic@gmail.com

Abstract

In last years has been observed a new wave of interest in the research and practical use of self-stressing concrete, now in combination with various types of non-traditional reinforcement. One of the widely used types of these reinforcements is FRP bars and long fibers (textile). We connect the major problems of FRP reinforcement using as a structural reinforcement with the development of exceeding deflections as well as crack opening under service loads. One of the most effective methods for its performance enhancing is chemical pre-stressing with self-stressing concrete. When self-stressing concrete matrix combined with textile forms a new composite material, namely according to Boxing Wang et al., textile -reinforced self-stressing concrete (TRSSC). This paper presents a critical analysis of some basic assumptions of the proposed models for assessment restraint strains/self-stresses distribution and calculation method of cracking load and deflection of textile reinforced self-stressing concrete.

Keywords: self-stressing concrete, FRP reinforcement, textile, restraint strain.

НЕКОТОРЫЕ ЗАМЕЧАНИЯ О ХИМИЧЕСКОМ ПРЕДВАРИТЕЛЬНОМ НАПРЯЖЕНИИ КОМПОЗИТНОЙ АРМАТУРЫ

В. В. Тур

Реферат

В последние годы наблюдается новая волна интереса в исследованиях и практическом применении напрягающего бетона, теперь в сочетании с нетрадиционными видами армирования. Одним из наиболее широко применяемых видов армирования считается композитная арматура и т.н. текстильные материалы на основе длинной фибры, применяемой в полимерных композитах. Главная проблема, связанная с применением таких материалов связана с чрезмерной шириной раскрытия трещин и развитием прогибов при действии эксплуатационных нагрузок. Одним из наиболее эффективных методов повышения эксплуатационных свойств конструкций армированных полимерными композитами является самонапряжение при использовании для этого напрягающего бетона. Напрягающий бетон в комбинации с текстильными материалами позволяет получить новый, по мнению Б. Ванга, строительный материал (TRSSC). В статье представлен критический анализ некоторых базовых положений расчётных моделей, предложенных Вангом для оценивания связанных деформаций и самонапряжений, а также моделей трещиностойкости и прогибов.

Ключевые слова: напрягающий бетон, композитная арматура, текстиль, связанная деформация.

> Theory is when you know everything and nothing works; practice is when everything works and nobody knows why. Here we combine theory with practice: nothing works and nobody knows why.
> **Albert Einstein**

Introduction

The main reason for this paper writing is my long-term interest in expansive cement, self-stressing concrete and self-stressed structures. Over 40 years I work with this unusual material and such type of prestressed structure in the research laboratory and at the building site. In various time periods, interest and assessments of the self-stressing concrete were very different: from admiration after its successful utilization in the civil engineering works (for instance, joint less self-stressed/post-tensioned slab-on-grade with size144x72m) to great criticism and sarcasm when shrinkage cracking appeared after full pre-stressing loosing or even self-damaging taking place in case for "unbalanced" expansion and strength development. In recent years number of publications dedicated to self-stressing and shrinkage-compensating concrete utilization increased sufficiently (from steel fibre concrete to textile-reinforced self-stressing concrete) and sometimes I can only briefly read a new article related to this issue. Among very interesting and fundamental research works, which show a very high scientific level (for example, Ito et al.) and open new horizons of practical utilization of the expansive composites, we can meet papers with very controversial individual statements or full content.

In this paper, I want to pay attention to the most controversial series of articles [10–12] dedicated to textile-reinforced self-stressed concrete (TRSSC), mainly the "*Theory of self-stressing distribution models*" and experimental results used for verification of these models. At the beginning, we have to tell some words about textile-reinforced concrete. In recent decades, it has developed various ways to replace conventional reinforcing steel (short fibre concrete, various type of FRP-reinforced concrete). Consideration to replace steel reinforcement by use of continuous fibres or grids that were made from continuous fibres began in the 1980s [18]. Among experts, *this new, innovative composite building material* is known today as *textile-reinforced concrete* (TRC). The mechanical and material properties of TRC have been extensively investigated [18]. In investigations [10-12] *"self-stressing concrete (SSC) matrix was combined with textile to form a new composite material, namely, textile-reinforced self-stressing concrete (TRSSC). In this material, textile functions as expansion confinements to SSC to attain self-stress."*

In the analysis process, we will pay attention to some statements from other articles related to this topic (for example, the priorities of expansive cement or self-stressing models development), which we are considered as not fully correct. Considering some important data (for instance, the 120-years Anniversary of prof. V.Mikhailov), I think that brief historical background will be useful.

1. Brief Historical review

Intensive development of the Portland cement concrete technology in the last decades allowed to obtain high-performance concrete (HPC) or even ultra-high performance concrete (UHPC) with a compressive strength above 120 MPa. Nevertheless, the inadequate ratio of any concretes compressive to tensile strength (as it was stated in our works [15-17], concretes of the new generation are still artificial stones with good performance under compression-only). Low tensile strength in combination with inherent to concrete early-age and long-term effects (autogenous as well as drying shrinkage, creep, temperature) lead to decreasing of the serviceability parameters of concrete structures. For instance, restrained shrinkage and temperature deformations lead to the additional tensile stresses appearance in the concrete structure causing cracks (cracks of varying sizes can be found in practically every reinforced concrete structures). Obviously, such cracking of concrete reduces structural durability in general. Based on the sustainable development strategy, ***fib*** Symposium 2020 in China defines concrete of the new generation as a High-durability concrete (HDC). To permit a more efficient utilization of structural concrete, the search for means of overcoming these weaknesses had led to mechanical pre-stressing of steel tendons. By keeping the concrete in compression, cracking is prevented. In the general case, mechanical pre-stressing requires elaborate equipment and techniques.

Considerable advantage can be derived from concrete which is expanding under the varying types of restraint induces a restrained strain and, as a result compressive pre-stress of sufficient magnitude to compensate for shrinkage effect (so-called shrinkage compensating concrete), or induces compressive stresses a high enough magnitude to result in significant compression in the concrete after autogenous and drying shrinkage has occurred (self-stressing concrete). The above-mentioned problem led to the idea of the physic-chemical (or sometimes called chemical) method of concrete structures volume pre-stressing. In 1953 **I. Giyon** wrote in his monograph: "*In case we reached a significant restrained expansion of the concrete that could provide an adequate reinforcement pre-tensioning, without doubts, we will get a principally new method of the beams pre-stressing*".

The history of the development of expansive cement (self-stressing and shrinkage-compensating concrete) application counts for about 90 years and can be said to have originated from an investigation of ettringite in cement. Ettringite ($3CaO\ Al_2O_3\ 3CaSO_4\ 32H_2O$) – is the phase formed during hydration of expansive cements which is the source of the expansion force. It is comparable to the natural mineral of the same name. This high sulfate calcium sulfoaluminate is also formed by sulfate attack on mortar and concrete (delayed ettringite) and was defined as "*cement bacillus*" in older literature. Candlot [1] reported in 1890 that this product resulted from reaction of ticalcium aluminate (C_3A) with calcium sulfate ($CaSO_4$). Michaelis [2] in 1892 suggested that ettringite was responsible for destructive expansion of Portland cement concretes in the presence of environmental containing sulfates.

One of the earliest investigators to recognize the potential of ettringite in the elimination of shrinkage and possibly of inducing pre-stress was Henry Lossier [3]. His works extended more than 20 years, starting in the mid-1930s and the cement he develops consisted of Portland cement, an expansive component (grinding gypsum, bauxites, and chalk to slurry burning the mixture to a clinker) and blast furnace slag.

Russian work by prof. V.Mikhailov [4, 5] in field of expansive cement followed two different courses to obtain an expansive cement to repairs and waterproofing and self-stressing cement. Expansive cement type M - is either a mixture of Portland cement, calcium aluminate cement and calcium sulfate or an inter-ground product made with Portland cement clinker, calcium aluminate clinker and calcium sulfate. In monograph [5], we can find the first formulation of the solid-state or solid-phase expansion mechanism of the matrix as a fundamental condition of concrete self-stressing under restraint and the related requirement to the expansive cement composition (for instance, the ratio Al2O3/SO3 in a binder and expansive component).

Studies by Klein [7,8] and his associates at the University of California are based on the formation of a stable anhydrous calcium sulfoaluminate compound by heat treating a mixture of bauxite, chalk, gypsum at about 2400F. While the ingredients were quite similar to those used in the Lossier cements, the material selection and clinkering conditions probably contributed to the formation of an anhydrous calcium sulfoaluminate, calcium sulfate and lime, produced a cement that could be handled much in the same manner as a regular cement and adjusted to offset shrinkage and produce large net expansion [9]. In recent years, some new types of the expansive cement and expansive additives to OPC are proposed, but all these materials based on the reaction of the ettringite formation (CSA-type). It should be mentioned that besides the use of expansive potential generated by ettringite formation, another type of expansive admixtures takes use of hydroxide formation. As well, periclase has been employed in dam construction as the expanding agent in China.

Therefore, it is strange to read the following statement from the one article:*" Calcium sulfoaluminate cements have essentially been developed in China in 1970s"*

At the beginning, after a short historical review I want briefly to present some most popular models for self-stresses values assessment and possibility of their application to design of the self-stressed elements with FRP reinforcement.

2 Design models for estimation early-ages restrained strains and self-stresses

2.1 Short review

There are following main direction with respect to the actual design models for assessment the early-age restrained expansion strains and stresses in self-stressing concrete element under restraint conditions:

1) Models based on the chemical energy conservation law [4, 5, 14, 22]. Apropos, professor V. Mikhailov formulated this method first in 1972, therefore the following statement from [14] *"the author (Tsuji) has proposed from some time ago a very convenient method based on conception of work quantity, and a general method for making estimations for the cases of applying expansive concrete in reinforced concrete"* is not fully correct. In this time period in SU was developed and implemented standard for self-stressed structures design [28] in which calculation method developed by V.Mikhailov was based on the energy conservation approach. On the other hand, Tsuji [14] developed a convenient practical method for estimating the strain/stress of reinforcing bars in RC members made of expansive concrete, based on the hypothesis that the quantity of work per unit volume by expansion is constant and do not include constants such as modulus of elasticity and creep coefficient of expansive concrete. In these methods, two hypotheses such as ones below are set: a) expansive strains are linearly distributed in the direction of cross-section height; b) the work quantity *U* that expansive concrete performs against restraint per unit volume is a constant regardless of the degree of restraint by external restraining objects. This method is more flexible and applicable for different types of self-stressed structural elements (mainly for composite beams and elements with asymmetrical longitudinal reinforcement distribution in cross-section) in comparison with the semi-empirical coefficient method [21] proposed by prof. V.Mikhajlov.
2) Analytical models [14-17, 23, 24]. As it was stated in [23], *"there have been particularly few analytical investigations on early-age induced stress in HSC containing expansive additive. Pointing this area, Sato et al. carry out two-dimensional FE analysis based on the effective modulus method considering the principle of superposition and the age at application of load on creep in order to evaluate early-age shrinkage/expansion-induced stress in RC-beams. A comparison of computes values indicated the necessity of adopting stricter creep analysis methods and actual creep coefficients."*

Fundamental approach developed by Ito et al. [23] consists of Finite element model and its practical realization as the method based on beam theory, which consider the principle of superposition and linear stress-strain relation of creep, in order to evaluate the early age shrinkage/expansion-induced stress in reinforced member. I think today it is the most progressive and perspective model for early-age self-stressing concrete strain/stress assessment. Some modification of this model for self-stressing concrete with high energy of expansion presents in our works [15-17].

3) Empirical exponential function models [12];
4) Semi-empirical models [13];

In last years, artificial neural network (ANN) and fuzzy inference system model (FIS) for predicting free expansion have been developed [20].

All listed above, models proposed for assessment early age strains/stresses in the self-stressing concrete elements are based on the following fundamental assumptions:

(1) Self-stressing is the specific type of the mechanical pre-stressing, in which the tensile force in the tendons and equal resultant compression force in concrete are induced gradually in time as a result the work that self-stressing concrete performs against restraint;
(2) Expansive strains are linearly distributed in the direction of cross-sectional height (plain section hypothesis is valid). In the first approximation, the cases considered are those when misalignments are not produced at the respective boundaries between expansive concrete and reinforcing bars. Based on the assumption that self-stresses in concrete are considered as the product of the *elastic strains* and modulus of elasticity $E_{cm}(t)$, at the state of stabilization of the expansion stresses are distributed linearly too.

On the other hand, the distribution of the stresses in the cross-section can be calculated as well as for the mechanically pre-stressed structure. Here, the resultant force in restraint is considered the pre-stressing force.

2.2 New Theory of self-stressing distribution model according to [10, 11]

What basic assumptions is used a new model for assessment self-stresses in TRCC according to [10, 11]? On the one hand, in article [10] we can to read the following: *"Self-stress is distributed along the fibre bundle in the textile and exhibits similar effect to that of mechanical pre-stress."* This statement complies with assumptions adopted in the models listed above and considered TRSSC element as the pre-stressed element. The next assumptions about stresses distributions look strange and require comments.

According to [10] *analysis of cracking load is based on the following three assumptions:*

a) The beam is in elastic stage and conforms to the assumption of small deformation before cracking-(no comments)
b) The relative displacement between matrix and the woven fabric is ignored- (no comments)
c) The self-stress value was distributed identically within range of 5mm above and below the textile (see Fig. 1) - (need comments)

Civil and environmental engineering
doi.org/10.36773/1818-1112-2021-126-3-21-30

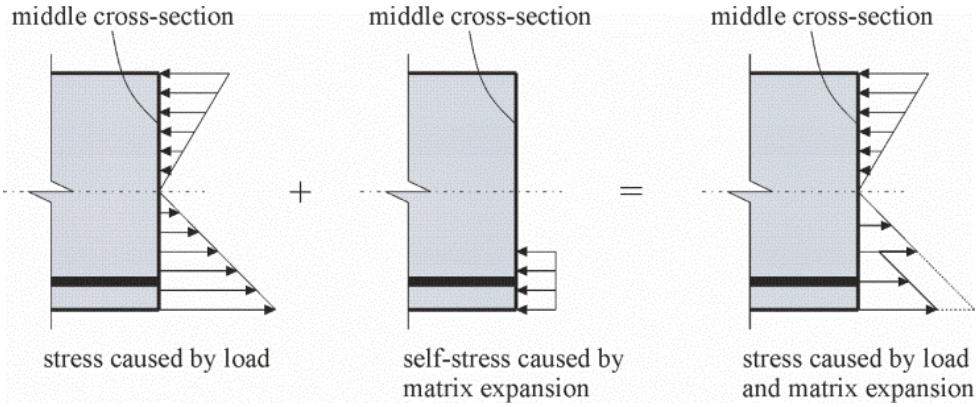

Figure 1 – Stressing distribution of TRSSC beam section according to [10]

Analysis of presented assumptions (mainly assumption c) and Figure 1 initiates following questions:

(1) Why self-stresses are distributed identically at the local area limited within the range of 5 mm above and below the textile? (Why not 5.5mm; 7mm; 5.6 mm...? What is the influence of bundle area? What is the scientific background of this range?);
(2) Is not valid for such new composites plain section law at the stage of expansion? Is the non-linear distribution of the strains in the section's depth in the test?
(3) Is the rest part of the section free from self-stressing if self-stresses concentrate within a limited range above and below textile reinforcement?

Maybe, philosophy of the authors [10-12] related to self-stressing of the concrete can be explained by a following statement from article [12]:*"steel bar-reinforced self-stressing concrete (SSC) and other types of reinforced SSC also have inherent shortcomings. The steel bar used to reinforce SSC cannot influence the entire concrete cross-section uniformly. Placing the concrete near steel bar could produce confinement, whereas placing the concrete far from the steel bar may cause deformation without confinement. Also, when the free expansion strain of the SSC matrix is too high, concrete located distant from the steel bar could incur cracks because* ***overexpansion****".*

The scientific background of this last assumption (c) authors proposed to find in article [11]. What can we read in this paper?

"The expansion of self- stressing concrete matrix was restricted by the interface between the textile and the matrix; therefore, self-stress was formed, and its value varied with the section height. The compacted level was different because of varied self-stressing values on different areas; thus, the elasticity modulus was not identical. Several fundamental assumptions were suggested for self-stressing distribution model:

(1) The self-stress value is generated because longitudinal fiber bundles resist the expansion of the matrix, and the effective range is higher than 10mm; conversely, the latitudinal bundles minimally influence the matrix expansion and is therefore neglected.
(2) The symmetry axis of self-stress is the axle center. Self-stress value is distributed as a quadratic function along z-axis.

.....

(4) Each layer shows deformation compatibility and does not slide relatively during tensile (?) testing. The self-stressing value along the z direction is ignored."

What are we reading now? The effective range of self-stresses distribution *is higher than 10mm* and self-stress value is distributed as *a quadratic function* along z-axis. Moreover, the symmetry axis of self-stress is the axle center (of the section?). I think that looking for your answers to these questions is useless; it is easier to use the results of your research on self-stressed elements reinforced with different FRP and compare it with proposed by authors [10-12] *"theory of self-stressing distribution model*" and cracking resistance model.

3. Experimental studies of self-stressed element reinforced with FRP

Let us consider the results of the two research works [16, 27], in which we used self-stressing concrete for beam elements reinforced with FRP bars. In the first research [16], we studied the possibility of applying self-stressing concrete to increase FRP reinforcement's effectiveness, mainly increasing crack resistance and flexural stiffness (satisfying of the serviceability limit state requirements). We adopted the following work hypothesis: expanding of self-stressing concrete in restraint conditions developed by FRP bars induces tensile force in restraint and compression forces (self-stresses) in concrete. The relatively low axial stiffness of FRP bars allows sufficient restrained strains that cannot be fully compensated for shrinkage development. In work [16] we studied the influence of the level of got self-stresses on the crack resistance and deflection of the beam elements reinforced with FRP longitudinal bars. In the second experiment presented in [27], we investigated the shear resistance of the self-stressed elements without stirrups and reinforced them with longitudinal FRP bars (GFRP and CFRP). For evaluation of the effects related to the usage of the self-stressing concrete jointly with FRP bars in first and second cases performed self-stressed elements with steel reinforcement and elements from OPC-concrete with FRP bars.

3.1 Experimental studies [16]

3.1.1Test specimens

Experimental studies [16] were carried out on two series of self-stressed concrete beams with different type of reinforcing bars. Experimental beams cross-section geometry with reinforcement areas and arrangement are shown in Fig. 2.

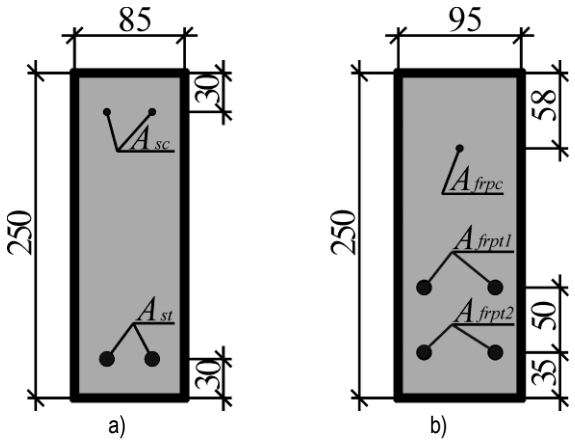

a) – self-stressed beams of the series I (I-BECS-(1…4): A_{sc} = 25,1 mm² (2Ø4); A_{st} = 157,0 mm² (2Ø10));
b) – self-stressed beams of the series II (II-BECF-(1,2): A_{frpc} = 13,7 mm² (1Ø4); A_{frpt1} = 143,5 mm² (2Ø10); A_{frpt2} = 143,5 mm² (2Ø10); II-BECF-(3): A_{frpc} = 13,7 mm² (1Ø4); A_{frpt1} = 143,5 mm² (2Ø10); A_{frpt2} = 330,5 mm² (2Ø14))

Figure 2 – Experimental beams cross-section geometry with reinforcement areas and arrangement [17]

Expansive cement composition was consisted of the following components in the following proportions (by weight): Ordinary Portland cement (CEMI-42,5N) – 71 %; metakaolin – 14 %; gypsum ($CaSO_4 \cdot 2H_2O$) – 15 %. The main mechanical characteristics of the hardened expansive cement established in accordance with [7, 8] are presented in Table 1.

Table 1 – Expansive cement characteristics

Expansion		Strength	
free expansion strain ε_f, %	reference self-stress $f_{CE,d}$, MPa	flexural f_{flex}, MPa	compressive f_{cm}, MPa
1,21	5,9	5,5	50,8

Notes: *1. Expansion and strength characteristics were established at the 28 days age of the mortar bars hardened in the unrestrained conditions;*

2. Reference self-stress, $f_{CE.\ d}$, was established in standard restraint conditions: ρ_l = 1% and E_s = 200 GPa.

Self-stressed beams of the both series were made of self-stressing concrete with characteristics presented in Table 2.

Table 2 – Average values of the self-stressing concrete characteristics

Series	Expansion characteristics at the concrete expansion stabilization		Mechanical characteristics	
	free expansion strain $\varepsilon_{CE,f}$, %	reference self-stress $f_{CE,d}$, MPa	compressive strength $f_{cm,28}$, MPa	modulus of elasticity $E_{cm,28}$, GPa
I	0,47	2,4	33,2	25,3
II	0,55	2,8	37,8	25,7

Notes: *1. Free expansion strain, $\varepsilon_{CE,f}$, was established on the unrestrained specimens;*

2. Reference self-stress, $f_{CE,d}$, was established in the standard restraint conditions: ρ_l=1 % and E_s=200 GPa;

3. Modulus of elasticity was established on the cylindrical specimens (Ø=150 mm, h=300 mm).

Steel and FRP reinforcing bars characteristics are listed in Table 3 and Table 4.

Table 3 – Average values of the mechanical characteristics of steel reinforcing bars (experimental values)

Nominal diameter, mm	Yield stress f_{ym}, MPa	Modulus of elasticity E_{sm}, GPa
4	573,2	200,0
10	625,7	

Table 4 – Average values of the mechanical characteristics of FRP reinforcing bars (experimental values)

Nominal diameter, mm	Type of fibers	Modulus of elasticity E_{frpm}, GPa	Tensile strength f_{frpm}, MPa	Ultimate tensile strain ε_{frpm}, %
5	Basalt	51,5	1262	2,45
10	Glass	45,2	1027	2,27
14	Glass			

3.1.2 Results of experimental research

3.1.2.1 Self-stressing stage, restrained strains distribution

Experimental values of the restrained strains and self-stresses in concrete on the depth of the cross-section gravity center immediately before static loading are listed in the Table 5.

Table 5 – Experimental values of restrained strains and self-stresses immediately before static loading

Unit code	Restrained strains, [%]			Self-stress
	$\Sigma(\Delta\varepsilon_{CE,t})_i$	$\Sigma(\Delta\varepsilon_{CE,m})_i$	$\Sigma(\Delta\varepsilon_{CE,b})_i$	σ_{CE}, [MPa]
I-BECS-(1)	0,342	–	0,128	2,69
I-BECS-(2)	0,372	–	0,144	2,95
I-BECS-(3)	0,443	–	0,144	3,00
I-BECS-(4)	0,499	–	0,154	3,46
II-BECF-(1)	0,481	0,330	0,269	1,78
II-BECF-(2)	0,556	0,365	0,276	1,92
II-BECF-(3)	0,429	0,267	0,197	2,10

As shown in Table 5, in all the tested beams, the initial value of self-stresses was got in the range from 1,8 to 3,5 MPa depending on the reinforcing bars' type, area, and arrangement. Reached pre-tensioning in reinforcing bars were at average 46 % from yield strain and 14 % from ultimate tensile strain for steel and FRP reinforcing bars respectively. It should be pointed that for the members pre-stressed with FRP reinforcing bars in accordance with [9], initial values of the pre-stress should be limited by the 24 % from the ultimate tensile strength.

Beams initial restrained expansion curvature values obtained on the basis of measured restrained strains and measures deflections varied in the diapason (1,16–1,82)·10^{-5} mm^{-1} and (3,7-4,1) mm respectively. These values of the initial restrained expansion curvature of the beams got at the self-stressing stage should be considered because two developed in time-superposed basic processes: (1) on the one hand–self-stressing concrete expansion in asymmetrical restraint conditions and (2) on the other hand–concrete elastic compressive strains accumulating under monotonically increasing in time restraint reaction [1, 5, 6]. It should be pointed that plane section hypothesis was valid for all tested beams. The so-called beam initial «elastic» curvature (that is determined from the accumulated concrete elastic compressive strains distribution) only have an influence on the self-stressed member behavior under the applied static load in terms of traditional decompression. In contrast with traditional pre-stressed members, in the self-stressed members the values of the beam initial «elastic» curvature is not possible to establish based on the direct strains measurement, but it can be obtained under the proposed MSDM concept [1, 2].

3.1.2.2. Load-deflection responses and failure modes

After the self-stressing concrete expansion stabilization was reached, self-stressed beams were tested with monotonically increasing load by means of two concentrated forces applied at the 1/3 and 2/3 points of the 1200 mm span. The main aim of the static loading consisted in the investigation of the influence of the achieved initial stress-strain state obtained to the self-stressing concrete expansion stabilization on the behavior of the tested beams under the load.

The moment-curvature and moment-deflection curves for specimens of series I and series II are shown in Fig. 3.

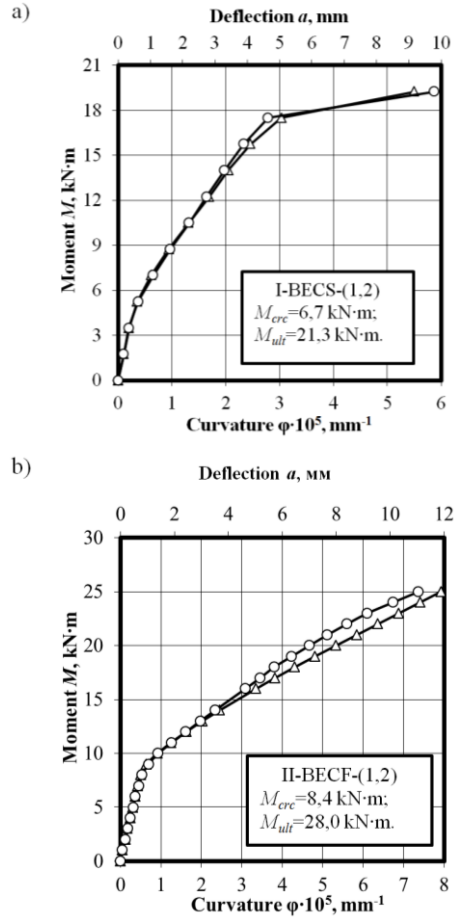

a) – self-stressed beams of the series I;
b) – self-stressed beams of the series II

Figure 3 – Relations «*M*-φ» and «*M*-*a*» obtained on the static loading stage

doi.org/10.36773/1818-1112-2021-126-3-21-30

Test results obtained within loading of the self-stressed beams are listed in Table 6 and Table 7.

Table 6 – Failure modes and experimental value of cracking and ultimate loads obtained within self-stressed beams testing

Unit code	Cracking load (force) P_{crc}, kN (M_{crc}, kN·m)	Ultimate load (force) P_{ult}, kN (M_{ult}, kN·m)	Failure mode
I-BECS-(1)	34 (6,8)	108 (21,6)	«B»
I-BECS-(2)	37,3 (6,5)	120 (21,0)	
I-BECS-(3)	39,5 (6,9)	120 (21,0)	
I-BECS-(4)	46,6 (8,2)	125,4 (22,0)	
II-BECF-(1)	40,5 (8,1)	150 (30,0)	«Sh»
II-BECF-(2)	43,5 (8,7)	130 (26,0)	
II-BECF-(3)	39,0 (7,8)	150 (30,0)	
Note: *«B» – flexural failure mode; «Sh» – shear failure mode.*			

Table 7 – Experimental values of the deflection and crack width obtained within self-stressed beams testing

Unit code	Deflection a, mm	Crack width (w_{max}/w_m), mm
I-BECS-(1)	2,3	0,1/0,1
I-BECS-(2)	2,7	0,15/0,07
I-BECS-(3)	2,9	0,1/0,09
I-BECS-(4)	3,2	0,1/0,1
II-BECF-(1)	4,9	0,7/0,59
II-BECF-(2)	4,6	0,6/0,38
II-BECF-(3)	4,6	0,6/0,47
Note: *In the table values of deflections, maximum and average crack width correspond to the loading rate of* $\approx 0,6 \cdot P_{ult}$*, where* P_{ult} *– ultimate load.*		

For beams of series I and series II, the first cracks occurred in the pure bending region at the load of 44 kN (7,1 kN•m) and 41 kN (8,2 kN•m) on average, respectively. After that in case of FRP reinforced beams, the slope of moment-curvature (moment-deflection) curves showed considerable drop and it was kept almost constant up to failure, as it is shown in Fig. 3. In case of steel reinforced beams, three characteristic branch sections with different slopes was observed: the first branch section – up to cracking; the second branch section – from cracking and up to reinforcing steel yielding; the third branch section – from reinforcing steel yielding and up to the failure (see Fig. 3). With increasing of the bending moment up to 24 kN·m, in the FRP reinforced beams, multiple inclined flexural shear cracks occurred outside the pure bending region and extended to a distance approximately 20 mm from the top surface of the beam. When applied load reached 143,3 kN (28,7 kN·m) at average, diagonal tension flexural shear failure mode was reached, but to this time FRP reinforcing bars did not reach its ultimate tensile strains (in accordance with test results: $\varepsilon_{rt,frp}$ = 0,933 %). Taking into account that FRP reinforced self-stressed beams reinforcement ratio was equal to 1,6 % and 2,1 % for II-BECF-(1,2) and II-BECF-(3) respectively, that is considerably higher of the both balanced reinforcement ratio (ρ_{bal} = 0,3 %) and recommended in accordance with [9] reinforcement ratio 1,4· ρ_{bal} = 0,42 %. For the real reinforcement ratio of the tested beams, expected failure mode is due to crushing of the concrete in compression, but an observed failure mode had changed on the flexural shear without crushing of the concrete in compression. Moreover, registered within testing value of the ultimate moment was at average in 2 times higher than predicted value of the ultimate moment in accordance with EN 1992-1-1 and based on the mean and established in tests values of the materials characteristics. In opposite to the FRP reinforced beams, failure mode and value of the ultimate load for steel reinforced self-stressed beams of series I was the same as it was predicted in accordance with EN 1992-1-1 (ratio between predicted and established within loading ultimate bending moments was equal to 0,90).

Characteristic modes of failure and crack patterns for beams of the both series I and series II are shown in the Fig. 4.

Based on the analysis of the obtained experimental results, it can be stated, that initial early age stress-strain state obtained on the expansion stage influenced on the beams behavior during loading. It was observed that for the both series I and series II self-stressed beams cracking load was near 30 % from the ultimate load (see Table 6). Flexural cracks development through the concrete cross-section depth was following: raised flexural cracks extended on the average depth about 180 mm and 195 mm (≈75 % from cross-section depth) for series I and series II beams respectively and saved this position almost up to the failure on the background of the gradually increasing cracks number and its opening. This effect is explained that in the self-stressed structures initial compressive stresses are saved in concrete under the crack. An observed cracks patterns in the member tensile zone (see Fig. 4) with an average distance between cracks 60±15 mm indicated about practically uniform distribution of the stresses longwise reinforcing bars in tension that is inherent for pre-stressed structures.

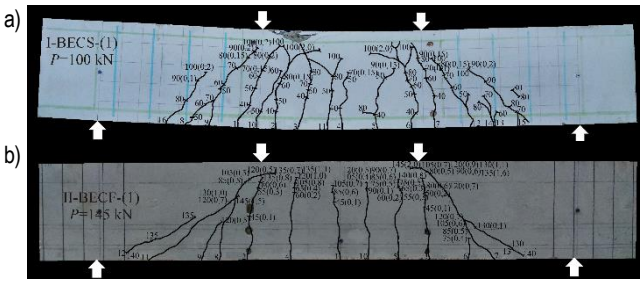

a) – self-stressed beams of the series I;
b) – self-stressed beams of the series II

Figure 4 – General view of the beam crack patterns after test [16]

3.1.3 Diagram method comparison with experimental results

To analyze results obtained within static loading of the self-stressed beams with non-symmetric both FRP and steel reinforcement arrangement the «M-$\varepsilon_{rt,x}$» diagram was proposed (where M is a bending moment; $\varepsilon_{rt,x}$ is a longitudinal tensile strain from the loading on depth of gravity center of the reinforcement in tension). The general view of the diagram is presented in the Fig. 5.

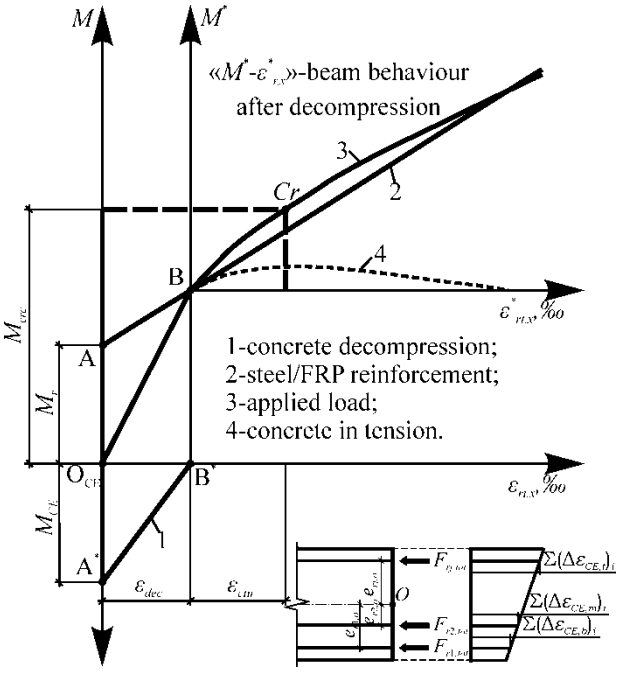

Figure 5 – Diagram for analysis of the initial stress-strain state influence on the behaviour under the loading of the non-symmetrically reinforced beams

Let us consider self-stressed beam under the monotonically increased load. Forces redistribution in the self-stressed beam cross-section under increasing load can be illustrated with the diagram presented in the Figure 1. Before load applying, in the beam cross-section balanced internal forces, obtained within self-stressing concrete expansion, are acting (see Fig. 1: $O_{CE}A = O_{CE}A^*, M_{CE} = M_r$). Moments from

the internal forces, accumulated to the end of the self-stressing stage, respectively concrete cross-section gravity center can be determined with respect to the value of the fixed restrained strains in reinforcement:

$$M_{CE} = M_r = \sum_{j=1}^{n} F_{rj,tot} \cdot e_{rj,o}, \quad (1)$$

where: M_{CE} and M_r are the balanced moments from self-stressing;

$e_{rj,o}$ – eccentricity of the force in the *j*-th restraint reinforcement line respectively concrete cross-section gravity center;

$F_{rj,tot}$ – force in the *j*-th restraint reinforcement line, accumulated on the self-stressing stage to the concrete expansion stabilization that is determined as follows:

$$F_{rj,tot} = \varepsilon_{rj}\left(t_{tot}\right) \cdot E_r \cdot A_r, \quad (2)$$

where: $\varepsilon_{rj}\left(t_{tot}\right)$ – strain in the *j*-th restraint reinforcement line, accumulated on the self-stressing stage to the concrete expansion stabilization, calculated in accordance with MSDM model [15-17];

E_r, A_r – modulus of elasticity and area of the restraint reinforcement respectively.

After applying and further monotonically increasing of the load, reducing of the initial concrete cross-section pre-compression, obtained on the self-stressing stage, was observed. Besides, up to decompression point B* (see diagram in the Fig. 5), cross-sectional tensile force is sustained by the reinforcement only (like it is in the traditional pre-stressed structures, line AB). Increment of the strains in reinforcement and increment of the bending moment, sustained by the reinforcement, before concrete decompression point B* is characterized by the AB line on the diagram in the Fig. 5. At the same time, reducing of the concrete initial compressive stresses corresponds to the internal moment changing along the A*B* line. At the point B* (see Fig. 5) concrete initial elastic compressive strains on the depth of gravity center of the reinforcement in tension reduces to 0 (so-called decompression stage). At the point B, line AB has the common point with the line O_{CE}B, characterized changing of the bending moment from the externally applied load. Within further loading after decompression point B*, behavior of the self-stressed member is the same like behavior of the conventional RC-beam without any initial pre-stressing (part of the diagram in the «M^*- $\varepsilon^*_{rt,x}$» axises). At this loading stage, a tensile force in concrete cross-section is sustained together by the concrete in tension and reinforcement right up to the flexural cracks appearing. Flexural cracks appear when tensile strains in concrete exceeds its ultimate values ε_{ctu} (see diagram in «M^*- $\varepsilon^*_{rt,x}$» axises in the Fig. 5).

Thus, to the flexural cracks formation, the total strains respect to cracking $\varepsilon_{rt,crc}$ on the depth of reinforcement gravity center, is considered as a sum of decompression starins ε_{dec} and ultimate concrete tensile strains ε_{ctu}.

Resultant value of the cumulative concrete elastic strains $\varepsilon_{CE,el}\left(t_{sl}\right)$, which corresponds to the decompression strains ε_{dec} at the static loading should be calculated as follows:

$$\varepsilon_{dec} = \varepsilon_{CE,el}\left(t_{sl}\right) = \frac{\varepsilon_{CE,eltot}\left(t_i\right) \cdot E_{c,aw}\left(t_i\right)}{E_{cm,sl}}, \quad (3)$$

where: $\varepsilon_{CE,eltot}\left(t_i\right)$ – concrete elastic strains accumulated to the end of the expansion stage and saved in structural memeber immediately before loading. It have to be calculated in accordance with proposed MSDM model [15-17];

$E_{c,aw}\left(t_i\right)$ – «average-weighted» expansive concrete modulus of elasticity, calculation procedure of it is presented in detail in [17];

$E_{cm,sl}$ – concrete modulus of elasticity to the static loading time;

t_i – age of concrete immediately before static loading.

Considering that decompression strains are a parameter that allows assessing the effectiveness of the initial self-stressing and to predict its further influence on the crack behavior of the beams, this parameter (ε_{dec}) was got from experimental results analysis with diagram «M- $\varepsilon_{rt,x}$», using and compared with the total tensile strains immediately before cracking measured on the depth of the reinforcement gravity center $\varepsilon_{rt,crc}$. This analysis of the self-stressing effectiveness was based on the assessment of the ratio between decompression strains ($\varepsilon_{dec,exp}$) and total tensile strains ($\varepsilon_{rt,crc}$), that is presented in Table 8.

Table 8 – Experimental values of the concrete tensile strains on the depth of the reinforcement gravity centre

Unit code	$\varepsilon_{dec,exp}$, ‰	$\varepsilon_{rt,crc}$, ‰	(2)/(3)
(1)	(2)	(3)	(4)
I-BECS-(1)	0,189	0,528	0,36
I-BECS-(2)	0,241	0,542	0,44
I-BECS-(3)	0,229	0,533	0,43
I-BECS-(4)	0,312	0,658	0,47
II-BECF-(1)	0,091	0,494	0,18
II-BECF-(2)	0,095	0,480	0,20
II-BECF-(3)	0,101	0,490	0,21

As it is shown in Table 8, from experimental research [17] this ratio was at average 0,43 and 0,20 for self-stressed beams of the series I and series II respectively.

For effectiveness of the FRP reinforcing bars application in the pre-stressed (self-stressed) structures, «M-$\varepsilon_{rt,x}$» diagram was utilized (see Fig. 5). It was assessed from the experimental results, that before loading in the beams of Series I and Series II almost equal values of the moments created by the pre-compression forces was obtained (was at average 3 kN·m). Therefore decompression strains in case of FRP bars using were less approximately in two times in comparison with decompression strains registered in self-stressed beams with steel reinforcement (see Table 8). It was stated, that up to decompression point, resultant force in tensile zone of the cross-section is sustained by the reinforcing bars only (at this stage concrete is under the initial compressive stresses). Taking into account that steel and FRP bars are characterized by the different values of modulus of elasticity (FRP bars modulus of elasticity E_{frpm} = 45,2 GPa, that was close to the concrete modulus of elasticity E_{cm} = 25,7 GPa), a different values of the moment increment was observed for the same levels of the longitudinal tensile strains in reinforcement (in case of FRP reinforcement, such increments were sufficiently less). To obtain equal values of the moment increments in case of FRP and steel bars utilizing, required area of FRP reinforcement have to be increased considerably and can be found based on the optimization procedure (it consists in the assessment of the FRP reinforcement axial stiffness, that is necessary to provide desired values of the moment increments within decompression stage as well as initial self-stresses at the expansion stage).

Nevertheless, it should be pointed that obtained self-stressing parameters in the members reinforced with FRP bars not only lead to the cracking moment increasing, but change series II self-stressed beams post-cracking behavior. A number of cracks, comparable with cracks number in series I self-stressed beams with steel reinforcing bars was observed (N=9 and N=12 at average respectively), and maximum flexural crack width was not exceed 0,6 mm under the loading rate near $0{,}6 \cdot P_{ult}$.

2.2 Experimental studies [27]

2.2.1Test specimens

Eight series of the self-stressed beams reinforced with FRP was tested in studies [27]. Beams in the experiment [27] were designed in such a way that they had asymmetric mixed reinforcement from steel and FRP bars near the bottom and top fiber of the section (see Fig. 6). However, despite different numbers and materials of reinforcement bars near the bottom and top fibres of the beam cross-section, their axial stiffness was very close ($A_s \cdot E_s = A_f \cdot E_f$).

Geometry, reinforcement arrangement and basic parameters of beams shown in Fig. 6.

doi.org/10.36773/1818-1112-2021-126-3-21-30

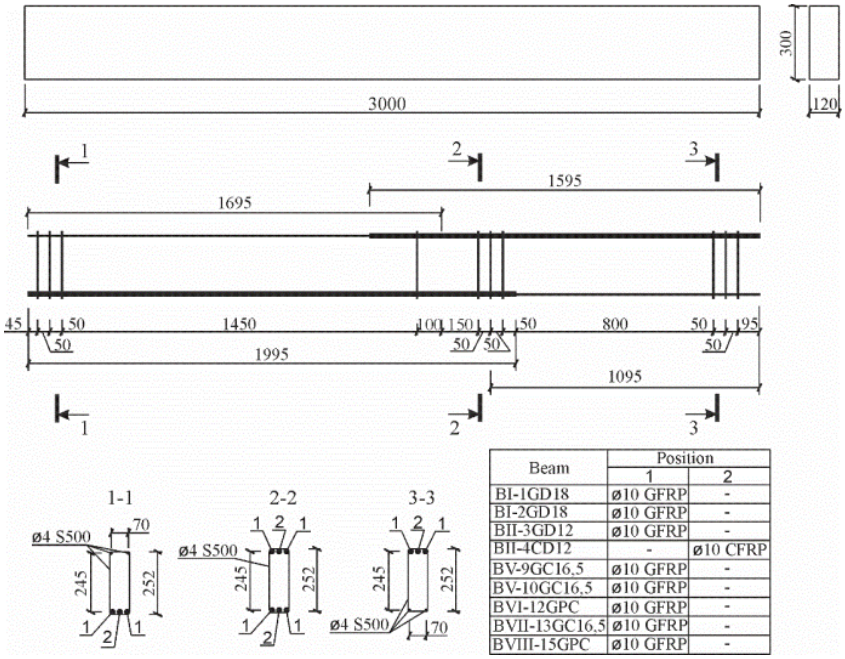

Beam	Position 1	Position 2
BI-1GD18	ø10 GFRP	-
BI-2GD18	ø10 GFRP	-
BII-3GD12	ø10 GFRP	-
BII-4CD12	-	ø10 CFRP
BV-9GC16,5	ø10 GFRP	-
BV-10GC16,5	ø10 GFRP	-
BVI-12GPC	ø10 GFRP	-
BVII-13GC16,5	ø10 GFRP	-
BVIII-15GPC	ø10 GFRP	-

Figure 6 – Geometry, reinforcement arrangement and parameters of tested beams [27]

Expansive concrete mix nominal composition per 1 m3 of the beams of series BI-BII, BV-BVIII are listed in Table 9 [27].

Table 9 – Expansive concrete composition

Series	1 м^3 in dry conditions, kg					
	Cement	Denka CSA	Fine aggregate	Coarse aggregate	Water, l	Stachement 2010
BI	510	90	600	960	240	-
BII	410	50	805	990	175	7,0
BV, BVII	515	85*	740	880	201	7,5
BVI, BVIII	360	-	900	1060	148	5,4
Note: «*» – CSA 20.						

Self-stressed beams of the series BI-BII, BV-BVIII were made of self-stressing concrete with characteristics presented in Table 10.

Table 10 – Average values of the self-stressing concrete characteristics

Series	Expansion characteristics at the concrete expansion stabilization		Mechanical characteristics	
	free expansion strain $\varepsilon_{CE,f}$, %	reference self-stress $f_{CE,d}$, MPa	compressive strength $f_{cm,28}$, MPa	modulus of elasticity $E_{cm,28}$, GPa
BI	1,12	2,55	53,1	31,7
BII	0,02	0,45	76,5	43,3
BV	0,45	2,20	53,2	33,7
BVI	-	-	47,1	40,5
BVII	0,42	2,35	50,2	31,2
BVIII	-	-	30,7	32,1

Notes: 1. Free expansion strain, $\varepsilon_{CE,f}$, was established on the unrestrained specimens;

2. Reference self-stress, $f_{CE,d}$, was established in the standard restraint conditions: ρ=1 % and E_s=200 GPa;

3. Modulus of elasticity was established on the cylindrical specimens (Ø=150 mm, h=300 mm).

Steel and FRP reinforcing bars characteristics are listed in Table 11 and Table 12.

Table 11 – Mechanical characteristics of steel reinforcing bars (experimental values)

Nominal diameter, mm	Yield stress f_{ym}, MPa	Modulus of elasticity E_{sm}, GPa
4	573,2	200,0

Table 12 – Mechanical characteristics of FRP reinforcing bars

Nominal diameter, mm	Type of fibers	Modulus of elasticity E_{frpm}, GPa	Tensile strength f_{frpm}, MPa	Ultimate tensile strain ε_{frpm}, %
10*	Glass	40,8	760	2,0
10*	Carbon	155	2000	1,5
10**	Glass	32	1244	2,7
Note: «*» – this reinforcement was used in beams of the series BI-BII; «**» – this reinforcement was used in beams of the series BV, BVI-12GPC, BVII-13GC16,5 and BVIII-15GPC.				

The measurement of the strains in the test beams at the stage of hardening and expansion of the self-stressing concrete underwater storage conditions was carried out using a strain meter with a digital indicator with a scale of 0.01 mm on a 270 mm basis (when measuring the deformations along the lateral face of the test beam). On each beam (series BI-BV) 4 strain meters are installed at the level of the reinforcement (in the middle sections of the span and cantilever part of the beam due to uneven reinforcement. On the beams of series BVII, two more strain meters are installed to study the process of self-stressing of concrete in a zone with the same reinforcement.

2.2.2 Results (self-stressing stage, expansive strains distribution)

Experimental values of the restrained strains at the level of reinforcement and self-stresses in concrete on the depth of the cross-section gravity center immediately before static loading are listed in the Table 13 and Table 14.

Table 13, 14 listed results of the measurement of the restrained strains on the level of the reinforcement, values of the calculated based on these strains tensile forces in reinforcement bars, and average self-stresses at the level of the center gravity of the section. Figures 7a,b show development in time tensile forces in restraint bars F_{s1} and F_{s2} near the top and bottom fibers of the cross-section respectively. We considered two series of beams performed from the self-stressing concrete with different values of standard self-stress grade in accordance with [...]. For beam BI-2SD18 from series BI standard self-stress was equal $f_{ce,m}$ = 2.55 MPa, and for beam BV-9GC16,5 from series BV, it was equal $f_{ce,m}$ = 2.2 MPa.

Table 13 – Experimental parameters of the self-stressing for beam BI-2GD18 (span)

Days	$\varepsilon_{s1}\cdot10^{-5}$	$\varepsilon_{s2}\cdot10^{-5}$	F_{s1}, kN	F_{s2}, kN	F_o, kN	M_o, kNm	$\varphi_M\cdot10^{-10}$, mm^{-1}	$\varphi_\varepsilon\cdot10^{-5}$, mm^{-1}	σ_{ce}, MPa
1	0	0	0	0	0	0	0	0	0
2	144,4	107,4	7,26	6,48	13,75	-0,11	-1,12	0,15	0,38
3	283,3	192,6	12,57	11,61	24,2	-0,14	-0,62	0,37	0,67
4	355,6	233,3	12,57	14,07	26,62	0,15	0,44	0,50	0,74
5	413	264,8	12,57	15,97	28,49	0,38	0,88	0,61	0,79
6	438,9	285,2	12,57	17,2	29,71	0,53	1,05	0,63	0,83
7	450	292,6	12,57	17,64	30,15	0,58	1,03	0,65	0,84
8	453,7	296,3	12,57	17,87	30,37	0,61	1,0	0,65	0,84
9	457,4	300	12,57	18,09	30,59	0,63	0,97	0,65	0,85
10	459,3	301,9	12,57	18,2	30,7	0,65	0,96	0,65	0,85
11	461,1	301,9	12,57	18,2	30,7	0,65	0,92	0,66	0,85
12	461,1	303,7	12,57	18,31	30,81	0,66	0,91	0,65	0,86
13	463	303,7	12,57	18,31	30,81	0,66	0,89	0,66	0,86

Table 14 – Experimental parameters of the self-stressing for beam BV-9GC16,5 (span)

Days	$\varepsilon_{s1}\cdot10^{-5}$	$\varepsilon_{s2}\cdot10^{-5}$	F_{s1}, kN	F_{s2}, kN	F_o, kN	M_o, kNm	$\varphi_M\cdot10^{-10}$, mm^{-1}	$\varphi_\varepsilon\cdot10^{-5}$, mm^{-1}	σ_{ce}, MPa
1	0	0	0	0	0	0	0	0	0
2	9,3	7,4	0,47	0,35	0,82	-0,02	-0,11	0,008	0,02
3	16,7	14,8	0,84	0,70	1,54	-0,02	-0,06	0,008	0,04
4	22,2	22,2	1,12	1,05	2,17	-0,01	-0,02	0	0,06
5	27,8	27,8	1,40	1,31	2,71	-0,01	-0,02	0	0,08
6	36,1	38,9	1,81	1,84	3,65	-0,001	-0,002	-0,01	0,10
7	44,4	50,0	2,23	2,36	4,59	0,01	0,02	-0,02	0,13
8	51,9	66,7	2,61	3,15	5,76	0,06	0,09	-0,06	0,16
9	55,6	72,2	2,79	3,41	6,20	0,07	0,10	-0,07	0,17
10	59,3	80,6	2,98	3,81	6,78	0,09	0,12	-0,09	0,19
11	63,0	88,9	3,17	4,20	7,36	0,12	0,16	-0,11	0,20
12	66,7	98,1	3,35	4,64	7,98	0,15	0,19	-0,13	0,22
13	70,4	102,8	3,54	4,86	8,39	0,15	0,19	-0,13	0,23
14	74,1	107,4	3,72	5,08	8,79	0,16	0,20	-0,14	0,24
…									
29	155,6	188,9	7,82	8,93	16,74	0,12	0,13	-0,14	0,47

As shown from Figure 7 for different reinforcement ratios near the top and bottom fibres of cross-section, but the very close value of the bars axial stiffness, the tensile forces in steel and FRP bars increased practically the same before expansion stabilization. At the stage of the expansion stabilization, the beam practically does not deflect (the value of the curvature is equal $\varphi_{ce} = 1{,}4\cdot10^{-6}$ mm^{-1}). The average value of the self-stress at the level of the center gravity of the cross-section was equal to 0.47 MPa (see Table 14 and Fig. 7b). Some different behavior at the expansion stage of the expansive concrete we can observe for beam BI-1GD18.

At the initial stage of expansion (near 2 days) the values of restrained strains and tensile forces in reinforcement, respectively, developed practically the same. However, at 3-day age restraint strain in steel reinforcement (Ø4 S500) exceeded yield strain for steel (ε_{s1} = 2,83‰ > ε_{sy} = 2,17‰). After that increasing of restrained strain does not provide to increasing of the tensile force in steel reinforcement (see Fig. 7a and Table 13) and this force remains practically constant $F_{s1} = f_y \cdot As$.

As a result, the main restraint element becomes FRP bars and additional tensile force is developed now in these bars. Because the difference in the values of the restrained strains at the level the top and bottom reinforcement took place the beam was deflected (the value of the curvature was equal $\varphi_{ce} = 6{,}6\cdot10^{-6}$ mm^{-1}), but sections remain plain.

Comparison with results obtained by testing the beams reinforced with steel reinforcement only (beams BIV-8SC16,5 and BIII-SD15) shows that, because axial stiffness of the bars near opposite fibres of section differs sufficiently, we can observe differences in the development of the axial tensile forces (see Fig. 8). Tensile forces in the bottom steel bars Ø12 S500 increased practically linearly before the self-stressed concrete expansion strain stabilization. In the top reinforcement bars Ø4 S500 at 17 days, tensile strains exceeded steel yielding strains (ε_{s1} = 2,33‰ > ε_{sy} = 2,17‰) and tensile force stabilized at the level $F_{s1} = f_y \cdot A_s$. The average self-stress value at the level of centre of gravity of section was equal to 1,7 MPa. The curvature of the beam now of expansion stabilization was equal φ_{ce}=19,2·10^{-6} mm^{-1} (for comparison curvature φ_{ce} = 6,6·10^{-6} mm^{-1} for the beams reinforced by FRP).

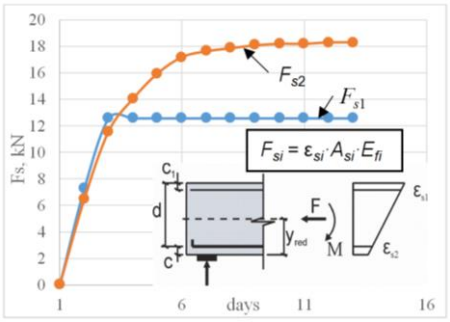

a)

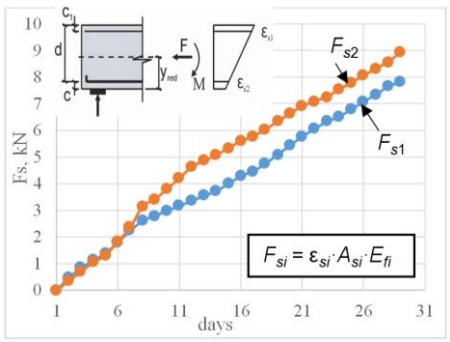

b)

a) – beam BI-2GD18 (span); b) – beam BV-9GC16,5 (span)

Figure 7 – Development of the tensile force in reinforcement at the expansion stage

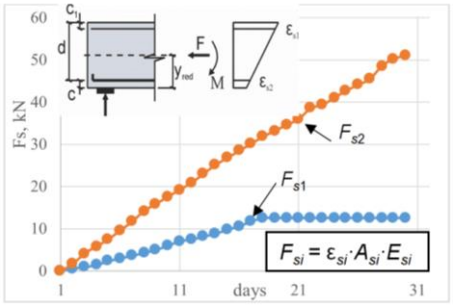

a)

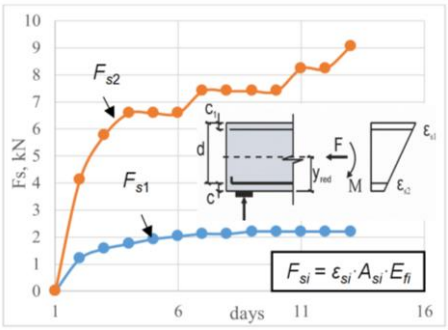

b)

a) – beam BIV-8SC16,5 (span); b) – beam BIII-6SD15 (span)

Figure 8 – Development of the tensile force in reinforcement at the expansion stage

doi.org/10.36773/1818-1112-2021-126-3-21-30

As with experiments [27], induced self-stresses influenced the shear resistance of the tested beams under uniformly distributed loads. Table 15 listed experimental results of the load testing of the self-stressed beams reinforced with FRP and beams performed from OPC-concrete reinforced with FRP too. Crack patterns after testing the beams are shown in Figure 9. The forces registered during static tests, corresponding to the formation of cracks and the ultimate forces, are presented in Table 15.

Table 15 – Results of static tests under the action of a uniformly distributed load in the span of a beam

Series	Beam	P_{cr}, kN	q_{cr}, kN/m	P_u, kN	q_u, kN/m	Mode of failure
BI	BI-1GD18 (without loading the cantilever)	-	29,6	-	87,3	Diagonal crack
	BI-2GD18	10,4	34,7	22,5	75,0	Diagonal crack in the span
BII	BII-3GD12	10,4	34,7	24,5	81,7	Diagonal crack in the cantilever
	BII-4CD12	8,4	28,0	24,5	81,7	--//--
BV	BV-9GC16,5	6,4	21,3	20,2	67,5	Diagonal crack in the span
	BV-10GC16,5	6,4	21,3	18,5	61,6	Diagonal crack in the cantilever
BVI	BVI-12GPC	6,4	21,3	18,2	60,6	Diagonal crack in the span

Notes: 1. P_{cr} – point force applied in the cantilever, corresponding to cracking;
2. q_{cr} – uniformly distributed load applied in the span of a beam corresponding to cracking;
3. P_u – point force applied in the cantilever, corresponding to failure;
4. q_u – uniformly distributed load applied in the span of a beam corresponding to failure.

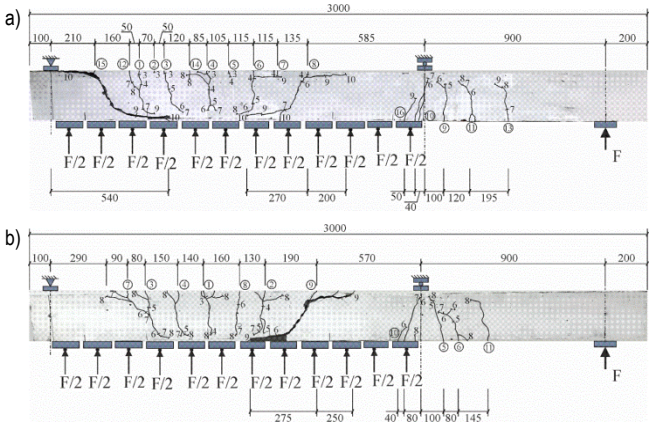

a) – BV-9GC16,5 (expansive concrete); b) – BVI-12GPC (opc-concrete)

Figure 9 – Cracks patterns for tested beams

Initial self-stresses now of the expansion stabilization for beams series BV was equal =0.47 MPa, and was partially compensated by shrinkage in the time before testing. So cracking loads for self-stressed beams BV-9GC16,5 and BV-10GC16,5 practically was the same as the cracking loads registered for beams performed from OPC-concrete (beam BVI-12GPC). However, for the beam series BII, cracking loads were on 31 % (beam BII-4CD12) and 62.5 % (beams series BI and BII-3GD12) greater than for beams performed from OPC-concrete. Analogical results were obtained for beams reinforced with steel bars. For the beams (series BIV) cracking loads were on 48 % and for the beam BIII-6SD15 even on 72 % greater than for the analogical beams performed from OPC-concrete (beam BVI-11SPC) (see Table 16). The cracks development and final crack pattern depend on the achieved value of self-stressing after failure (see Fig. 10). For self-stressed beams reinforced with steel bars and FRP bars, the cracks development and final crack pattern depend on the achieved value of self-stressing after failure.

Table 16 – Results of static tests under the action of a uniformly distributed load in the span of a beam

Series	Beam	P_{cr}, kN	q_{cr}, kN/m	P_u, kN	q_u, kN/m	Mode of failure
BIII	BIII-6SD15	14,5	48,2	36,6	122,1	Diagonal crack in the span
BIV	BIV-7SC16,5	12,4	41,4	34,6	115,3	--//--
	BIV-8SC16,5	12,4	41,4	37,9	126,3	--//--
BVI	BVI-11SPC	8,4	28,0	26,5	88,5	--//--

Notes: 1. P_{cr} – point force applied in the cantilever, corresponding to cracking;
2. q_{cr} – uniformly distributed load applied in the span of a beam corresponding to cracking;
3. P_u – point force applied in the cantilever, corresponding to failure;
4. q_u – uniformly distributed load applied in the span of a beam corresponding to failure.

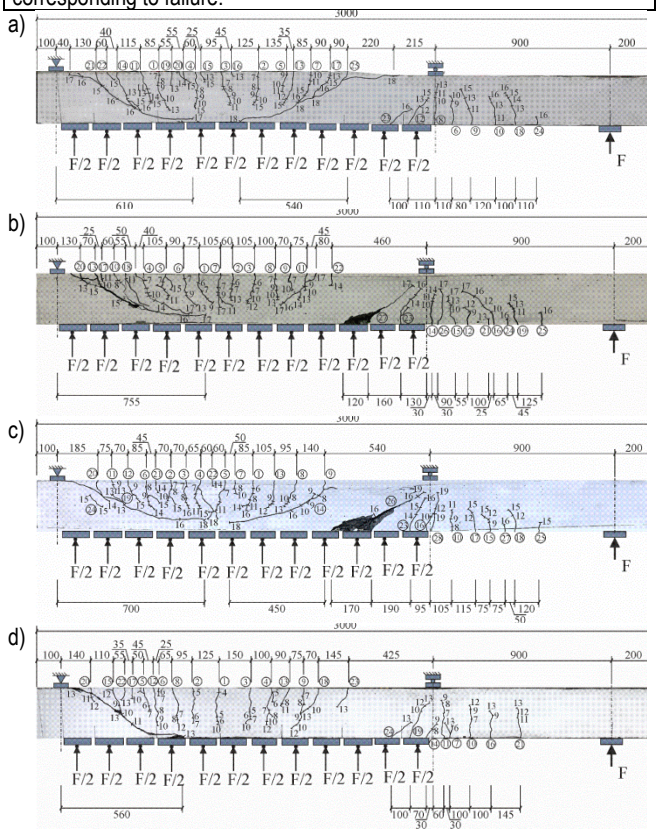

a) – BIII-6SD15 (expansive concrete);
b) – BIV-7SC16,5 (expansive concrete);
c) – BIV-8SC16,5 (expansive concrete); d) – BVI-11SPC (opc-concrete)

Figure 10 – Cracks patterns for tested beams

The behavior of the self-stressed beams reinforced with FRP at the ultimate limit state needs a separate analysis and does not subject to this paper.

Conclusions

What can we conclude from the results of the presented experimental and theoretical investigations?

(1) A self-stressed structure -is a pre-stressed structure, in which we create the tension of the reinforcement by the work that self-stressing concrete performs against restraint at the expansion stage. Resultant pre-stressing force transfers from tendons to expanding concrete by the bond or anchorage and depends on the degree of restraint. The cases considered are those when misalignments are not produced at the respective contact surface between expansive concrete and reinforcing bars.

(2) Independently from the type of restraint (steel bars or FRP bars) transferring of the chemical pre-stressing force to self-stressing concrete is realized like for traditional pre-stressed structure. At all stages of the self-stressing expansive strains are linearly distributed in the direction of the cross-sectional height. Considering, that self-stresses distribution is related to the restrained strain distribution, I can not imagine why such local stress distribution was adopted by Boxing Wang as a basic assumption in the "*theory of self-stressing distribution model*" [11], and repeated in a more controversial form as an assumption to " *calculation model of cracking load and deflection of textile reinforced self-stressing concrete*" [10].

(3) Self-stressing is related to the elastic part of deformations only. All rules applied to the design of the pre-stressed structures (for checking of the serviceability limit states) are valid for self-stressed structures reinforced with FRP. In such a case, why do we have to apply the finite difference method for the calculation of cracking load and deflection of TRSSC beams? According to the modern crack resistance theory cracking load depends mainly on the ultimate tensile strain of concrete (no tensile strength). Based on the obtained test results authors [10] conclude that *" the comparison of calculated and test values indicates an error of less than 30%, which is consistent with each other, thus verifying the applicability of calculation method*". It is a very optimistic statement!

The following conclusion is optimistic too: *"self-stress can significantly improve the cracking resistance of TRSSC beams. Although the tensile strength of the matrix of TRSSC is 26.07% lower than that TCR, the cracking loads of the TRSSC beam are increased by 33.39% and 30.29 %".* In first, in the experiment self-stressing cement grade 4.0 (self-stress in standard condition is equal to $f_{ct,m}$ = 4.0 MPa) was used. Matrix specimens were cured before tensile testing in non-restrained conditions. In such conditions unbalanced expansion of the active self-stressing cement matrix, leads to self-damaging of the own material structure and decreasing of the tensile (and compressive) strength. Testing these specimens after curing in the restrained conditions (as if it was in tested prisms) will get higher values of the tensile strength. Now it is difficult to assess what is the value of tensile strength we have to account for when we want to verify the proposed crack resistance model. Moreover, experimental results presented in [10,11] are very unclear and non-representative. For instance, the same mix proportions for matrix type NC and SSC; dimensions of the reinforced TRSSC beams (prisms 100x100x400mm for testing so sensitive parameter as crack resistance); measurement (with unknown error) of the longitudinal deformations with the usage of the laser rangefinder only at the level of the layer of textile; curing under standard conditions, etc.)

At the finish of this paper, I want to point out there one of my impressions and write one curt remark. I always considered the CBM journal as a very serious and high-level edition and publication in this journal was a great honor…

References

1. Peligot, E.-M. Bulletin Societe d'Encougrament pour L'Industrie Nationale / E.-M. Peligot, C. A. Gagout. – Paris : Incentive Company for the Development of National Industry, 1890. – Vol. 5. – P. 682.
2. Michaelis, W. Tonindustrie-Zetung (Goslar). – 1892. – Vol. 16. – P. 105.
3. Lossier, H. Expanding Cements and Their Application- Self-stressed concrete / H. Lossier, A. Gagout // Le Genie Civil (Paris). – 1944. – Vol. 121. №8, April 15. – P. 61–65.
4. Mikhailov, V. V. Stressing Cement and the Mechanism of self-stressing concrete regulation / V. V. Mikhailov // Proceeding of IV Symposium Chemistry of Cement. – 1960. – Washington. – P. 134.
5. Mikhailov, V. Expansive and self-stressing cement and self-stressed reinforced structures / V. Mikhailov, S. Litver. – Moscow : Stroyizdat, 1974. (in Russian)
6. Mather, B. Expansive cement / B. Mather // Miscellaneous paper C-7-21, National Technical Information Service. – 1970.
7. Klein, A. Stadies of Calcium Sulfoaluminate Admixtures for Expansive Cement / A. Klein, A. Troxell // ASTM. – 1958. – Vol. 58. – P. 968–1008.
8. Metha, P. K. Formation of Ettringite by Hydration of System Containing an Anhyrous Calcium Sulfoaluminate / P. K. Metha, A. Klein // Journal ACI. – 1965. – P. 435–436.
9. Guttman, P. V. Expansive cement in USA / P. V. Guttman // ASCE. – 1967. – Vol. 37. № 11. – P. 135.
10. Calculation method of cracking load and deflection of textile reinforced self-stressing concrete / B. Wang [et al.] // Construction and Building Materials. – 2021. – № 304. – 124622. – DOI: 10.1016/j.conbuildmat.2021.124622.
11. Wang, B. Distributed models of self-stress value in textile reinforced self-stressing concrete / B. Wang, J. Zhao, Q. Wang // Construction and Building Materials. – 2016. – № 126. – P. 286–296. – DOI: 10.1016/j.conduildmat.2016.06.149.
12. Man, T. Expansion behaviour of self-stressing concrete confined by glass-fiber composite meshes / T. Man, B. Wang, H. Jin, X. Zhang // Construction and Building Materials. – 2016. – № 128. – P. 38–46. – DOI: 10.1016/j.conbuildmat.2016.10.022.
13. He, H. Performance of steel fiber reinforced self-stressing concrete / H. He, B. Wang, J. Lin // Key Engineering Materials. – 2009. – № 400–402. – P. 427–432. – DOI: 10.4028/www.scientific.net/-KEM.400-402.427.
14. Tsuji, Y. Methods of estimating chemical prestress and expansion distribution in expansive concrete subjected to uniaxial restraint / Y. Tsuji // Concrete Library of JSCE. – 1984. – № 3. – P. 131–143.
15. Tur, V. Self-stressed concrete members reinforced with FRP bars / V. Tur, M. F. Herrador, V. Semianiuk // Proceeding of the ***fib*** Symposium. – 2017. – P. 431–438.
16. Semianiuk, V. Crack resistance of self-stressed members reinforced with FRP bars / V. Semianiuk, V. Tur // Solid state phenomena. – 2018. – № 272. – P. 244–249. – DOI: 10.4028/www.scientific.net/-ssp.272.244.
17. Early age strain and self-stresses of expansive concrete members under uniaxial restraint conditions / V. Semianiuk [et al.] // Construction and building materials. – 2017. – № 131. – P. 39–49.
18. Scheerer, S. Textile reinforced concrete – from the idea to a high performance material / S. Scheerer, F. Schladitz, M. Gurbach // 11th International symposium on ferrocement and textile reinforced concrete, 3rd ICTRC. – 2015. – P. 15–33.
19. Mather, B. Expansive cement / B. Mather // Miscellaneous paper C-7-21, National Technical Information Service. – 1970.
20. Wang, V. Prediction of expansion behaviour of self-stressing concrete by artificial neural networks and fuzzy inference systems / V. Wang, T. Han, H. Jin // Construction and Building Materials. – 2015. – № 84. – P. 184–191.
21. TCP 45-5.03-158-2009. Concrete and reinforced concrete structures from self-stressing concrete: design rules. – Minsk, 2010. (in Russian)
22. Ishikava, Y. Initial stress analysis of expansive material under restrictions based on chemical conservation law / Y. Ishikava, K. Shibata, T. Tanabe // Creep, shrinkage and durability mechanics of concrete and concrete structures. – 2009. – P. 437–443.
23. Early age deformation and resultant induced stress in expansive high strength concrete / H. Ito [et al.] // Journal of Advanced Concrete Technology. – 2004. – № 2 (2). – P. 155–174.
24. Zdanowicz, K. Chemical prestress on concrete with carbon textile reinforcement: Theoretical and analytical approaches / K. Zdanowicz, S. Marx // Proceedings of the ***fib*** Symposium. – 2019. – P. 259–265.
25. STB 2101-2010. Self-stressing concretes: specifications. – Minsk, 2011. (in Russian)
26. He, H. Research of long-term expansive deformation of stress fiber reinforcement self-stressing concrete / H. He, J. Qin, C. Huang // Journal of building materials. – 2009. – № 12 (5). – P. 595–598.
27. Varabei, A. Experimental studies of the resistance shear of self-stressed concrete beams under different loading conditions / A. Varabei, V. Tur // Vestnik PSU, Series F. – 2021. (in Russian)
28. Guide for self-stressed concrete structures design SN-511. – P. 32. (in Russian).

Accepted 19.11.2021

UDC 624.012

ROBUSTNESS ASSESSMENT OF PRECAST REINFORCED CONCRETE STRUCTURAL SYSTEMS IN AN ACCIDENTAL DESIGN SITUATION

V. V. Tur[1], A. V. Tur[2], A. A. Lizahub[3]

[1] Doctor of Technical Sciences, Professor, Head the Department of Concrete Technology and Building Materials, Brest State Technical University, Brest, Belarus, e-mail: profturvic@gmail.com
[2] PhD in Engineering, Associate Professor, Department of Building Structures, Brest State Technical University, Brest, Belarus, e-mail: aturphd@gmail.com
[3] Master of Engineering Science, Postgraduate of Department of Building Structures, Brest State Technical University, Brest, Belarus, e-mail: p_332_14lizogub@mail.ru

Abstract

The article presents the simplified implementation of the method of alternative load paths based on the energy balance approach. This method should be used to checking the global resistance of a damaged structural system after the occurrence of an accidental event. It is necessary to provide (reserve) enough ties with the required continuity and ductility in the original prefabricated structural system to ensure the integrity of the damaged system. We consider the system of ties as the "second line of defense" of the structural system after the exhaustion of the flexural resistance of its elements. The continuity and ductility of the tie elements provide a resistance of the damaged structural system under an accidental combination of actions by mobilizing alternative load paths after the support or key element has been removed. Ductility is the ability of the tie to obtain significant plastic bond elongation before rupture. The ductility is important properties of the ties for redistributing internal forces and getting large deflections. It is necessary for the realization of the chain (membrane) effect, as well as a measure that provides energy absorption (damping) during the dynamic application of an accidental action after the vertical support losing.

The article presents analytical solutions and the working example for the design of horizontal ties in precast hollow-core slabs floor, which are obtained based on the energy approach.

Keywords: robustness, dynamic resistance, ties, energy balance method, membrane effect.

ОЦЕНКА ЖИВУЧЕСТИ СБОРНЫХ ЖЕЛЕЗОБЕТОННЫХ КОНСТРУКТИВНЫХ СИСТЕМ В ОСОБОЙ РАСЧЕТНОЙ СИТУАЦИИ

В. В. Тур, А. В. Тур, А. А. Лизогуб

Реферат

В статье представлена упрощенная реализация метода альтернативных траекторий нагрузок на основе энергетического подхода. Этот метод следует использовать для проверки глобального сопротивления поврежденной конструктивной системы после реализации особого события. Для обеспечения целостности поврежденной системы в исходной сборной конструктивной системе необходимо предусматривать (резервировать) достаточное количество связей, обладающих требуемой степенью неразрывности и пластической деформативности. Система связей рассматривается как «вторая линия защиты» конструктивной системы после исчерпания ее элементами сопротивления изгибу. Неразрывность и пластичность связевых элементов обеспечивают сопротивление поврежденной конструктивной системы при особой комбинации воздействий за счет мобилизации альтернативных путей нагрузки после удаления опоры или ключевого элемента. Пластичность подразумевает собой способность связи достигать значительного пластического удлинения перед разрывом и является важным свойством связей для перераспределения внутренних сил и развития больших прогибов. Что в свою очередь необходимо для реализации цепного (мембранного) эффекта, который обеспечивает поглощение (демпфирование) энергии при динамическом приложении особого воздействия после удаления вертикальной опоры.

В статье представлены аналитические решения и пример для расчета горизонтальных связей в перекрытии из сборных пустотных плит, полученные на основе энергетического подхода.

Ключевые слова: живучесть, динамическое сопротивление, связи, метод энергетического баланса, мембранный эффект.

1 Introduction

Resonant building disasters over the last century [1], [2] have shown that checking the robustness of damaged systems in accidental design situations should be considered as one of the most important stages of the design and detailing of structural elements of the building. Structural system should fulfil the requirements regarding robustness at the stage of conceptual design, considering the use of various strategies for protection against progressive collapse.

We should note that in the scientific and technical literature, definitions of the term "*robustness*" are widely presented [1]–[6]. For example, ***fib*** Bulletin 43 [7] guidelines define *structural robustness as the insensitivity of a structural system to local failure*. In this context, insensitivity is understood as the state of a modified structural system, when damage to individual elements (so-called key elements respect to the system as a whole) causes only insignificant changes in its structural behaviour (its response). The ability of the system to redistribute additional action effects that appear after damaging the structure under the accidental actions achieves this. In this case, we expect to observe a ductile (not brittle) behaviour for structural components without global collapse mode for the structural system.

In the current standards [8]–[13], the requirement for robustness checking is implicit where an accidental situation causes by events such as fires, explosions, impacts of vehicles in parts of the building, the consequences of human errors made at various stages of the structure's lifetime.

It should be noted that almost all known definitions of the term "robustness" [2] are based mainly on the phenomenon of disproportionate collapse, and only a few, for example, [5] consider robustness as an aspect of the safety of a structural system. According to [13] *"robustness is a specific aspect of structural safety that refers to the ability of system subject to accidental of exceptional loadings (such as fire, explosions, impact or consequences of human error) to sustain local damage to some structural components without experiencing a disproportionate degree of overall distress or collapse"*.

The draft new *fib* MC2020 develops provisions related to the assessment of the robustness of structural systems, which are based on the risk assessment format as presented in ISO 2394:2015 [14]. According to *fib* MC2020 structural robustness, checks should include the following basic steps: (1) identification of the intended hazard (*H*) or the list of hazards to which the structural system is likely to be exposed during

a lifetime. At the same time, it should be taken into account that we may not identify some hazards at the designing stage (for example, terrorist and/or criminal attacks); (2) determination of the local resistance of an individual key element (*D*); (3) determination of subsequent indirect damage to the system (*S*) following direct local failure, also described as progressive collapse; (4) quantifying the values of direct C_{dir} and indirect C_{ind} consequences, including economic, social, environmental losses, as well as the cost of loss of human lives (human victims) in monetary terms according to ISO 2394:2015. Direct costs (damage) are usually localized because of damage to individual structural components, while indirect losses are associated with the loss of system functionality because of the implementation of direct losses. The total risk R_{tot} associated with a system failure in an accidental design situation is calculated according to ISO 2394:2015.

The main strategies for protecting structural systems from progressive collapse and requirements for assessing the robustness of reinforced concrete structural systems are detailed in [1], [10], [12], [15]–[18]. In this article, we will consider only the alternative load path strategy (ALP) in more detail.

The combination of horizontal (internal and perimetric) and vertical ties placed in floor elements, columns and walls ensures the integrity of the structural system. In an accidental design situation, the system of ties is considered as the "*second line of defence*" of the structural system after the exhaustion of the flexural resistance of its elements.

When the internal support is removed in the floor elements, the arched effect, bending (beam) and membrane (chain) effects can be realized in succession (depending on the vertical displacement development for the different boundary conditions). If the slab deflection exceeds the critical value and the ties collapse or lose anchorage in adjacent spans, this will indicate that the limit state has been exceeded.

Compared to monolithic reinforced concrete structural systems, precast RC- buildings are more sensitive to the effects of accidental actions. This is due to the presence of different types of butt joints that ensure the integrity of the structural system and the continuity of alternative load paths. At the same time, prefabricated systems distinguish between joints working in tension, compression, bending, torsion, and shear. When designing precast buildings, all requirements are taken into account, both strategies for protection against progressive collapse, and checks of the robustness of the structural system.

In traditional prefabricated reinforced concrete systems, friction forces on the contact of elements, restraining deformations on supports (arch effect) and welded joints of embedded parts slightly increase the resistance of the system under the action of vertical (gravity) loads. However, this is not enough to ensure sufficient resistance of the structural system in accidental design situations. In this way, in the original precast RC-structural system, it is necessary to reserve enough ties that have the required continuity and ductility to ensure the integrity of the damaged system. The continuity of the tie elements provides resistance to an accidental combination of actions by mobilizing alternative load paths after the support have been removed. Ductility is the ability to obtain significant plastic bond elongation before rupture. Such property is important for redistributing forces and obtaining large deflections necessary for the realization of the chain (membrane) effect, as well as a measure that provides energy absorption (damping) during the dynamic application of an accidental action after the vertical support losing.

In structural systems made of prefabricated reinforced concrete elements, all key elements, which failure can lead to the disproportionate collapse of the complete system, should be identified at the stage of conceptual design. Therefore, at the first stage, it is recommended to analyse the local resistance of key elements, as it is performed, for example, in case of the panel buildings designing.

In a two-stage design, it performed a structural system robustness check using non-linear static (NLS) or dynamic (NLD) models that consider the spatial work (3D) of the structural system. Adequate modelling of ties is important when using computer software and it should be based on fairly simple and reasonable relationships. ("*Make everything as simple as possible, but not simpler*" – Albert Einstein).

The article presents simplified analytical solutions for the design of horizontal ties in precast hollow-core slabs floor, which are obtained on the basis of the provisions of the energy balance approach [16]–[19]. Using the example of a real prefabricated floor, we compared the calculation results of the required parameters of horizontal ties designed according to the proposed method and calculation models included in the structural codes of various countries [8]–[13], [20]. It has been established that the ductility of ties is one of the basic parameters that should be controlled when calculating ties.

2 Analytical models for horizontal ties resistance

2.1 Membrane (chain) effects in a damaged structural system

As shown above, redundancy of alternative load paths is considered as the main strategy for protecting the structural system from progressive collapse. Alternative load paths in a damaged structural system are realized through "chain" (or "membrane") effects for floor slabs, cantilever and beam effects for precast walls, vertical suspension of walls and columns, diaphragm effect in the floor plane. When implemented chain (membrane) of the mechanism in the damaged structural system, all gravitational loading perceived due to reactions in the tensioned horizontal ties.

As follows from [2], until now there is no consensus on the magnitude of the vertical deflection, after exceeding which chain effects are accounted in the structural system resistance. It is generally accepted that this is a state when compressive axial forces become tensile, or a state in which the tie elements begin to actively perceive tensile forces.

In RC frames, the beam-end-moment effect is initially implemented. Flexural plastic hinges are formed in the near support sections. After the exhaustion of their bending resistance at large deflections, chain (membrane) resistance mechanisms come into operation.

In accordance with the requirements of the standards [8], [10]–[13], [20] calculation of chain (membrane) forces in a deformed structural system are performed, as a rule, separately, without taking into account its bending behaviour during the formation of plastic hinges.

Chain (membrane) effects should be considered as the "second line of defence" of the structural system against progressive collapse, if the damaged structural system is capable of mobilizing alternative loading paths.

2.2 Basic assumptions of simplified analytical models

For damaged structural systems, the resistance will depend on the dynamic effects during the transition to a deformed shape under an accidental action combination, as well as the nonlinear behaviour of the connections. In the design, we should consider these effects in the calculation model. Bulletin 43 [7] proposed a simplified approach for such an analysis. The basic provisions of a simplified model for calculating modified systems with alternative load paths based on the application of the energy approach were developed in [16]–[19]. We apply the considered model for simplified analysis of the damaged load-bearing structural systems for which the global resistance depends on the resistance of the horizontal ties loaded by tension. However, the basic principles adopted in described model are valid also to the analysis of another type of collapse mechanism where the plastic displacements are localized in connections. Considering the collapse mechanisms of the structural system, authors carried the development of analytical models of the resistance of horizontal tensile ties based on the following assumptions:

1) we assume the key element to be removed from the structural system suddenly after the accidental action applied;
2) we assume that gravity forces only load the damaged system with the removed element. The accidental combination includes the characteristic value of dead load and quasi-permanent value of the imposed load. Basic rules for accidental load combinations when checking damaged structural systems are discussed in detail in [21], [22];
3) prefabricated elements under displacement of the system are assumed to be perfectly rigid bodies connected by deformable ties;
4) the global resistance of the damaged structure depends only on the resistance of some critical ties. During development of the deflection of the damaged structural system, maximum forces arise in the ties;
5) at the stage when the support has suddenly been removed these connections providing alternative load paths are assumed to be unstrained.

The gravity forces on the system are modelled by the resultant $Q = mg$ applied at the centre of gravity of the prefabricated elements. The actual position of the damaged system is determined by the generalized displacement a_q at the centre of gravity and a rotation θ (here,

doi.org/10.36773/1818-1112-2021-126-3-31-39

in the general case, a_{qz} is the vertical component of displacement). It is possible to establish simple geometric relationships between the vertical deflection of the system a_{qz} and the linear elongation w_i of the ductile joints by assumptions (2) and (4). The load-displacement relationship "*N*-w_i" should describe the nonlinear behaviour for each tie connection *i* (see section 2.2).

2.3. Modelling the dynamic resistance of a structural system based on energy balance: design equations

According to assumption 5, immediately after support is removed, the vertical displacements of the structural system are practically not limited because the ductile joints are unloaded. The system when moving down is under acceleration. The resultant tie forces in the damaged system can be taken as the system resistance R, which balances the gravity force acting in its centre of gravity. We can define resistance as static (quasi-static) or dynamic. According to the energy approach [16]–[19], the static resistance varies depending on the value of displacement and can be expressed by the resistance function R_{stat} (a_{qz}) associated with the "*N*-*w*" relationship for ductile ties in the joints of precast elements [7].

In the general case, the energy balance equation for the vertical displacement a_q and rotation θ of the moving system can be written in the traditional form as:

$$\frac{m}{2}\cdot\left(\frac{da_q}{dt}\right)^2+\frac{I_m}{2}\cdot\left(\frac{d\theta}{dt}\right)=m\cdot g\cdot a_{qz}-\sum_{i=1}^{n}N_i\left(w_i\right)dw_i \quad (1)$$

The first term on the right-hand side of equation (1) describes the potential energy, and the last term is the absorbed strain energy of the tie. The two terms on the left-hand side of this equation describes the kinetic energy because of displacement and rotation, respectively. To get a deformed state of equilibrium, the motion of the system must stop. At the downward position, the kinetic energy of the structural system has the value W_k = 0. In this case, we assume that the maximum vertical deflection $a_{qz,max}$ of the centre of gravity of the damaged part of the structural system and of the tie linear displacements w_i to be reached. The equilibrium equation for the deformed state of a system with single-degree-of-freedom (SDOF) in the first half-period of oscillations can be written in the traditional way (Eq. 2):

$$Q\cdot a_{qz,max}=\sum_{i=1}^{n}\int_{0}^{w_{i,max}}N_i\left(w_i\right)dw_i \quad (2)$$

where $a_{qz,max}$ is the maximum vertical deflection in the point where the driving force Q applied, when the downward motion stop;

$w_{i,max}$ is horizontal displacement of the *i*-th connections.

According to [7], the strain energy capacity of the tie can be obtained from the relationship *"N-w"* as follows:

$$\xi\left(w\right)=\frac{W_{int}\left(w\right)}{N_u\cdot w}=\frac{\int_0^w N\left(w\right)dw}{N_u\cdot w} \quad (3)$$

Therefore, Eq. 2 expressing the energy balance of the deformed system can be written:

$$Q\cdot a_{qz,max}=\sum_{i=1}^{n}\xi_i\left(w_{i,max}\right)\cdot N_{i,u}\cdot w_{i,max} \quad (4)$$

At the stage when the motion stops at the downward position, the system is not necessarily in equilibrium. Therefore, besides Eq. 4, the following inequality should be met:

$$R_{stat}\left(a_{qz,max}\right)\geq m\cdot g \quad (5)$$

If inequality (5) is not met, the accepted value of $a_{qz,max}$ is not correct, since before it is reached, the tie elements are broken. The process of successive destruction of the tie elements with increasing displacement of the modified system is called the zipper-type mode.

The conditions of the equilibrium of forces in the deformed state for the proposed collapse mechanism are checked using Eq. 4 and Eq. 5. The dynamic resistance of the damaged system gets based on the resistance of horizontal ties to the maximum driving force $Q = mg$ after a sudden removal of the column.

As follows from Eq. 4, the dynamic resistance R_{dyn} $(a_{qz,max})$ depends on the maximum vertical deflection $a_{qz,max}$, which is chosen to consider 1) the availability of free space for the downward movement of the system (for example, according to [7] and [11] it is the distance to the underlying floor) and 2) the ductility of the ties..

A quantitative assessment of the uncertainties of the proposed simplified method based on energy balance, in comparison with direct nonlinear dynamic analysis, is considered in [16]–[19], in particular in the most recent of them [23]. In [23], it was noted that instead of the cumbersome nonlinear dynamic analysis (NLD), which contains a number of uncertainties (for example, load history, damping coefficient, etc.), the method based on energy balance (EBM) is a promising approach for determining the maximum dynamic response of the structure. Despite some errors adopted in the estimation, authors [23] show that the method based on the energy balance is quite accurate and effective both 1) in implementing the bending mechanism (the formation of plastic hinges at small deformations) and 2) at the stage of implementation of the membrane (chain) effect in ties that perceive tension (the stage of large displacements). Studies [23] show that the model describing the uncertainty (modelling error) of the energy balance method (EBM) compared to nonlinear dynamic analysis (NLD) well describes by a lognormal distribution with the following statistical parameters LN (0.95; 0.20). (*It should be noted that there is a certain amount of slyness here: the finite element model should be tested based on classical laws, and not vice versa*).

3 Prefabricated building with hollow-core slabs

3.1 Static and dynamic resistance

As shown above (see Eqs. 2-4), the resistance of a damaged system with alternative loading paths almost directly depends on the ductility of the tie connections.

Let us consider a prefabricated floor with hollow-core slabs of equal spans. The internal support of the continuous girder is removed under accidental action. When the support is removed, a longitudinal strip of prefabricated floor together with the ties forms an alternative load-bearing bridging system. In accordance with the formulated assumptions (see Section 2.2), in the ultimate state, prefabricated floor elements are considered as rigid bodies connected by ductile ties.

After the sudden removal of the mid-column of the continuous girder, the prefabricated slabs rotate at the adjacent supports and move in the horizontal direction.

As follows from [2] and [7], the resistance model considers a longitudinal strip of prefabricated floor elements (for example, hollow-core slabs). In this simplified model, the resistance in the transverse direction, arch, and beam effects in the longitudinal direction are neglected and are not taken into account.

We assume that the horizontal ties of the system have the same mechanical characteristics; therefore, for any state of deflection, the three ties have the same tensile force and the same elongations, because the characteristic load-deflection *N-w* relationships for each tie are the same. For each precast floor element, the resultant Q, which is assumed to be placed in the centre of gravity of the element, represents the self-weight and other permanent loads. The deformed state is described by the deflection a_{qz} of the driving force [7] (see Fig. 1).

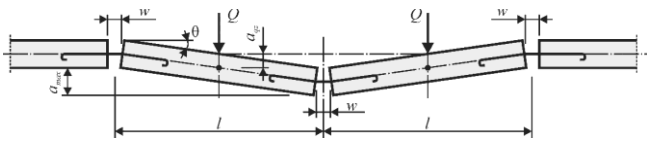

Figure 1 – Deformed scheme of a prefabricated floor for the catenary (chain) forces calculation. Source: own study

From the conditions of static equilibrium of the system in a deformed state, we can write:

$$Q \cdot \frac{l}{2} = N(w) \cdot 2 \cdot a_{qz} \quad (6)$$

For the certain displacements w of the horizontal ties, the vertical deflection a_{qz} can be calculated directly from the deformed geometric scheme (see Fig. 1) as:

$$a_{qz} = \frac{\sqrt{3 \cdot l \cdot w}}{2} \quad (7)$$

where l is the length of the prefabricated elements.

Considering Eq. 7, static resistance expresses as:

$$R_{max}\left(a_{qz,max}\right) = 2 \cdot N(w) \cdot \sqrt{\frac{3 \cdot w}{l}} \quad (8)$$

The maximum value of the static resistance is associated with the maximum displacement $a_{qz,max}$, at which the downward movement of the system must be stopped and is determined by the formula:

$$R_{\max}\left(a_{qz,\max}\right) = 2 \cdot N_u \cdot \sqrt{\frac{3 \cdot w_{\max}}{l}} \quad (9)$$

We can express the energy equilibrium condition for the doubled span system as:

$$2Q \cdot a_{qz,max} = 3\xi(w_{max}) \cdot N_u \cdot w_{max} \quad (10)$$

By introducing Eq. 7 and Eq. 9 into Eq. 10, we obtain dynamic resistance as:

$$R_{dyn}\left(a_{qz,max}\right) = \frac{1}{2}\xi(w_{max}) \cdot R_{max} \quad (11)$$

As stated in [2] even if the tie will have an ideally plastic response, the static response of the system based on the chain (catenary) actions increases almost linearly with increasing displacement, therefore Eq. 11 uses a factor of 1/2.

3.2 Modelling of the tie elements. "*N-w*" relationship for reinforcing bar

The "*N-w*" relationship relates the tensile force N in the tie connection and its end displacement w (local end-slip displacement). To obtain the "*N-w*" diagram, it is necessary to have an adequate local bond-slip relationship "τ-s" (Fig. 2). Based on extensive experimental research [24], including our own, we adopted the dependence in accordance with [8] and [13].

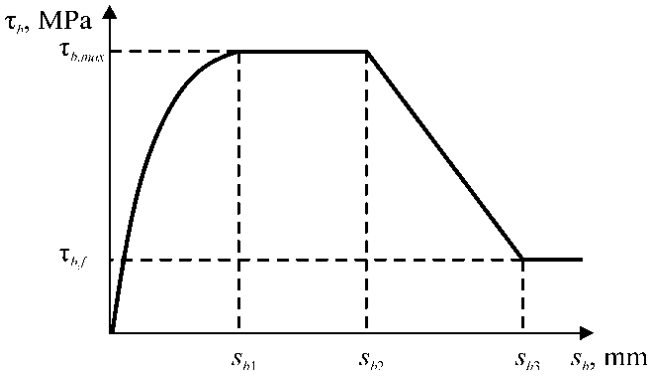

Figure 2 – Analytical bond stress-slip relationship [8], [13]

The advantage of the relationship (Fig. 2) is the applicability for both ribbed and plain bars, as well as an almost complete range of concrete classes, including high-strength ones [8], [13], [24]. The bond-slip behavior for reinforcement bars is modelled according to [13].

According to [24] for the "*N-w*" diagram developing, it is necessary (a) to determine the transmission length l_t and (b) the strain $\varepsilon_s(x)$ and $\varepsilon_{ct}(x)$ distribution along this length.

In the general case, the transmission zone length increases with increasing tensile stress. In this case, for a steel bar embedded in concrete, the following cases are possible: (1) the length of the transmission zone is shorter or equal to the anchorage length; (2) the transmission zone length is greater than the anchorage length. It should be noted that for continuous tie elements passing through the overlap, case (1) is usually valid.

According to [8] and [13] for monotonic loading the reference value of τ_b of the bond stresses between concrete and reinforcing bar can be calculated as follows:

$$\tau_b = \tau_{b,max} \cdot s_b^{0.4} \quad (12)$$

where $\tau_{b,max}$ is the maximum bond-shear stresses between concrete and reinforcing bar in accordance with [8];

s_b is the current value of the relative slip displacement of the reinforcing bar in concrete.

If the anchorage length is greater than the transmission length, to determine the slip displacement we assume to consider the concrete element rigid in relation to the reinforcing bar. Such an assumption gives a slight overestimation of the designed value of the end slip. According to works [7] and [24] the relation (13) is valid if the following requirements are satisfied: 1) the steel bar works in an elastic stage; 2) the net end-slip is less than 1.0 mm:

$$w_{end} = 0.288 \cdot \left(\frac{\varnothing \cdot \sigma_s^2}{\tau_{b,max} \cdot E_s}\right)^{0.714} + \frac{\sigma_s}{E_s} \cdot 2 \cdot \varnothing \quad (13)$$

where $\tau_{b,max} = 2.5\sqrt{f_{cd}}$ for "good" bond conditions; (14a)

$\tau_{b,max} = 1.25\sqrt{f_{cd}}$ for "all other" bond conditions; (14b)

$\varnothing$ is bar diameter, in [mm].

In Eq. 13 the first term on the right-hand side describes the end-slip displacement caused by bond stresses along that part of the transmission length where bond stresses appear, here defined as the "net end-slip" $s_{end,net}$:

$$s_{end,net} = 0.288 \cdot \left(\frac{\varnothing \cdot \sigma_s^2}{\tau_{b,max} \cdot E_s}\right)^{0.714} \quad (15)$$

The last term of Eq. 13 considers the effect of local concrete failure near the free end over a length of approximately $2\varnothing$.

The relationship between stress σ_s and a given end-slip displacement can be rewritten from Eq. 15 as follows:

$$\sigma_s = 2.39 \cdot \sqrt{\frac{\tau_{b,max} \cdot E_s}{\varnothing} \cdot s_{end,net}^{1.4}} \quad (16)$$

where $s_{end,net} = w_{end} - \frac{\sigma_s}{E_s} \cdot 2 \cdot \varnothing$ (17)

The transmission length according to works [7] and [24] is calculated as:

$$l_t = 0.583 \cdot \frac{\varnothing \cdot \sigma_s}{\tau_{b,max} \cdot s_{end,net}^{0.4}} + 2 \cdot \varnothing \quad (18)$$

When yielding in steel reinforcement starts, the end-slip $w_{end,y}$ and the transmission length $l_{t,y}$ can be obtained by inserting $\sigma_s = f_{yd}$ into Eq. 16 and Eq. 18. In the general case, the relationship "N-w_{end}" is nonlinear before steel yielding is reached. However, the pull-out stiffness of the joint $k_a(w_{end})$ is generally defined as a secant at point $N(w_{end})$:

$$k_a\left(w_{end}\right)=\frac{N\left(w_{end}\right)}{w_{end}} \quad (19)$$

As the first approximation, we can get the value of the connection pull-out stiffness based on the stiffness it reached just before yielding:

$$k_a=\frac{N_y}{w_{end,y}} \quad (20)$$

where N_y is the force corresponding to the steel yielding in the tie connection;

$w_{end,y}$ is end-slip corresponding to $\sigma_s = f_{yd}$.

It should be noted that Eq. 19 underestimates the stiffness for loads less than N_y. A more accurate value of the axial stiffness calculates by Eq. 20 for a given loading range or the end-slip.

According to [7], the "plastic zone length" defines as the part of the transmission length where the reinforcement bar has reached yielding. Within the "plastic zone length", the bond-shear stress decreases due to steel yielding to [24].

If the anchorage length of the reinforcement bar in the concrete body is sufficient, the maximum value of the "plastic zone length" along the transmission length can be calculated accounting that the reinforcing steel reaches rupture tensile strength f_u. Along the "plastic zone" length, the tensile stress in reinforcement increases from the value of yield strength f_y to the value of the ultimate tensile strength f_{ud} at the loaded end of the bar.

The ultimate value of the plastic zone length can be calculated according to [24] as:

$$l_{t,pl}=\left(\frac{f_{ud}-f_{yd}}{\tau_{bm,pl}}\right)\cdot\frac{\varnothing}{4} \quad (21)$$

where $\tau_{bm,pl}$ is the average value of bond-shear stress, calculated by Eq. 22.

To calculate the average shear-bond stress for ribbed bars of ductile type (classes B and C according to [8] determined as the "*high ductility*") in [7], [24] it has been proposed the following formula:

$$\tau_{bm,pl}=0.27\tau_{b,max} \quad (22)$$

where $\tau_{b,max}$ is determined by Eq. 14a or Eq. 14b depending on the bond conditions.

The ultimate end-slip of the tie bar can be calculated as follows:

$$w_{end,u}=l_{t,pl}\cdot\varepsilon_{sm,pl}+w_{end,y} \quad (23)$$

where $\varepsilon_{sm,pl}$ is the average strain of the reinforcing bar along the plastic zone length, according to [7] can be estimated as $\varepsilon_{sm,pl} = 0.5\varepsilon_{su}$.

As follows from Eq. 23, with an increase of the plastic zone length $l_{t,pl}$. the ultimate displacement of the tie increases. An idealized three-line the "*N-w*" relationship shown in Fig. 3 can be proposed based on the recommendations of [7].

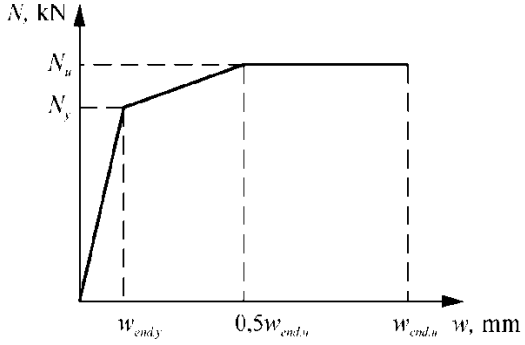

Figure 3 – Idealized "*N-w*" relationship [7], [24]

4 Example of checking the robustness of precast multi-story building

4.1 Structural system description, input data for analysis

As an example, we will consider the structural system of an 18-storey building, the plan of which is shown in Fig. 4. In the considered structural system, monolithic (cast-in-place) columns with a section of 300x300 mm (along axes 2, 6) and prefabricated panel walls (along axes 1, 4, 7) are used as supporting vertical elements. Floors are made of prefabricated hollow-core slabs (1.2x6.0x0.22 m) with modification in the support nodes. The slabs are supported on prefabricated girders with a height of 0.26 m (see Fig. 4). At the stage of preliminary analysis and design, it designed an integrated system of horizontal and vertical ties under the requirements of [8] and [10].

In accordance with the input data, the following characteristic values of actions were adopted for the design: (1) dead load of floor slabs g_{k1} = 3.05 kPa; (2) dead load of the floor finishing g_{k2} = 0.6 kPa; (3) imposed load q_k = 1.5 kPa. An accidental load combination is taken as:

$$p_A = g_{k1} + g_{k2} + \psi_2 \cdot q_k = 3.05 + 0.6 + 0.3 \cdot 1.5 = 4.1 \text{ kPa}.$$

According to the proposed analytical model, we check the robustness of the structural system, taking into account the chain (membrane) effects.

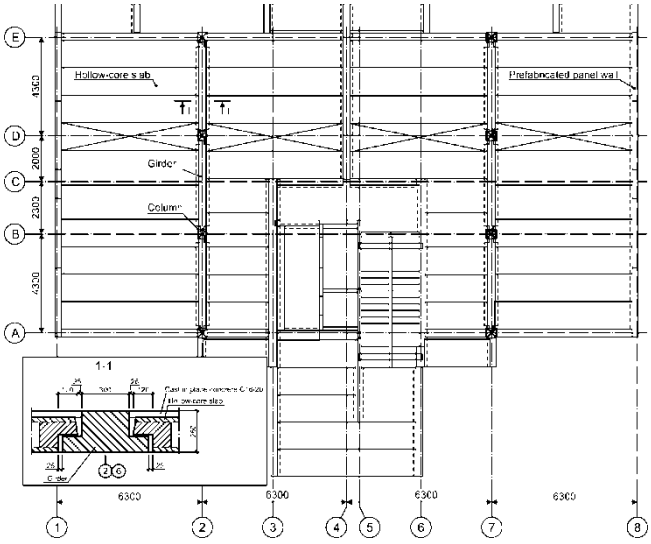

Figure 4 – The first floor of an analyzed 18-storey prefabricated framed building.

Within the framework of the approaches in the current codes and guidelines [8]–[12] the resistance of precast floor slabs in one direction and resistance of prefabricated girders in the other (transverse) direction are considered separately. To determine the required cross-sectional areas of horizontal ties in girders and slabs, the principle of compatibility of vertical displacements at the point of removal of the column is used. In accordance with this principle (the principle of compatibility), the force-deformation connections parameters of the ties in the beams and slabs are determined from the condition of equality of displacements: $a_{max,p} = a_{max,b}$ (here, $a_{max,p}$ and $a_{max,b}$ is the maximum deflection of slabs and girders at the remote element, respectively).

4.2 Modelling of the horizontal tie

We accept plain bars Ø28S240, which have significant plastic deformability, as tie connections. The following reinforcement steel properties are taken: f_{yk} = 240 MPa; $(f_u/f_y)_k$ = 1.3; E_s = 200 GPa; $\varepsilon_{suk} = 1.5 \cdot 10^{-2}$; A_s = 616 mm^2. It is assumed, that the tie bar is anchored in confined concrete of compressive strength class C20/25 (f_{ck} = 20 MPa; f_{cm} = 20 + 8 = 28 MPa), "good" bond conditions. In Tab. 1 presents the values of the main parametric points of the "*N-w*" relationship (Fig. 3) for tie connections, which are calculated based on the proposed end-slip approach.

Table 1 – The "*N-w*" relationship basic points for plain bars Ø28S240

№	Reinforcement	Parameters for "*N-w*" diagram			
		N_y, kN	N_u, kN	$w_{end,y}$, mm	$w_{end,u}$, mm
1	2Ø28S240	295.68	384.38	0.658	28.94
2	4Ø28S240	591.40	768.76	0.658	28.94
Note: general view of the "*N-w*" diagram see Fig. 3.					

4.3 Analytical solution for ties sections area

Let us consider a strip of girders along axis 2 (Fig. 4). We consider that the internal tie connections in the direction of axis 2 are concentrated in prefabricated girders. The girders are loaded with an accidental loads combination as follows: Q = 4.1x6.0x4.0 = 98.4 kN. The girders have a loop connection at the column (2Ø25S500) and have additionally reserved horizontal tie connections (4Ø28S240). The deflection of the middle joint (at the joint with the removed column) should not exceed 2.3 m (free floor space). In Tab. 2 presents the main design parameters and the results of robustness checking.

Table 2 – The robustness checking results for an analysed precast building (by EBM)

Calc. step	Design Parameter	Reference	Value	Units
Girders (l = 4.3 m)				
1	w_{max}	Tab. 1	0.02894	m
2	$a_{max,b} = 2\,a_{qz,max}$	Eq. 6	0.61	m
3	R_{max}	Eq. 9	218.47	kN
4	R_{dyn}	Eq. 11	218.47	kN
5	$R_{dyn} > Q$	Eq. 5	105.8>98.4	
Hollow-core slabs (l = 6.3 m)				
6	$a_{max,s} = a_{max,b}$	see note(1)	0.61	m
7	w_{max}	Eq. 6	0.0206	m
8	R_{max}	Eq. 9	77.94	kN
9	R_{dyn}	Eq. 11	37.80	kN
10	$R_{dyn} > Q$	Eq. 5	37.8>29.52	
Notes: 1) based on the compatibility hypothesis $a_{max,s} = a_{max,b}$.				

Based on the accepted concept of the deflection compatibility, we will show how to determine the required cross-sectional area of the tie connections for a given type of reinforcement (S240).

Based on the results from Table 2, the required ultimate force to break the bar can be calculated from Eq. 9 as:

$$N_u = \frac{R_{max}}{2\cdot\sqrt{\frac{3\cdot w_{max}}{6.0}}} = \frac{60.86}{2\cdot\sqrt{\frac{3\cdot 0.0206}{6.0}}} = 299.8\ kN;$$

Since 2Ø28S240 N_u = 384 kN > 299.8 kN, required reinforcing bar area is equal:

$$A_{s,req} = \frac{N_u}{1.3\cdot f_{yk}} = \frac{299.8\cdot 10^3}{1.3\cdot 240} = 960.9\ mm^2;$$

We accept 2Ø25S240 (A_s = 982 mm^2).

4.4 Comparison of the required tie sections area and dynamic resistance designed by the energy balance method (EBM) and by the current standards

At the first stage, we verified the proposed model based on the results of our own investigations [25] obtained by testing span-to-span hollow-core slab fragments under uniformly distributed load and sudden support removal (see Fig. 5). The authors found that the obtained experimental results have a good agreement with the calculation based on EBM.

Figure 5 – Experimental investigation of the fragment of the hollow-core slabs [25]

Let us compare now the calculation results obtained by the proposed model (EBM) and the models included in the codes and standards of various countries. In Tab. 3 gives the results of calculating the required cross-sectional area of horizontal tie connections according to the current standards.

Analysis of standards [8], [10]–[12] shows that all the design models for calculation of the chain (membrane) force presented in Tab. 3 are based on the equations, which are got from the of static equilibrium of the deflected system at maximum vertical displacement:

$$T_j = (1+\alpha)\cdot\frac{(g_k + \psi_i\cdot q_k)\cdot l_b^2}{2\cdot\delta_s} \qquad (24)$$

where δ_s is the vertical displacement of the joint with the removed element.

Table 3 – Designing of the horizontal ties according to the current standards

№	Reference	Expression	Tie Force, T_j		a_{max}(2)	δ_s	Reinforcement (A_s, mm^2)
			kN	kN/m	m		
1	[10]	$0.8(g_k^{(1)} + q_k)sL$	75	62.5	1.3	$\le \frac{l_s}{4.8}$	1Ø20S240 (314)
2	[10] [11] [12]	$\frac{(g_k+q_k)}{7.5}\cdot\frac{l_r}{5}\cdot F_t$ $F_t = 20 + 4n_s$ or 60 kN/m	62.69	51.91	1.97	$\le \frac{l_s}{3.2}$	1Ø20S240 (314)
3	[12] [8]	$3(1.2\,g_k + 0.5q_k)l_b$ $3(g_k + 0.3q_k)l_b$	116.34	96.57	1.05	$\le \frac{l_s}{6}$	1Ø25S240 (491)
Notes: 1) input data l_b = 6.3 m; g_k = 3.65 kPa; q_k = 1.5 kPa; 2) the value of the maximum deflection $a_{max} = \delta_s = (g_k + q_k)\cdot l_b^2 / (2\cdot T_j)$							

In work [2] it is shown that the design model of [10] and [11] is based on the following formula for determining the vertical displacement:

$$\delta_s = 18.75\cdot(1+\alpha)\cdot\frac{l_b}{T_j} \qquad (25)$$

doi.org/10.36773/1818-1112-2021-126-3-31-39

When determining α from 0 to 1.5 (according to [2]) and F_t from 24 to 60 kN/m (when the number of floors changes from 1 to 10 or more), we obtain the maximum displacement $a_{max} = \delta_s \le l_b / 1.28$(**!**). The design model of [12] was obtained with $a_{max} = \delta_s \le l_b / 6$.

Based on the analysis of the results got from testing of the full-scale slab-to-slab joint tests carried out by PCA [2], it is implied that the catenary action will stop at an ultimate deflection greater than $\delta s = lb / 6.67$ which agrees well with the [12] requirements and other research studies. Furthermore, experimental studies [2], [18], [23] shown that in bar fracture failure mode the system is collapsed at $\delta s \approx lb / 10$. The discrepancy in the value of an ultimate vertical displacement according to the different standards [8], [10], [11] and another research provision (e.g. energy balance method) is remarkable and standard [12] is more relaxed.

Comparison of calculation results obtained using energy balance method and standard methods [8]–[12] (see Tab. 3) shows that the required areas of reinforcing bars used as horizontal ties are significantly different. So, when calculating according to the codes [8]–[11] 1Ø20S240 is required, [12] 1Ø25S240 standards (see Tab. 3), while from the calculation according to the energy balance method using the dependences "*N*-*w*" is 2Ø25S240.

Assuming of fixed values of maximum vertical deflection (from $l_b / 1.28$ to $l_b / 10$) in the codes [8]–[12] leads to rather optimistic and relaxed results when the horizontal ties designed.

Tab. 4 compares the values of the parametric points of the "*N*-*w*" relationship for the tie connections which were calculated according to standards [8], [9] and Tab. 5 presents robustness criteria checking results of the precast floor using the resistances R_{max}, R_{dyn}, assessed based on the energy balance method.

The calculation result presented in Tab. 5 shows that checking criterion $R_{dyn} \ge Q$ for horizontal ties designed according to the standards [8], [10]–[12] is not satisfied. At the same time, the designed tie connection, despite the significant plastic deformability of the reinforcement S240 ($\varepsilon_{suk} = 1.5 \cdot 10^{-2}$), does not provide the *a priori* assumed vertical deflections without the bar rupture. A sudden failure mode of the structural system occurs. The vertical deflection of the damaged floor a_{max} = 0.73 m with horizontal steel ties 1Ø20S240, determined by the energy balance method considering the ultimate (rupture) steel force, turns out to be insufficient for resisting the accidental action effects. Tie forces determined by the standards [8], [10]–[12] correspond to a_{max} from 1.05 m to 1.968 m, which is not realistic for this type of reinforcement (Ø20S240).

Table 4 – The "*N*-*w*" relationship basic parameters for analysed horizontal ties according to [7] and [24]

№	Reinforcement	Parameters of the "*N*-*w*" diagram			
		N_y, kN	N_u, kN	$w_{end,y}$, mm	$w_{end,u}$, mm
1	1Ø25S240	117.84	153.19	0.492	38.49
2	1Ø20S240	75.4	97.97	0.612	30.8
Note: "*N*-*w*" diagram see Fig. 5.					

Table 5 – Design values of resistances R_{max}, R_{dyn} for the damaged system

№	Reference	Required reinforcement	Resistance of ties, kN		Maximum displacement a_{max}, m		Criterion $R_{dyn} \ge Q$
			R_{max}	R_{dyn}	according to the standards(1)	according to the energy balance(2)	
1	[10]	1Ø20S240	23.73	11.03	1.3	0.73	not done
2	[10]–[12]				1.968	0.73	not done
3	[8], [12]	1Ø25S240	41.63	19.44	1.05	0.85	not done
4	according to EBM	2Ø25S240	60.87	29.52	-	0.61	done
Note: 1) max deflection corresponding to the ultimate force in the tie calculated by the current standards; 2) max deflection by the energy balance method (EBM)							

As follows from Eq. 24, obtained from the equilibrium condition of the deflected system, at a constant value of the tie force $T_j = f_{yd} \cdot A_{st}$ (after yielding of steel), the global resistance of the structure linearly depends on the value of the vertical deflection δ_s. After rewriting equation (Eq. 24), considering that $(g_k + \psi_i \cdot q_k) = R_{max}$, we obtain:

$$R_{max} = \frac{2 \cdot f_{yd} \cdot A_{st}}{l_b^2} \cdot \delta_s \tag{26}$$

For the considered case of horizontal tie 1Ø25 S240 at l_b = 6300 mm, A_{st} = 491 mm²:

$$R_{\max} = 0.0059 \cdot \delta_{s,\max} \tag{27}$$

4.5 Reliability assessment of the load-bearing capacity models

The next stage of the comparison of the proposed energy balance method (EBM) and standard methods considered in actual codes was performed based on the reliability assessment of the damaged system with the horizontal ties designed according provisions (requirements) of the codes and EBM. To determine failure probability, the probabilistic model for the dynamic resistance is combined with the probabilistic model for accidental load combination acting on the typical floor. We calculated failure probabilities for the damaged system according to the following limit state function g(***X***):

$$g(\boldsymbol{X}) = \theta_R \cdot R_{dyn} - \theta_E \cdot (G + Q) \tag{28}$$

Probabilistic models for most important basic variables adopted in the probabilistic models for the dynamic resistance and effects of actions, which are used in limit state function (Eq. 28) are listed in Tab. 6.

Table 6 – Probabilistic models of basic variables for reliability analyses

Category of variables	Name of basic variables	Sym. *X*	Dimension	Distrib.	Mean μ_X	St. dev. σ_X
Actions	Permanent	G	kN	N	G_k = 27,59	0,1μ_G = 2,759
	Imposed	Q	kN	GU	0,2Q_k = 2,268	1,1μ_Q = 2,495
Material strengths	Concrete (C20/25)	f_c	MPa	LN	28	4,8
	Reinforcement (S240)	f_y	MPa	LN	300	30
	Reinforcement (S500)	f_y	MPa	LN	560	30
Model uncertainties	Load effect factor	θ_E	–	N	1	0,10
	Resistance factor	θ_R	–	N	1	0,05
Notes: N – normal distribution; LN – lognormal distribution; GU – Gumbel distribution; l_s = 6,3 m; b_s = 1,2 m; g_k = 3,65 kPa; q_k = 1,5 kPa; $G_k = g_k \times l_s \times b_s$ = 27,59 kN; $Q_k = q_k \times l_s \times b_s$ = 11,34 kN						

The probability density distribution functions for the different analyzed design cases are shown in Fig. 6 and Fig. 7. The results of the failure probability calculations are presented in Tab. 7. Probabilistic modelling of the limit state function was performed with usage Monte Carlo simulation method (N=10⁸).

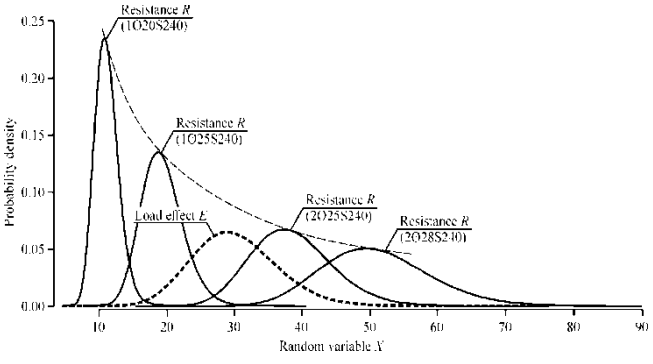

Fig. 6 – Load effect E and resistance R as random variables for ties from reinforcement class S240

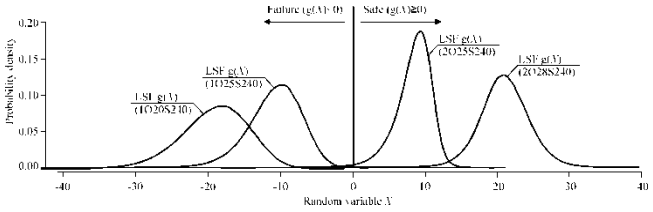

Figure 7 – Limit state function $g(\boldsymbol{X})$ as random variables for ties from reinforcement class S240

Table 7 – Results of probability simulation of performance function of damaged system with hollow-core slabs

№	Reference	Req. reinforcement	Resistance, R		Load Effect, E		Performance function, $g(\boldsymbol{X})$		p_f ($g(\boldsymbol{X})$<0)	β
			mean	sd	mean	sd	mean	sd		
Ties from reinforcement of class S240 (k = 1.3; ε_u = 15%)										
1	[10]-[12]	1Ø20 S240	11.03	1.74	30.14	6.28	-19.12	4.74	0.999999	< -4.8
2	[8], [12]	1Ø25 S240	19.26	3.03			-10.88	3.70	0.999971	-4.02
3	according to EBM	2Ø25 S240	38.53	6.07			8.39	2.53	0.007649	2.42
Force-equivalent ties from reinforcement of class S500 (k = 1.08; ε_u = 5%)										
1	[10]-[12]	1Ø20 S500	7.25	0.64	30.14	6.28	-22.89	5.70	0.999999	< -4.8
2	[8], [12]	1Ø25 S500	12.67	1.12			-17.47	5.28	0.999998	-4.6
3	according to EBM	2Ø25 S500	25.34	2.23			-4.80	4.33	0.877255	-1.16

Notes: sd – standard deviation; $k = f_u / f_y$; β is reliability index according to the Laplace function.

As we can see from results presented in Tab.7, only energy balance method (EBM) in which ductility of the steel ties considered, allow to design reliable structural system in damaged state (failure probability $p_f(g(\boldsymbol{X})<0)$ = 0.007649 in case 2Ø25S240). From analysis of the numerical results (see Tab. 7) one can conclude that the design under actual design according to codes [8], [10]–[12] is non-robust and would collapse in case of the notional column removal, even if the requirements by the codes are fulfilled. The very close conclusions were formulated in [26] based on own numerical investigations ("*It is concluded that in case of the removal of an inner column, the original design according to the Eurocodes is very likely to fail.*"). We relate the main reason of this problem of the non-robust designing with requirements of the actual codes in which neglecting the ductility and rotation capacity of the slab elements in the damaged system.

5 Brief algorithm for simplyfied calculation of the dynamic resistance

As shown earlier, one of the main issues in the tie force assessment is to determine the value of deflection at which the catenary effect is mobilized. For a statically indeterminate structural system, this point can be determined using a simplified approach. As the deflection at which the catenary effect starts, point a_0 of the "*F*-δ" relationship should be taken as shown in Fig. 8. We assumed it as the point where the nonlinear flexural response crosses with a straight-line response of the catenary effect (see Fig. 8).

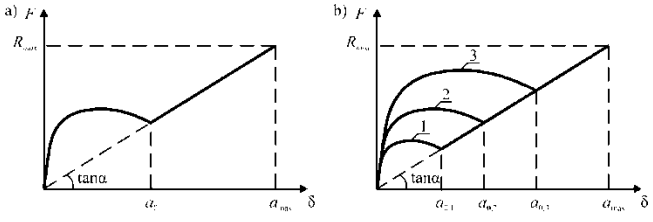

Figure 8 – For the position of point a_0 assessment

It should be borne in mind that the horizontal tie in the structure is either unloaded before being put into operation (when it is designed as an independent link), or has compressive strained (when it is part of the reinforcement). The amount of horizontal tie reinforcement should be designed in such a way that a chain (membrane) effect is provided for the perception of an accidental combination of actions and that a smooth transition from a disengaging flexural plastic hinge to an engaging tensile tie is ensured. Here, the amount and ductility properties of flexural reinforcement should provide a sufficient length of the plastic deformation branch of the "*F*-δ" response to achieve the deflection a_0 (see Fig. 9). We should base the structural design procedure for robustness checks on ensuring a smooth and consistent transition to the mobilization of alternative loading paths.

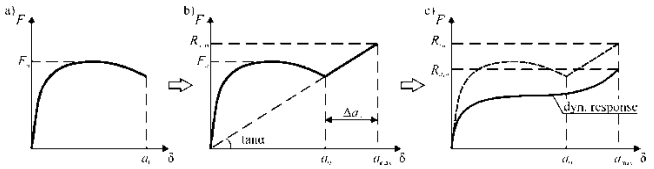

a) the response "*F*-δ" when a flexural plastic hinge realizing;
b) common response "*F*-δ" for the flexural joint and horizontal tie connection; c) the dynamic response of the damaged system

Figure 9 – The calculation steps to the determination of the parameters of a system of the horizontal ties

In this case, the maximum deflection a_{max} and the resistance R_{max} should be determined based on the energy balance equations, as shown earlier. To ensure compatibility (consistency) in the response of flexural hinges and horizontal tensile ties in statically indeterminate systems, the following procedure can be proposed:

1) a nonlinear calculation of the modified structural system is performed and the nonlinear reaction "*F*-δ" is determined taking into account only flexural plastic hinges behavior (Fig. 9a). A linear reaction "*F*-δ" will pass through this point (a_0), which describes, with an acceptable approximation, the operation of the horizontal tie. The slope tangent is the axial stiffness of the horizontal tie;
2) the parameters of the horizontal tie connections necessary to ensure the resistance of the accidental combination are calculated. For a given R_{max}, the deformation parameters of the ties are determined, which will ensure the achievement of the maximum displacement a_{max} (Fig. 9b);
3) to perform complex nonlinear analysis of the damaged structural system with flexural and tension plastic hinges using computer software;
4) to calculate parametric points of a dynamic diagram and determine the global resistance of the damaged structural system (Fig. 9c), accounting of the value of the global safety factor according to [11].

5 Conclusions

Based on the obtained results, we can make the following conclusions:

1. The proposed method for determining membrane (chain) forces based on the provisions of the energy balance method of the damaged structural system (EBM) is a promising method for calculating its maximum dynamic response. This method for determining the total dynamic response of a system can be successfully applied both in the case of simple analytical models and for complex nonlinear finite element models instead of cumbersome nonlinear dynamic analysis (NLD), which contains a number of uncertainties (for example, load history, damping coefficient, modeling error etc.).
2. Comparison of the calculation results according to the current standards [8]–[12] with proposed energy balance method, has shown that the calculation models of the codes can give an unsafe result, for example, underestimating the required cross-sectional area of horizontal ties. This is because it based all dependencies for calculating the tie force on constant values of the ultimate deflection (usually from 1/6 to 1/10 of the span) without checking the ultimate deformability of horizontal ties. As follows from the analysis performed, with the unchanged value of the accidental combination of actions, the calculated

doi.org/10.36773/1818-1112-2021-126-3-31-39

tie force (for which its cross-section is selected) will change in inverse proportion to the deflection. The approach adopted in the standards [8]–[12] can lead to unrealistic results when the adopted reinforcement is horizontal tie cannot ensure the achievement of the *a priori* maximum deflection due to insufficient deformability. The model included in [12], in which the constant deflection of 1/10 span is used to derive the design equations, is most similar to the solutions based on the energy balance. Changes should be made to the current standards [8]–[10] in terms of the application of methods based on the energy balance of the system for the design of horizontal ties.

3. Taking into account a number of assumptions made in the formulation of the basic provisions of the method based on the energy approach, it is necessary to perform a statistical analysis of the uncertainty modeling based on the results of experimental studies, but not the results of dynamic calculations of the finite element model as done in [23].

References

1. Research and practice on progressive collapse and robustness of building structures in the 21st century / J. M. Adam [et al.] // Engineering Structures. –2018. – Vol. 173. – P. 122–149. – DOI: https://doi.org/10.1016/j.engstruct.2018.06.082.
2. Tohidi, Mosleh. Effect of floor-to-floor joint design on the robustness of precast concrete cross wall buildings. A Thesis Submitted to the University of Birmingham for the Degree of Doctor of Philosophy / M. Tohidi ; College of Engineering and Physical Sciences School of Civil Engineering, The University of Birmingham. – August 2015. – 400 p.
3. El-Tawil, S. Computational simulation of gravity-induced progressive collapse of steel-frame buildings: Current trends and future research needs / S. El-Tawil, H. Li, S. Kunnath // Journal of Structural Engineering. – 2014. – Vol. 140, № 8. – A2513001. – DOI: https://doi.org/10.1061/(ASCE)ST.1943-541X.0000897.
4. A review of progressive collapse research and regulations / M. Byfield [et al.] // Proceedings of the Institution of Civil Engineers-Structures and Buildings. – 2014. – Vol. 167, № 8. – P. 447–456.
5. Fang, Z. X. Redundancy of structural systems in the context of structural safety / Z. X. Fang, H. T. Fan // Procedia engineering. – 2011. – Vol. 14. – P. 2172–2178. – DOI: https://doi.org/10.1016/-j.proeng.2011.07.273.
6. Folic, Radomir. Structural Robustness of monolitic and precast RC building / R. Folic // First Scientific-applied Conference with International Participation Reinforced Concrete and Masonry Structures-Theory and Practice, Sofia, October 22, 2015.
7. Structural connections for precast concrete buildings. Guide to good practice. – 2008. – № 43. – 370 p. – DOI: https://doi.org/10.35789/-fib.BULL.0043.
8. SP 5.03.01-2020. Concrete and reinforced concrete structures. – Published on November 16, 2020. – Minsk : RUE "STROYTECHNORM", 2020. – 245 p.
9. SN 2.01.01-2019. Basis of structural design. – Published on September 8, 2020. – Minsk : RUE "STROYTECHNORM", 2020. – 90 p.
10. EN 1991-1-7:2006. Eurocode 1. Impact on building structures. Part 1-7. General influences. Accidental influences. – Published on September 19, 2006. – Brussels : CEN/TC 250 Construction Eurocodes, 2006. – 66 p.
11. BS 8110-1. The structural use of concrete in building – Part 1: Code of practice for design and construction. – Published on March 15, 1997. – London : BSI, 1997. – 172 p.
12. UFC 4-023-03. Design of Buildings to Resist Progressive Collapse, with Change 3. – Published on January 25, 2005. – Washington : National Institute of Building Sciences, 2005. – 176 p.
13. fib Model Code for Concrete Structures 2010 / International Federation for Structural Concrete (fib), Federal Institute of Technology Lausanne – EPFL ; Proofreading and editing: Paul Beverly. – Ulm : CPI Books GmbH – Ebner & Spiegel, 2013. – 434 p.
14. ISO 2394:2015. General principles on reliability of structures. International Standard. – Published on March 1, 2015. – Warszawa : ISO/TC 98/SC 2 Reliability of structures, 2020. – 120 p.
15. Qian, Kai. Research advances in design of structures to resist progressive collapse / K. Qian, B. Li // Journal of Performance of Constructed Facilities. – 2014. – Vol. 29, № 5. – B4014007. – DOI: 10.1061/(ASCE)CF.1943-5509.0000698.
16. Tur, A. Reliability Approaches to Modeling of the Nonlinear Pseudo-Static Response of RC-structural Systems in Accidental Design Situations / A. Tur, V. Tur // Journal of Sustainable Architecture and Civil Engineering. – 2018. – Vol. 22, № 1. – P. 76–87.
17. Herraiz, B. Energy-based method for sudden column failure scenarios: theoretical, numerical and experimental analysis / B. Herraiz, T. Vogel, J. Russell // IABSE Workshop Helsinki 2015: Safety, Robustness and Condition Assessment of Structures. Report International Association for Bridge and Structural Engineering IABSE. – Madrid : IABSE, 2015. – P. 70–77. – DOI: https://doi.org/10.3929/ethz-a-010389549.
18. Progressive collapse of multi-storey buildings due to sudden column loss – Part I: Simplified assessment framework / B. A. Izzuddin [et al.] // Engineering structures. – 2008. – Vol. 30, № 5. – P. 1308–1318. – DOI: https://doi.org/10.1016/j.engstruct.2007.07.011.
19. Progressive collapse of multi-storey buildings due to sudden column loss – Part II: Application / A. G. Vlassis [et al.] // Engineering structures. – 2008. – Vol. 30, № 5. – P. 1424–1438. – DOI: https://doi.org/10.1016/j.engstruct.2007.08.011.
20. ASCE/SEI 7-10. Minimum design loads for buildings and other structures. – Reston : American Society of Civil Engineers, 2013. – DOI: https://doi.org/10.1061/9780784412916.
21. Accidental actions values and combinations for key-elements checking / V. Tur [et al.] // E3S Web of Conferences. – 2020. – Vol. 212. – Les Ulis : EDP Sciences, 2020. – DOI: https://doi.org/10.1051/-e3sconf/202021202019.
22. Permanent and live load model for probabilistic structural fire analysis: a review / R. Van Coile [et al.] // CONFAB 2019, 3rd International Conference on Structural Safety under Fire and Blast Loading, Brunel University, London, 2019, 2nd – 4th September 2019. – London : Brunel University, 2019. – URL: http://hdl.handle.net/1854/LU-8630908.
23. Quantification of model uncertainties of the energy-based method for dynamic column removal scenarios / L. Ding [et al.] // Engineering Structures. – 2021. – Vol. 237. – P. 112057. – DOI: https://doi.org/-10.1016/j.engstruct.2021.112057.
24. fib Bulletin 72. Bond and anchorage of embedded reinforcement: Background to the fib Model Code for Concrete Structures 2010. [Technical report] / International Federation for Structural Concrete (fib). – Lausanne, 2014. – 170 p. – DOI: https://doi.org/10.35789/-fib.BULL.0072.
25. Tur, A. V. Experimental research of the robustness of disk of overlapping from the hollow core slabs with removing the carrier element / A. V. Tur, T. M. Petsold, T. A. Tsimbarevich // Bulletin of the Brest State Technical University. – 2018. – Vol. 1. – P. 104–109.
26. Parametric study and reliability-based evaluation of alternate load path design in reinforced concrete slabs / D. Droogné [et al.] // 39th IABSE Symposium-Engineering the Future, September 21-23, 2017, Vancouver, Canada. – Zurich : IABSE, 2017. – P. 1106–1113.

Accepted 27.10.2021

UDC 624.012.45: 539.415

ESTIMATION OF THE SHEAR RESISTANCE MODELS OF REINFORCED CONCRETE ELEMENTS WITHOUT STIRRUPS ACCORDING TO VARIOUS DESIGN CODES

V. V. Tur[1], A. P. Varabei[2], S. S. Derechennik[3]

[1] Doctor of Technical Sciences, Professor, Head the Department of Concrete Technology and Building Materials, Brest State Technical University, Brest, Belarus, e-mail: profturvic@gmail.com
[2] Master of Engineering Science, Postgraduate of Department of Building Structures, Brest State Technical University, Brest, Belarus, e-mail: mag01414@g.bstu.by
[3] Ph.D in Engineering, Head the Department of Electronic Computing Machines and Systems, Brest State Technical University, Brest, Belarus, e-mail: 1@mail.ru

Abstract

This paper presents the results of assessments shear design models with experimental data, included in the current and developed standards for the design of reinforced concrete structures.

Keywords: reinforced concrete, shear resistance, beams, estimation, design models, order statistics, confidence level, 5%-quantile.

ОЦЕНКА ПРОЧНОСТИ СРЕЗУ МОДЕЛЕЙ ЖЕЛЕЗОБЕТОННЫХ БАЛОЧНЫХ ЭЛЕМЕНТОВ БЕЗ ПОПЕРЕЧНОГО АРМИРОВАНИЯ ПО РАЗЛИЧНЫМ ПРОЕКТНЫМ КОДАМ

В. В. Тур, А. П. Воробей, С. С. Дереченник

Реферат

В данной статье представлены результаты оценок расчетных моделей на сдвиг с экспериментальными данными, включенные в действующие и разрабатываемые стандарты на проектирование железобетонных конструкций.

Ключевые слова: железобетон, сопротивление сдвигу, балки, оценка, расчетные модели, статистика заказов, уровень достоверности, 5% -квантиль.

Introduction

As shown in [10], the application of Eurocodes allows to development of a common understanding of the design problem and provides, on the one hand, the applying of harmonized design strategies for European countries, and on the other hand, opens up broad opportunities for international cooperation.

With the influx of a new generation of engineers in the countries of the united Europe and considering the fact that in the overwhelming majority of countries, national standards do not receive further development (funding for the development of national-level regulatory documents and research carried out for the purpose of normalization has been discontinued), in the design practice of Europe. There is practically no alternative to Eurocodes. But here, the absence of an alternative with broad harmonization creates serious problems. So, according to the current strategy in European standardization, the second generation of Eurocodes (EC - G2) was to be introduced in 2020. The fib Model Code 2010 forms the basis for the new reinforced concrete code. However, despite a rather extensive version of a new fib MC 2010, developed to replace MC 90, the new code for the design of reinforced concrete and pre-stressed structures (prEN 1992-1-1) was not accepted and implemented in 2020. Judging by the report of the chairman of the TG4 / TC250 working group on EC2 A. Muttoni, made in November 2019 at the 26th – Concrete Days (Czech Republic), the introduction of these codes may not take place by 2024.

One of the most open to question due to which a consensus among the scientific community has not been reached is still the problem of shear, including local shear (punching shear). So, according to [11], only based on the analysis of the results of the application of EN1992 (EC2), 1168 remarks and comments related to shear resistance models were collected. At the same time, until now, the thematic group TG4 / TC250 cannot choose for one of the considered variants of the shear resistance model and, accordingly, the local shear (punching shear).

Shear resistance models of elements without stirrups: a brief review

We accepted the following design models of the shear resistance of elements without stirrups for the analysis (see table 1):

1. The shear resistance design model according to the actual EC 2;
2. The shear design model according to ***fib*** Model Code 2010 (for two levels of approximation LoA I and LoA II) based on the Modified Compression Field Theory (MCFT) and Critical Shear Crack Theory (CSCT), that was recommended to introduce in a new version of the EC2. This model largely strives to get closer to understanding the physical phenomenon of the shear;
3. Semi-empirical shear resistance model based on the Critical Shear Crack Theory (CSCT), introduced in the prEN 1992 project.

Not so long ago, at conferences and seminars at various levels, passionate debates took place, in which the following issues were considered: for example, which model of resistance in bending, shear, punching shear is adequate, makes it possible to better describe the physical behavior of a structural element under load, etc.

As a rule, in the process of discussion, the results of verification of the proposed model against the background of experimental data obtained both in their own research and by various researchers are cited as an argument.

Let us briefly explain this using the example of the design models for calculating the shear resistance of elements without stirrups introduced in *fib* MC2010 [5] and prEC 2 [6] (see table 1). The design model equations are such that they consider one basic variable $\sqrt[3]{f_{ck}}$ or $\sqrt{f_{ck}}$, which expresses the characteristic shear strength of concrete as a function of the characteristic compression strength. The transition to the design values performs by dividing the characteristic values of the shear resistance by a partial coefficient $\gamma_c = 1{,}5$. In this situation, it should be noted that, ideally, the ratio $V_{theo} / V_{test} \cong 1$ is in the position corresponding to the 5% quantile of the distribution of the ratios of theoretical and experimental resistance, not the average value. Obviously, in this case, the average value must be a priori higher than 1.

It should be borne in mind that determining the position of the 5% quantile from the ratio of calculated and experimental values is also associated with certain problems. First of all, the estimation accuracy is due to the reasonable choice of the probability distribution function for the obtained empirical sample. As a rule, highly asymmetric distributions are obtained, for which the required quantile must still be calculated accordingly. In these cases, it can be very useful to use the method of order statistics [2], which was used in our analysis.

doi.org/10.36773/1818-1112-2021-126-3-40-47

Table 1 – Shear resistance models of RC- elements without stirrups

Codes	Design equations	Note
EC 2 [1]	$V_{Rd,c} = \left[C_{Rd,c} \cdot k \cdot (100 \cdot \rho_l \cdot f_{ck})^{\frac{1}{3}} + k_1 \cdot \sigma_{cp} \right] \cdot b_w \cdot d,$ but not less $V_{Rd,c} = (\nu_{min} + k_1 \cdot \sigma_{cp}) \cdot b_w \cdot d,$ $\nu_{min} = 0,035 \cdot k^{3/2} \cdot f_{ck}^{1/2}$ if $0,5 \cdot d \le a_v < 2 \cdot d$ the value V_{Ed} is reduced by the coefficient $\beta = \frac{a_v}{2 \cdot d}$ $V_{Ed} \le 0,5 \cdot b_w \cdot d \cdot \nu \cdot f_{cd},$	$C_{Rd,c} = \frac{0,18}{\gamma_c};$ $k = 1 + \sqrt{\frac{200}{d}} \le 2,0;$ $\rho_l = \frac{A_{sl}}{b_w \cdot d} \le 0,02;$ $\nu = 0,6 \cdot \left(1 - \frac{f_{ck}}{250}\right).$
fib Model Code 2010 (LoA I) [5]	$V_{Rd,c} = k_v \frac{\sqrt{f_{ck}}}{\gamma_c} \cdot z \cdot b_w,$ $k_v = \frac{180}{1000 + 1,25 \cdot z},$ if $d \le a_v < 2 \cdot d$ the value V_{Ed} is reduced by the coefficient $\beta = \frac{a_v}{2 \cdot d}$	–
fib Model Code 2010 (LoA II) [5]	$V_{Rd,c} = k_v \frac{\sqrt{f_{ck}}}{\gamma_c} \cdot z \cdot b_w,$ $k_v = \frac{0,40}{1 + 1500 \cdot \varepsilon_x} \cdot \frac{1300}{1000 + k_{dg} \cdot z},$ $\varepsilon_x = \frac{1}{2 \cdot E_s \cdot A_s} \cdot \left(\frac{M_{Ed}}{z} + V_{Ed} + N_{Ed} \left(\frac{1}{2} \mp \frac{\Delta e}{z} \right) \right)$ if $d \le a_v < 2 \cdot d$ the value V_{Ed} is reduced by the coefficient $\beta = \frac{a_v}{2 \cdot d}$	$k_{dg} = \frac{32}{16 + d_g} \ge 0,75;$
prEC 2 [6]	$\tau_{Rd,c} = \frac{V_{Rd,c}}{b_w \cdot d} = \frac{0,6}{\gamma_c} \cdot \left(100 \cdot \rho_l \cdot f_{ck} \cdot \frac{d_{dg}}{d} \right)^{1/3},$ $\tau_{Rd,c} \ge \tau_{Rd,c,min},$ when $\tau_{Rd,c\,min} = \frac{10}{\gamma_c} \cdot \sqrt{\frac{f_{ck}}{f_{yd}} \cdot \frac{d_{dg}}{d}},$ if $d \le a_v < 2 \cdot d$ the value V_{Ed} is reduced by the coefficient $\beta = \frac{a_v}{2 \cdot d}$	if $f_{ck} \le 60 MPa;$ $d_{dg} = 16 + D_{lower} \le 40$ if $f_{ck} > 60 MPa;$ $d_{dg} = 16 + D_{lower} \cdot (60 / f_{ck})^2 \le 40$ $\rho_l = \frac{A_{sl}}{b_w \cdot d};$ if $a_{cs} \le 4d$ $d = a_v = \sqrt{\frac{a_{cs}}{4} \cdot d}$ when $a_{cs} = \lvert M_{Ed} / V_{Ed} \rvert \ge d$

Despite the different methods for obtaining the design equations of the shear resistance models included in the current EC2 and the project prEC2, the latter are quite similar both as recording and in the list of basic variables included in these models. The main difference should be considered that the prEN1992 model attempts to take into account the scale factor (through the ratio d_{dg} / d). At the same time, in prEC2, the value of the coefficient $C_{Rd,c}$ was changed and a different form of notation $\tau_{Rdc,min}$ was proposed.

Some problems associated with estimating the accuracy of the shear resistance models

The shear resistance models included in the actual structural codes are still empirical or semi-empirical. They are based on different types of tests performed under different conditions (in particular, calibrations of empirical coefficients $C_{Rd,c}$).

We should bear in mind that the databases of experimental results used for statistical assessment of the model uncertainties are not always homogeneous and represent the complete sets of input basic variables

necessary for performing calculations by theoretical models. For example, at present, extensive databases have been collected containing the results of shear resistance tests of reinforced concrete beams Instance, at present, extensive databases have been collected containing the results of shear tests of the different reinforced concrete beams. However, most of the recent database comprises the results of tests of rectangular beams with the section depth up to 600 mm, tested by concentrated forces applied in the span (only about 8% of test data are beams tested with a uniformly distributed load). To eliminate bending failure mode, most of the beams have, as a rule, so high values of the longitudinal reinforcement ratio ρ_l that they are unrealistic for practice.

Of course, the methodological approaches taken during testing do not fully simulate the physical behavior of an element during shear (for instance, plane stress-strain state).

Another, and even more serious problem relates to the development of empirical models of shear resistance against a background of sets of test results. Moreover, it should be borne in mind that most of the test results from the analyzed databases were obtained on specimens that are not representative of respect to structural elements used in engineering practice, the behavior of which they should model.

As a typical example, we can present the model for estimation of the shear resistance of deep elements without stirrups, included in the current standards EN1992 [1].

Obviously, the proposed model can indeed be most suitable for checking the ultimate limit state of punching of the solid slabs under concentrated (local) load, which, for practical and economic reasons, do not have shear reinforcement (stirrups).

At the same time, actual structural code requirements prohibit reinforced concrete beams without stirrups for practice. In structural elements subjected to bending moments and shear forces, according to the standards [1, 5-6], we have to set the minimum amount of stirrups, even when the condition $V_{Rd,c} \geq V_{Ed}$ is met.

As noted in [10], the sensitivity of slabs to local defects and damages (for example, caverns, unconsolidated places, etc.) is much lower than that of beams. In addition, tests of beams are almost always performed by concentrated forces applied in the immediate vicinity of the support (as a rule, the shear span a / d is from 2.0 to 6.0). With such a test scheme, the maximum shear force coincides with the maximum moment, and, in fact, in the slabs on the supports, the maximum shear force V_{Ed} acts, which decreases to zero in the section with the maximum bending moment M_{Ed} under a uniformly distributed load.

Database containing test results for beam elements without stirrups

We carried the estimation of the uncertainties of the shear models with the usage of test results from our own experimental database, which included 377 beams without stirrups with a wide range of the investigated basic variables. The experimental database was compiled based on the results of laboratory studies, described in detail in the article [8].

The ranges of variation of the main parameters of the analyzed beam elements are presented in Tables 2 and 3.

All beams included in the database (see tables 2 and 3) have a rectangular cross-section, single-span and simply supported, subjected to one or two concentrated forces applied in the span or uniformly distributed load.

Table 2 – Parameters of beam elements subjected to point loading in span

Autor	Number of samples	b, mm	d, mm	ρ_l, %	f_{cm}, MPa	a/d	V_{exp}, kN
Morrow, Viest (1957)	12	305	363 – 375	1,24 – 3,83	14,7 – 45,7	2,76 – 7,86	88,96 – 177,9
Kim, Park (1994)	16	170 – 300	142 – 915	1,01 – 4,68	53,7	3 – 4,5	39,34 – 332,1
Collins, Kuchma (1999)	21	169 – 300	110 – 925	0,5 – 1,03	36 – 99	2,5 – 3,07	40 – 249
Kani, Huggins, Wiltkopp (1979)	32	155	135 – 1097	0,5 – 2,84	17,7 – 34,5	2,5 – 7	24,5 – 165,1
Johnson, Ramirez (1998)	1	305	610	2,49	55,8	3,1	191,3
Elzanaty, Nilson, Slate (1986)	11	177,8	273	1 – 2,5	20,6 – 79,2	4 – 6	44,81 – 78,53
Mphonde, Frantz (1984)	12	152	298	2,32 – 3,36	22,4 – 101,8	2,5 – 3,6	64,6 – 117,9
Islam, Pam, Kwan (1998)	10	150	205	2,02 – 3,22	26,6 – 83,3	2,9 – 3,94	45,5 – 96,9
Ahmad, Khaloo, Poveda (1986)	14	127	184 – 208	1,77 – 6,64	60,8 – 67	2,7 – 4	44,48 – 75,63
Yoon, Cook, Mitchell (1996)	3	375	655	2,8	36 – 87	3,23	249 – 327
Ahmad, Park, El-Dash (1995)	4	102 – 127	178 – 215,9	1,04 – 2,07	40,3 – 89,1	3 – 3,7	19,79 – 43,39
Bazant, Kazemi (1991)	18	38,1	40,6 – 165,1	1,65	46,8	3	2,95 – 10,14
Thorentfeldt, Drangsholt (1990)	16	150 – 300	207 – 442	1,82 – 3,23	54 – 97,7	3 – 4	56,16 – 280,7
Cladera (2002)	4	200	359	2,24	49,9 - 87	3,01	99,69 – 117,9
Adebar, Collins (1996)	6	290 – 360	178 – 278	1 – 3,04	46,2 – 58,9	2,88 – 4,49	74,3 – 128
Xie, Ahmad, Yu, Nino, Chung (1994)	2	127	215,9	2,07	37,7 – 98,9	3	36,68 – 45,72
Salandra, Ahmad (1989)	4	101,6	171,4	1,45	52,1 – 69,1	2,59 – 3,63	20,02 – 29,8
Kulkarni, Shah (1998)	3	102	152	1,37	41,9 – 45	3,5 – 5	19,52 – 24,24
Gonzalez-Fonteboa (2002)	4	200	306	2,87 – 2,93	39,65 – 46,77	3,28	83,88 – 100,5
Hou, Chen, Xu (2015)	3	120	146	3,25	48,85	2,06 – 4,11	29,15 – 94,16
Moody, Viest, Elstner, Hognestad (1954)	21	152 – 178	262 – 533	1,62 – 4,25	17,3 – 36,7	1,52 – 3,41	51,2 – 436,1
Mathey, Watstein (1963)	16	203	403	0,75 – 3,05	21,9 – 27	1,51	180 – 313
Kani (1967)	17	154	132 – 1097	2,58 – 2,84	24,8 – 31,5	1 – 2,5	51,4 – 585,6
Papadakis (1996)	8	140	200	0,8 – 1,2	25	1,5 – 2,5	42,6 – 103,8
Leonhardt, Walther (1961-1962)	8	190	274	2,04	30	1 – 5,83	60,3 – 388,3
Van Den Berg (1962)	30	229	359	4,53	19,1 – 50,3	2,76 – 4,88	99,2 – 177,9
Cao	3	300	1845 – 1925	0,36 – 1,52	27 – 34	2,9	224 – 402
Niwa	3	300 – 600	1000 – 2000	0,14 – 0,28	25,4 – 28	2,98	227 – 804
Quach	1	250	3840	0,66	43,2	3,13	342,3
Sherwood	2	300	1400	0,83	39	2,90	242 – 265

Table 3 – Parameters of beams subjected to uniformly distributed loading

Autor	Number of samples	b, mm	d, mm	ρ_l, %	f_{cm}, MPa	L, mm	V_{exp}, kN
Krefeld, Thurston (1966)	51	152,4 – 254	239,8 – 482,6	1,31 – 4,28	11,2 – 37,2	1829 – 4877	48,7 – 636,5
Shioya (1989)	8	158 – 1500	200 – 3000	0,4	21,2 – 28,5	2161 – 32805	36,1 – 1927,5
Brown, Bayrak (2006)	1	203	406	3,07	26,9	2439	336,7
Stanik, Bentz, Collins (2007)	3	113 – 300	230 – 617	0,76 – 1,15	31,3 – 35,8	1007 – 5815	64,1 – 255,5
Smith (1970)	3	150	200	2,01	28 – 36,2	2452 – 3664	50,5 – 59
de Cossio, Seiss (1960)	6	152	252 – 276	1,01 – 1,35	19,2 – 41,2	1674 – 2795	59,9 – 135

doi.org/10.36773/1818-1112-2021-126-3-40-47

Estimation methodology and results of estimation

We carried the estimation of the shear resistance models from Table 1 based on random samples made up of the ratios V_{theo} / V_{test}. Considering the fact that the shear strength depends *mainly* on the variation in the concrete compressive strength $\sqrt{f_{ck}}$, we checked the requirements declared by the researches, according to which the 5% - quantile of the distribution of the ratio V_{theo} / V_{test} should be close to 1. At the same time, at the first stage, a suitable probability distribution function was established for the samples N = 35 of results using the Kolmogorov – Smirnov test, and then for the selected distribution the value of the 5% -quantile of the statistical distribution of the ratio V_{theo} / V_{test} was calculated. Additionally, the 5% quantile of the statistical distribution was calculated using the method of Order statistics detailed in [2, 4]. The method of Order (non-parametric) statistics allows calculating the quantile of a given order without determining the probability density distribution function (*pdf*) and for a required confidence level (γ = 0,5; 0,75; 0,9).

The results of estimations of 5 % quantiles using both the empirical distributions and the method based on Order statistics theory are shown in Table 4.

Table 4 – Calculation results of the 5% -quantile of the distribution of the shear resistance ratio V_{theo} / V_{test} according to various models

Prediction model	The value of the 5% -quantile of the distribution of the V_{theo} / V_{exp} ratio				
	Empirical distribution		Method based on Order statistics for confidence level		
	pdf	Value	γ=0,5	γ=0,75	γ=0,9
Beam elements subjected to uniformly distributed loading at L/d < 10,0					
Model Code 2010 (LoA I)	G	0,146	0,143	0,135	0,122
Model Code 2010 (LoA II)	LN	0,338	0,325	0,307	0,276
prEN 1992-1-1	N	0,353	0,354	0,334	0,301
EN 1992-1-1	N	0,208	0,205	0,194	0,174
Beam elements subjected to uniformly distributed loading at L/d ≥ 10,0					
Model Code 2010 (LoA I)	LN	0,248	0,299	0,283	0,256
Model Code 2010 (LoA II)	G	0,659	0,701	0,673	0,625
prEN 1992-1-1	LN	0,824	0,838	0,834	0,826
EN 1992-1-1	G	0,501	0,563	0,546	0,517
Beam elements subjected to point loading at a/d < 2,0					
Model Code 2010 (LoA I)	G	0,144	0,144	0,142	0,139
Model Code 2010 (LoA II)	G	0,350	0,339	0,334	0,325
prEN 1992-1-1	N	0,375	0,381	0,371	0,353
EN 1992-1-1	N	0,307	0,303	0,299	0,293
Beam elements subjected to point loading at a/d ≥ 2,0					
Model Code 2010 (LoA I)	LN	0,323	0,381	0,313	0,255
Model Code 2010 (LoA II)	N	0,560	0,673	0,650	0,639
prEN 1992-1-1	N	0,628	0,749	0,689	0,622
EN 1992-1-1	LN	0,614	0,711	0,686	0,653
Note: LN – lognormal distribution; N – normal distribution; G – Gumbel distribution.					

As seen from the results shown in Table 4 for various cases of loading, including slender and rigid beams subjected to uniformly distributed loading, practically none of the analyzed models gives the expected value of the ratio V_{theo} / V_{test} 1,0 in the 5 % -quantile, which was declared, for example, in [9]. The closest to unity values of the ratio V_{theo} / V_{test} are given by the prEC2 design model for the slender beams ($L / d \geq 10$) subjected to uniformly distributed loading (0.824 - with an empirical N-distribution and 0.826 with an estimate by the method of order (non-parametric) statistics with confidence level γ = 0,90). If we rely on the obtained results, we can conclude that almost all the analyzed models provide quite significant reserves (in particular, for the beams with shear span to depth ratio $a / d < 2{,}0$ and rigid beams with $L / d < 10$ analyzed models underestimate the shear resistance by up to 7 times!). The following question arises: how it can be explained? Is the result obtained random or are the empirical coefficients in the models specially selected in this way? These questions require additional analysis, considering the previously shown errors associated with the estimation, starting with the formation of reliable samples of experimental data.

However, we can make some preliminary remarks. So, according to prEC2, the shear resistance model has the following formulation:

$$\tau_{Rd,c} = \frac{0,6}{\gamma_c} \cdot \left(100 \cdot \rho_l \cdot f_{ck} \cdot \frac{d_{dg}}{d} \right)^{1/3} \geq \tau_{Rdc,min}, \quad (1)$$

The coefficient (partial factor for concrete) is used to transform from the characteristic value of the shear resistance $\tau_{Rk,c} = f(f_{ck})$ to its design value $\tau_{Rd,c}$ .It should be noted that when equation (1) was derived, the authors of [9] obtained a coefficient equal to 0.87. If we assume that the transition to the design value of shear resistance $\tau_{Rd,c}$ is equivalent to the application of the design value of concrete compressive strength (f_{ck} / γ_c) in the design model (1), then the characteristic value of the shear resistance should correspond to a 5% quantile of the resistance distribution.

The estimation of the reliability of the design shear resistance models was carried out on the basis of samples of experimental data that have the same or very close parameters with variable values f_{cm}. Next, a sample of experimental data with close values f_{cm} is estimated (selected experimental values of shear stress in Figure 1). We applied the method based on the order (non-parametric) statistics for assessing the shear stress value corresponding to the 5% quantile shear resistance distribution with a required confidence level. The experimental values of the shear stress in 5% quantiles are compared with the dependence function $\tau_{Rc,theo} = f(f_{ck})$ of the estimated design model (see Figure 1). We may consider the shear resistance model conditionally accurate with an assigned confidence level if the ratio $\tau_{Rc,theo} / \tau_{Rc,exp,5\%-кв.}$ 1,0. Otherwise, the model is adjusted by changing the value of the coefficient until the model is suitable for the accepted criterion.

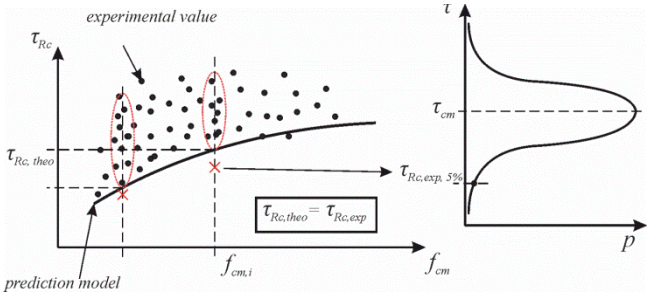

Figure 1 – Estimation of the shear resistance model uncertainty

Some problems of this method are in the difficulty of selecting experimental data with the same or close parameters and variable values f_{cm}. Figures 2-4 show the diagrams of the estimation of the shear resistance models according to the EC2, prEC2 and *fib* Model Code 2010 (LoA II), for beams subjected to point and uniformly distributed loadings.

The results of estimating the reliability of shear resistance models according to the described method based on non-parametric statistics for various types of loading are presented in Tables 5-13.

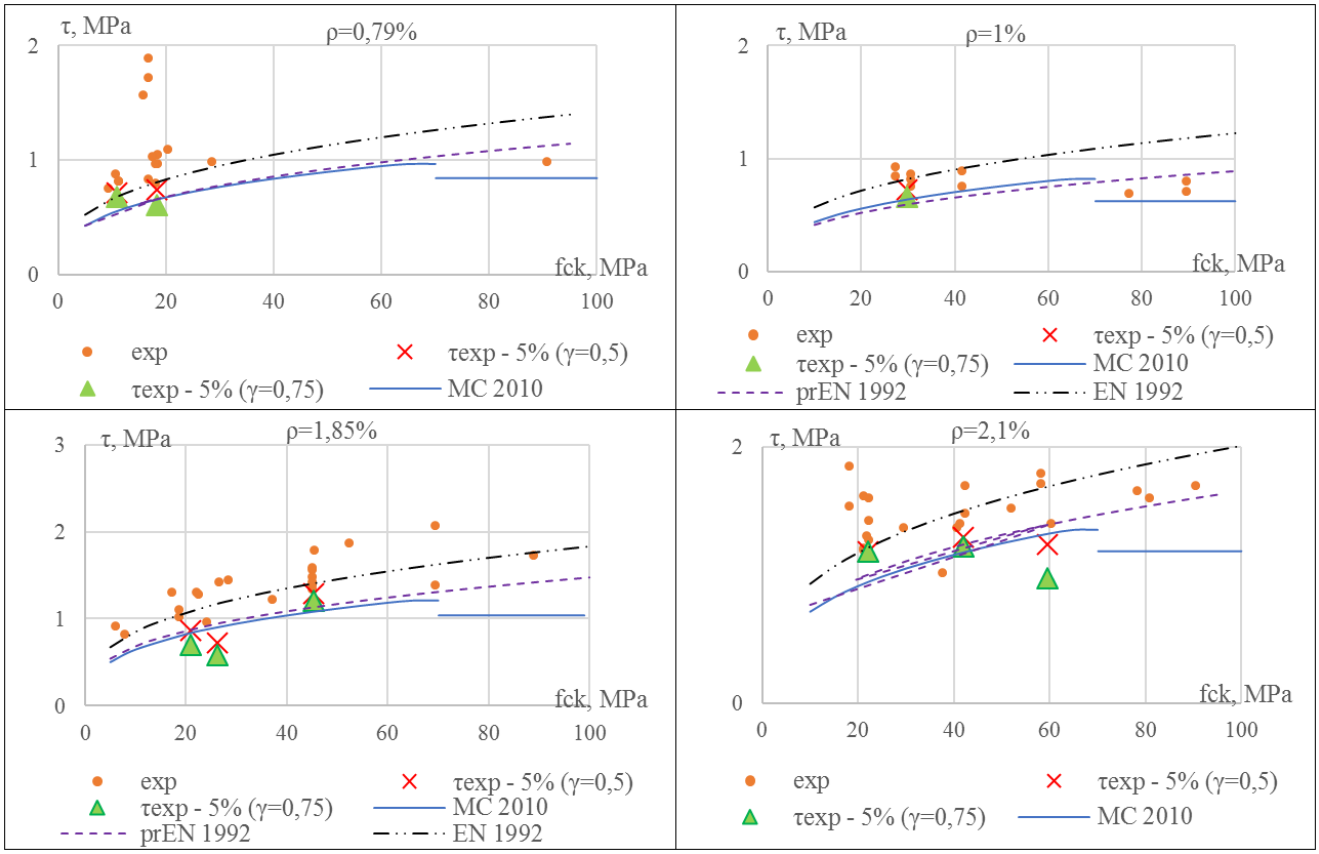

Figure 2 – Estimates of various shear resistance models at $a / d \geq 2{,}0$

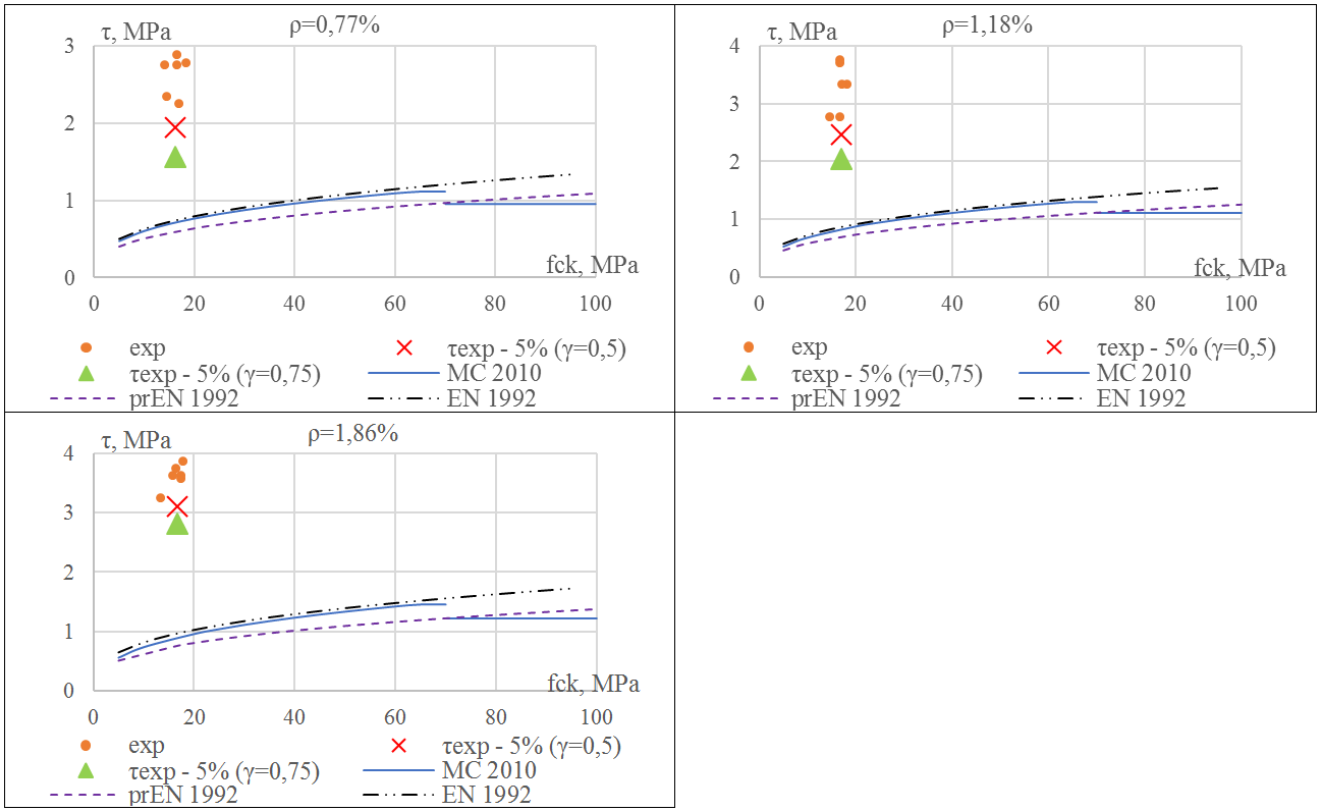

Figure 3 – Estimates of various shear resistance models at $a / d < 2{,}0$

doi.org/10.36773/1818-1112-2021-126-3-40-47

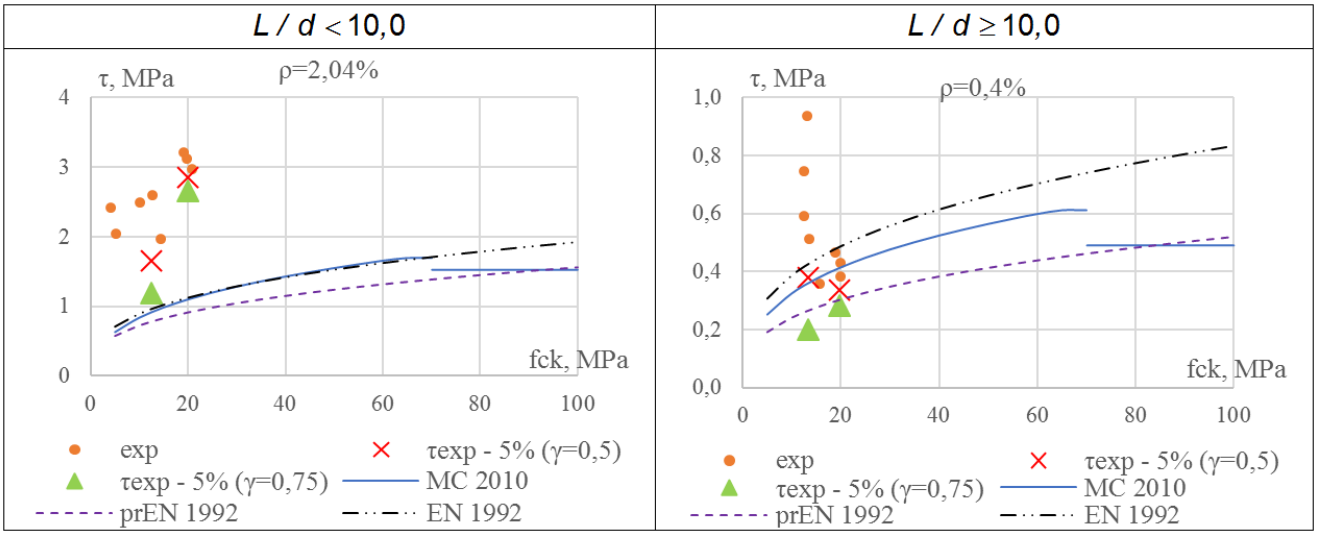

Figure 4 – Estimates of various shear resistance models (uniformly distributed loading)

Table 5 – The results of estimating the reliability of the shear resistance model according to the EC2 ($a / d \geq 2,0$)

Prediction model	Reinforcement ratio ρ_l	f_{ck}, MPa	Confidence level, γ	5% -quantile τ_{test}, MPa	τ_{theo}, MPa	Ratio $\tau_{theo} / \tau_{test}$ for 5% -quatile τ_{test}
EC2	$\rho_l = 0,79\%$	11,1	$\gamma = 0,5$	0,71	0,68	0,96
			$\gamma = 0,75$	0,66		1,04
		18,3	$\gamma = 0,5$	0,73	0,81	1,12
			$\gamma = 0,75$	0,61		1,34
	$\rho_l = 1,0\%$	29,8	$\gamma = 0,5$	0,71	0,59	0,84
			$\gamma = 0,75$	0,65		0,92
	$\rho_l = 1,85\%$	21	$\gamma = 0,5$	0,86	1,09	1,26
			$\gamma = 0,75$	0,67		1,62
		26,7	$\gamma = 0,5$	0,70	1,18	1,69
			$\gamma = 0,75$	0,57		2,09
		45,7	$\gamma = 0,5$	1,27	1,41	1,11
			$\gamma = 0,75$	1,20		1,17
	$\rho_l = 2,1\%$	22,4	$\gamma = 0,5$	1,17	1,22	1,04
			$\gamma = 0,75$	1,16		1,05
		42,2	$\gamma = 0,5$	1,29	1,51	1,17
			$\gamma = 0,75$	1,21		1,24
		59,6	$\gamma = 0,5$	1,23	1,69	1,38
			$\gamma = 0,75$	0,97		1,74

Table 6 – The results of estimating the reliability of the shear resistance model according to the EC2 ($a / d < 2,0$)

Prediction model	Reinforcement ratio ρ_l	f_{ck}, MPa	Confidence level, γ	5% -quantile τ_{test}, MPa	τ_{theo}, MPa	Ratio $\tau_{theo} / \tau_{test}$ for 5% -quatile τ_{test}
EC2	$\rho_l = 0,77\%$	16,5	$\gamma = 0,5$	1,94	0,75	0,38
			$\gamma = 0,75$	1,54		0,48
	$\rho_l = 1,18\%$	17,3	$\gamma = 0,5$	2,43	0,87	0,36
			$\gamma = 0,75$	2,02		0,43
	$\rho_l = 1,86\%$	16,8	$\gamma = 0,5$	3,09	0,97	0,31
			$\gamma = 0,75$	2,81		0,34

Table 7 – The results of estimating the reliability of the shear resistance model according to the EC2 (uniformly distributed loading)

Prediction model	Reinforcement ratio ρ_l	f_{ck}, MPa	Confidence level, γ	5% -quantile τ_{test}, MPa	τ_{theo}, MPa	Ratio $\tau_{theo} / \tau_{test}$ for 5% -quatile τ_{test}
$L / d < 10,0$						
EC2	$\rho_l = 2,04\%$	12,7	$\gamma = 0,5$	1,63	0,97	0,59
			$\gamma = 0,75$	1,19		0,81
		20,3	$\gamma = 0,5$	2,82	1,13	0,40
			$\gamma = 0,75$	2,66		0,43
$L / d \geq 10,0$						
EC2	$\rho_l = 0,4\%$	13,5	$\gamma = 0,5$	0,37	0,43	1,15
			$\gamma = 0,75$	0,20		2,14
		20	$\gamma = 0,5$	0,33	0,49	1,48
			$\gamma = 0,75$	0,27		1,78

Table 8 – The results of estimating the reliability of the shear resistance model presented in the prEC2 ($a / d \geq 2,0$)

Prediction model	Reinforcement ratio ρ_l	f_{ck}, MPa	Confidence level, γ	5% - quantile τ_{test}, MPa	τ_{theo}, MPa	Ratio $\tau_{theo} / \tau_{test}$ for 5% -quatile τ_{test}
prEC2	$\rho_l = 0,79\%$	11,1	$\gamma = 0,5$	0,71	0,56	0,79
			$\gamma = 0,75$	0,66		0,85
		18,3	$\gamma = 0,5$	0,73	0,66	0,90
			$\gamma = 0,75$	0,61		1,08
	$\rho_l = 1,0\%$	29,8	$\gamma = 0,5$	0,71	0,59	0,83
			$\gamma = 0,75$	0,65		0,91
	$\rho_l = 1,85\%$	21	$\gamma = 0,5$	0,86	0,88	1,02
			$\gamma = 0,75$	0,67		1,31
		26,7	$\gamma = 0,5$	0,70	0,95	1,36
			$\gamma = 0,75$	0,57		1,67
		45,7	$\gamma = 0,5$	1,27	1,14	0,90
			$\gamma = 0,75$	1,20		0,95
	$\rho_l = 2,1\%$	22,4	$\gamma = 0,5$	1,17	1,01	0,86
			$\gamma = 0,75$	1,16		0,87
		42,2	$\gamma = 0,5$	1,29	1,24	0,96
			$\gamma = 0,75$	1,21		1,03
		59,6	$\gamma = 0,5$	1,23	1,39	1,13
			$\gamma = 0,75$	0,97		1,43

Table 9 – The results of estimating the reliability of the shear resistance model presented in the prEC2 ($a / d < 2,0$)

Prediction model	Reinforcement ratio ρ_l	f_{ck}, MPa	Confidence level, γ	5% - quantile τ_{test}, MPa	τ_{theo}, MPa	Ratio $\tau_{theo} / \tau_{test}$ for 5% -quatile τ_{test}
prEC2	$\rho_l = 0,77\%$	16,5	$\gamma = 0,5$	1,94	0,60	0,31
			$\gamma = 0,75$	1,54		0,39
	$\rho_l = 1,18\%$	17,3	$\gamma = 0,5$	2,43	0,70	0,29
			$\gamma = 0,75$	2,02		0,35
	$\rho_l = 1,86\%$	16,8	$\gamma = 0,5$	3,09	0,76	0,25
			$\gamma = 0,75$	2,81		0,27

Table 10 – The results of estimating the reliability of the shear resistance model presented in the prEC2 (uniformly distributed loading)

Prediction model	Reinforcement ratio ρ_l	f_{ck}, MPa	Confidence level, γ	5% - quantile τ_{test}, MPa	τ_{theo}, MPa	Ratio $\tau_{theo} / \tau_{test}$ for 5% -quatile τ_{test}
$L / d < 10,0$						
prEC2	$\rho_l = 2,04\%$	12,7	$\gamma = 0,5$	1,63	0,78	0,48
			$\gamma = 0,75$	1,19		0,66
		20,3	$\gamma = 0,5$	2,82	0,92	0,33
			$\gamma = 0,75$	2,66		0,35
$L / d \geq 10,0$						
prEC2	$\rho_l = 0,4\%$	13,5	$\gamma = 0,5$	0,37	0,27	0,73
			$\gamma = 0,75$	0,20		1,35
		20	$\gamma = 0,5$	0,33	0,30	0,91
			$\gamma = 0,75$	0,27		1,11

Table 11 – The results of estimating the reliability of the shear resistance model according to the *fib* Model Code 2010 (LoA II) ($a / d \geq 2,0$)

Prediction model	Reinforcement ratio ρ_l	f_{ck}, MPa	Confidence level, γ	5% - quantile τ_{test}, MPa	τ_{theo}, MPa	Ratio $\tau_{theo} / \tau_{test}$ for 5% -quatile τ_{test}
fib MC 2010 (LoA II)	$\rho_l = 0,79\%$	11,1	$\gamma = 0,5$	0,71	0,56	0,79
			$\gamma = 0,75$	0,66		0,85
		18,3	$\gamma = 0,5$	0,73	0,66	0,90
			$\gamma = 0,75$	0,61		1,08
	$\rho_l = 1,0\%$	29,8	$\gamma = 0,5$	0,71	0,64	0,90
			$\gamma = 0,75$	0,65		0,99
	$\rho_l = 1,85\%$	21	$\gamma = 0,5$	0,86	0,84	0,98
			$\gamma = 0,75$	0,67		1,25
		26,7	$\gamma = 0,5$	0,70	0,91	1,30
			$\gamma = 0,75$	0,57		1,60
		45,7	$\gamma = 0,5$	1,27	1,09	0,86
			$\gamma = 0,75$	1,20		0,91
	$\rho_l = 2,1\%$	22,4	$\gamma = 0,5$	1,17	0,95	0,81
			$\gamma = 0,75$	1,16		0,82
		42,2	$\gamma = 0,5$	1,29	1,18	0,92
			$\gamma = 0,75$	1,21		0,98
		59,6	$\gamma = 0,5$	1,23	1,32	1,07
			$\gamma = 0,75$	0,97		1,36

doi.org/10.36773/1818-1112-2021-126-3-40-47

Table 12 – The results of estimating the reliability of the shear resistance model presented in the *fib* Model Code 2010 (LoA II) ($a / d < 2,0$)

Prediction model	Reinforcement ratio ρ_l	f_{ck}, MPa	Confidence level, γ	5% - quantile τ_{test}, MPa	τ_{theo}, MPa	Ratio $\tau_{theo} / \tau_{test}$ for 5% -quatile τ_{test}
fib MC 2010 (LoA II)	$\rho_l = 0,77\%$	16,5	$\gamma = 0,5$	1,94	0,72	0,37
			$\gamma = 0,75$	1,54		0,47
	$\rho_l = 1,18\%$	17,3	$\gamma = 0,5$	2,43	0,83	0,34
			$\gamma = 0,75$	2,02		0,41
	$\rho_l = 1,86\%$	16,8	$\gamma = 0,5$	3,09	0,89	0,29
			$\gamma = 0,75$	2,81		0,32

Table 13 – The results of estimating the reliability of the shear resistance model according to the *fib* Model Code 2010 (LoA II) (uniformly distributed loading)

Prediction model	Reinforcement ratio ρ_l	f_{ck}, MPa	Confidence level, γ	5% - quantile τ_{test}, MPa	τ_{theo}, MPa	Ratio $\tau_{theo} / \tau_{test}$ for 5% -quatile τ_{test}
$L / d < 10,0$						
fib MC 2010 (LoA II)	$\rho_l = 2,04\%$	12,7	$\gamma = 0,5$	1,63	0,92	0,56
			$\gamma = 0,75$	1,19		0,77
		20,3	$\gamma = 0,5$	2,82	1,11	0,39
			$\gamma = 0,75$	2,66		0,42
$L / d \geq 10,0$						
fib MC 2010 (LoA II)	$\rho_l = 0,4\%$	13,5	$\gamma = 0,5$	0,37	0,36	0,97
			$\gamma = 0,75$	0,20		1,8
		20	$\gamma = 0,5$	0,33	0,42	1,27
			$\gamma = 0,75$	0,27		1,56

Conclusions

Based on the results of evaluating the reliability of the calculated shear resistance models presented in this work, the following conclusions can be drawn:

1. One of the key characteristics affecting the accuracy of estimating the reliability of prediction models is the need for a reasonable choice of the probability distribution function based on the empirical sample obtained. Due to the asymmetric distribution, difficulties arise in calculating the 5% quantile.
2. Since in most prediction models the conversion from the characteristic value of concrete strength at shear $\sqrt{f_{ck}}$ is performed by dividing by a partial coefficient γ_c = 1,5, it would be methodologically correct for the ratio of theoretical and experimental resistance $V_{theo} / V_{test} \cong 1$ to correspond to the 5% quantile of the distribution, and not to the average value.
3. Taking into account the above remarks, a proprietary method for estimating the reliability of shear resistance models was proposed, based on the method of ordinal statistics, which does not require the determination of the probability and density distribution function, and also allows calculating the quantile of the required order for a predetermined security.

The results of estimating the reliability of the models according to the generally accepted and proposed methods show that practically none of the analyzed models gives the expected ratio $V_{theo} / V_{test} \approx 1,0$ in the 5% quantile. The closest to unity values of the ratio V_{theo} / V_{test} are given by the considered design models for flexible beams subjected to uniformly distributed loading ($L / d \geq 10$) and beams with shear span to depth ratio $a / d \geq 2,0$, subjected to point loading. For rigid beams ($a / d < 2,0$ and $L / d < 10$), all the models under study provide a fairly significant margin. Based on the results obtained, the question arises about the applicability of these models to the required level of reliability.

References

1. European Committee for Standardization. Eurocode 2: Design of Concrete Structures, Part 1-1: General rules and rules for buildings. – 2018. – 293 p.
2. Derechennik, S. S. A new approach to assessing the IN-SITU characteristic strength of concrete in existing reinforced concrete structures with a limited number of field test results / S. S. Derechennik, V. V. Tur // Bulletin of the Brest State Technical University. Series: Building and architecture. – 2018. – № 1. – P. 109–115.
3. Tur, V. V. Influence of the size effect on the shear resistance of beam elements without transverse reinforcement / V. V. Tur, A. P. Vorobiev // Construction and reconstruction. Oryol State University named after I. S. Turgenev. – 2019. – № 2. – P. 43–60.
4. Derechennik, S. S. A new IN-SITU method for assessing the characteristic strength of concrete taking into account the reliability of existing reinforced concrete structures / S. S. Derechennik, V. V. Tur // Perspective Directions of Innovative Development of Construction Industry and Engineering Training: collection of scientific articles XXI International Scientific and Methodological Seminar, Brest, October 25-26, 2018: in 2 parts / Ministry of Education of the Republic of Belarus, Brest State Technical University, Faculty of Civil Engineering; editorial board: V. V. Tur [et al.]. – Brest : BrSTU, 2018. – Part 2. – P. 23–38.
5. fib Model Code for Concrete Structures 2010 / International Federation for Structural Concrete (fib), Federal Institute of Technology Lausanne – EPFL ; Proofreading and editing: Paul Beverly. – Ulm : CPI Books GmbH – Ebner & Spiegel, 2013. – 434 p.
6. European Committee for Standardization. Eurocode 2: Design of Concrete Structures. – Part 1 : General rules, rules for buildings, bridges and civil engineering structures. Draft for committee works, April 2018. – 293 p.
7. Tur, V. V. New approaches to determining the shear resistance of beam elements without transverse reinforcement: Part 1 - Review of design models / V. V. Tur, A. P. Vorobey // Bulletin of the Brest State Technical University. Series: Building and architecture. – 2019. – № 1. – P. 13–20.
8. Tur, V. V. New approaches to determining the shear resistance of beam elements without transverse reinforcement: Part 2 - Verification of design models / V. V. Tur, A. P. Vorobey // Bulletin of the Brest State Technical University. Series: Building and architecture. – 2019. – № 1. – P. 20–28.
9. Cavagnis, F. A mechanical model for failures in shear of members without transverse reinforcement based on development of a critical shear crack / F. Cavagnis, M. Fernández Ruiz, A. Muttoni // Engineering Structures. – 2018. – № 157. – P. 300–315. – DOI: https://doi.org/10.1016/j.engstruct.2017.12.004.
10. Tur, V.V. New in the design of concrete structures: the second generation of Eurocodes and national norms / V. V. Tur, T. M. Petsold // Bulletin of Polotsk State University. Construction. Applied Sciences. Building construction. – 2018. – № 8. – P. 131–146.
11. Ignatiadis, A. Eurocode 2 – analysis of National Annexes [Technical Paper] / A. Ignatiadis [et al.] // Structural Concrete. – 2015. – № 1. – P. 3–16. – DOI: https://doi.org/10.1002/suco.201400060.

Accepted 27.10.2021

UDC 691.32:539.421

FRACTURE TOUGHNESS OF CARBON NANOTUBES MODIFIED CEMENT BASED MATERIALS

S. A. Zhdanok[1], E. N. Polonina[2], E. A. Sadovskaya[3], S. N. Leonovich[4]

[1] Doctor of Physical and Mathematical Sciences, Academician of the National Academy of Sciences of Belarus, LLC "Advanced Research and Technologies", Minsk district, village Leskovka, Belarus, e-mail: ceo@art-pte.com
[2] Master of Technical Sciences, Belarusian National Technical University, Minsk, Belarus, e-mail: grushevskay_en@tut.by
[3] Master of Technical Sciences, Belarusian National Technical University, Minsk, Belarus, e-mail: elena_koleda@bk.ru
[4] Doctor of Technical Sciences, Professor, Foreign Academician of RAASN, Belarusian National Technical University, Minsk, Belarus, Qingdao University of Technology China, Qingdao, e-mail: snleonovich@yandex.ru, CEF@bntu.by

Abstract

In order to increase the fracture toughness of concrete, dispersed fiber reinforcement is increasingly used in practice. The initiation of crack initiation occurs at the nanoscale in the cement matrix. Thus, the use of nano-reinforcement with dispersed nanoparticles can have a positive effect on the fracture toughness of the cement composite. It is proposed to consider carbon nanotubes (CNTs) as such nanofibers.

This article discusses the possibility of using nanocarbon tubes as elements for restraining the development of cracks at the nanoscale in cement composite. The results of testing nanomodified cement stone for strength indicators, fracture toughness indicators, results of nanoindentation, ultrasonic sounding and infrared spectroscopy are presented. A structural model of a cement stone dispersed-reinforced with nanocarbon tubes is considered.

Keywords: fracture toughness, crack resistance, strength, nanoconcrete, carbon nanotubes, stress intensity factor.

ВЯЗКОСТЬ РАЗРУШЕНИЯ ЦЕМЕНТНЫХ МАТЕРИАЛОВ, МОДИФИЦИРОВАННЫХ УГЛЕРОДНЫМИ НАНОТРУБКАМИ

С. А. Жданок, Е. Н. Полонина, Е. А. Садовская, С. Н. Леонович

Реферат

С целью повышения вязкости разрушения бетона на практике все чаще используют дисперсное армирование волокнами. Начало зарождения трещин происходит на наноуровне в цементной матрице. Таким образом, использование наноармирование дисперсными нановолокнами может оказать положительное влияние на трещиностойкость цементного композита. В качестве таких нановолокон предлагается рассмотреть углеродные нанотрубки (УНТ).

В данной статье рассматривается возможность использования наноуглеродных трубок в качестве элементов сдерживания развитию трещин на наноуровне в цементном композите. Приведены результаты испытаний наномодифицированного цементного камня на прочностные показатели, показатели трещиностойкости, результаты наноиндентирования, ультразвукового прозвучивания и инфракрасной спектроскопии. Рассматривается структурная модель цементного камня дисперсно-армированного наноуглеродными трубками.

Ключевые слова: вязкость разрушения, трещиностойкость, прочность, нанобетон, углеродные нанотрубки, коэффициент интенсивности напряжений.

Introduction

Concrete is the most commonly used building material around the world. One of its main disadvantages is fracture fragility and low fracture toughness. The use of dispersed reinforcement of concrete composites is a promising direction in solving this type of problem. Dispersed fibers, evenly distributed over the entire volume of the material, create a spatial framework and contribute to the inhibition of developing cracks under the action of destructive forces [1, 2].

The authors put forward a working hypothesis according to which the fracture toughness of cement composites increases with the introduction of carbon nanotubes.

The initiation of crack initiation occurs at the nanoscale in the cement matrix. Thus, the use of nano-reinforcement with dispersed nanofibers can have a positive effect on the fracture toughness of a cement composite. Carbon nanotubes (CNTs) can be considered as such nanofibers. The effect of CNTs on the microstructure and nanostructure of the modified cement stone depends on the type of carbon material, its physical and chemical characteristics, the geometric parameters of the fibers and the uniformity of dispersion in the composite [3-6].

Structural modeling

The presence of carbon nanofibers changes the microstructure and nanostructure of the CNT-modified cement. A decrease in capillary porosity and a decrease in total porosity are observed, followed by an improvement in the pore structure. Reverse micromechanical analysis shows a shift from micropores and mesopores with a size of 100 nm in ordinary Portland cement to small gel pores with a size of 5–12 nm in cement modified with CNTs [7].

In the views of Ange-Therese Akono [7], the model of the modified CNT cement composite consists of 4 scale levels. At the nanoscale, calcium silicate hydrate products are packaged in various structural units, resulting in low C – S – H densities, high C – S – H densities, and ultrahigh C – S – H densities. On a submicron scale, the C – S – H grains are linked by a network of carbon nanofibers forming a C – S – H matrix. On a microscopic scale, capillary pores and unhydrated clinker grains are embedded in the C – S – H matrix.

The physical model of the kinetics of destruction of Guzeev-Piradov-Leonovich concrete [8] is represented by a structure consisting of a system of different-scale grains (clinker, sand, crushed stone) with mutual attraction relations in the form of active forces (N_{act}) created by physical (N_{ph}), chemical (N_{ch}) and adhesion (N_{adh}) processes as a result of cement hydration, and a subsystem of voids in the hydrated mass (in the form of capillaries (K), pores (P), cracks (T), in which a complex of reactive forces within the limits of their geometric dimensions in the structure (figure). The result of the processes occurring in the capillaries and cracks are deformations in the intergranular matrix, the free flow of which is impeded by rigid clinker grains and nanocarbon tubes, which creates a certain stress intensity at the tops of the dividing cracks (figure 1) The stress intensity, as well as the stress-strain state near the capillary tops and cracks are determined by the criterion of crack resistance (K_C) and the coefficients stress intensity (K_{IC}, K_{IIC}) [8–10].

doi.org/10.36773/1818-1112-2021-126-3-48-53

I – grains of crushed stone; II – sand grains;
III – clinker grains; IV – hydrated mass of cement;
C_i – physical and chemical bonds; C_j – adhesive contacts;

1 – capillaries filled with water symmetrically; 2 – capillaries filled with water asymmetrically; 3 – microcracks; 4 – cracks in contact with grains; 5 – cavities of contacts; 6 – carbon nanotubes [8]

Figure 1 – Physical model of Guzeev-Piradov-Leonovich concrete (scale dimensions not respected)

Practical research

Preparation for testing

The additives were pre-mixed with mixing water and introduced into the cement, intensively stirring for 5 minutes. The amount of mixing water was selected in such a way as to obtain a dough of normal density in all cases. The obtained dough was used to make beams with dimensions of 40x40x160 mm and 10x10x20 mm. The experimental research methods were in accordance with the provisions of GOST 310.1-5, GOST 310.3.

When conducting research on the effect of CNTs on cement stone, the following materials were used as the main components:

1. Portland cement PC 500 D0 was used as a binder according to GOST 10178 of JSC "Belarusian Cement Plant" with the following mineral composition, w_t%: C_3S – 58.31, C_2S – 13.38, C_3A – 8.01, C_4AF – 10.64.
2. Modifying substance - carbon nanomaterial (CNT): average diameter of pipes and fibers 10-300 nm, average length of tubes and fibers 0.01-20 μm, bulk density 0.15-0.22 g / cm^3, ash content not more than 5%, specific adsorption surface from 60 m^2 / g.
3. Superplasticizer (SP) in the form of an aqueous solution - a polycarboxylate copolymer with a density of 1.1-1.14 g / ml, pH = 6-8, a viscosity of 230-330 cps, a content of non-volatile substances of 39–41%, a water-reducing capacity of over 40 %.
4. Water for mixing and subsequent hardening complying with the requirements of STB 1114 GOST 23732.

The formulations of the investigated compositions are presented in table 1.

Table 1 – The composition of the raw mix of cement stone

Composition №	The composition of the raw mixture, wt. %		The amount of added additive from the mass of cement,%	V/C	Supplement composition		Normal Density Coefficient (K_{nd})
	Cement	Additive			Mass fraction of superplasticizer to cement,%	Mass fraction of solid nanocarbon to cement,%	
1	99,2	0,8	-	0,26	-	-	0,26
2			0,8	0,21	0,4	-	0,21
3			0,8	0,21	0,4	0,000 4	0,21

Fracture toughness

The conditional critical stress intensity factor when testing beams for bending is calculated according to GOST 29167 according to the formula:

$$K_c^* = \frac{3F_c^* L_0}{2b^{1/2}t}\sqrt{a_0/b}\left(1{,}93 - 3{,}07\lambda + 14{,}53\lambda^2 - 25{,}11\lambda^3 + 25{,}8\lambda^4\right)$$

where a_0, b, t, L_0 – geometric dimensions of the sample, m;

F_c^* – load corresponding to the dynamic initiation of the main crack during non-equilibrium tests, MN;

$$\lambda = a_0 / b$$

The effect of carbon nanotubes on fracture toughness is shown in Figure 2.

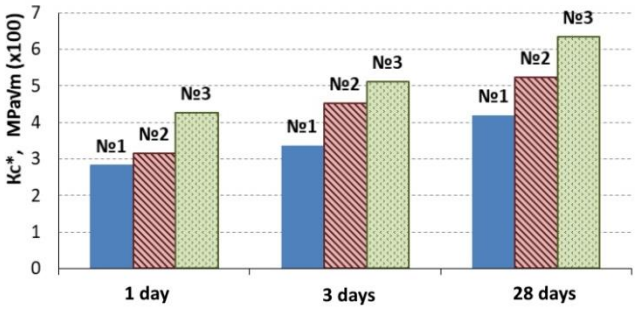

Figure 2 – Histogram of changes in the conditional critical stress intensity coefficient at different ages for composition № 1 (without additive), composition № 2 (SP), composition № 3 (SP + CNT)

Ultrasound examinations

Ultrasonic measurements were performed with Pulsar-2.2 devices (frequency 50 kHz, wavelength 100 mm) and an ultrasonic rectangular receiver model 50777PR in combination with an oscilloscope and corresponding u-shaped sensors (frequency 5 MHz, transverse wavelength 0.5 mm, longitudinal wavelength 1 mm). The test results are presented in table 2.

Table 2 – Results of ultrasound tests

Composition №	Average longitudinal and transverse velocity data		Young's modulus E,10^{9}Pa	Poisson's ratio υ	Shear modulus G, 10^{9}Pa	Density, kg/m^3
	V_{long}, km/s	V_{trans}, km/s				
2	4,735	2,556	34,98	0,288	13,57	2077,8
	4,763	2,622				
3	4,816	2,614	37,20	0,293	14,39	2225,9
	4,828	2,605				

In the composition with nanocarbon tubes, the effect of increasing the elastic modulus by 6 %, density by 7 %, shear modulus by 6 %, Poisson's ratio by 2 % is observed. An increase in density indicates a decrease in pore volume due to a more compact structure of the C-H-S gel. The values of the modulus of elasticity are quite high and indicate good elastic-plastic characteristics of solid samples.

Nanoindentation

The nanoindentation method is one of the direct methods for studying the mechanical properties of cement materials at the nanoscale. During testing, it is not the size of the sample that decreases, but the size of the deformed region. C-S-H exists in at least three structurally different forms: low, high and ultra-high density, which have different average values of hardness and hardness and different volume concentrations. Nanoparticles of different chemical composition with a high specific surface area and high surface energy are used to target the CSH gel nanostructure. The nanoindentation method makes it possible to assess the effect of nanoparticles directly on the volume fraction of different forms of CSH gel at an early age (6-24 hours) and adulthood (4-6 months) (Figure 3, 4).

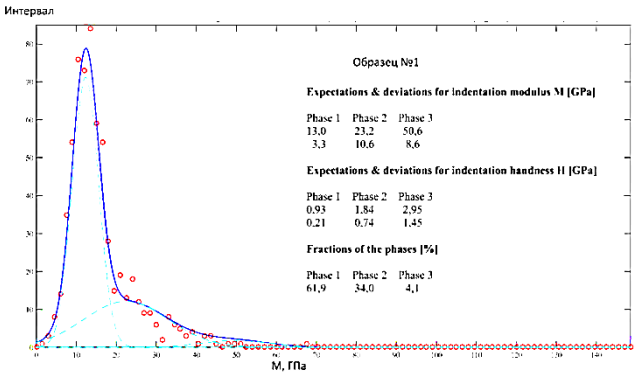

(a)

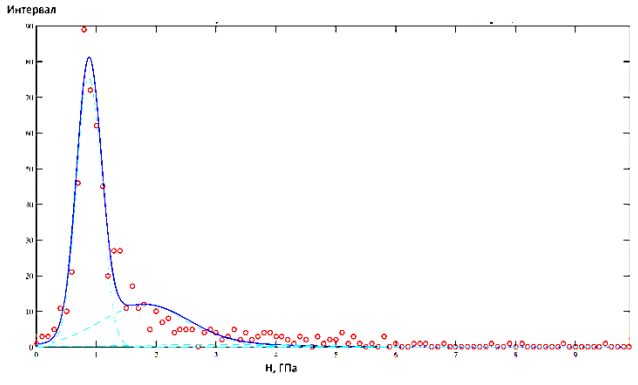

(b)

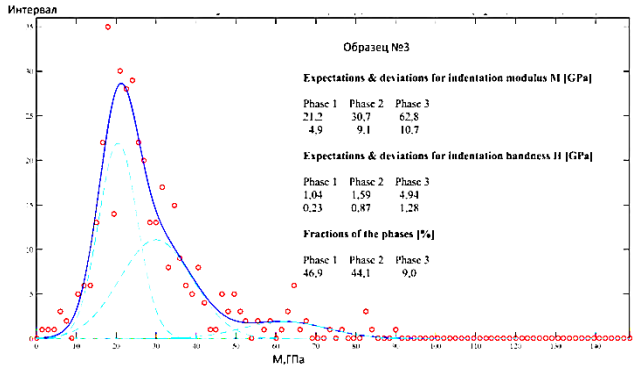

(c)

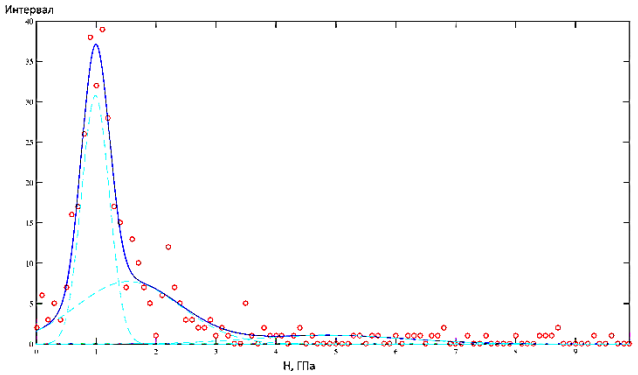

(d)

Figure 3 – Histograms of the distribution of nanoindentation points by the modulus of elasticity (a, c) and hardness (b, d) for composition No. 2 (a, b) and composition No. 3 (c, d)

Table 3 – Average values of the modulus of elasticity *M* and stiffness *H* in three phases. / – after the dividing line, the standard deviation in this phase is indicated

Options		№1	№3
Elastic modulus M, GPa / Standard deviation SD	Phase 1	13,0/3,3	21,2/4,9
	Phase 2	23,2/10,6	30,7/9,1
	Phase 3	50,6/8,6	62,8/10,7
Hardness H, GPa / Standard deviation SD	Phase 1	0,93/0,21	1,04/0,23
	Phase 2	1,84/0,74	1,59/0,87
	Phase 3	2,95/1,45	4,94/1,28
Phase volume fraction,%	Phase 1	61,9	46,9
	Phase 2	34,0	44,1
	Phase 3	4,1	9,0

According to the results obtained, the distribution in the modulus of elasticity M shifted to the right in the composition nanomodified with carbon nanotubes in comparison with the composition without nanotubes. At the same time, the volume fraction of phase 1 with lower average values of M and H decreased and the volume fraction of phases 2 and 3 with large average values of M and H and with a denser volumetric packing of CSH gel particles increased.

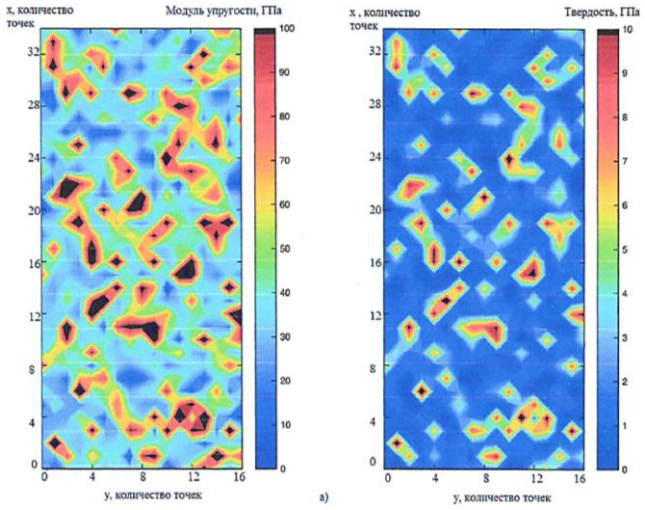

(a)

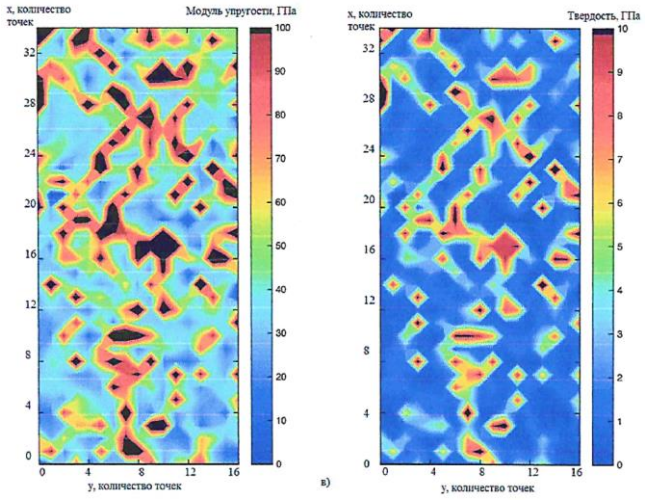

(b)

Figure 4 – Distribution of M and H in the horizontal XY plane, perpendicular to the motion of the nanoindentor: a) sample Composition № 2 (SP); b) sample Composition № 3 (SP + CNT)

doi.org/10.36773/1818-1112-2021-126-3-48-53

For phases 1, 2, 3 of the distribution Mav for phase 3, which has the maximum average value of Hav of the distribution in H in samples with CNTs, the width of the distribution according to the corresponding Gaussian function has decreased, which is characterized by a decrease in the ratio SD / Mav (SD is the standard deviation - exponent in the Gaussian function), and shows a higher structural ordering of the CSH gel in the sample with CNTs. The change in the relative values of the Gaussian function (Figure 5) indicates a change in the structure of the CSH gel in the samples modified with CNTs.

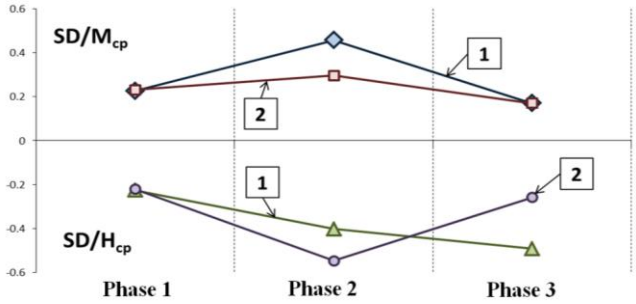

Figure 5 – The ratio of the standard deviation to the mean value of the modulus of elasticity M and stiffness H in three phases (relative values of the Gaussian function)
1 – composition № 2 (SP); 2 – composition № 3 (SP + CNT)

According to tests by nanoindentation methods in studies [11], it is concluded that when CNTs are added to the cement matrix, there is a tendency to increase the high density CSH gel due to the low density CSH gel.

Infrared spectroscopy (IR)

Using the method of IR spectroscopy, the effect of CNT nanoparticles introduced into the SP-WB super-plasticizer with high water-reducing ability on the structure of Portland cement stone was assessed. Low doses of nanoparticles in relation to cement make it possible to isolate the effect of the effect of nanoparticles on the degree of polymerization of CSH gel separately from the effect on the rate of formation of CSH gel [12].

Table 4 – Dependence of the *K* coefficient on the modifier introduced into the cement

Composition №	Position of the maxima of the absorption band of stretching vibrations of a silicon-oxygen tetrahedron				$K_1^1/K_2^1/K_3^1$ K_1^{28}/K_2^{28}
	Main maximum, cm^{-1}	Absolute intensity	Shoulder, cm^{-1}	Absolute intensity	
Hardening of samples - 1 day					
$K = I_{abs}^{955}/I_{abs}^{992}$					
№1	955	0.0278	973 / 988 / 993	0.0230 / 0.0188 / 0.0168	1.21 / 1.48 / 1.65
№2	953	0.0327	976 / 989 / 992	0.0261 / 0.0219 / 0.0203	1.25 / 1.49 / 1.61
№3	953	0.0360	976 / 987 / 991	0.0296 / 0.0262 / 0.0243	1.21 / 1.37 / 1.48
Hardening of samples - 28 days					
$K_1^{28} = I_{abs}^{957}/I_{abs}^{994}$, $K_2^{28} = I_{abs}^{957}/I_{abs}^{1017}$					
№1	958	0.0114	993 / 1018	0.0047 / 0.0022	2.43 / 5.19
№2	957	0.0157	994 / 1018	0.0077 / 0.0030	2.04 / 5.30
№3	956	0.0164	994 / 1016	0.0085 / 0.0028	1.93 / 5.86

*K – the ratio of the relative intensities of the main maximum and the shoulder.

According to the data obtained (Table 4), the absolute intensity of the bands at the maximum of 953-955 cm^{-1} and at the inflection points for composition № 3 (SP + CNT) is significantly higher than for compositions № 1 and № 2 (without CNTs), and the value of the coefficients K_{123}^1 is significantly lower than for compositions without CNTs. Analysis of the IR spectra of the control and modified samples shows that by the 1st day of hardening, the introduced CNTs contribute to some acceleration of the hydration of the main clinker minerals due to the high specific surface area and high surface energy of nanoparticles, which are additional centers of crystallization on the nuclei of neoplasms.

For ages 1 and 28 days, the data of thermogravimetry and IR-spectroscopy, the amount of hydrate water and total chemically bound water did not differ significantly in samples with CNTs compared to samples without nanoparticles. For an age of 28 days in the range $(1/\lambda) = 3000\text{-}3600$ cm^{-1}, there is no significant advantage in the rate of hydration of alite, the formation of hydrated water, CSH gel, and portlandite in the composition with CNTs. According to IR data in the range $(1/\lambda) = 900\text{-}1100$ cm^{-1}, the following changes in the structure of the CSH gel are expressed: 1) transition of hydrosilicates with degrees of polycondensation of silicon-oxygen tetrahedra n_2, n_3 close to 1, observed in IR-spectra at the age of 1 days, due to their combination into structures with a higher degree of polycondensation (28 days); 2) the content of hydrosilicates of calcium with the degree of polycondensation n4 in the composition № 3 (SP + CNT) in comparison with the sample of composition № 2 - 10.4%.

Strength indicators

To carry out mechanical tests of specimens for compression and bending, a Testing 2.1005 testing machine was used. The studies were carried out on cement specimens-beams with dimensions of 40x40x160 mm, hardening under normal conditions. The test results are shown in the figure 6.

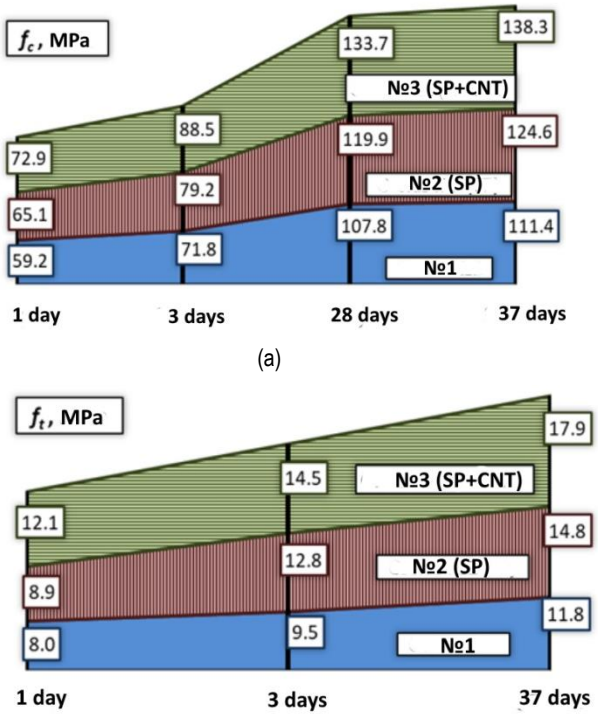

Figure 6 – Results of tests of cement matrix on a) axial compression, b) bending tension

Analysis of the results obtained indicates the effect of carbon nanotubes on the compressive and bending strength of cement matrix [13]. The increase in compressive strength with the introduction of CNTs was 12% relative to composition № 2 containing a plasticizer without CNTs as an additive. The combined effect of the plasticizer and CNT (composition № 3) had an increase in compressive strength by 21-23% relative to the composition without additive (composition № 1). The increase in

the bending strength of the cement stone was 21% (37 days) with the introduction of CNTs into the plasticizer (composition №3 relative to the composition № 2) and 51% (37 days) with the addition of CNTs and a plasticizer (composition № 3) in relation to the composition without additive (composition № 1)

Heavy Nano Concrete Research

To determine the strength characteristics and fracture toughness indices of nano-concrete, prism samples 100x100x400 mm and cube samples 100x100x100 mm were made [14-15]. The compositions differed among themselves by different contents of the main components of the mixture (table 5)

Table 5 – Recipes for nanoconcrete compositions

Composition №	Component consumption, %						Workability grade
	% - the ratio of the components of the concrete matrix				CNT modified additive		
	Cement	Crushed stone FR 5-10 mm	Crushed stone FR 5-20 mm	Sand	% from the mass of the binder	Mass fraction of solid nanocarbon to cement, %	
A	18	-	45	37	0,8	0,0006	П5
B	19	-	45	36	0,5	0,00038	П5
C	20	38	-	42	0,7	0,00038	Р4
D*	23	39	-	38	0,7	0,0006	Р6

* Composition *D* contains 8% (by weight of cement) sulfoaluminate additive, 9% (by weight of cement) condensed compacted silica fume.

The tests of the samples were carried out on the specialized equipment of the Research Laboratory of PGS BNTU (Figure 7). The test results are shown in Figure 8.

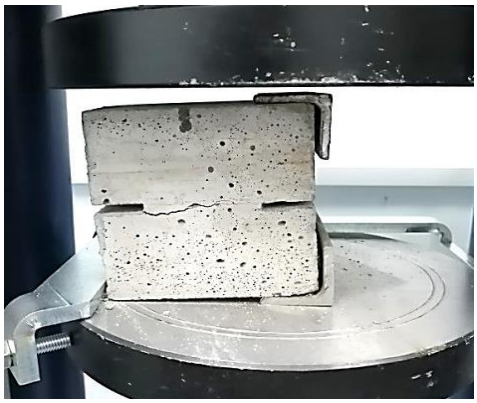

a)

b)

c)

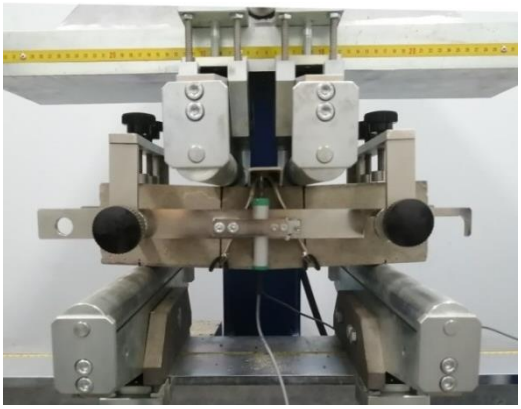

d)

Figure 7 – Tests of nanoconcrete a) normal separation (K_{IC}), b) transverse shear (K_{IIC}), c) axial compression, d) flexural tensile

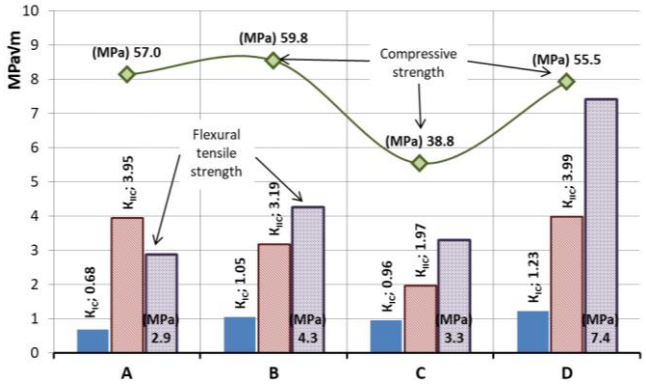

Figure 8 – Test results of nanoconcrete specimens for compression, bending tension, fracture toughness

Analysis of research results

1. The results of our studies of fracture toughness are confirmed [7], where it is shown that carbon nanofibers lead to an increase in the fracture toughness of the cement composite. Thus, the addition of 0.1 wt% CNTs led to an increase in fracture toughness by 4.5 % (0.69 ± 0.02 MPa√m), and the addition of 0.5 wt% CNTs - by 7.6 % (0, 71 ± 0.04 MPa√m). For the unmodified cement composite, the fracture toughness was 0.66 ± 0.02 MPa√m.
2. Our position on the containment of cracking by carbon fibers at the nano-level coincides with the studies of Ange-Therese Akono [7, 16], which show that carbon nanofibers fill nanopores and connect grains of calcium hydrates (C – S – H), which leads to the effect of bridging and facilitating load transfer, individual CNTs are embedded in hydration products and delay nanocracks. Also in [17], SEM images are demonstrated that confirm the effects of the formation of bridges that transfer the load along nano- and microcracks.

doi.org/10.36773/1818-1112-2021-126-3-48-53

3. Similar to our values of Young's modulus were obtained as a result of studies [7], where it was also established that the presence of carbon nanofibers affects the stochastic distribution of the macroscopic Young's modulus, causing a shift towards higher values (29.66 GPa for simple Portland cement, 31.43 GPa for cement + 0.1 wt% CNT and 36.12 GPa for cement + 0.5 wt% CNT).
4. The results of our studies using nanoindentation coincide with the results [18] in which the author concluded that CNTs modify C–S–H by increasing the amount of C–S–H with high rigidity, enhancing the cement paste matrix on a nanoscale and reducing porosity. It was also established in [7] that the presence of carbon nanofibers affects the stochastic distribution of the macroscopic Young's modulus, causing a shift towards higher values, which is fully confirmed by our studies.
5. The influence of CNTs on the increase in the strength characteristics of the cement composite in our studies coincides with the results of the studies by Bryan M. Tyson [17] - the increase in the values of flexural strength was 82 %. Also in the research of P.V. Ryabchikov [19], it was shown that the increase in the compressive strength of fine-grained concrete with the introduction of CNT was 14.1 % (without CNT - 67.4 MPa, with CNT - 76.9 MPa); an increase in tensile strength with a bend of 15.6 % (without CNTs - 8.22 MPa, with CNTs - 10.2 MPa); increase in tensile strength during splitting 24.1 % (without CNT - 2.20 MPa, with CNT - 2.73 MPa). Our results are also confirmed by the research of S.N. Tolmachev [20]: the strength of cement stone with CNTs increases by 1.5-1.9 times, the strength of solutions increases by 1.3-1.4 times, and the strength of concrete increases by 1.25-1.35 times compared with control formulations.

Conclusion

The studies carried out make it possible to assert that nanocarbon tubes have a significant effect on the properties of cement composites, including their fracture toughness. The use of dispersed reinforcement at the nanoscale is one of the methods for obtaining high-performance concrete, allowing the design of elements of buildings and structures with low strength indicators, but resistant to cracking and durability in general.

References

1. Composite materials based on cement binders modified with SiO_2 nanoadditives / B. M. Khrustalev [et al.] // Nauka i tekhnika. – 2017. – № 16 (6). – P 459–465. – DOI: https://doi.org/10.21122/2227-1031-2017-16-6-459-465.
2. Modification of cement concretes with additives containing nanosized materials / S. A. Zhdanok [et al.] // Inzhenerno-fizicheskiy zhurnal. – 2020. – Vol. 93, № 3. – P. 669.
3. Physical and mechanical characteristics of concrete modified with a plasticizing additive based on nanostructured carbon / S. A. Zhdanok [et al.] // Inzhenerno-fizicheskij zhurnal. – 2019. – Vol. 92, № 1. – P. 14–20.
4. Polonina, E. N. Physico-mechanical characteristics of nanobeton / E. N. Polonina, S. N. Leonovich, E. A. Koleda // Vestnik Inzhenernoj shkoly Dal'nevostochnogo federal'nogo universiteta. – 2018. – № 4 (37). – P. 100–111.
5. Influence of a plasticizing additive containing carbon nanomaterial on the properties of self-compacting concrete / S. A. Zhdanok [et al.] // Vestnik grazhdanskih inzhenerov. – 2018. – № 6 (71). – P. 76–85.
6. Mechanism of increasing the strength of cement material modified with SiO_2 nanoparticles and MWCNT / E. N. Polonina [et al.] // Inzhenerno-fizicheskij zhurnal. – 2021. – T. 94, No. 1. – P. 72.
7. Akono, A. T. Nanostructure and Fracture Behavior of Carbon Nanofiber-Reinforced Cement Using Nanoscale Depth-Sensing Methods / A. T. Akono // *Materials.* – 2020. – № *13.* – P. 3837. – DOI: https://doi.org/10.3390/ma13173837.
8. Strength, crack resistance and durability of structural concrete under temperature and corrosion effects : 2 parts / S. N. Leonovich [et al.] ; ed. S. N. Leonovich. – Minsk : BNTU, 2016. – Part 1. – 390 p.
9. Koleda, E. A. Characteristics of crack resistance of fiber-reinforced concrete as a determining factor of quality / E. A. Koleda, S. N. Leonovich // Construction and reconstruction technology: TCR-2015 : collection of reports of the International Scientific and Technical Conference / Technical University and the National Academy of Sciences of Belarus ; ed. B. M. Khrustalev, S. N. Leonovich. – Minsk : BNTU, 2017. – P. 282–287.
10. Sadovskaya, E. A. Multilevel structure of concrete: analysis and classification of the levels of organization of the structure of conglomerate building composites / E. A. Sadovskaya, E. N. Polonina, S. N. Leonovich // Problems of modern construction: materials of the International Scientific and Technical Conference, Minsk, May 28, 2019 / Belarusian National Technical University; editorial board: V. F. Zverev, S. M. Koleda. – Minsk : BNTU, 2019. – P. 285–297.
11. Barbhuiya, S. Nanoscaled mechanical properties of cement composites reinforced with carbon nanofibers / S. Barbhuiya, P. Chow // Materials. – 2017. – № 10. – P. 662. – DOI: https://doi.org/10.3390/ma10060662.
12. Zhdanok, S. A. Investigation by the method of IR spectroscopy of the degree of activation of carbon nanomaterials for modifying structural concrete / S. A. Zhdanok, E. N. Polonina, S. N. Leonovich // Stroitel'nye materialy. – 2020. – № 7. – P. 49–53. – DOI: https://doi.org/10.31659/0585-430X-2020-782-7-49-53.
13. Increasing the strength of concrete with a plasticizing additive based on nanostructured carbon / S. A. Zhdanok [et al.] // Stroitelnye materialy. – 2018. – № 6. – P. 67–72.
14. Strength of nanofibreconcrete tensile / E. A. Sadovskaya [et al.] // Inzhenerno-fizicheskij zhurnal. – 2020. – Vol. 93, № 4. – P. 1051–1055.
15. Physicomechanical properties of medium-strength concrete modified with a carbon nanostructured additive / E. A. Koleda [et al.] // Vestnik Povolzhskogo gosudarstvennogo tekhnologicheskogo universiteta. Series: Materials. Constructions. Technologies. – 2018. – № 2. – P. 24–34.
16. Metaxa, Zoi. Carbon nanofiber cementitious composites: Effect of debulking procedure on dispersion and reinforcing efficiency / Z. Metaxa, M. S. Konsta-Gdoutos, S. P. Shah // Cement and Concrete Composites. – 2013. – № 36. – P. 25–32. – DOI: https://doi.org/10.1016/j.cemconcomp.2012.10.009.
17. Tyson, Bryan. Carbon Nanotubes and Carbon Nanofibers for Enhancing the Mechanical Properties of Nanocomposite Cementitious Materials / B. Tyson [et al.] // Journal of Materials in Civil Engineering. – 2011. – № 23. – P. 1028–1035. – DOI: https://doi.org/10.1061/(ASCE)MT.1943-5533.0000266.
18. Sanchez, F. Nanotechnology in Concrete / F. Sanchez, K. Sobolev // Construction and Building Materials. – 2010. – № 24. – P. 2060–2071. – DOI: http://dx.doi.org/10.1016/j.conbuildmat.2010.03.014.
19. Ryabchikov P.V. Influence of carbon nanomaterials on the properties of cement / P. V. Ryabchikov, E. I. Batyanovsky // Science - to education, production, economy: materials of the Seventh International Scientific and Technical Conference: in 3 volumes / Belarusian National Technical University; editorial board: B. M. Khrustalev, F. A. Romanyuk, A. S. Kalinichenko. – Minsk : BNTU, 2009. – T. 2. – P. 91.
20. Tolmachev, S. N. Features of the influence of carbon nanoparticles on the level of the structure of road cement concretes / S. N. Tolmachev, E. A. Belichenko // Tekhnologii betonov. – 2014. – № 8 (97). – P. 13–17.
21. The influence of a plasticizing additive based on nanostructured carbon in a self-compacting concrete mixture on its technological properties / S. A. Zhdanok [et al.] // Inzhenerno-fizicheskij zhurnal. – 2019. – Vol. 92, № 2. – P. 391–396.

Accepted 01.11.2021

MECHANICAL ENGINEERING

UDC 621.85.01

RESEARCH OF RIGIDITY OF TOOTHEDS OF THE TOOTHED BELT IN CONDITIONS OF THE DYNAMIC LOADING

A. G. BAKHANOVICH

Doctor of Technical Sciences, Associate Professor, Rector of Brest State Technical University, Belarus, Brest, email: rector@bstu.by

Abstract

The article results of experimental researches of rigidity of tootheds of a toothed belt within the limits of zones of a deficient profile gearing are presented by transmission of capacity.

Keywords: toothed-belt transmission, rigidity of tootheds, deficient profile gearing, intense-deformed condition.

ИССЛЕДОВАНИЕ ЖЁСТКОСТИ ЗУБЬЕВ ЗУБЧАТОГО РЕМНЯ В УСЛОВИЯХ ДИНАМИЧЕСКОГО НАГРУЖЕНИЯ

А. Г. Баханович

Реферат

В статье представлены результаты экспериментальных исследований жёсткости зубьев зубчатого ремня в пределах зон неполнопрофильного зацепления при передаче мощности.

Ключевые слова: зубчато-ременная передача, жесткость зубьев, неполнопрофильное зацепление, напряженно-деформированное состояние.

The rigidity of belt teeth is one of the parameters, defining the distribution of loading in a toothed-belt gearing, and, hence, defining the load carrying capacity and the operational resource of transmission.

As a result of the theoretical research of the complex stress condition of the elements of a toothed-belt transmission it is established that the deformation of belt teeth is defined by the stresses of a bearing strain, shear and bending. Solving the problem of the theoretical definition of the deformation of a belt tooth at the known combination of force factors and mechanical properties of a belt, the ratio of the deformations, making a total tangential deformation, is determined. It is established that in the condition of full gearing at $\beta_p = \beta_w$ the shear deformations make up the main quantity.

The theoretical research of the stress-strained state of a belt tooth, carried out by the author [1], is also devoted to the analysis of the tooth, which has completely input in gearing of a belt. Considering the problem, the author notes that finding of the analytical solution is extremely complicated, since the problem refers to the type of the non-classical mixed contact problems of the theory of elasticity.

The researches of the stress-strained state with the application of the method of finite elements [2–5] are also known. However, the results of these researches are presented in the form of the diagrams of stress in the material of a belt tooth, received on the basis of numerous approximations. It is not possible to find the value of the total tangential deformation of a tooth with their help, especially when a tooth is in the state of the incomplete profile gearing. Thus, we can come to the conclusion, made in the work [6], that it is expedient to define the value of the rigidity of teeth experimentally.

At the experimental determination of EZ the following dependence is used (Fig.1):

$$EZ = \frac{F}{\Delta s}, \tag{1}$$

where F – the effort on a belt tooth;

Δs – the tangential deformation of a tooth.

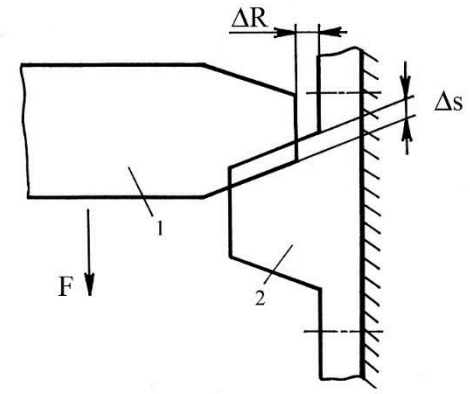

1 – penetrator; 2 – belt tooth

Figure 1 – Loading of a belt tooth

It is established that the value EZ is better to be expressed in relation to the module of shear of rubber of the tooth G, defined by the hardness. In this case:

$$EZ = \frac{G}{a_z}, \tag{2}$$

where a_z – the empirical factor: a_z = 0,230...0,239 – for the belts with the module m = 1...10 mm; a_z = 0,251...0,264 – for the belts *MXL–XXH* [7].

The values EZ, received in such a way, cannot be used for the description of the deformation of teeth in the conditions of the incomplete gearing that is characteristic of the angles ψ_1 and ψ_2 (Fig.2). It is possible to assume that in such conditions the value EZ is less than its value at full gearing, since the centroid of the effort F is displaced to the tip of a belt tooth.

doi.org/10.36773/1818-1112-2021-126-3-54-56

This conjecture is proved implicitly by the researches of EZ in the conditions of the incomplete profile gearing, characterized by the existence of the radial clearance ΔR [8]. The behavior of EZ within the limits of the angle ψ_1 is described in the work [9], however, the influence of the phase of gearing within the limits of the angle ψ_2 on EZ is not established. Due to the opposite direction of loading, applied to the tooth in the zones ψ_1 and ψ_2, different dependences of the change of EZ (within the limits of the given angles) appear. The experimental researches were conducted to prove the given hypothesis.

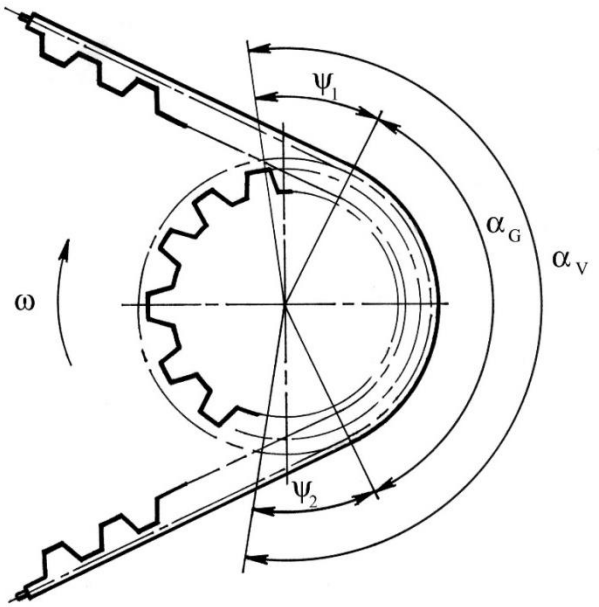

Figure 2 – Scheme of the interaction of a toothed belt with a pulley (ψ_1, ψ_2 – the angles of an input of teeth in gearing and an output from it accordingly – the zones of an incomplete profile gearing of teeth)

The toothed belts with the following parameters: 1) m = 7 mm; z_p = 71; B_p = 32 both 50 mm and 2) m = 3 mm; z_p = 48; B_p = 16 mm with hardness of teeth HS = 58,6; 64,2; 74,3; 85,2 relative units are the objects of the researches. The belts are made by the method of diaphragm vulcanizations and of pressing by rigid elements, made of rubber mixture 1453 with the use of kapron fabric facing of the art.56320, gum-dipped (№ 420).

The values of the angles ψ_1 and ψ_2 vary within the limits, corresponding to $z_ш$ = 8...30. The effort on the examined tooth changes within the limits 0...F_{max}, where $F_{max} = 2[F_t] / z_ш$. $[F_t]$ according to [10] for m = 3 and 7 mm are taken as10 and 45 N/mm. The replication of carrying out of the experiments is 7 at their reliability 0,95 [11].

The developed special stand (Fig.3) is used for the experimental researches. It consists of the frame 1 with the guides 2, in which the movable carriage 3 is established. The fragment of the examined belt 4 is fixed on the carriage 3. In the top part of the frame 1 the axis 5 with the lever of the variable length 6 with the penetrator 7 on the end, is placed. The profile of the penetrator corresponds to the profile of the pulley tooth. The lever 8 is positively connected with the lever 6. The lever 8 is equipped with a set of loads 9 and the displacement indicator 10 in the form of the indicator of a clock type with the division value 0,01 mm.

At the given value $\psi_{1(2)}$, defined from the value $z_ш$, the tooth of the belt (by moving of the carriage 3) is fixed at the distance X from the axis of symmetry of the pulley, corresponding to the demanded arc of traverse of the pulley φ_2 within the limits of 0...$\psi_{1(2)}$. The length of the lever 6 is adjusted up to the value $R = mz_ш / 2$. After that the penetrator 7 is engaged with the tooth of the examined belt. Consequently, increasing the effort on the tooth of the belt from 0 to F_{max} by means of the loads 9, the angular displacement $\Delta\varphi_2$ of the lever 6 is registered.

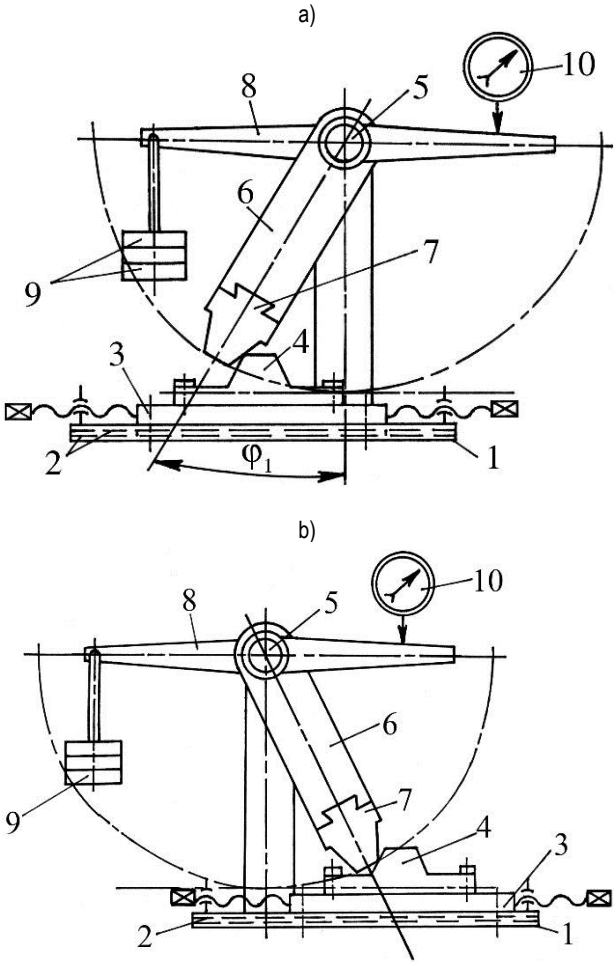

a) input in gearing; b) output from gearing

Figure 3 – Stand for the research of rigidity of belt teeth

The value of the tooth rigidity for each effort F_i, acting on it, is determined by the formula:

$$EZ_i = \frac{F_i}{Rtg\left(\Delta\varphi_2\right)}. \quad (3)$$

Discretely changing the distance X that corresponds to getting of different phases of gearing within the limits of the angles $\psi_{1(2)}$, we make loading of a belt tooth. As a result of the researches the dependences EZ of the phase of gearing, the module of a belt and hardness of its teeth are received (Fig.4).

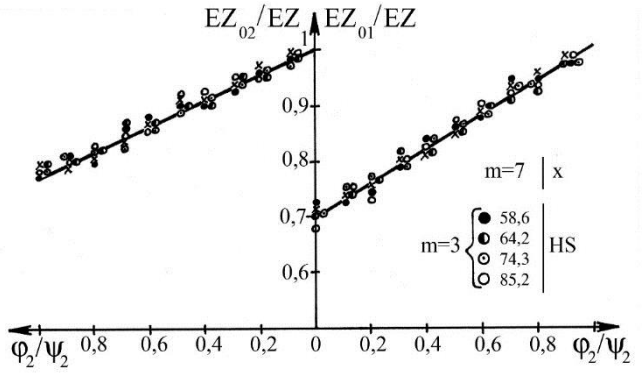

Figure 4 – Rigidity of belt teeth at different phases of an input in gearing and an output from it

The dependences EZ of the phase of a pulley turn within the limits of the angles of the input in gearing and the output from it can be expressed as the empirical equations:

$$EZ_{01} = EZ\left(0,7 + 0,3\frac{\varphi_2}{\psi_1}\right), \quad (4)$$

$$EZ_{02} = EZ\left(1 - 0,23\frac{\varphi_2}{\psi_2}\right). \quad (5)$$

The analysis of the dependences shows the unequal influence of the angles ψ_1 and ψ_2 on the rigidity of teeth. At the equal change of ψ_1 and ψ_2 the increase of EZ_{01} is 1,3 times more intensive than the reduction of EZ_{02}. At the same time the limiting values of EZ_{01} at $\varphi_2 / \psi_1 = 0$ are 10 % less than EZ_{02} at $\varphi_2 / \psi_2 = 1$. It is explained by the fact that the initial contact of teeth at their input in gearing takes place in the zone of the tip of the belt teeth. The disconnection of teeth at the output, as a rule, occurs in the middle part of a belt tooth.

Thus, the empirical dependences, allowing to define the rigidity of the belt teeth in the zones of the incomplete profile gearing, are received.

References

1. Pogrebnyak, A. P. Determination of the parameters of gear belt gears, ensuring an increase in their reliability: dis. ... Candidate of Technical Sciences : 05.02.02 / A. P. Pogrebnyak. – Kiev, 1977. – 126 p.
2. Murukami, Y. Study of belt toughness through an examination of the strain on belt cords / Y. Murukami // SAE tech. rap. ser. – 1988. – № 880415.
3. Load distribution in timing belt / G. Gerbert [et al.] // Mech. des. – 1978. – Vol. 100, No 4. – P. 208–215.
4. Gurevich, Yu. Loading belt drive operating without a slip / Y. Gurevich // Izv. vuzov, Ser. life. – 1989. – No. 4. – P. 139–144.
5. Kravtsov, E. D. investigation of the stress-strain state of a timing belt finite element / E. D. Kravtsov, A. A. Klimenko // Machine parts. – 1983. – No. 37. – P. 19–22.
6. Natalevich, A. N. Investigation of conditions for improving the efficiency of gear-belt gears: dis. ... Candidate of Technical Sciences: 05.02.02 / A. N. Natalevich. – Minsk, 1982. – 196 p.
7. Boikov, V. P. Toothed belts / V. P. Boikov, Yu. N. Gorodnichev, G. G. Kozachevsky. – M. : Chemistry, 1989. – 192 p.
8. Shpilevsky, V. I. Increasing the bearing capacity and durability of gear belts based on the use of rational methods of their pre-tension: dis. ... Candidate of Technical Sciences: 05.02.02 / V. I. Shpilevsky. – Minsk, 1993. – 185 p.
9. Kravtsov, E. D. The influence of the design parameters of gear belt transmission on the design load: dis. ... Candidate of Technical Sciences: 05.02.02 / E. D. Kravtsov. – Odessa, 1987. – 154 p.
10. Gear belt transmission. Calculation method: OST 38 05227-81. – Introduction. 01.01.82. – Moscow : NIIRP Minneftekhimprom of the USSR, 1981. – 22 p.
11. Kane, M. M. Fundamentals of scientific research in mechanical engineering technology / M. M. Kane. – Minsk : Higher School, 1987. – 231 p.

Accepted 29.10.2021

UDC 621.85.01

RESEARCH OF DYNAMIC CHARACTERISTICS OF POWER TRANSFERS BY FRICTIONAL TYPE FLEXIBLE LINK

A. G. Bakhanovich

Doctor of Technical Sciences, Associate Professor, Rector of Brest State Technical University, Belarus, Brest, email: rector@bstu.by

Abstract

Functioning of power transfer by flexible link of frictional type in conditions of a dynamic loading is theoretically described. Small motions of power transfer by flexible link of frictional type which allows to forecast unstable transfer operating modes are presented. Experimental research in the obtained dependences are given and recommendations as to the choice of rational operational transfer parameters which ensure the rise in stability of its movement are offered.

Keywords: power transfer, frictional flexible coupling, dynamic loading, unstable operation, operating parameters, movement stability

ИССЛЕДОВАНИЕ ДИНАМИЧЕСКИХ ХАРАКТЕРИСТИК ПЕРЕДАЧИ МОЩНОСТИ ГИБКИМ ЗВЕНОМ ФРИКЦИОННОГО ТИПА

А. Г. Баханович

Реферат

Теоретически описано функционирование передачи мощности гибким звеном фрикционного типа в условиях динамической нагрузки. Представлены малые движения передачи мощности гибким звеном фрикционного типа, что позволяет прогнозировать нестабильные режимы работы передачи. Приведены экспериментальные исследования полученных зависимостей и предложены рекомендации по выбору рациональных эксплуатационных параметров передачи, обеспечивающих повышение устойчивости ее движения.

Ключевые слова: передача мощности, фрикционная гибкая муфта, динамическая нагрузка, нестабильная работа, рабочие параметры, устойчивость движения.

Introduction

Despite the quasi-constant nature of the transmitted torque, slip oscillations are inevitable in a frictional belt drive (FBD), which in some cases leads to slipping of the belt relative to the pulleys. and thus affects the stability of the gear movement. This phenomenon contributes to the occurrence of vibration in the drives on the whole, and the vibrations of the belt legs contribute to the intense production of noise. The durability of belts in suchlike conditions is also low, however, theoretically, such a phenomenon has not been described up to now.

When analyzing large displacements, it was shown [1] that in certain modes the FBD, as a coupling, is nonholonomic. In the work [2], a linear equation of nonholonomic coupling was obtained, which is the result of considering non-vibrational loading of the transmission. The authors of works [3, 4] made an attempt to experimentally substantiate slip zones, in which transmission can be represented as a holonomic system. The drawback of these works is that the authors do not take into account the change in the slip coefficient when the load fluctuates, and that is why they could not explain the significant discrepancy between empirical and analytical results in the resonant modes of operation. Thus, the issue of the criterion for transmission holonomy at small vibrations remains open.

The aim of this work is to describe small motions of a system with a FBD in a nonholonomic setting, which makes it possible to predict unstable transmission modes. It is known that a nonholonomic dynamical system will occur if the generalized coordinates of the system are related to the generalized velocities of the system and the kinematic coupling equation is not integrable.

Main part

To derive a FBD coupling equation, let's consider the processes of changing the speeds of the driving and driven pulleys over a period of time Δt when oscillating relative to stationary motion. Similar processes of changing the speeds of the transmission pulleys occur in non-stationary loading conditions and in the absence of torsional vibrations. For the simplicity of analytical conclusions, let's assume the calculated FBD gear ratio equal to one and $\Delta t_1 = \Delta t_2 = \Delta t$ in accordance with Fig. 1. Furthermore, we linearize the sections of speed change over the period Δt, corresponding to the drop and increase in the load. At t_0, the angular velocities of the driving and driven pulleys are respectively equal to $\dot{\varphi}_{10}$ and $\dot{\varphi}_{20}$.

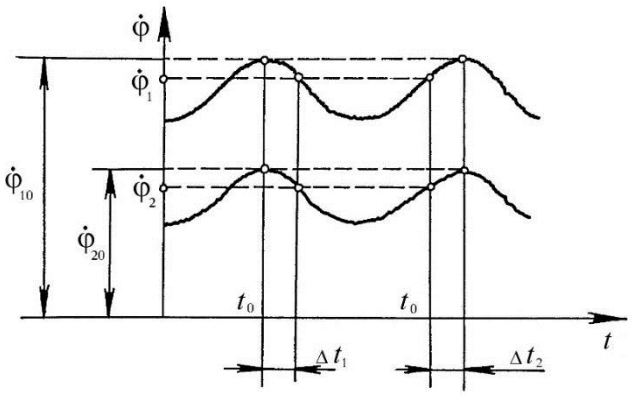

Figure 1 – Change of angular speeds of the leader and follower pulleys of power transmission by flexible link of frictional type at loading oscillations

During the time Δt, these speeds will change and become equal, respectively, $\dot{\varphi}_1$ and $\dot{\varphi}_2$. In this case, the angles of rotation of the pulleys during the time Δt will be equal: for the case Δt_1

$$\varphi_1 = \dot{\varphi}_{10}\Delta t_1 - \frac{\varepsilon_1 \Delta t_1^2}{2}, \quad (1)$$

$$\varphi_2 = \dot{\varphi}_{20}\Delta t_1 - \frac{\varepsilon_2 \Delta t_1^2}{2}, \quad (2)$$

where ε_1 and ε_2 — angular acceleration of the transmission pulleys.

For the case Δt_2

$$\varphi_1 = \dot{\varphi}_{10}\Delta t_2 + \frac{\varepsilon_1 \Delta t_2^2}{2}, \quad \varphi_2 = \dot{\varphi}_{20}\Delta t_2 + \frac{\varepsilon_2 \Delta t_2^2}{2}.$$

With uniform rotation, the angular accelerations of the pulleys are equal to:

for the case Δt_1

$$\varepsilon_1 = \frac{\dot{\varphi}_{10} - \dot{\varphi}_1}{\Delta t_1}, \quad (3)$$

$$\varepsilon_2 = \frac{\dot{\varphi}_{20} - \dot{\varphi}_2}{\Delta t_1}. \quad (4)$$

for the case Δt_2

$$\varepsilon_1 = \frac{\dot{\varphi}_1 - \dot{\varphi}_{10}}{\Delta t_2}, \quad \varepsilon_2 = \frac{\dot{\varphi}_2 - \dot{\varphi}_{20}}{\Delta t_2}.$$

We substitute expressions (3) and (4), respectively, in (1) and (2) and express the time from these dependencies. We perform a similar procedure with other formulas.

Taking into account that the time Δt is the same for the driving and driven pulleys, we obtain the FBD coupling equation, both for the case of Δt_1 and for the case of Δt_2 in the form

$$\frac{\varphi_1}{\dot{\varphi}_1 + \dot{\varphi}_{10}} = \frac{\varphi_2}{\dot{\varphi}_2 + \dot{\varphi}_{20}}, \quad (5)$$

or

$$\varphi_1\left(\dot{\varphi}_2 + \dot{\varphi}_{20}\right) = \varphi_2\left(\dot{\varphi}_1 + \dot{\varphi}_{10}\right). \quad (6)$$

Since the type of connections and their properties determine the form of the differential equations of motion of the system, it is necessary to find out the properties of the obtained kinematic coupling equation. Let's make an integrability analysis with the help of the elements of the Pfaffian forms theory [5].

We write the equation (6) in the following form

$$\varphi_1 \frac{d\varphi_2}{dt} - \varphi_2 \frac{d\varphi_1}{dt} + \left(\varphi_1\dot{\varphi}_{20} - \varphi_2\dot{\varphi}_{10}\right) = 0,$$

$$\varphi_1 d\varphi_2 - \varphi_2 d\varphi_1 + \left(\varphi_1\dot{\varphi}_{20} - \varphi_2\dot{\varphi}_{10}\right)dt = 0. \quad (7)$$

It follows (7)

$$Adx + Bdy + Cdz = 0, \quad (8)$$

where $A = \varphi_1;\ B = -\varphi_2;\ C = \left(\varphi_1\dot{\varphi}_{20} - \varphi_2\dot{\varphi}_{10}\right);$
$dx = d\varphi_2;\ dy = d\varphi_1;\ dz = dt.$

An integrating factor for the differential equation (8) exists if the condition is fulfilled

$$A\left(\frac{\delta B}{\delta z} - \frac{\delta C}{\delta y}\right) + B\left(\frac{\delta C}{\delta x} + \frac{\delta A}{\delta z}\right) + C\left(\frac{\delta A}{\delta y} - \frac{\delta B}{\delta x}\right) = 0. \quad (9)$$

We calculate particular derivatives entering the condition (9)

$$\frac{\delta B}{\delta z} = -\frac{\delta\varphi_2}{\delta t} = -\dot{\varphi}_2; \quad \frac{\delta A}{\delta z} = \frac{\delta\varphi_1}{\delta t} = \dot{\varphi}_1;$$

$$\frac{\delta C}{\delta y} = \frac{\delta\left(\varphi_1\dot{\varphi}_{20} - \varphi_2\dot{\varphi}_{10}\right)}{\delta\varphi_1} = \dot{\varphi}_{20}; \quad \frac{\delta A}{\delta y} = \frac{\delta\varphi_1}{\delta\varphi_1} = 1;$$

$$\frac{\delta C}{\delta x} = \frac{\delta\left(\varphi_1\dot{\varphi}_{20} - \varphi_2\dot{\varphi}_{10}\right)}{\delta\varphi_2} = -\dot{\varphi}_{10}; \quad \frac{\delta B}{\delta x} = -\frac{\delta\varphi_2}{\delta\varphi_2} = -1.$$

Substituting these values of the derivatives into the condition (5), after a number of transformations we find

$$\frac{\varphi_1}{\dot{\varphi}_{10} - \dot{\varphi}_1} = \frac{\varphi_2}{\dot{\varphi}_{20} - \dot{\varphi}_2}; \text{ или } \frac{\varphi_1}{\Delta\dot{\varphi}_1} = \frac{\varphi_2}{\Delta\dot{\varphi}_2}.$$

This condition means that the increment of the rotation angles per unit of speed change for the driving and driven pulleys of the transmission must remain equal during torque fluctuation.

However, in real conditions, because of the presence of an irreparable lag of the driven pulley due to elastic sliding, we have

$$\varphi_1 > \varphi_2;\ \Delta\dot{\varphi}_1 \neq \Delta\dot{\varphi}_2;\ \text{или } \frac{\varphi_1}{\dot{\varphi}_{10} - \dot{\varphi}_1} \geq \frac{\varphi_2}{\dot{\varphi}_{20} - \dot{\varphi}_2}.$$

Consequently, the equation of the kinematic connection of the FBD (6) is non-integrable, that is, a kinematic connection carried out by a belt in a friction-type transmission — flat-belt, V-belt is nonholonomic. Its equation in general form [5]

$$\sum_{j=1}^{n} A\nu_j\dot{\varphi}_j + a_\nu = 0,$$

where $\upsilon = 1, 2, 3, \ldots, \rho$; ρ – the number of linear nonholonomic connections, for our case $\rho = 1$; n – the number of the system generalized coordinates ($n = 2$);

$$A_{11} = -\varphi_2, \quad A_{12} = \varphi_1, \quad a_1 = \left(\varphi_1\dot{\varphi}_{20} - \varphi_2\dot{\varphi}_{10}\right). \quad (10)$$

In differentials an equation general form can be presented in the following way:

$$\sum_{j=1}^{n} A\nu_j d\varphi_j + a_\nu dt = 0. \quad (11)$$

As is known from analytical mechanics, a coupling type (11) meets basic Hertz-Hölder principle for the analytical mechanics of nonholonomic systems. It follows from this principle that the relations for coordinates $\delta\varphi_j$ variations in the presence of nonholonomic coupling are obtained from the equations of differential connections by discarding the term which, in the equation, contains value dt (54) and replacing $d\varphi_j$ by $\delta\varphi_j$. Thus, the coordinate variations $\delta\varphi_j$ are bound by the relation $\sum_{j=1}^{n} A\nu_j\delta\varphi_j = 0.$

For the case under consideration, this allows to obtain

$$\sum_{j=1}^{2} A\nu_j\delta\varphi_j = 0, \text{ или } A_{12}\delta\varphi_2 + A_{11}\delta\varphi_1 = 0,$$

$$\varphi_1\delta\varphi_2 - \varphi_2\delta\varphi_1 = 0.$$

Considering small oscillations with respect to stationary motion and assuming that the possible displacements $d\varphi_j$ meet a number of coordinate variation values $\delta\varphi_j$, we write, for small oscillations, a coupling equation without a free term in differential form $\varphi_1 d\varphi_2 - \varphi_2 d\varphi_1 = 0.$

Dividing this equation by dt we obtain the constraint equation for small oscillations

$$\varphi_1\dot{\varphi}_2 - \varphi_2\dot{\varphi}_1 = 0, \text{ или } \dot{\varphi}_2 = \frac{\varphi_2}{\varphi_1}\dot{\varphi}_1 = 0. \quad (12)$$

Thus, a free term a_1 does not have a significant effect on dynamic processes during vibrations of friction belt drives and actually determines only the initial state of the system. In the further analysis, we use equations with indefinite Lagrange multipliers and a coupling equation (12). Such an equation has the form

doi.org/10.36773/1818-1112-2021-126-3-57-62

$$\frac{d}{dt}\frac{\delta T}{\delta \dot{x}_j} - \frac{\delta T}{\delta x_j} = -\frac{\delta \Pi}{\delta x_j} - \frac{\delta \Phi}{\delta \dot{x}_j} + \lambda_1 A_1 + \ldots + \lambda_l A_j e, \quad (13)$$

where j = 1, 2, …, n – the number of generalized coordinates; l – the number of linear nonholonomic links; T – the kinetic energy of the system; Π – potential energy of the system; Φ – dissipation function.

In addition, a linear nonholonomic coupling is laid on FBD system in the form

$$A_{1R}\dot{x}_1 + A_{2R}\dot{x}_2 + \ldots + A_{SR}\dot{x}_R; \quad R = 1, 2, \ldots, l. \quad (14)$$

To use these equations in the study of small oscillations with respect to stationary motion, it is necessary to pass from the original equations to the equations in variations, replacing the coordinates x_j with q_i j

$$\left.\begin{aligned} x_j &= x_j(t) + q_j \\ \dot{x}_j &= \dot{x}_j(t) + \dot{q}_j \end{aligned}\right\}.$$

For the PBd, the generalized coordinates are φ_1 и φ_2 (n = 2). That's why

$$\left.\begin{aligned} \varphi_1 &= \varphi_1(t) + q_1 \\ \dot{\varphi}_1 &= \dot{\varphi}_1(t) + \dot{q}_1 \end{aligned}\right\}, \quad \left.\begin{aligned} \varphi_2 &= \varphi_2(t) + q_2 \\ \dot{\varphi}_2 &= \dot{\varphi}_2(t) + \dot{q}_2 \end{aligned}\right\}, \; \varphi_2\dot{\varphi}_1 - \varphi_1\dot{\varphi}_2 = 0. \quad (15)$$

Thus, a dynamic FBD system has one degree of freedom of movement, since n = 1.

The transition to equations in variations is carried out as follows. We perform the calculations of the terms $\frac{d}{dt}\frac{\delta T}{\delta \dot{x}_j}$, $\frac{\delta T}{\delta x_j}$, $\frac{\delta \Pi}{\delta x_j}$, and then, in the obtained equations, we expand all the terms in the degrees of variation and restrict ourselves to only terms of the lowest orders.

Generalized forces are calculated taking into account the selected new variables. These forces can be calculated as coefficients for possible displacements in the expression of virtual work. The transition from the coordinates x_j to their variations q_j must also be performed for the nonholonomic coupling equation (14). For the considered movement of the belt drive, we will have a nonholonomic coupling equation in the form

$$A_1\dot{\varphi}_1 + A_2\dot{\varphi}_2 = 0. \quad (16)$$

Expanding $A_1 = A_1(\varphi_1; \varphi_2)$ и $A_2 = A_2(\varphi_1; \varphi_2)$ in the degrees of variation and restricting ourselves to terms of the lowest orders, we obtain

$$\begin{aligned} A_1 &= A_1 l_0 + \frac{\delta A_1}{\delta \varphi_1} l_0 q_1 + \frac{\delta A_1}{\delta \varphi_2} l_0 q_2 + \ldots; \\ A_2 &= A_2 l_0 + \frac{\delta A_2}{\delta \varphi_1} l_0 q_1 + \frac{\delta A_2}{\delta \varphi_2} l_0 q_2 + \ldots \end{aligned} \quad (17)$$

When decomposing, we use a usual method: we assume all coefficients to be constant. In the equations (13), the terms with the index "0" correspond to stationary motion.

The equations with indefinite factors for the FBD then take the form

$$\frac{d}{dt}\frac{\delta T}{\delta \dot{\varphi}_1} - \frac{\delta T}{\delta \varphi_1} = Q_1 + A_1\lambda, \quad \frac{d}{dt}\frac{\delta T}{\delta \dot{\varphi}_2} - \frac{\delta T}{\delta \varphi_2} = Q_2 + A_2\lambda,$$

where Q_1, и Q_2 – generalizing forces.

An indefinite factor λ is the function of coordinates and velocities. Expanding it into a Taylor series after the transformations, we obtain

$$\lambda = \lambda_0 + \sum_{j=1}^{n} \frac{\delta \lambda}{\delta \varphi_j} l_0 q_j + \sum_{j=1}^{n} \frac{\delta \lambda}{\delta \dot{\varphi}_j} l_0 \dot{q}_j.$$

For simplicity, we denote all lower-order terms by λ'. Then

$$\lambda = \lambda_0 + \lambda'.$$

Kinetic energy is expressed as a quadratic form of generalized velocities with coefficients a_{ij}, which are determined by the coordinates of the system

$$T = \frac{a_{11}\dot{\varphi}_1^2 + 2a_{12}\dot{\varphi}_1\dot{\varphi}_2 + a_{22}\dot{\varphi}_2^2}{2}. \quad (18)$$

After the differentiation operations with respect to generalized coordinates, we have

$$\begin{aligned} &a_{11}\ddot{\varphi}_1 + a_{12}\ddot{\varphi}_2 + \frac{1}{2}\frac{\delta a_{11}}{\delta \varphi_1}\dot{\varphi}_1^2 + \frac{\delta a_{11}}{\delta \varphi_2}\dot{\varphi}_1\dot{\varphi}_2 - \frac{1}{2}\frac{\delta a_{22}}{\delta \varphi_1}\dot{\varphi}_2^2 + \\ &+ \frac{\delta a_{11}}{\delta \varphi_2}\dot{\varphi}_2^2 = Q_1(\varphi_1; \varphi_2; \dot{\varphi}_1; \dot{\varphi}_2) + A_1\lambda, \end{aligned} \quad (19)$$

$$\begin{aligned} &a_{12}\ddot{\varphi}_1 + a_{22}\ddot{\varphi}_2 + \frac{1}{2}\frac{\delta a_{22}}{\delta \varphi_2}\dot{\varphi}_2^2 + \frac{\delta a_{22}}{\delta \varphi_1}\dot{\varphi}_1\dot{\varphi}_2 - \frac{1}{2}\frac{\delta a_{11}}{\delta \varphi_2}\dot{\varphi}_1^2 + \\ &+ \frac{\delta a_{12}}{\delta \varphi_1}\dot{\varphi}_1^2 = Q_2(\varphi_1; \varphi_2; \dot{\varphi}_1; \dot{\varphi}_2) + A_2\lambda. \end{aligned} \quad (20)$$

We obtain the equation of disturbed motion. Using (15), limiting ourselves to terms of lower orders and omitting transformations, we have the following equations:

- for stationary movement

$$\begin{aligned} &\frac{1}{2}\frac{\delta a_{11}}{\delta \varphi_1} l_0 \dot{\varphi}_1^2(t) + \frac{\delta a_{11}}{\delta \varphi_2} l_0 \dot{\varphi}_1(t)\dot{\varphi}_2(t) + \\ &+ \frac{\delta a_{12}}{\delta \varphi_2} l_0 \dot{\varphi}_2^2(t) = Q_1 l_0 + A_1 l_0 \lambda_0, \end{aligned} \quad (21)$$

$$\begin{aligned} &\frac{1}{2}\frac{\delta a_{22}}{\delta \varphi_2} l_0 \dot{\varphi}_2^2(t) + \frac{\delta a_{22}}{\delta \varphi_1} l_0 \dot{\varphi}_1(t)\dot{\varphi}_2(t) + \\ &+ \frac{\delta a_{12}}{\delta \varphi_1} l_0 \dot{\varphi}_1^2(t) - \frac{1}{2}\frac{\delta a_{11}}{\delta \varphi_2} l_0 \dot{\varphi}_1^2(t) = Q_2 l_0 + A_2 l_0 \lambda_0. \end{aligned} \quad (22)$$

- for oscillations (in variations)

$$\begin{aligned} &a_{11} l_0 \ddot{q}_1 + a_{12} l_0 \ddot{q}_2 + \frac{\delta a_{11}}{\delta \varphi_1} l_0 \dot{\varphi}_1(t) l_0 \dot{q}_1 + \frac{\delta a_{11}}{\delta \varphi_2} l_0 \dot{\varphi}_2(t) l_0 \dot{q}_1 + \\ &+ \frac{\delta a_{11}}{\delta \varphi_2} l_0 \dot{\varphi}_1(t) l_0 \dot{q}_2 + 2\frac{\delta a_{12}}{\delta \varphi_2} l_0 \dot{\varphi}_2(t) l_0 \dot{q}_2 - \\ &- \frac{\delta a_{12}}{\delta \varphi_1} l_0 \dot{\varphi}_2(t) l_0 \dot{q}_2 = \frac{\delta Q_1}{\delta \varphi_1} l_0 q_1 + \frac{\delta Q_1}{\delta \varphi_2} l_0 q_2 + \frac{\delta Q_1}{\delta \dot{\varphi}_1} l_0 \dot{q}_1 + \\ &+ \frac{\delta Q_1}{\delta \dot{\varphi}_2} l_0 \dot{q}_2 + \frac{\delta A_1}{\delta \varphi_1} l_0 \lambda_0 q_1 + \frac{\delta A_1}{\delta \varphi_2} l_0 \lambda_0 q_2 + A_1 l_0 \lambda', \end{aligned}$$

$$\begin{aligned} &a_{12} l_0 \ddot{q}_1 + a_{22} l_0 \ddot{q}_2 + \frac{\delta a_{22}}{\delta \varphi_2} l_0 \dot{\varphi}_2(t) l_0 \dot{q}_2 + \frac{\delta a_{22}}{\delta \varphi_2} l_0 \dot{\varphi}_2(t) l_0 \dot{q}_1 + \\ &+ \frac{\delta a_{22}}{\delta \varphi_1} l_0 \dot{\varphi}_1(t) l_0 \dot{q}_2 + 2\frac{\delta a_{12}}{\delta \varphi_1} l_0 \dot{\varphi}_1(t) l_0 \dot{q}_1 + \\ &+ \frac{\delta a_{11}}{\delta \varphi_2} l_0 \dot{\varphi}_1(t) l_0 \dot{q}_1 = \frac{\delta Q_2}{\delta \varphi_1} l_0 q_1 + \frac{\delta Q_2}{\delta \varphi_2} l_0 q_2 + \frac{\delta Q_2}{\delta \dot{\varphi}_1} l_0 \dot{q}_1 + \\ &+ \frac{\delta A_2}{\delta \varphi_1} l_0 \lambda_0 q_1 + \frac{\delta A_2}{\delta \varphi_2} l_0 \lambda_0 q_2 + A_2 l_0 \lambda'. \end{aligned}$$

We divide the generalized forces into two categories. To the first, we refer the forces that have potential (Π), to the second – all dissipative ones (Φ)

$$\Pi = \frac{1}{2}\left(b_{11}\varphi_1^2 + 2b_{12}\varphi_1\varphi_2 + b_{22}\varphi_2^2\right),$$

$$\Phi = \frac{1}{2}\left(l_{11}\varphi_1^2 + 2l_{12}\varphi_1\varphi_2 + l_{22}\varphi_2^2\right).$$

Then

$$Q_1 l_0 = -\frac{\delta\Pi}{\delta\varphi_1}l_0 - \frac{\delta\Phi}{\delta\dot{\varphi}_1}l_0;\quad Q_2 l_0 = -\frac{\delta\Pi}{\delta\varphi_2}l_0 - \frac{\delta\Phi}{\delta\dot{\varphi}_2}l_0;$$

$$\frac{\delta Q_1}{\delta\varphi_1}l_0 = -\frac{\delta^2\Pi}{\delta\varphi_1^2}l_0;\quad \frac{\delta a_1}{\delta\varphi_2}l_0 = \frac{\delta Q_2}{\delta\varphi_1}l_0 = \frac{\delta^2\Pi}{\delta\varphi_1\delta\varphi_2};$$

$$\frac{\delta Q_2}{\delta\varphi_2}l_0 = -\frac{\delta^2\Pi}{\delta\varphi_2^2}l_0;\quad \frac{\delta Q_2}{\delta\dot{\varphi}_1}l_0 = -\frac{\delta^2\Phi}{\delta\dot{\varphi}_1^2}l_0;$$

$$\frac{\delta Q_1}{\delta\dot{\varphi}_2}l_0 = \frac{\delta Q_2}{\delta\dot{\varphi}_1}l_0 = -\frac{\delta^2\Phi}{\delta\dot{\varphi}_1\delta\dot{\varphi}_2}l_0;\quad \frac{\delta Q_2}{\delta\dot{\varphi}_2}l_0 = -\frac{\delta^2\Phi}{\delta\dot{\varphi}_2^2}l_0.$$

If we introduce a double notation, then the equations of small oscillations of the system under consideration with respect to stationary motion can be written in the form:

$$\begin{aligned}
&a_{11}\ddot{q}_1 + a_{12}\ddot{q}_2 + \left(l_{11} + \tilde{l}_{11}\right)\dot{q}_1 + l_{12}\dot{q}_2 + \tilde{\gamma}_1 q_2 + \\
&+\left(b_{11} + b'_{11}\right)q_1 + \left(b_{12} + b'_{12}\right)q_2 = A_1 l_0\lambda', \\
&a_{12}\ddot{q}_1 + a_{22}\ddot{q}_2 + l_{12}\ddot{q}_1\left(l_{22} + \tilde{l}_{22}\right)\dot{q}_2 + \tilde{\gamma}_2 q_1 + \\
&+\left(b_{12} + b'_{21}\right)q_1 + \left(b_{22} + b'_{22}\right)q_2 = A_2 l_0\lambda',
\end{aligned} \tag{23}$$

where

$$a_{11} = a_{11}l_0;\ a_{12} = a_{12}l_0;\ a_{22} = a_{22}l_0;\ l_{11} = -\frac{\delta Q_1}{\delta\dot{\varphi}_1}l_0;\ l_{22} = -\frac{\delta Q_2}{\delta\dot{\varphi}_2}l_0;$$

$$l_{12} = -\frac{\delta Q_1}{\delta\dot{\varphi}_2}l_0;\ l_{21} = -\frac{\delta Q_2}{\delta\dot{\varphi}_1}l_0;\ \tilde{l}_{11} = \frac{\delta a_{11}}{\delta\varphi_1}l_0\dot{\varphi}_1 + \frac{\delta a_{11}}{\delta\varphi_2}l_0\dot{\varphi}_2;$$

$$\tilde{l}_{22} = \frac{\delta a_{22}}{\delta\varphi_2}l_0\dot{\varphi}_2 + \frac{\delta a_{11}}{\delta\varphi_1}l_0\dot{\varphi}_1;\ \tilde{\gamma}_1 = \frac{\delta a_{11}}{\delta\varphi_2}l_0\dot{\varphi}_1 + 2\frac{\delta a_{12}}{\delta\varphi_2}l_0\dot{\varphi}_2 - \frac{\delta a_{22}}{\delta\varphi_1}l_0\dot{\varphi}_1;$$

$$\tilde{\gamma}_2 = \frac{\delta a_{11}}{\delta\varphi_2}l_0\dot{\varphi}_2 + 2\frac{\delta a_{22}}{\delta\varphi_1}l_0\dot{\varphi}_1 + \frac{\delta a_{22}}{\delta\varphi_1}l_0\dot{\varphi}_2;\ b_{12} = \frac{\delta Q_1}{\delta\varphi_2}l_0 = -\frac{\delta Q_2}{\delta\varphi_1}l_0;$$

$$b_{11} = -\frac{\delta Q_1}{\delta\varphi_1}l_0;\ b_{22} = -\frac{\delta Q_2}{\delta\varphi_2}l_0;\ b'_{11} = \frac{\delta A_1}{\delta\varphi_1}l_0\lambda_0;\ b'_{12} = \frac{\delta A_1}{\delta\varphi_2}l_0\lambda_0;$$

$$b'_{21} = \frac{\delta A_2}{\delta\varphi_1}l_0\lambda_0;\ b'_{22} = \frac{\delta A_2}{\delta\varphi_2}l_0\lambda_0.$$

In this case, the terms $l_{11}\dot{q}_1$, $l_{12}\dot{q}_2$, $l_{22}\dot{q}_2$ have the form of dissipative forces, although they are not connected with the dissipative function. The terms $\tilde{\gamma}_1\dot{q}_2$ и $\tilde{\gamma}_2\dot{q}_1$ are "gyroscopic" forces силы $\left|\tilde{\gamma}_1\right| = \left|\tilde{\gamma}_2\right| = \gamma$.

Then, after a series of transformations, the equations in variations can be written in the form

$$\begin{aligned}
&a_{11}\ddot{q}_1 + a_{12}\ddot{q}_2 + \left(l_{11} + \tilde{l}_{11}\right)\dot{q}_1 + \left(l_{12} + \tilde{l}_{12}\right)\dot{q}_2 + \\
&+\gamma\dot{q}_2 + \left(b_{11} + b'_{11}\right)q_1 + \left(b_{12} + b'_{12}\right)q_2 = A_1 l_0\lambda',
\end{aligned} \tag{24}$$

$$\begin{aligned}
&a_{12}\ddot{q}_1 + a_{22}\ddot{q}_2 + \left(l_{12} + \tilde{l}_{22}\right)\dot{q}_1 + \left(l_{22} + \tilde{l}_{22}\right)\dot{q}_2 - \\
&-\gamma\dot{q}_1 + \left(b_{12} + b'_{21}\right)q_1 + \left(b_{22} + b'_{22}\right)q_2 = A_2 l_0\lambda'.
\end{aligned} \tag{25}$$

We obtain the value λ_0 using equations (21) or (22) and assume it to be known. Since in the above two equations (24) and (25) there are three unknown values – q_1, q_2 и λ', it is necessary to add the nonholonomic coupling equation to them (16), replacing the variables in it with their variations

$$\begin{aligned}
&\dot{\varphi}_1\frac{\delta A_1}{\delta\varphi_1}l_0 q_1 + \dot{\varphi}_1\frac{\delta A_1}{\delta\varphi_2}l_0 q_2 + \dot{\varphi}_2\frac{\delta A_2}{\delta\varphi_1}l_0 q_1 + \\
&+\dot{\varphi}_2\frac{\delta A_2}{\delta\varphi_2}l_0 q_2 + + A_1 l_0\dot{q}_1 + A_2 l_0\dot{q}_2 = 0.
\end{aligned} \tag{26}$$

To determine the expansion terms of the lowest orders λ', which are equal to $\lambda' = \sum_{j=1}^{n}\frac{\delta\lambda}{\delta\varphi_j}l_0 q_0 + \sum_{j=1}^{n}\frac{\delta\lambda}{\delta\varphi_j}l_0 q_j,$, it is necessary to find an indefinite factor λ as the function of the coordinates and velocities of the system $\lambda = \lambda\left(\varphi_j;\ \dot{\varphi}_j\right)$. To do this, it is necessary to differentiate the nonholonomic coupling equation (6) $\frac{d}{dt}\left(\sum_{j=1}^{n}A_{vj}q_j + a_v\right) = 0.$

Transforming (19) and (20) to the form $\ddot{\varphi}_1 = \frac{Q_1 + A_1\lambda}{a_{11}}$, $\ddot{\varphi}_2 = \frac{Q_2 + A_2\lambda}{a_{22}}$, and substituting them in (10), we express $\lambda = \lambda\left(\varphi_j;\ \dot{\varphi}_j\right)$, which expands into a Taylor series with the definition of the expansion terms of the lowest orders.

To draw up the equations of motion of the belt contour as an autonomous drive system, it is necessary to determine the kinetic and potential energy of the system.

Kinetic energy:

- for the drive pulley

$$T_1 = \frac{1}{2}J_1\dot{\varphi}_1^2,$$

- for driven pulley

$$T_2 = \frac{1}{2}J_2\dot{\varphi}_2^2,$$

where J_1 и J_2 are respectively the reduced moments of inertia of the driving and driven pulleys.

On the other hand, in the accepted notation

$$T_1 = \frac{1}{2}a_{11}\dot{\varphi}_1^2;\ T_2 = \frac{1}{2}a_{22}\dot{\varphi}_2^2.$$

We define potential energy as

$$\Pi = \frac{C_\varphi\left(\varphi_1 - \varphi_2\right)^2}{2},$$

where C_φ is the torsional stiffness of the transmission.

Since the influence of elastic slip on the relative rotation of the pulleys is several times higher than the deformations of the belt legs, the value C_φ will be set as depending on the value of resilient slip ξ

$$C_\varphi = \frac{M_2 l_0}{2\pi\xi}.$$

The angle of rotation of the driven pulley can be determined from the coupling equation (12), setting the angle of rotation of the driving pulley

doi.org/10.36773/1818-1112-2021-126-3-57-62

$$\varphi_2 I_0 = \frac{\dot{\varphi}_2}{\dot{\varphi}_1} I_0.$$

Since J_1 и J_2 do not depend on the angles of rotation of the FBD shafts, the equations of stationary motion (21) and (22) will take the form

$$Q_1 I_0 + A_1 I_0 \lambda_0 = 0,$$
$$Q_2 I_0 + A_2 I_0 \lambda_0 = 0. \quad (27)$$

From the equation (27) we find λ_0

$$Q_1 I_0 = -\frac{\delta\Pi}{\delta\varphi_1} I_0 = C_\varphi \left(\varphi_1 - \varphi_2 + \frac{\dot{\varphi}_2^2 \varphi_1}{\dot{\varphi}_1^2} \right) A_1 I_0 = \varphi_2 I_0,$$

$$\lambda_0 = \frac{Q_1}{A_1} I_0 = C_\varphi \left(\frac{\varphi_1}{\varphi_2} - 1 + \frac{\varphi_2}{\varphi_1} \right) I_0.$$

The equations in variations (24) and (25) for the belt drive at $J_1 = \text{const}$ и $J_2 = \text{const}$ will assume the form

$$a_{11}\ddot{q}_1 + l_{11}\ddot{q}_1 + l_{12}\ddot{q}_2 + \gamma q_2 + (b_{11} + b'_{11}) q_1 + \\ + (b_{12} + b'_{12}) q_2 = A_1 I_0 \lambda', \quad (28)$$

$$a_{22}\ddot{q}_2 + l_{12}\ddot{q}_1 + l_{22}\ddot{q}_2 + (b_{12} + b'_{21}) q_1 + \\ + (b_{22} + b'_{22}) q_2 = A_2 I_0 \lambda'. \quad (29)$$

We reveal the values of the terms on the left-hand sides of the equations (28) and (29)

$$l_{11} = C_\varphi \left(\frac{\varphi_2}{\dot{\varphi}_2} + \frac{\varphi_2}{\varphi_1} - \frac{\dot{\varphi}_2^2 \varphi_1}{\dot{\varphi}_1^4} \right) I_0 = C_\varphi N_1 I_0,$$

$$l_{12} = C_\varphi \left(-\frac{\varphi_1}{\dot{\varphi}_2^2} - \frac{\varphi_1}{\dot{\varphi}_1} + \frac{2\varphi_2}{\dot{\varphi}_1} \right) I_0 = C_\varphi N_2 I_0,$$

$$b_{11} = C_\varphi \left(1 - \frac{\dot{\varphi}_2}{\dot{\varphi}_1} + \frac{\dot{\varphi}_2^2}{\dot{\varphi}_1^2} \right) I_0 = C_\varphi N_3 I_0.$$

$$b'_{11} = 0; \quad b_{12} = C_\varphi \left(\frac{\dot{\varphi}_1}{\dot{\varphi}_2} - 1 + \frac{\dot{\varphi}_2}{\dot{\varphi}_1} \right) I_0 = C_\varphi N_4 I_0,$$

$$b'_{12} = \lambda_0; \quad l_{22} = C_\varphi \left(-\frac{\varphi_1 \dot{\varphi}_1}{\dot{\varphi}_2^3} + \frac{\varphi_1}{\dot{\varphi}_2} + \frac{\varphi_1}{\dot{\varphi}_1} \right) I_0 = C_\varphi N_5 I_0, \quad (30)$$

$$b_{22} = C_\varphi \left(-\frac{\dot{\varphi}_1^2}{\dot{\varphi}_2^2} - \frac{\dot{\varphi}_1}{\dot{\varphi}_2} + 1 \right) I_0 = C_\varphi N_6 I_0,$$

$$b'_{21} = -\lambda_0, \quad b'_{22} = 0.$$

In what follows, for simplicity of notation, the index "0" will be omitted, i.e. $\lambda_0 = \lambda$.

Differentiating the nonholonomic coupling equation (17), we obtain

$$\ddot{\varphi}_2 = \frac{\varphi_2 - \ddot{\varphi}_1 - \dot{\varphi}_1 \dot{\varphi}_{20} + \dot{\varphi}_2 \dot{\varphi}_{10}}{\varphi_1}. \quad (31)$$

From the equations of stationary motion (21), we express φ_1 и φ_2, respectively

$$\ddot{\varphi}_1 = -\frac{C_\varphi}{J_1} \left(\varphi_1 - \varphi_2 + \frac{\varphi_2 \dot{\varphi}_2}{\dot{\varphi}_1} \right) + \frac{\varphi_2}{J_1} \lambda, \quad (32)$$

$$\ddot{\varphi}_2 = -\frac{C_\varphi}{J_2} \left(\frac{\varphi_1 \dot{\varphi}_1}{\dot{\varphi}_2} - \varphi_1 + \varphi_2 \right) - \frac{\varphi_1}{J_2} \lambda. \quad (33)$$

Substituting (32) and (33) into (31), we obtain

$$\lambda = k_1 q_1 + k_2 q_2 + k_3 \dot{q}_1 + k_4 \dot{q}_2.$$

Expanding (18) in a Taylor series and discarding higher-order terms, we obtain

$$\lambda = \frac{\frac{C_\varphi}{J_2} \left(\frac{\varphi_1 \dot{\varphi}_1}{\dot{\varphi}_2} - \varphi_1 + \varphi_2 \right) - \frac{C_\varphi \varphi_2}{J_1 \varphi_1} \left(\varphi_1 - \varphi_2 + \frac{\varphi_2 \dot{\varphi}_2}{\dot{\varphi}_1} \right) - \frac{\dot{\varphi}_1 \dot{\varphi}_{20}}{\varphi_1} + \frac{\dot{\varphi}_2 \dot{\varphi}_{10}}{\varphi_1}}{\frac{\varphi_2^2}{J_1 \varphi_1} + \frac{\varphi_1}{J_2}}, \quad (34)$$

where

$$k_1 = \frac{\frac{C_\varphi}{J_2} \left(\frac{\dot{\varphi}_1}{\dot{\varphi}_2} - 1 + \frac{\dot{\varphi}_2}{\varphi_1} \right) + \frac{C_\varphi \varphi_2}{J_1 \varphi_1} \left(1 - \frac{\dot{\varphi}_2}{\dot{\varphi}_1} - \frac{\varphi_2^2}{\varphi_1^2} \right) + \frac{\dot{\varphi}_1 \dot{\varphi}_{20}}{\varphi_1} - \frac{\varphi_2 \varphi_{10}}{\varphi_1^2}}{\frac{1}{J_2} - \frac{\varphi_2^2}{J_1 \varphi_1^2}},$$

$$k_2 = \frac{\frac{C_\varphi}{J_2} \left(-\frac{\varphi_1^2}{\varphi_2^2} + 1 + \frac{\dot{\varphi}_1}{\dot{\varphi}_2} \right) - \frac{C_\varphi}{J_1 \varphi_1} \left(\frac{\dot{\varphi}_1}{\dot{\varphi}_2} - 1 + \frac{\dot{\varphi}_2}{\varphi_1} \right) + \frac{\dot{\varphi}_2 \dot{\varphi}_{20}}{\varphi_2^2} + \frac{\dot{\varphi}_1 \dot{\varphi}_{10}}{\varphi_1^2}}{\frac{2\varphi_2}{J_1 \varphi_1} + \frac{\varphi_1}{J_2 \varphi_2}},$$

$$k_3 = \frac{\frac{C_\varphi}{J_2} \left(\frac{\varphi_1}{\dot{\varphi}_2} - \frac{\varphi_2}{\dot{\varphi}_2} - \frac{\dot{\varphi}_2 \dot{\varphi}_1}{\dot{\varphi}_1^2} \right) + \frac{C_\varphi \varphi_2}{J_1 \dot{\varphi}_1^2} \left(\frac{\varphi_2}{\dot{\varphi}_2} - \frac{\dot{\varphi}_2 \varphi_1}{\dot{\varphi}_1^2} - \frac{\varphi_2 \dot{\varphi}_2}{\dot{\varphi}_1^2} \right) - \frac{\dot{\varphi}_{20}}{\varphi_1} + \frac{\varphi_2 \dot{\varphi}_{10}}{\varphi_1^2}}{\frac{\varphi_2}{J_2 \dot{\varphi}_2} - \frac{\varphi_2 \dot{\varphi}_2}{J_1 \dot{\varphi}_1^2}},$$

$$k_4 = \frac{\frac{C_\varphi}{J_2} \left(\frac{\varphi_1 \dot{\varphi}_1}{\dot{\varphi}_2} + \frac{\varphi_2 \dot{\varphi}_1}{\dot{\varphi}_2} + \frac{\varphi_1}{\dot{\varphi}_1} \right) - \frac{C_\varphi}{J_1 \varphi_1} \left(-\frac{\varphi_2 \dot{\varphi}_1}{\dot{\varphi}_2^2} - \frac{\varphi_1}{\dot{\varphi}_1} + \frac{\varphi_2}{\dot{\varphi}_1} \right) - \frac{\dot{\varphi}_{20}}{\varphi_2} + \frac{\dot{\varphi}_{10}}{\varphi_1}}{\frac{2\varphi_1 \dot{\varphi}_2}{J_1 \dot{\varphi}_2^2} - \frac{\varphi_2 \varphi_1^2}{J_2 \dot{\varphi}_1^2}}.$$

After substituting the obtained coefficients (30) into the equations (28) and (29), taking into account (34), we will obtain

$$J_1 \ddot{q}_1 + C_\varphi N_1 \dot{q}_1 + C_\varphi N_2 q_2 + C_\varphi N_3 q_1 + \left(C_\varphi N_4 + \lambda_0 \right) q_2 = \\ = A_1 \left(k_1 q_1 + k_2 q_2 + k_3 \dot{q}_1 + k_4 \dot{q}_2 \right), \quad (35)$$

$$J_2 \ddot{q}_2 + C_\varphi N_3 \dot{q}_1 + C_\varphi N_5 q_2 + \left(C_\varphi N_4 - \lambda_0 \right) q_1 + C_\varphi N_6 q_2 = \\ = A_2 \left(k_1 q_1 + k_2 q_2 + k_3 \dot{q}_1 + k_4 \dot{q}_2 \right). \quad (36)$$

To the obtained equations of motion (35) and (36), it is necessary to add a nonholonomic coupling equation in variations, which, taking into account (26), will have the form

$$\dot{\varphi}_1 q_2 - \dot{\varphi}_2 q_1 + \varphi_2 \dot{q}_1 - \varphi_1 \dot{q}_2 = 0.$$

For the joint solution of (35) and (36), it is necessary to determine from the coupling equation in variations the variation of the coordinate q_1, equal to $q_1 = \frac{\dot{\varphi}_1 q_2 - \varphi_2 \dot{q}_1 - \varphi_1 \dot{q}_2}{\dot{\varphi}_2}$ and substitute it into the equation of motion of the driven pulley (36).

Similarly, the deduced coordinate variation must be substituted into the equation of motion of the driving pulley (35).

Omitting the transformations, having performed these operations and made the adduction of similar terms, we obtain an FBD analytical model for torsional vibrations, i.e. equation of small oscillations regarding stationary movement

$$\left.\begin{aligned} J_1\ddot{q}_1 + z_{11}\dot{q}_1 + z_{12}q_1 + z_{13}\dot{q}_2 = 0 \\ J_2\ddot{q}_2 + z_{21}\dot{q}_2 + z_{22}q_2 + z_{23}\dot{q}_1 = 0 \end{aligned}\right\}, \quad (37)$$

where

$$z_{11} = C_\varphi N_1 - \left(C_\varphi N_4 + \lambda_0\right)\frac{\varphi_2}{\dot{\varphi}_1} + \frac{\varphi_1\varphi_2 k_2}{\dot{\varphi}_1} - A_2 k_3,$$

$$z_{12} = C_\varphi N_3 + \left(C_\varphi N_4 + \lambda_0\right)\frac{\varphi_2}{\dot{\varphi}_1} + \frac{\varphi_1\varphi_2 k_2}{\dot{\varphi}_1} - A_2 k_1,$$

$$z_{13} = C_\varphi N_2 + \left(C_\varphi N_4 + \lambda_0\right)\frac{\varphi_1}{\dot{\varphi}_1} + \frac{\varphi_1^2 k_2}{\dot{\varphi}_1} - A_2 k_4,$$

$$z_{21} = C_\varphi N_5 - \left(C_\varphi N_4 - \lambda_0\right)\frac{\varphi_1}{\dot{\varphi}_2} + \frac{\varphi_1^2 k_1}{\dot{\varphi}_2} - A_2 k_4,$$

$$z_{22} = C_\varphi N_6 + \left(C_\varphi N_4 - \lambda_0\right)\frac{\dot{\varphi}_1}{\dot{\varphi}_2} + \frac{\varphi_1\dot{\varphi}_1 k_1}{\dot{\varphi}_2} - A_2 k_2,$$

$$z_{23} = C_\varphi N_2 - \left(C_\varphi N_4 - \lambda_0\right)\frac{\varphi_2}{\dot{\varphi}_2} + \frac{\varphi_1\varphi_2 k_1}{\dot{\varphi}_2} - A_2 k_3.$$

To study the stability of the FBD motion, it is required to solve a system of motion equations (37) or obtain a characteristic equation and solve its roots. We use the operator notation. The system (12) is transformed to the form

$$\left.\begin{aligned} \left(J_1 p^2 + z_{11}p + z_{12}\right)q_1 + z_{13}pq_2 = 0, \\ z_{23}pq_1 + \left(J_2 p^2 + z_{21}p + z_{22}\right)q_2 = 0 \end{aligned}\right\}.$$

As a result, a homogeneous system of linear algebraic equations was obtained. For its solution to be non-trivial, the determinant of this system must be equal to zero. Expanding the determinant, we obtain a characteristic equation of the system in operator form:

$$\begin{aligned} D_p = {} & J_1 J_2 p^4 + \left(J_2 z_{11} + J_1 z_{21}\right)p^3 + \\ & + \left(z_{11}z_{21} + J_1 z_{22} - z_{13}z_{23}\right)p^2 + \\ & + \left(J_2 z_{12} + z_{12}z_{21} + z_{11}z_{22}\right)p + z_{12}z_{22} = 0. \end{aligned} \quad (38)$$

In view of a significant complexity of calculating the roots of the characteristic equation of high orders, we will use the method of approximate calculation with the help of stability criteria. We use Mikhailov stability criterion [6]. This criterion envisages the use of a frequency hodograph $D(j\upsilon)$, which can be obtained from the characteristic equation at $p = j\upsilon$.

We replace p by $j\upsilon$ in polynomial (23) and select substantial and imaginary parts

$$D(j\nu) = U(\nu) + jV(\nu). \quad (39)$$

Taking into account (116), the expression (117) is transformed to the form

$$U(\nu) = J_1 J_2 p^4 - \left(z_{11}z_{21} + J_1 z_{22} - z_{13}z_{23}\right)\nu^2 + z_{12}z_{22},$$

$$V(\nu) = -\left(J_2 z_{11} + J_1 z_{21}\right)\nu^3 - \left(J_2 z_{12} + z_{12}z_{21} + z_{11}z_{22}\right)\nu.$$

The curve described by the end of the vector $D(j\upsilon)$ when the frequency changes from zero to infinity, is shown in accordance with Figure 2. It was obtained for the FBD of the RUVI kitchen machine with the parameters: J_1 = 0,009 Нмс^2; J_2 = 0,004 Нмс^2; D_1 = 18,5 мм; D_2 = 82,5 мм.

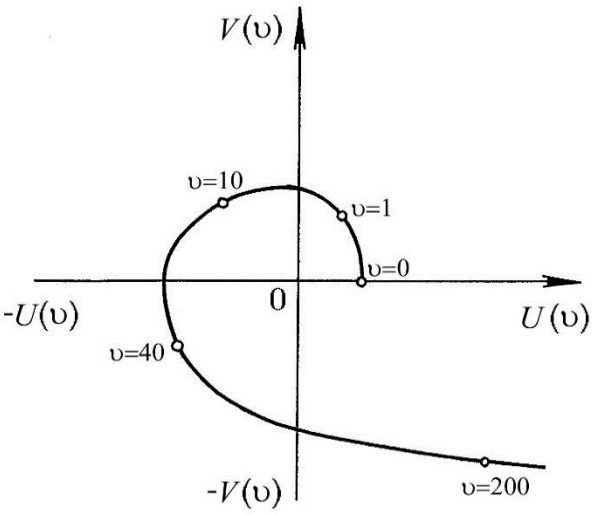

Figure 2 – Mihajlov Frequency hodograph for the transmission of power by friction type flexible link

Conclusions

The frequency hodograph begins on the positive part of the real axis and traverses four quadrants sequentially in the positive direction. Therefore, in accordance with Mikhailov's criterion, the dynamic system of the transmission under consideration is stable. The boundaries of the stability regions of the stationary motion of the FBD can be estimated by the decrease (loss) in the angular velocity of the driven pulley from the load. If, as is customary in the theory of belt drives [7-10], the loss of angular velocity is estimated by the value of the resilient slip coefficient, then a stable operation of the considered FBD under the condition $\xi \le 5\%$ will be observed at $2F_0 \ge 53{,}5\ N$. Thus, for increasing the stability of movement, the value of the belt pre-tension should not be less than the permissible values.

References

1. Skoybeda, A. T. Automation of running systems of wheeled machines / A. T. Skoybeda ; ed. V.V. Guskov. – Minsk : Science and Technology, 1979. – 280 p.
2. Panovko, Ya. G. Introduction to the theory of mechanical vibrations / Ya. G. Panovko. – Moscow : Nauka, 1971. – 304 p.
3. Rivin, E. N. Dynamics of machine tool drive / E. N. Rivin. – Moscow : Mechanical Engineering. – 1966. – 204 p.
4. Shchedrov, V. S. Fundamentals of flexible thread mechanics / V. S. Shchedrov. – Moscow : Nauka, 1980. – 238 p.
5. Dobronravov, V. V. Fundamentals of the mechanics of nonholonomic systems / V. V. Dobronravov. – Moscow : Higher School. – 1970. – 264 p.
6. Mathematical foundations of the theory of automatic regulation / B. K. Chemodanov [et al.]. – Moscow: Higher school, 1977. – Volume 2. – 455 p.
7. Skoybeda, A. T. Belt transmissions / A. T. Skoybeda, A. N. Nikonchuk. – Minsk : Science and Technology, 1995. – 383 p.
8. Tamulevich, G. D. Drive belts / G. D. Tamulevich, G. G. Bobylev. – Moscow : Chemistry, 1990. – 23 p.
9. Sokolovskaya, F. M. V-belts / F. M. Sokolovskaya, G. D. Tamulevich. – Moscow : Chemistry, 1973. – 160 p.
10. Vorobiev, I.I. Belt transmissions / I. I. Vorobiev. – Moscow : Mechanical Engineering, 1979. – 168 p.

Accepted 26.10.2021

UDC 621.793:66.088

THE TRIBOTECHNICAL CHARACTERISTICS OF DIAMOND-LIKE COATINGS FORMED BY HYBRID TECHNOLOGY

N. M. Chekan[1], Y. V. Auchynnikau[2], Y. I. Eysimont[3], V. M. Khvisevich[4], A. I. Verameychyk[5], D. S. Kolynov[6], G. A. Kostyukovich[7]

[1] Ph.D in Physical and Mathematical Sciences, Head of the Laboratory of Nanomaterials and Ion-Plasma Processes, State Scientific Institution "Physico-Technical Institute of the National Academy of Sciences of Belarus", e-mail: pec@bas-net.by
[2] Doctor of Technical Sciences, Associate Professor, Associate Professor of the Department of Logistics and Management Methods, Grodno State University named after Y. Kupala, Grodno, Belarus, e-mail: ovchin_1967@mail.ru
[3] Ph.D in Engineering, Associate Professor, Associate Professor of the Department of Logistics and Management Methods, Grodno State University named after Y. Kupala, Grodno, Belarus
[4] Ph.D in Engineering, Associate Professor, Professor of the Department of Applied Mechanics of Brest State Technical University, Brest, Belarus, e-mail: vmhvisevich@bstu.by
[5] Ph.D in Physics and Mathematics, Associate Professor, Senior Research Associate of Brest State Technical University Testing Center, Brest, Belarus, e-mail: vai_mrtm@bstu.by
[6] Consultant of LLC "Vikon-Auto", Chkalovsk, Nizhny Novgorod region, Russian Federation, e-mail: vikon_v@mail.ru
[7] Ph.D in Engineering, Professor of the Department of Materials Science and Resource-Saving Technologies, Grodno State University named after I. Kupala. Deputy Director of JSC "Belcard" for Development, Grodno, Belarus

Abstract

The use of low temperatures to improve the performance of steel products is a widely used technology in mechanical engineering. Another direction of increasing the efficiency of machine parts and mechanisms is the creation of thin-layer systems using vacuum technologies. The combination of these technological approaches made it possible to obtain antifriction vacuum superhard coatings with increased tribotechnical characteristics. The effect of increasing the wear resistance of hybrid coatings is the formation of nanodisperse structures in the steel substrate and coating, the decay of residual austenite, which leads to an increase in martensite in the structure of steel subjected to cold treatment, a significant change in the values of internal stresses in superhard coatings.

Keywords: diamond-like coating, cryogenic treatment, coefficient of friction, steel, wear resistance.

ТРИБОТЕХНИЧЕСКИЕ ХАРАКТЕРИСТИКИ АЛМАЗОПОДОБНЫХ ПОКРЫТИЙ, СФОРМИРОВАННЫХ ПО ГИБРИДНОЙ ТЕХНОЛОГИИ

Н. М. Чекан, Е. В. Овчинников, Е. И. Эйсымонт, В. М. Хвисевич, А. И. Веремейчик, Д. С. Колынов, Г. А. Костюкович

Реферат

Применение низких температур для повышения эксплуатационных характеристик стальных изделий является широко применяемой технологией в машиностроении. Другим направлением увеличения работоспособности деталей машин и механизмов является создание тонкослойных систем с применением вакуумных технологий. Сочетание данных технологических подходов позволило получить антифрикционные вакуумные сверхтвердые покрытия с повышенными триботехническими характеристиками. Эффект увеличения износостойкости гибридных покрытий заключается в образовании нанодисперсных структур в стальной подложке и покрытии, распадом остаточного аустенита, что приводит к увеличению мартенсита в структуре стали, подвергнутой обработке холодом, существенному изменению значений внутренних напряжений в сверхтвердых покрытиях.

Ключевые слова: алмазоподобное покрытие, криогенная обработка, коэффициент трения, сталь, износостойкость.

Introduction

There are various ways to impart surface strength. The most famous is the thermal hardening with high-speed heating and cooling of the laser beam or electron beam, treatment with plasma compression flows, leading to stirring of surface layers and administration of alloying additives [1–5]. However, from the point of view of vacuum methods of engineering of the surface, the surface treatment with bunches of nitrogen ions is the most profitable. Almost all modern sets of physical precipitation of coatings from the steam phase are equipped with sources of argon ions for precleaning and activating the surface before applying coatings. This means that there is already a necessary toolkit for the implementation of ion-beam nitriding. In this case, the single vacuum technological cycle of applying solid coatings is not disturbed. This is the great advantage of the method being developed.

Simple and effective way is the modification of the structure of materials by cryogenic processing. The sharp cooling of the surface layers leads to significant temperature gradients, which in turn causes the appearance of high compressive stresses. Such treatment is important for structural steels, which temperature of the end of martensitic transformations is significantly lower than room temperature. Transformation of residual austenite in martensite, as well as the appearance of a significant amount of dislocations leads in some cases to crushing the grain and a significant increase in surface hardness. In this case, the depth of the modified layer is several hundred micrometers [2]. As a result of cryogenic effects, nanodisperic phases are formed in the modifiable material.

The hardness of vacuum coatings increases by the formation of an ultrafine structure characteristic of thin-layer vacuum coatings. In the process of creating low-dimensional structural formations, it is necessary to consider the change in the thermodynamic properties of coatings, which, ultimately, can change phase fields on the status diagrams. One of the main tasks in the formation of thin-layer coatings in the field of mechanical engineering is to increase their physical and mechanical properties, which makes it possible to increase the operational resource of the processing tool. This is achieved by studying the peculiarities of the transformation of the coating structure of refractory compounds at high temperatures. The study of crystallization processes, recrystallization of carbonitrides, nitrides, carbides, including in thin-layer systems, is a priority in the field of surface engineering.

The aim of the present work was to study the influence of the processes of the hybrid technology of hardening metal surfaces on the tribotechnical characteristics of obtained nanocomposition coatings.

The technique of experiment

The application of composite coatings based on titanium nitride was carried out on a vacuum installation UVNIPA-1-001, equipped with a cathode-arc evaporator with a plasma electromagnetic filtering system,

doi.org/10.36773/1818-1112-2021-126-3-63-67

as well as an ion source II-4-0.15. H11steel was usedas a substrate. The surface of the substrates from steels was hardened and grinding to cleanliness not lower than grade 11. Before applying of the coatings the surface of the sample was cleaned and heatedby titanium ions under such conditions: the evaporator current 105–110 A; the potential on the sample 1,0 kV. The coating precipitation was carried out at a current of the stabilizing coil of 1,7 A, the current of the control coil 2,0 A and the current of the arc 90 A. The pressure of the reaction gas (nitrogen) was within $(0{,}87\text{-}5)\times10^{-2}$ Pa. During the deposition of the coating on the substrate, the displacement voltage was supplied from -50 V to -100 V. Pre-processing of metal substrates in liquid nitrogen was carried out at a boiling point of liquid nitrogen (-195,6 °C), processing time was 30 minutes – 72 hours. Coatingsformed on activated substrates were exposed by cryogenic liquids at a temperature of -195,6 ° C in the time range from 30 minutes to 72 hours.

Tribotechnical studies were carried out on the friction machine FT-2 (Microtestmachines Co.), which operates according to the "Finger-Disk" scheme by dry friction of three spherical samples D = 1,5 mm on a flat surface of the disk (counter body), made of steel and polished on a flat surfaces usingabrasive paper or grinding paste to the average arithmetic deviation of the surface profile Ra = 0,1-0,3 μm. The tests were carried out at a normal load from 20 H to 100 H and a linear slide speed of 0,1-0,5 m/s. The tribotechnical characteristics for a "diamond-coating" pair were determined on the device J&L TEX.

Research results

The requirement of increased strength of mechanical components, which are used in heavily-grooved conditions and at high slip velocity led to the creation of materials for coatings with high hardness to ensure greater wear resistance of modifiedbodies [3]. Due to the high tribotechnical characteristics of carbon-based coating, widespread use for modifying products used in mechanical engineering: bearings, gears, sleeves and other components of transmissions, machines, automotive units [4]. According to classical representations, there are two main types of carbon coating: diamond-like carbon [5] and ceramic coatings [6]. Ceramic materials with high hardness and Jung modules as coatings for steel parts are widely used to ensure resistance to abrasive wear. Coatings on the basis of diamond-like carbon (DLC), on the other hand, provide low coefficients of friction, as well as high wear resistance by friction in a pair with steel counter bodies [7]. Typically, the friction coefficient values of DLC are in the range from 0,01 to 0,5, depending on the type of coating and conditions of testing conditions [8].

DLCare usually amorphous, consisting of different phases with sp^2 and sp^3-hybridized C-C and C-H bonds. In the process of friction, in particular, in the process of sliding, local or general heating of the rubbing body with a coating occurs, as a result of which sp^2-hybridized carbon bonds can form a graphite-like tribolayer, which can reduce and/or stabilize the process of friction of the contacting bodies. In case of inobservance of technological regimes of the DLC coatings precipitation in the coating structurethe formation of cracks and delamination of coatings from the substrate can be observed due to the presence of high internal stresses in the coating [9].

Diamond-like coatings (DLC) containing hydrogen in their structure are thermally unstable and can be transformed into graphite when heated over 300°C. This process of the complete transition of the DLC to graphite in air occurs at a temperature of 450–600°C [9].

To increase the thermal, tribotechnical characteristics, various non-metallic materials such as: silicon (Si), fluorine (F), nitrogen (N), as well as metals chrome (Cr), titanium (Ti) and tungsten (W) are introduced into the DLC. The introduction of non-metallic materials improves the mechanical properties of the coating (N, Si). Thus, the introduction of fluorine into the structure of the coating allows to change the surface energy [10].

The introduction of metals in the DLC leads to the formation of nanocrystals, usually carbides of metal. These formations are statistically distributed over the volume of the coating matrix.Uniform distribution over the volume of the coating and low-dimensional geometric characteristics of the formations significantly reduces the internal residual stresses in the coating.

Conducted research show that a perspective direction for modifying diamond-like coatings may be a hybrid technology consisting in the preliminary modification of the steel substrate in a cryogenic medium, the formation of a diamond-like coating and the subsequent processing of this system at a low temperature.

The studies show the change in the tribological characteristics of the DLC of coatings formed according to this technology (Figures 1–5).

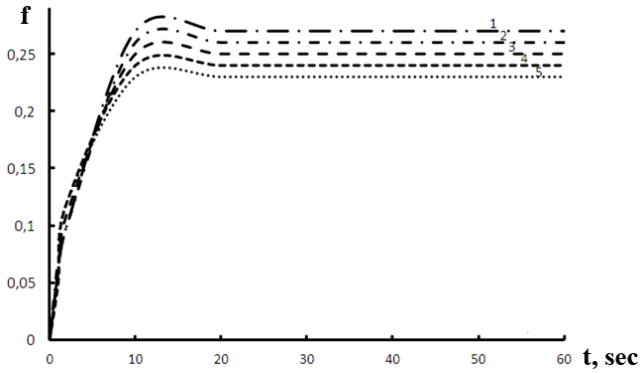

The substrate of steel H11 was subjected to pretreatment in liquid nitrogen: 1 – source substrate; 2 – during 60 min; 3 – during 180 min; 4 – during 1440 min; 5 – during 4320 min. V = 0.1 m/s, load 30 H, counterbody – steel 52100

Figure 1 – Dependence of the coefficient of friction of the diamond-like coating formed on steel H11 (1–5)

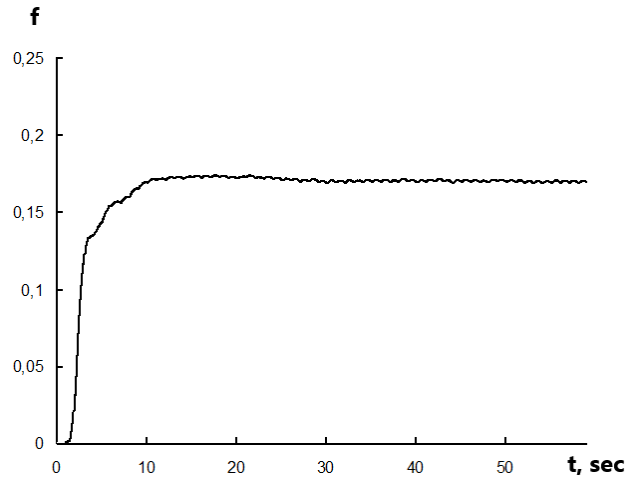

V = 0,1 m/s, load 30 H, counterbody – steel 52100

Figure 2 – Dependence of the coefficient of friction of a diamond-like coating formed on steel H11 and subjected to cryogenic processing for 30 minutes

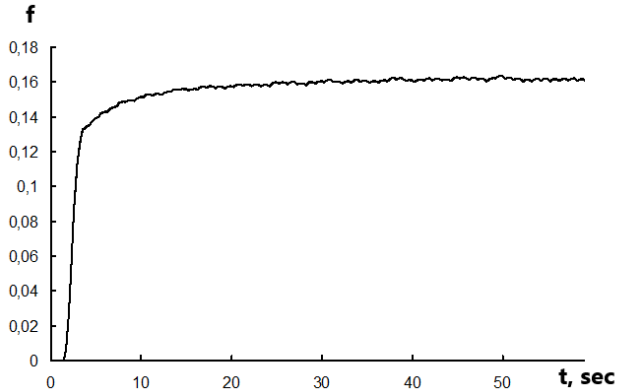

V = 0,1 m/s, load 30 H, counterbody – steel 52100. The substrate was subjected to pre-processing in liquid nitrogen for 60 minutes

Figure 3 – Dependence of the coefficient of friction of a diamond-like coating formed on steel H11 and subjected to cryogenic processing for 30 minutes

doi.org/10.36773/1818-1112-2021-126-3-63-67

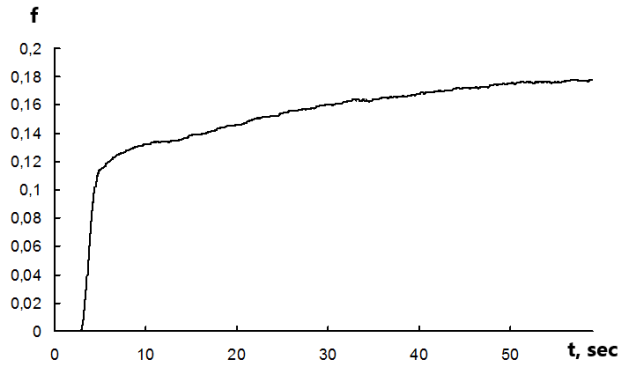

V = 0,1 m / s, load 30 H, counterbody- steel 52100. The substrate was subjected to pre-processing in liquid nitrogen for 4320 min

Figure 4 – Dependence of the friction coefficient of a diamond-like coating formed on steel H11 and subjected to cryogenic processing for 30 minutes

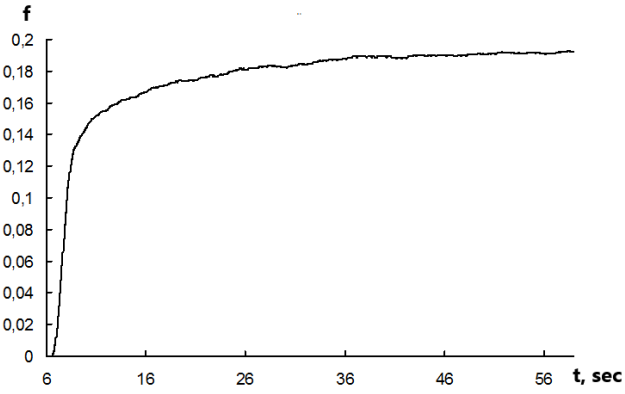

V = 0,1 m/s, load 30 H, counterbody – steel 52100

Figure 5 – Dependence of the coefficient of friction of the diamond-like coating formed on the steel H11 and subjected to cryogenic processing to 60 minutes

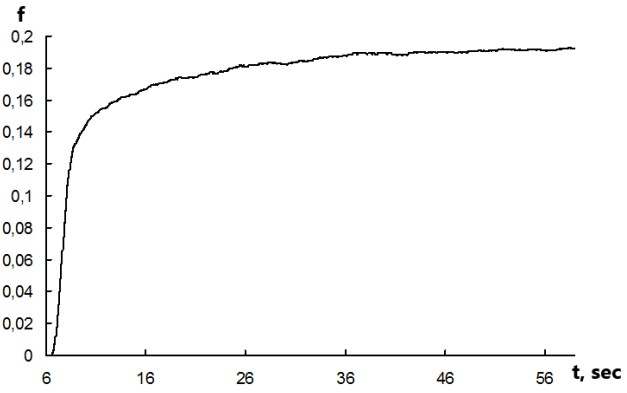

V = 0,1 m/s, load 30 H, counterbody – Steel 52100. The substrate was subjected to pre-processing in liquid nitrogen for 60 minutes

Figure 6 – Dependence of the coefficient of friction of a diamond-like coating formed on steel H11 and subjected to cryogenic processing for 60 minutes

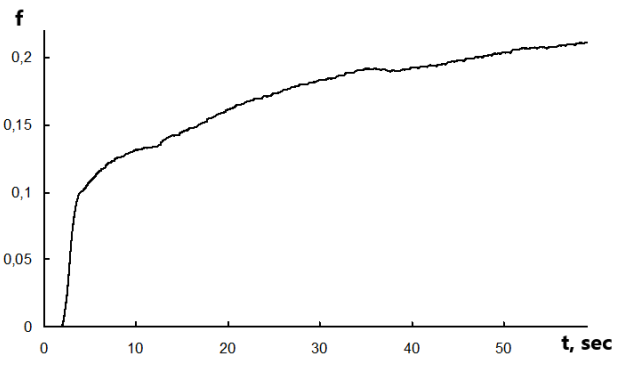

V = 0,1 m/s, load 30 H, counterbody – Steel H11. The substrate was subjected to pre-treatment in liquid nitrogen for 180 minutes

Figure 7 – Dependence of the coefficient of friction of a diamond-like coating formed on steel 52100 and subjected to cryogenic processing for 60 minutes

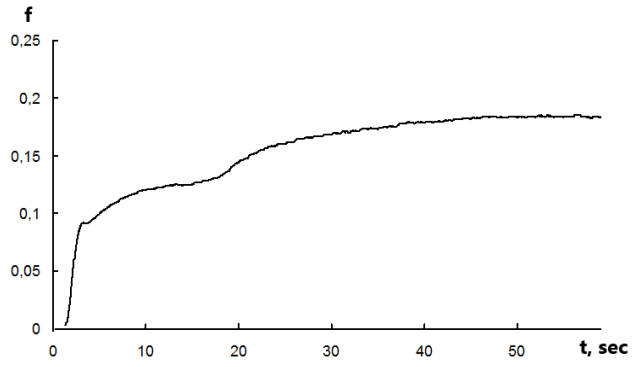

V = 0,1 m/s, load 30 H, counterbody – Steel 52100. The substrate was subjected to pretreatment in liquid nitrogen for 1440 minutes

Figure 8 – Dependence of the coefficient of friction of the diamond-like coating formed on steel H11 and subjected to cryogenic processing to 60 minutes

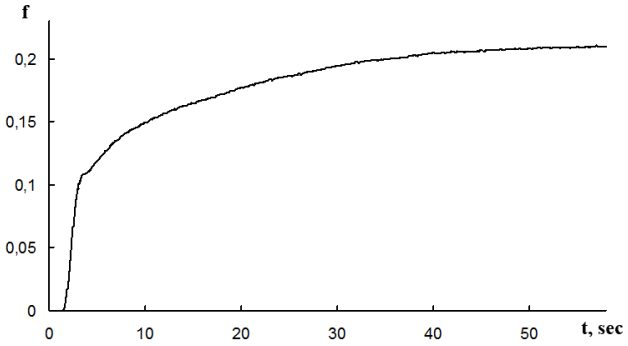

V = 0,1 m/s, load 30 H, counterbody – Steel 52100. The substrate was subjected to pre-processing in liquid nitrogen for 4320 min

Figure 9 – Dependence of the coefficient of friction of a diamond-like coating formed on steel H11 and subjected to cryogenic processing for 60 minutes

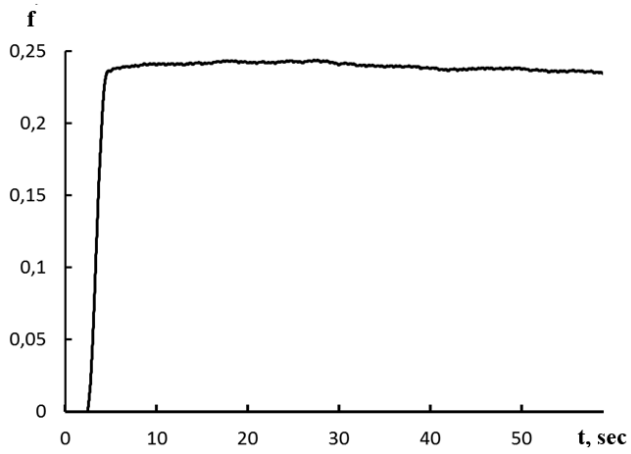

V = 0,1 m/s, load 30 H, counterbody – Steel 52100. The substrate was subjected to pre-treatment in liquid nitrogen for 180 minutes

Figure 10 – Dependence of the coefficient of friction of the diamond-like coating formed on steel H11 and subjected to cryogenic processing for 180 minutes

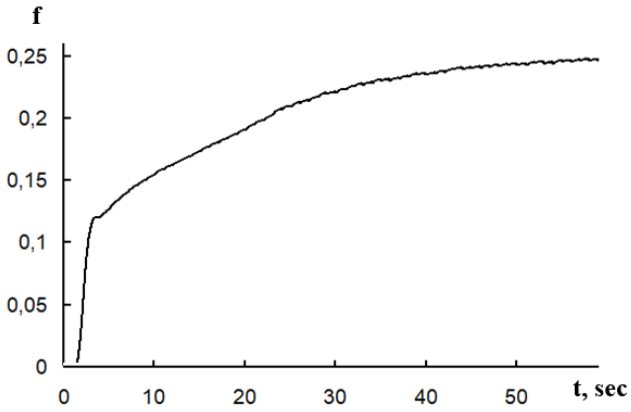

V = 0,1 m/s, load 30 H, counterbody – Steel 52100. The substrate was subjected to pretreatment in liquid nitrogen for 1440 minutes

Figure 11 – Dependence of the coefficient of friction of a diamond-like coating formed on steel H11 and subjected to cryogenic processing for 180 minutes

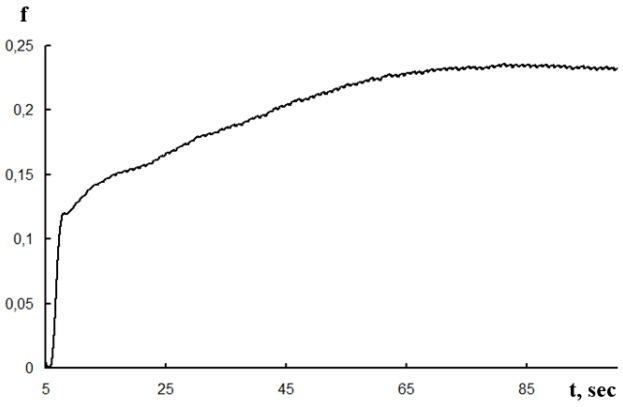

V = 0,1 m/s, load 30 H, counterbody – Steel 52100. The substrate was subjected to pre-processing in liquid nitrogen for 4320 min

Figure 12 – Dependence of the coefficient of friction of a diamond-like coating formed on steel H11 and subjected to cryogenic processing for 180 minutes

A general tendency associated with the tribotechnical characteristics of diamond-like coatings is the increase in the friction coefficient in hybrid processing for the friction pair "modified diamond-like coating - Steel 52100". This effect can be explained on the basis of an increase in the SP^3-hybridization phase, which leads to an increase of the coating hardness and, as a result, increase the friction coefficient for the studied friction pair.

Based on the data obtained, it can be seen that the pretreatment of the steel substrate in the cryogenic medium leads to a certain decrease in the coefficient of friction of the pair "diamond-like coating-steel 52100". The value of reducing the valuesof the friction coefficient depends on the exposure time in the cryogenic liquid. It is possible to assume the next mechanism of the friction process flowing in the system "diamond-like coating - solid". At the initial stages of contacting the DLC surfaces and solid body, the wear of nanoirregularities of a softer solid body (SS) occurs due to the penetration of nano- and microroughnesses of the diamond-like coating into the surface layers of the SS, as a result of which plastic deformation of the mating surfaces occurs in the low-dimensional range and is accompanied by local plastic deformation, plastic flow of the material occurs in the contact zone. This process leads to an increase in the physicomechanical characteristics of rubbing surfaces. The formation of wear products of solid leads to the closure of microirregularities in surface layers of the counterbody and the beginning of the abrasive wear. This process is intensified as the temperature and friction force increases in the contact zone. At the same time, carbon diffusion occurs in the near-surface metal layers, there is an aliament of the source relief of the substrate and the formation of nano- and microcracks on it. Diffusion of carbon in the counterbody, the formation of carbon-containing friction products in the contact area leads to a decrease in the friction coefficient.

Pre-treatment of substrate at low temperatures and then the subsequent treatment at cryogenic temperatures leads to an increase in the microhardness of diamond-like coatings, and then, as a result, to the intensification of the above-described processes occurring during the friction of the modified DLC, which ultimately affects the increase in the wear resistance of coatings and reducing the friction coefficient. However, tribotechnical characteristics depend on the processing technology. An increase in carbon diffusion in the steel substrate leads to stabilization of friction force, smoothing the surface layers of both the DLC and the counterbody, which leads to a significant reduction in wear intensity. The lowest coefficient of friction is possessed by diamond-like coatings formed on a steel substrate pretreated in a cryogenic medium for 60 min, followed by treatment of the formed DLC in liquid nitrogen for 30 min.

The similar nature of the friction of the DLC, formed on a hybrid technology, is characteristic of the friction pair of "DLC-diamond" (Figures 13–18).

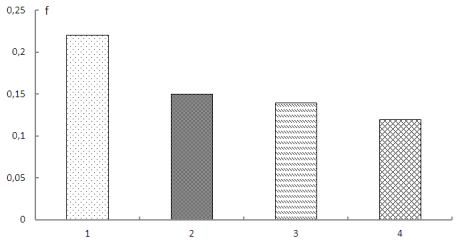

1 – initial steel; Steel is treated in a cryogenic medium for 60 min (2), 180 min (3), 4320 min (4). The friction coefficient was determined at the time of complete destruction of the diamond-like coating

Figure 13 – Dependence of the coefficient of friction of diamond-like coatings (a pair of friction "DLC-diamond") formed on the H11 steel substrate on the time of activation of the substrate in the cryogenic medium

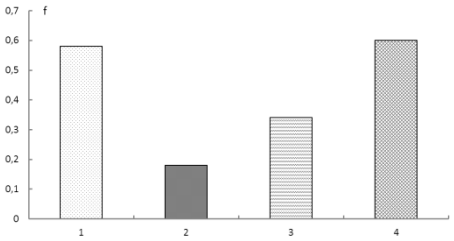

1 – initial steel; Steel is treated in a cryogenic medium for 60 min (2), 180 min (3), 4320 min (4). The friction coefficient was determined with the load on the indenter 20 H

Figure 14 – The dependence of the coefficient of friction of diamond-like coatings (the pair of friction "DLC -diamond") formed on the H11 steel substrate on the activation time of the substrate in the cryogenic medium

doi.org/10.36773/1818-1112-2021-126-3-63-67

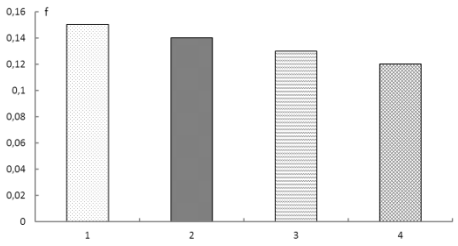

The coating was formed on the H11 steel substrate, which was activated in the cryogenic medium. 1 – initial steel; Steel is treated in a cryogenic medium for 60 min (2), 180 min (3), 4320 min (4). The friction coefficient was determined at the time of complete destruction of the diamond-like coating

Figure 15 – Dependence of the coefficient of friction of a diamond-like coating formed on H11 steel and cryogenic processing for 30 minutes, counterbody-diamond

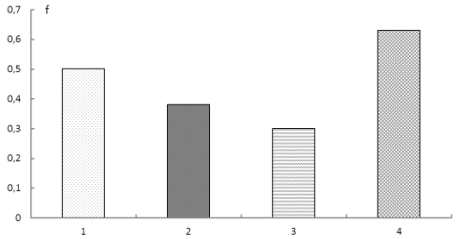

The coating was formed on the 4x5mfs steel substrate, which was activated in the cryogenic medium. 1 – initial steel; Steel is treated in a cryogenic medium for 60 min (2), 180 min (3), 4320 min (4). The friction coefficient was determined with the load on the indenter 20

Figure 16 – The dependence of the coefficient of friction of a diamond-like coating formed on H11steel and cryogenic processing for 30 minutes, counterbody-diamond

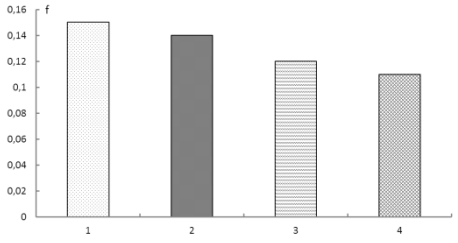

The coating was formed on the H11 steel substrate, which was activated in the cryogenic medium. 1 – initial steel; Steel is treated in a cryogenic medium for 60 min (2), 180 min (3), 1440 min (4). The friction coefficient was determined at the time of complete destruction of the diamond-like coating

Figure 17 – Dependence of the coefficient of friction of a diamond-like coating formed on H11 steel and cryogenic processing for 60 minutes, counterbody -diamond

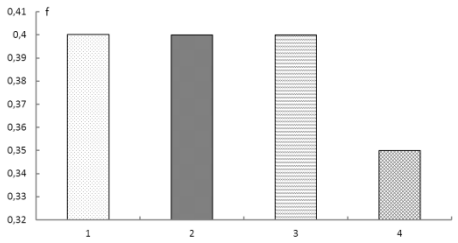

The coating was formed on the H11 steel substrate, which was activated in the cryogenic medium. 1 – initial steel; Steel is treated in a cryogenic medium for 60 min (2), 180 min (3), 1440 min (4). The friction coefficient was determined with the load on the indenter 20 H

Figure 18 – Dependence of the coefficient of friction of a diamond-like coating formed on steel H11 and cryogenic processing for 30 minutes, counter body-diamond

Conclusions

Conducting additional cryogenic processing of the "DLC- activated substrate" system affects the internal stresses in the coating structure. Taking into account the fact that the diamond-like coatings themselves are metastable systems with high internal stresses in the region 1–2 GPa, additional increase in the internal voltages values of the order of 80–500 MPa in the system "DLC – activated substrate" should result in further increase in the dispersion of structural components diamond-like coating and, as a result, to an increase in the physicomechanical characteristics of coatings (microhardness, adhesion strength).

Conducting hybrid treatment of diamond-like coatings leads to a decrease in the values of the friction coefficient and a decrease in the intensity of wear in the friction pairs "DLC – steel", "DLC-modified steel substrate".

References

1. Ermakov, B. S. Effect of magnetic transformations on the properties and destruction of austenitic steels at cryogenic temperatures / B. S. Ermakov, V. V. Prudnikova, S. A. Vologhjanina // The strength of materials and structures at low temperatures. – SPb.: SPBTTAPT, 1999. – P. 40–53.
2. Lovchenko, G. F. Nanostructured mechanically doped dispersed and strengthened materials based on metals: author. dis. ... Doct. tech. sciences : 05.02.01 / G. F. Lovchenko ; FTI NANB – Minsk, 2009. – 49 p.
3. The investigation of the structures and tribological properties of F-DLC coatings deposited on Ti-6Al-4 V alloys / J. Wang [et al.] // Surf. Coat. Technol. – 2017. – Vol. 316. – P. 22–29.
4. Szeri, A. Z. Tribology: Friction, lubrication, and wear / A. Z. Szeri. – New York : Hemisphere Publishing Corp. McGraw Hill Book Co, 1980. – P. 1–99.
5. Wan, S. Tribological performance of CrN and CrN/GLC coated components for automotive engine applications / S. Wan // J. Alloys Compd. – 2017. – Vol. 695. – P. 433–442.
6. Seokil, Kang. Effects of TiCN interlayer on bonding characteristics and mechanical properties of DLC-coated Ti-6Al-4V ELI alloy / Kang Seokil, Lim Hyun-Pil, Lee Kwangmin // Journal of Refractory Metals and Hard Materials. – 2015. – Vol. 53. – P. 13–16.
7. Charitidis, C. A. Nanomechanical and nanotribological properties of carbon-based thin films: A review / C. A. Charitidis // Journal of Refractory Metals and Hard Materials. – 2010. – Vol. 28. – P. 51–70.
8. Dittrich, Karl-Heinz. Production and characterization of dry lubricant coatings for tools on the base of carbon / Karl-Heinz Dittrich, Daniel Oelsner // Journal of Refractory Metals and Hard Materials. – 2002. – Vol. 20. – P. 121–127.
9. Haubner, R. Superhard materials / R. Haubner // Journal of Refractory Metals and Hard Materials. – 2002. – Vol. 20. – P. 91–92.
10. Morphology and growth aspects of Cr(N) phases on gas nitridation of electroplated chromium on AISI 316 LN stainless steel / P. K. Ajikumar [et al.] // Surf. Coat. Technol. – 2006. – Vol. 201. – P. 102–107.

Accepted 01.11.2021

UDC 621.9.06

OPTIMISATION OF THE DESIGN OF THE BASIC ELEMENTS OF THE BEARING SYSTEM OF A HEAVY CNC MACHINING CENTRE

V. P. GORBUNOV[1], A. S. TROFIMCHUK[2]

[1] Ph.D in Engineering, Associate Professor, Associate Professor of the Department of Mechanical Engineering, Brest State Technical University, Brest, Belarus
[2] Master of Engineering Science, engineer of LLC "Machine-building enterprise "COMPO", Brest, Belarus

Abstract
By the example of a three-dimensional model of the bearing system of a heavy multi-purpose CNC machine, the influence on the deformation displacements of the structural design of the basic elements, the location of the supports is considered, which made it possible to identify weak points in the structure and outline ways to improve the processing accuracy.

Keywords: multi-purpose machine, spindle, axis, accuracy, modeling, loading, stiffness, deformation movements, modification of structures.

ОПТИМИЗАЦИЯ КОНСТРУКЦИИ БАЗОВЫХ ЭЛЕМЕНТОВ НЕСУЩЕЙ СИСТЕМЫ ТЯЖЕЛОГО МНОГОЦЕЛЕВОГО СТАНКА С ЧПУ

В. П. Горбунов, А. С. Трофимчук

Реферат
На примере трехмерной модели несущей системы тяжелого многоцелевого станка с ЧПУ рассмотрено влияние на деформационные перемещения конструктивного оформления базовых элементов, расположения опор, что позволило выявить слабые места в конструкции и наметить пути повышения точности обработки. Расчеты выполнены с использованием метода конечных элементов.

Ключевые слова: многоцелевой станок, шпиндель, ось, точность, моделирование, нагружение, жесткость, деформационные перемещения, модификация конструкций.

Preamble

Processing accuracy is significantly influenced by deformations of basic elements of the machine bearing system which result in readjustment of mounting surfaces carrying a billet and a tool, that is, geometrical accuracy parameters. The multipurpose machine is by its design a complicated system with considerable electric power availability compared to common machines and the load and heat sharing in it is problematic to describe analytically. Deformations of machine units and parts are of a complex spatial nature and depend upon many factors [1]: structure and arrangement of machine units, machine operating modes, sequence and duration of operation in this or other mode, thermo-physical properties of materials of which the machine is made, geometric form of the machine units and many other parameters. The result of basic component displacement caused by elastic deformations of the technological system is spatial deviation of the spindle axis. This deviation results in processing error increase and in the absence of machine accuracy reserve the size got at surface processing may exceed the bounds of tolerance zone, which is a parametric failure [2]. Spindle deviation in consequence of deformation of machine major units and its entire bearing system will be a variable and primarily depends upon machine operating conditions.

If in case of light and medium machines the main influence on spindle axis displacement is equally exercised by force and thermal factors of action on the spindle unit and the surfaces it is based on [3], in case of heavy and unique machines the following matters deserve special attention: basic components' weight, gravity centre shifts of moving elements while in operation, residual voltages.

Conducting experimental researches of such deviations under different operating conditions is a long-term and labor-intensive process and in case of multipurpose machines (especially heavy machines) it produces a need for transition to computer modelling of deformation processes during diagnosis of elastic deformations of machine bearing system and to forecasting of its geometrical accuracy change. The forecasting is possible if the behavior of spindle axis time shifting is known. Instead of experimental determination of such dependence one may use an elastic model of the multipurpose machine basic component.

The use of modeling of deformation processes occurring in the processing equipment with the help of computers and special-purpose software substantially reduces the laboriousness of similar problems solution on changing the subject of research, because once produced model can be adapted to new conditions or a new subject in the shortest possible time. Modelling makes it possible to solve the problems of design optimization with the purpose of increase in stiffness and consequently in accuracy of the entire machine.

Workobjective

The objective of this work is assessment of the impact of deformations of the basic elements of the heavy multi-purpose CNC machine's bearing system on the spindle shift and assessment of a possibility of optimization of these elements' design.

Body

The research technique set forth in this work [4] was applied for modelling the assessment of displacements caused by elastic deformations. A heavy horizontal multipurpose CNC machine was considered as the subject of research. The machine is intended to processing of large parts weighing up to 50 tons. The machine structure includes a spindle head with a moving slide and horizontal bar spindle, a rack along which a spindle head moves, a sledge with a fixed rack, a frame along which the sledge with the rack move, a swivel table and a stationary table placed apart from the frame. Also the machine is equipped with an automatic tool changing apparatus (ATC apparatus). The maximum working travels of: the rack horizontally along the axis X – 8000 mm; the spindle head vertically along the axis Y – 3000 mm; the slide along the axis Z – 1500 mm. The machine overall dimensions are length x width x height – 17000 x 10800 x 6970 mm. Examination of the main part of the machine assembly (without reference to the stationary and longitudinal swivel tables) weighing 103960 kg is performed. The total height of the machine geometrical model is equal to 6500 mm. The weight of prismatic parts is shown in Figure 1.

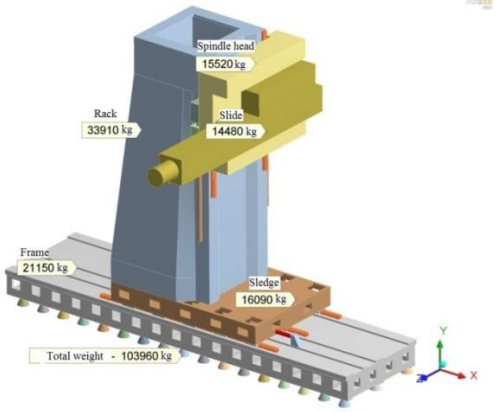

Figure 1 – Weight of prismatic parts of the machine

doi.org/10.36773/1818-1112-2021-126-3-68-71

Rails, carriage support bearings, drive screws, shoes are presented in the model in a stylistic way. Three rails X (the distance between the end rails is 2000 mm) carry 15 bearings. The stiffness of 3000 N/mkmis attributed to each bearing. Two rails have three carriage support bearings each in respect to the coordinate Y, their stiffness is also 3000 N/mkm. The distance between the axes of these rails is 1650 mm.

The linear guideways along the axis Z carry only the slide and their standard size is less than that of linear guideways along the axes X and Y. That is why the spindle head carries 12 carriage support bearings Z with stiffness 2000 N/mkm each. They are connected to three rails on the slide.

The frame rests on three rows of bearings running along the axis X with a step 500 mm. The bearings are presented in a stylistic way as hollow truncated cones (shoes). It is assumed that the vertical stiffness of each bearing is equal to 1000 N/mkm. The example of representation of the stylized rails and bearings is given in Figure 2.

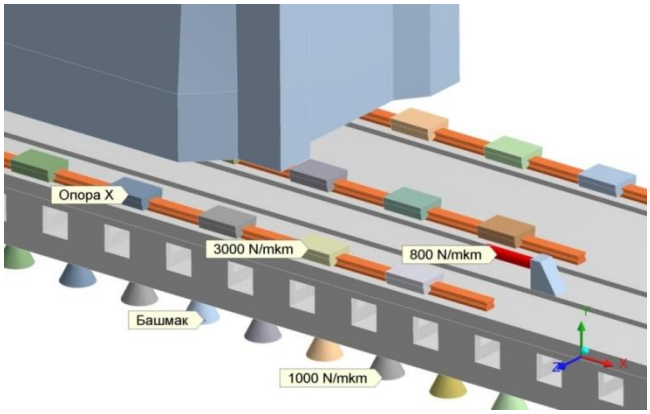

Figure 2 – Stylized representation of rails and carriage support bearings illustrated bythe carriage support bearing along the axis X

There are contact fining elements present in the model. They are located on the borders of all connected bodies. The so-called contact pairs are formed. Initially all contact elements are in a “bonded” state, that is, the contact pairs are blocked against slipping and releasing.

Modelling is performed in the linear setting. Geometrical nonlinearities are not taken into consideration because considerable deformations of the structure (compared to its size) are not expected. Physical nonlinearities associated with plastic deformation are not considered either, since the loads on the system are small with regard to its carrying capacity.

We have considered three versions of locking and loading of the machine basic units.

Figure 3 shows the first version of locking and loading of the rack assembly. It is assumed that all the parts are linked to each other with the help of contact elements. They jointly base themselves on the shoes. All the shoes (51 piece in this model) are fixed on the lower butt ends (marker A – “Fixed Support”). Here the rigid footing virtually begins. Marker B – “Standard Earth Gravity” – indicates the gravity direction. The structure is loaded with its own weight only.

The second version of loading consists in application of the testing force to the top of the rack. Two testing forces 500 N each act on the rail ends Y in the direction X. The total force 1000 N tries to shift right and bend the machine rack. If the bearings X are not blocked, the force is transmitted to the drive X as a result. Such loading characterizes stiffness of the rack and all the underlying parts. The testing force may be directed both along X and along Z. The spindle head and the slide do not participate in loading. The force of gravity is considered to be absent.

The third version of loading is application of the testing force tothe spindle butt end on the slide. The force value is 1000 N (in a linear modelthe force value is notessential). It is alternately directed along the axes X, Y, Z. In this way it is possible toreveal supplenessof all system parts and primarily of the slide, spindle head and their carriage support bearings. This testing force simulates the cutting force.

Preliminary analysis of machine loading versions has shown that the main impact on deformation displacements ofthe basic parts is caused by their weight, gravity center shifts of moving elements, residual voltages. The cutting forces applied to the spindle butt end produce only a slight impact. That is why we leave the first version of loading as the basic one.

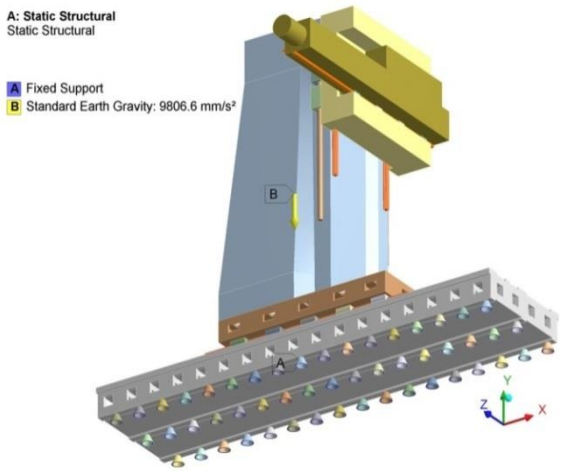

Figure 3 – The first version of locking and loading (A – bottom of the shoes, B – force of gravity) of the rack assembly.

In the work [5] the pattern of total deformation displacements USUM in the rack assembly in the basic version of loading is presented. The pattern of to tal deformation displacements USUM is divided into horizontal displacements along the axis X and vertical displacements Y. Assessment of the obtained results is conducted by the techniques submitted in [6].

Results of researches and discussion

With the reference to analysis of the obtained results it can be seen that the rack performs a deformation clock-wise rotation under the action of a heavy 30-tonspindle head. The rack's turn is related to a deformation “break” of the sledge. The sledge bends exactly under the front wall of the rack. The spindle heads weight is passed down along it. The sledge deflection is also caused by sagging of the under lying carriage support bearing along the axis X. Visually the deformation of the rack itself is not big. When turning, its profile gets moderately distorted. Also the frame on the bearings looks stiff enough. As for the slide, it is rather supple. Displacement patterns examined below are obtained by FEM-calculation at the blocked guides.

The general manifestation of deformation is “a dive” of the rack (clockwise turn). The suppleness of sledge and its carriage support bearings are responsible for it in the first place. Also a can tilevered bending of the extended slide has an impact. These deformations lead to vertical and horizontal shifting of the spindle butt end axis.

The mode of “dive” is illustrated by the section in Figure 4. It shows a deformation situationinside the sledge. The rack locally weighs on the sledge with its front wall by sagging to “248.03” mkm. The sledge bottom is relatively thin (bottom thickness $h_D = 40$ мм and bulges over the bearings X (for example, marker “186.72”). Sledge vertical ribs go into inter bearing gaps. The bearings X also sag under load (see Figure 4). This happens quite non-uniformly. The bearings under the front wall of the rack go down to about 104 mkm, and at the sledge edges – only to 42-48 mkm.

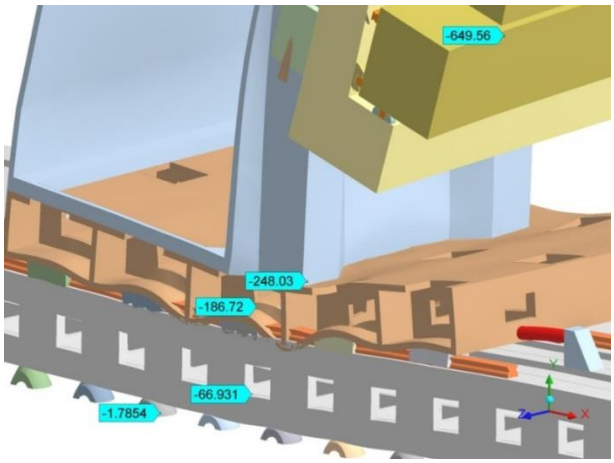

Figure 4 – Vertical displacements (mkm) under gravity in the section in the sledge area (×1200)

Table 1 and Figure 5 show vertical reactions that act on the carriage support bearingsin the directionX (see Figure 2). Let's take the next to us rail as the first one. Ordinal numbers will be assigned to the bearings on each railfrom right to left. The nearest bearing in Figure 5 will be designated as bearing 1–1, and the farthest bearing – as bearing 3–5 (the first digit is a number of a rail). The highest overall reaction is present on the bearing 1-3. This bearing is close to the front wall of the rack that forms a load. The bearings at the edges of each railare loaded about three times as weak. It can be observed that the maximum load accrues to the first rail of the third row. The minimum reaction accrues tothe angle bearing 3-5. Forces in these bearings differ by a factor of 7, 9.

Following the results of modeling described above the sledge design was virtually modified. Firstly, the sledge bottom thickness h_D was increased. Secondly, the search was tried out for the optimal layout of carriage support bearings (roller bearings) with smaller number of bearings and their more uniform loading. Also the model material was changed in order to increase its stiffness.

Table 1 – Vertical reactions R_y in the bearings X in rows and rails (sledge bottom thickness is 40 mm), in N

	Rail 1	Rail 2	Rail 3	Portion - rows
Row 5	35728	19879	12870	8.6%
Row 4	70004	46281	48374	20.6%
Row 3	101740	84603	84767	33.9%
Row 2	74580	67189	66910	26.1%
Row 1	29957	30638	25497	10.8%
Portion – rails	39.0%	31.1%	29.9%	100%

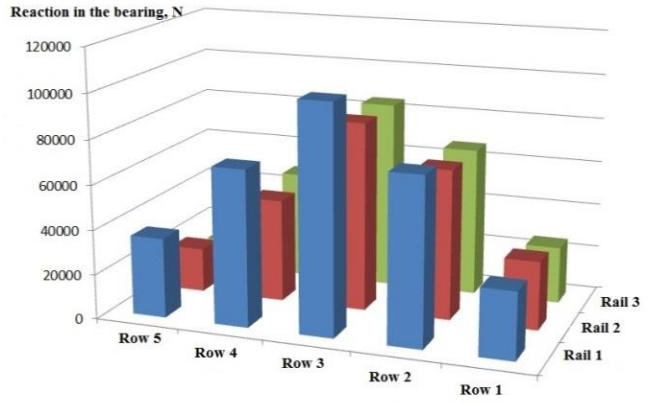

Figure 5 – Vertical reactions in the bearings X under the weight of rack assembly

Different versions of structural design (SD) are accumulated in Table 2. The case of SD1 refers to the basic version. Sledge bottoms were by turn enlarged to the thickness 80 and 120 mm (SD3 and SD4 respectively).

The maximum deformation displacement by gravity along the spindle axes X and Y is observed in the top position of the spindle headon the frame (SD1). At this point the maximum angle of obliquity is observed at sagging of the sledge on the bearings. The minimum displacement along the axis X is observedat the maximum descending of the spindle head (SD2). The problem may be solvedby increase in the bottom thickness to 40 mm.

ForacaseSD3 ch_D = 80 мм there can be observed a positive effect – spindle end hanging decreased by 9% - from 939 mkm up to 859 mkm (Table 2). "The dive" to the right decreased approximately by a factor of 1, 2. The cause of it is a smaller bulging of the sledge bottomover the bearings. The sledgebends to a lesser extendunder the front wall of the rack. The rack leans clockwise to a lesser extend.

Table 2 – Aggregate displacements of the spindle for different structural cases of the test (load – own weight)

Structural case	Description	Spindle, displacement X		Spindle, displacement Y	
		mkm	%	мкм	%
SD1	h_D = 40 мм	505	100,0%	939	100,0%
SD2	h_D = 40 мм and spindle head descending to 2 m	206	40,8%	952	101,4%
SD3	h_D = 80 мм	423	83,8%	859	91,5%
SD4	h_D = 120 мм	397	78,6%	821	87,4%
SD5	h_D = 80 мм and 11 bearings	411	81,4%	885	94,2%
SD6	h_D = 80 мм, and 11 bearings	393	77,8%	873	93,0%
SD7	h_D = 80 мм and sledge material stiffness increased up to	344	68,1%	790	84,1%
SD8	h_D = 80 ммand bearing X material stiffness increased	391	77,4%	821	87,4%

In the case SD 4 there is observed a slight difference in displacements from SD 3. Though the growth of the walls up to 120 mm results in a substantial increase of weight of the structure, it does not bring a substantial increase in stiffness of the machine.

Duetonon-uniformed loading of the bearings a version was modulated with decrease in the number of bearingsup to 11 (SD5) with simultaneous increase of bottom wall thickness up to 80 mm. The bearing row 4 and the bearing 1-2 are cut down. Displacements on the spindle have hardly changed compared to the version SD3. Loading of the bearings increases, for example, of the bearing 1-3 by 40%, though the reaction forceremains with in the limits of dynamic load rating of the bearings. The increase in sledge wall thickness to (SD6) does not make difference for spindle displacements compared to the version SD5.

The considered version with the increase in bearing thickness SD8 has shown a slight increase in stiffness compared to the version SD3 and worse values compared to the version SD7.

Thus, by degree of labor inputs and reduction of values of spindle displacement in the directions X and Y it is possible to offer the design change according to the versions SD3 and SD7.

Figure 6 showsthe degree of impact of the basic elements of the bearing system of the machine concernedat the structural cases of modeling SD1, SD3, SD7. If in the basic version the maximum impact on the deformation "dive" is made by the sledge and the bearings, in the offered versions the main impact is made bythe rack.

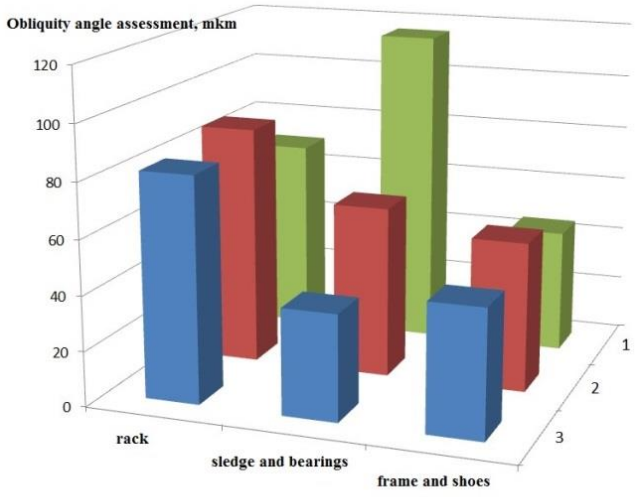

Figure 6 – The role of the rack assembly partsin forming the deformation "dive" (1 – SD1, 2 – SD3,3 – SD7)

doi.org/10.36773/1818-1112-2021-126-3-68-71

The results of virtual variation of stiffness of the main parts of the machine assembly are presented in Table 3. Stiffness has been changed for each part by turn, twice: both downward and upward. For that end one operated the elastic modulus of the corresponding model material. We shall speak about a stiffness coefficient which in the initial state is equal to one f_j= 1 for design SD3, at the decrease in stiffness it is f_j = 0,5, at the increase it is f_j = 2. The result of modeling is displacement of the spindle end along the axis X ("dive").

Table 3 – Spindle "dive" along the coordinate X depending on the stiffness coefficient of the part, in mkm

Stiffness coefficient	Shoe	Bearing	Frame	Sledge	Rack
0,5	443	458	447	562	572
1	423	423	423	423	423
2	401	391	396	344	343

It is evident from Table 3 that the greatest impact on "the dive" is made by stiffness of the sledge and the rack. After increase of the sledge stiffness the further lowering of "the dive" should be attained by elaboration of the rack design. The frame, the shoes and bearings X have roughly the same and moderate effect on "the dive". Expenditures for their reinforcement are unreasonable.

Conclusion

It is evident from the obtained results of modelling that the greatest deformations of the machine are due to sledge and rack deflection along the axis X, the reat the deflection increases when the spindle head goes upward. To increase the sledge stiffness, the most preferred method will be to increase its bottom thickness to 80 mm. Also, in order to achieve an even load distribution on the frame guides, it is necessary to change the installation diagram of roller bearings. To reduce the impact of the rack deflection on processing accuracy by using a mathematical model describing deviations, it is possible to negate errors with the help of correction ofthe control programme in the machine CNC system.

References

1. Reshetov, D. N. Accuracy of Metal-Cutting Machines / D. N. Reshetov, V. T. Portman. – M. : Machine-building industry, 1986. – 336 p.
2. Pronikov, A. S. Parametric Reliability of Machines / A. S. Pronikov. – M. : Moscow State Technical University named after N.E. Bauman, 2002. – 560 p.
3. Gorbunov, V. P. Modeling of Spindle Axis Shifting of a Plane Horizontal Milling Machine under the Action of Force and Thermal Factors / V. P. Gorbunov, L. V. Kasian // Bulletin of Brest State Technical University. Mechanical engineering. – 2012. – № 4 (76). – P. 69–72.
4. Gorbunov, V. P. Modeling of Spindle Axis Shifting from Elastic Deformations of the Rack of a Plane Horizontal Milling CNC Machine / V. P. Gorbunov, A. S. Trofimchuk // New Technologies and Materials, Production Automation: materials of the International Science and Technology Conference, Brest, May 27–28, 2019. – Brest : Brest State Technical University, 2019. – P. 42–46.
5. Gorbunov, V. P. Modeling of Shiftings from Elastic Deformations of the Bearing System of a Horizontal Milling and Boring CNC Machine / V. P. Gorbunov, A. S. Trofimchuk // Bulletin of Brest State Technical University. Mechanical engineering. – 2019. – № 4. – P. 35–38.
6. ANSYSUserManual. Theoretic Manual. [Electronic resource]. – Access mode: www.twirpx.com.

Accepted 26.10.2021

UDC 620.179.18

THE USE OF ARTIFICIAL NEURAL NETWORK MODELS IN THE ACOUSTIC DIAGNOSTICS OF MULTI-SHAFT GEAR DRIVES

A. N. Parfievich[1], V. A. Sokol[2], M. V. Neroda[3]

[1] Master of Technical Sciences, Senior Lecturer of the Department of Mechanical Engineering and Operation of Vehicles, Brest State Technical University, Brest, Belarus, e-mail: parfievichand@gmail.com
[2] Master of Technical Sciences, Senior Lecturer of the Department of Mechanical Engineering and Operation of Vehicles, Brest State Technical University, Brest, Belarus, e-mail: sokolva@mail.ru
[3] The First Vice Rector, Ph.D in Engineering, Associate Professor, Brest State Technical University, Brest, Belarus, e-mail: nerodamv@mail.ru

Abstract

The article considers the possibility of diagnosing a multi-shaft gear mechanical system based on the analysis of an acoustic signal using artificial neural network models on the example of the speed box of the SN-501 lathe. A sufficiently high efficiency and accuracy of detecting a local defect of the gear wheel in conditions of high acoustic activity of all components of the drive when monitoring its condition is shown.

Keywords: gear wheel, local defect, artificial neural network model, diagnostics, acoustic signal, multi-shaft gear drive.

ИСПОЛЬЗОВАНИЕ ИСКУССТВЕННЫХ НЕЙРОСЕТЕВЫХ МОДЕЛЕЙ ПРИ АКУСТИЧЕСКОЙ ДИАГНОСТИКЕ МНОГОВАЛЬНЫХ ЗУБЧАТЫХ ПРИВОДОВ

А. Н. Парфиевич, В. А. Сокол, М. В. Нерода

Реферат

В статье рассмотрена возможность диагностики многовальной зубчатой механической системы на основе анализа акустического сигнала с применением искусственных нейросетевых моделей на примере коробки скоростей токарного станка SN-501. Показана достаточно высокая эффективность и точность выявления локального дефекта зубчатого колеса в условиях высокой акустической активности всех составляющих привода при проведении мониторинга его состояния.

Ключевые слова: колесо зубчатое, локальный дефект, искусственная нейросетевая модель, диагностика, акустический сигнал.

Introduction

Currently, diagnostic specialists who study various kinds of mechanisms on the basis gear wheels are faced with a difficult task associated with the formalization of the monitoring procedure, but at the same time it is important not to lose in the process of simplification that amount of information which carries information about changes in the diagnosed object. To achieve this goal, they are increasingly resorting to the joint use of the known methods of representing oscillatory processes accompanying the operation of the device, and modern mathematical means.

One of the most widespread methods for representing a oscillation signal is a spectral analysis, the mathematical basis of which has been sufficiently well studied and implemented practically on all modern control and diagnostic tools. To diagnose periodic oscillatory processes using amplitude-frequency analysis, the Fourier transformation procedure is most often used. This method of representing an acoustic signal makes it possible to evaluate its composition and the amplitude of the characteristic frequencies generated by each element of the mechanical drive, as well as to track their changes determined by the change in the state of cog wheels.

Object and subject of research

As an object of research, a complex mechanical system was chosen − a gearbox of the drive of the main movement of a SN-501 lathe model. When the drive is operating, both the gearings of the kinematic chain of rotation transmission to the output shaft and its other elements that do not affect the rotation of the spindle (guitar drives of replaceable wheels, reverse, brake mechanism and parasitic gear wheels), but influencing the formation of the final acoustic signal of the drive are in motion. This leads to the appearance on the spectrum of a large number of additional components, which complicate the identification and analysis of harmonics at the frequencies of interest.

As a source of information was used an acoustic signal generated by a VIK-MA hardware-software complex on the basis of data obtained from a measuring microphone with an M101 capsule, installed at a distance of 300 mm from the body of the gearbox in the horizontal plane [1]. The measurement of acoustic signals was carried out at the input shaft rotation frequencies which correspond to the operational ones both under load and without it.

The simultaneous use of angular displacement transformers on the input and output shafts of the drive made it possible to determine with high accuracy the rotational frequences of the input and output shafts, as well as the frequencies of the characteristic components on the spectrum of the analyzed signal.

On Z = 43 gear of shaft II, which is included in the studied kinematic chain of the gearbox, an operational local defect of the working part of the tooth of various sizes was simulated (25 %, 50 %, 75 %) of the length at the top of the tooth and without a tooth (Fig. 1). The measurements were carried out for each condition of the tooth multiple times to accumulate the required amount of data for statistical processing. The results obtained while using serial wheels are taken as reference.

Figure 1 – Experimental Z = 43 gear with operational local tooth defect

doi.org/10.36773/1818-1112-2021-126-3-72-75

The spectral characteristics of an acoustic signal obtained during the experiment indicate that each of the drive elements makes its own contribution to its formation. But with a large number of sources of acoustic activity, a highly qualified diagnostician is needed to identify the characteristics of each element of the object and then make the appropriate diagnosis, therefore, spectral analysis has limitations in diagnosing complex mechanical systems on the basis of gear wheels and requires formalization and automation of processing of incoming data for analysis.

Analyzing the obtained spectra of acoustic activity of the investigated object, one can point out the problem of its excessive saturation with various components from the drive operating elements, but at the same time, a decrease in the spectrum resolution can lead to the loss of data that can carry diagnostic information.

As is known from a number of literary sources [2, 3, etc.], the following number of frequency components have the greatest diagnostic value, the change in the amplitudes of which carries significant information about the state of the investigated element of the object:

– in the low-frequency area – reverse f_o and multiple components of the all gear wheels of the kinematic chain;
– in the area of tooth connection – toothed f_z, multiple components of the gear wheels, as well as other frequency components at the combined frequencies $l \cdot f_z \pm n \cdot f_o$, arising from various kinds of signal modulations (l, n = 1; 1,5; 2, etc.).

Taking into account a very large number of characteristic frequency components to be analyzed for each gear wheel, determining their characteristics 'manually' is a very painstaking process. For its automation in the software part of the complex, a new function 'Harmonics analysis' has been developed and implemented, which allows to automatically obtain the values of the frequencies and amplitudes of the circulating and cogging spectrum components, their multiple harmonics, as well as the combined components formed during operation of each gear wheel and forming a set of the most informative frequency components when detecting defects and errors of gear wheels (Fig. 2).

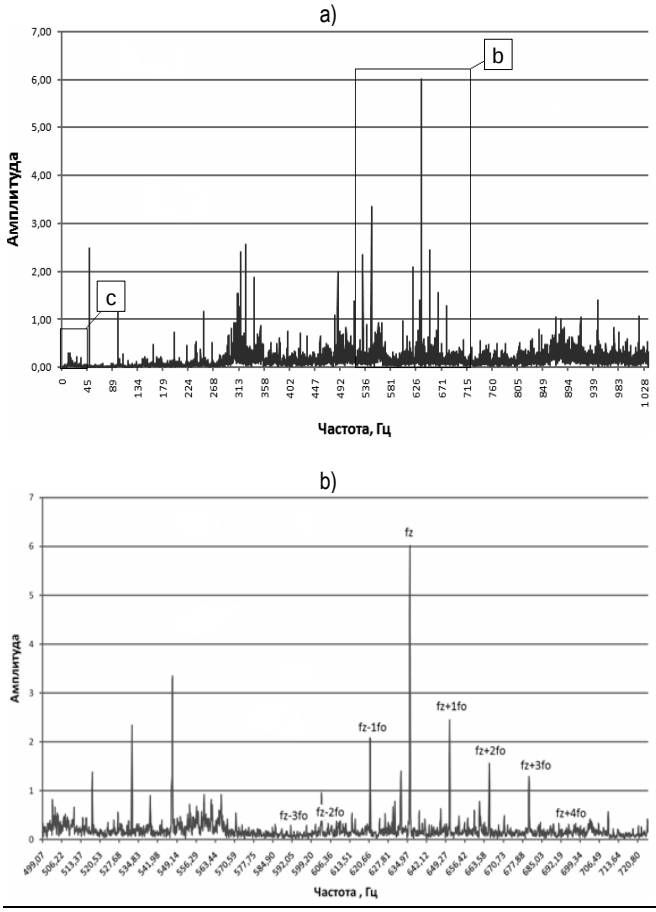

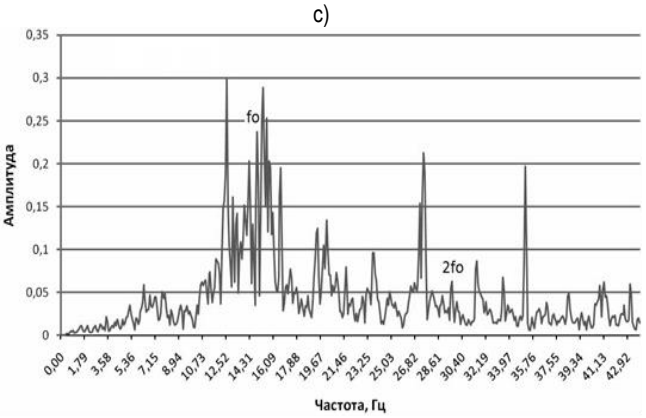

d)

i	Amplitudes of harmonics							
	reverse frequency f_{oi}	cog frequency f_{zi}	combined frequencies $f_{zi} + f_{oi}$					
			j=-3	j=-2	j=-1	j=1	j=2	j=3
1	0,237	6,018	0,2877	0,2203	2,0718	2,2243	1,5597	1,1467
2	0,0632	1,473	1,1489	0,9026	0,3780	2,037	0,2023	0,1939
3	0,0205	0,355	0,3953	0,1080	0,3725	0,1903	0,1491	0,1451
4	0,0405	0,073	0,0465	0,0588	0,0535	0,0524	0,0304	0,0312
5	0,0290	0,022	0,0814	0,0513	0,0295	0,0251	0,0349	0,0369

a) a fragment of the spectrum of the acoustic signal of the object under study; b); a fragment of the spectrum of the acoustic signal in the frequency range $(f_z - 5f_o) - (f_z + 5f_o)$ of the gear under study; c) a fragment of the spectrum of the acoustic signal in the area of the reverse frequencies of the gear under investigation; d) experimental data obtained using the «Harmonic Analysis» complex function for the gear under study

Figure 2 – The spectrum of an acoustic signal of the multi-shaft gear drive and the result of its processing by the software of the VIKMA complex

The developed technique for automatic spectral characteristics processing makes it possible to simplify the procedure for analyzing the parameters of acoustic noise. This gives a possibility to narrow the set of analyzed data for making a diagnosis and to take steps to formalize the diagnostic procedure through the use of powerful modern mathematical means, by way of proposing the use of the capabilities of artificial neural networks.

Neural network diagnostic method

The obtained volume of experimental data on the acoustic activities of the drive was divided into 5 classes, depending on the condition of the tooth (Table 1) and used to solve the classification problem. As a training excerpts, 25 samples of each of the analyzed states were formed, 5 of which were provided to the network for testing.

The description of each sample was carried out by the amplitudes of the acoustic signal harmonics obtained from the high-resolution spectra by the software of the complex using the «Harmonics analysis» function. For each toothed wheel, the amplitudes of at least 5 harmonics of the reverse f_o and the tooth f_z frequency and 10 amplitudes of the modulated side bands $f_z - if_o$, i = -5…5 were taken as such.

Table 1 – Classification of the state of the experimental Z = 43 gear.

Class Number	Tooth condition
1	No defects
2	25% of the tooth surface is damaged
3	50% of the tooth surface is damaged
4	75% of the tooth surface is damaged
5	Chipped tooth

A multilayer neural network with one hidden layer consisting of Kohonen neurons [4], the structure of which is shown in Figure 3, was chosen as a classifier.

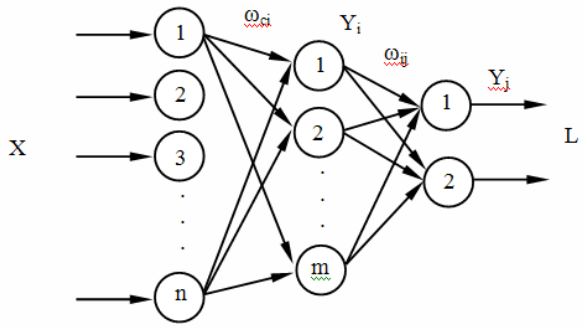

Figure 3 – The structure of a neural network classifier on the basis of Kohonen neurons.

The choice of the given structure of an artificial neural network is determined by the limited set of analyzed data. Thus, when using a multilayer perceptron as a classifier, the following size of the training excerpt is necessary [5]:

$$L \approx \frac{V}{\varepsilon} \quad (1)$$

where ε – the permissible classification accuracy;

V – the total number of adjustable parameters (weight coefficients and threshold values) is calculated by the formula:

$$V = m \cdot (n + 3) + k \quad (2)$$

where m – the number of neurons in the hidden layer;

n – the number of neurons in the distribution (input) layer;

k – the number of neurons in the output layer.

Let's assume, n = 60, m = 30, k = 5 and ε = 0.1. Then $L \approx 18950$.

A similar result can be obtained for multi-recurrent neural networks [6], as well as for deep learning neural networks [7].

For the selected structure of the neural network classifier, there are no strict requirements for the dimension of the training excerpt. It is sufficient that the size of the training excerpt is as follows:

$$L \geq 2 \cdot m \quad (3)$$

The first layer of neural elements is designed to distribute input signals to the Kohonen hidden layer neurons. The dimension of the input layer (the number of neurons in the input layer) is determined by the dimension of the analyzed data. In our case, data with a dimension of 60 are used, therefore, the number of neurons in the distribution layer is n = 60. The input signals are parameters formed on the basis of the function of the hardware-software 'Harmonics Analysis' complex (Fig. 2, r).

The second, the artificial neural network hidden layer consists of Kohonen neurons. The Kohonen layer plays a key role in the classification of data and performs the clustering of the input image space, as a result of which clusters of different images are formed, each of which corresponds to its own neural element. The optimal number of neurons in the hidden layer of Kohonen is determined experimentally, and may differ from the type of tasks, data structure, etc. In the given case, the experiments showed good results, with the number of neurons in the hidden layer equal to m = 30.

To train the Kohonen layer, a competitive teaching method is used [4, 5]. The essence of this learning method is that in the teaching process there is competition between neural elements, as a result of which a winning neural element is determined, which characterizes the class of analyzed data. To determine the winner neuron, the Euclidean distance between the input and weight vectors is used, which is defined as:

$$D_i = \left|X - \omega_i\right| = \sqrt{(X_1 - \omega_{1i})^2 + (X_2 - \omega_{2i})^2 + \ldots + (X_c - \omega_{ci})^2}, \quad (4)$$

where ωci – the weight coefficient between the c-m neuron of the distribution layer and the i-m neuron of the Kohonen layer;

X = [$X1$, $X2$ ... Xn] - input image.

During the teaching process, synaptic connections for the winner neuron are strengthened, but for the rest of the neurons they are not change. Thus, after training the artificial neural network, when the input image is submitted, the activity of the winning neuron is taken equal to one, and the remaining neurons are 'reset' to zero [4-6]. This teaching rule is known under the name "the winner-takes-it-all" [4, 5].

The third layer consists of five linear neural elements and realizes the representation of the clusters, formed by the Kohonen layer, into 5 classes, respectively. The activity of the output neuron, when its value is equal to one, characterizes this or that class. In this case, all other output neurons have an activity equal to zero.

The neural network training algorithm can be represented as the following sequence of steps:

1. Random initialization of the weight coefficients ωci of the neurons of the Yi layer.
2. Distribution of the input image from the training excerpt to the neural network and the calculation of the following parameters:

a) the Euclidean distance between the input image and the weight vectors of the neural elements of the Yi layer is determined:

$$D_i = \left|X - \omega_i\right| = \sqrt{(X_1 - \omega_{1i})^2 + (X_2 - \omega_{2i})^2 + (X_n - \omega_{ni})^2}, \quad (5)$$

where $i = \overline{1,m}$.

b) neural element winner with number k:

$$D_k = \min_j D_j. \quad (6)$$

c) the output value of the winner neuron is set to '1', and the output of the remaining neural elements is set to '0':

$$Y_i = \begin{cases} 1, i = k \\ 0, \text{иначе} \end{cases} \quad (7)$$

d) the weighting coefficients of the winner neuron are modified in accordance with the following expression:

$$\omega_{ck}(t+1) = \omega_{ck}(t) + \gamma\,(X_c - \omega_{ck}(t)), \quad (8)$$

e) if the winner neuron is the neuron corresponding to the presented image (so, when the number of neurons in the Yi layer is equal to 5, when the image corresponding to the whole gear wheel is fed to the input of the network, the winner neuron must be with index 1; when feeding the image corresponding to 25% damage, the winner neuron should be indexed 2, etc). Otherwise:

$$\omega_{ck}(t+1) = \omega_{ck}(t) - \gamma\,(X_c - \omega_{ck}(t)). \quad (9)$$

The process is repeated starting with item 2 for all input images.

3. Training is performed to the desired degree of agreement between the input and weight vectors.

The value of discernment reliability in the course of training the neural network was 93.3%, the mistakenly recognized images corresponded to neighboring classes.

Neural network testing

At the initial stage, the z = 24 gears of shaft III and z = 27 of shaft IV of the SN-501 lathe gearbox in a technically correct state were used as test objects. The accuracy of the diagnosis with the trained neural network was 100%.

To check the adequacy of the proposed method of acoustic diagnostics, in addition to the gearbox of the SN-501 lathe main movements drive as a base object, the elements of such gear drives as a PM-250 model horizontal reducer with cylindrical spur wheels and a gearbox of a model 2K52 radial boring mill were tested.

On the z = 40 gear wheel of the PM-250 horizontal reduction gear with spur wheels, similar local defects in the form of tooth damage were simulated, as in the lathe gearbox (25 %, 50 % and 75 % of the tooth length, and no tooth).

When diagnosing the gearbox of the 2K52 radial boring mill, the object of the research was a technically serviceable z = 42 gear wheel of the kinematic chain. At the stage of data collection, various situations were simulated: operation of the gearbox at idle stroke and work under load (in the course of using the lathe during mechanical processing).

The results of using a neural network to detect gears with damaged teeth are shown in Table 2.

doi.org/10.36773/1818-1112-2021-126-3-72-75

Table 2 – Reliability of detecting tooth damage of multi-shaft drives by acoustic data using an artificial neural network

Classes of diagnosed parameters of a cogwheel	Accuracy of diagnosis, %				
	Whole tooth	25% of tooth length	50% of tooth length	75% of tooth length	No tooth
Serviceable gears z = 24 and z = 27 of the SN-501 lathe gear box					
Whole tooth	100%	-	-	-	-
25% of tooth width	-	-	-	-	-
50% of tooth width	-	-	-	-	-
75% of tooth width	-	-	-	-	-
No tooth	-	-	-	-	-
Gear wheel Z = 40 of the PM-250 reducer with a whole chipped tooth					
Whole tooth	-	-	-	-	-
25% of tooth width	-	-	-	-	-
50%of tooth width	-	-	-	-	-
75% of tooth width	-	-	-	13,3%	-
No tooth	-	-	-	-	86,7%
Gear wheel Z = 40 of the PM-250 reducer with 75% damage of the tooth length					
Whole tooth	-	-	-	-	-
25% of tooth width	-	-	-	-	-
50% of tooth width	-	-	3,3%	-	-
75% of tooth width	-	-	-	96,7%	-
No tooth	-	-	-	-	-
Gear wheel Z = 40 of the PM-250 reducer with 50% damage of the tooth length					
Whole tooth	-	-	-	-	-
25% of tooth width	-	-	-	-	-
50% of tooth width	-	-	100%	-	-
75% of tooth width	-	-	-	-	-
No tooth	-	-	-	-	-
Gear wheel Z = 40 of the PM-250 reducer with 25% damage of the tooth length					
Whole tooth	13,3%	-	-	-	-
25% of tooth width	-	83,3%	-	-	-
50% of tooth width	-	-	3,3%	-	-
75% of tooth width	-	-	-	-	-
No tooth	-	-	-	-	-
Serviceable gear wheel Z = 40 of the PM-250 reducer					
Whole tooth	100%	-	-	-	-
25% of tooth width	-	-	-	-	-
50% of tooth width	-	-	-	-	-
75% of tooth width	-	-	-	-	-
No tooth	-	-	-	-	-
Serviceable gear z = 42 of the radial 2K52 boring mill gearbox					
Whole tooth	100%	-	-	-	-
25% of tooth width	-	-	-	-	-
50% of tooth width	-	-	-	-	-
75% of tooth width	-	-	-	-	-
No tooth	-	-	-	-	-

The accuracy of the diagnosis of an artificial neural network trained on one object when using it on other gear drives was no less than 83%, since the diagnostic features describing the classes of the state of gear wheels for similar objects are identical. Moreover, in all cases, the erroneous results corresponded to the neighboring class of tooth condition, and the wheels with undamaged teeth were assessed without error as serviceable. It is obvious that the selected set of acoustic signal parameters for describing the state of damaged wheels is sufficient for adequate operation of the neural network analyzer.

Conclusion

Thus, the method for diagnosing elements of multi-shaft in-line gear drives developed in the course of experimental studies using neural network models has shown a fairly high efficiency and accuracy. The proposed structure of a neural network immune detector for the classification of the proposed states of the gear tooth is characterized by a small volume of the training excerpt and is distinguished by a high level of clustering accuracy in the analysis of the acoustic signal, which is the 'product' of the activities of all elements of the kinematic chain of the SN-501 lathe gearbox. This approach in the study of multi-shaft gear drives is supposed to minimize human participation directly in the diagnosis procedure, which, in turn, is intended to increase its objectivity. Despite the fact that this method requires additional actions that are not directly related to the diagnostic process (training the network on theoretically and practically grounded diagnostic features, determining the data preparation technology), the prepared artificial neural network can further be used to make a diagnosis on other similar objects that have a similar nature of the formation of the analyzed signal.

References

1. New hardware and software means for research and diagnostics of mechanical systems / A.V. Dragan [et al.] // Bulletin of Brest State Technical University. − 2006. − № 4. − P. 17−26.
2. Barkov, A. V. Monitoring and diagnostics of rotary machines by vibration [Electronic resource] / A.V. Barkov, N.A. Barkova, A. Yu. Azovtsev. – Access mode: http://www.vibrotek.com/russian/articles/-book/index.htm.
3. Jacob Anil. Gear diagnosis using a new method for monitoring the condition of rotary equipment: Translated from English. [Electronic resource] / Anil Jacob, Dr. Y. I. Sharaf-Eldeen. – Access mode: http://www.vibration.ru/d_zub_peredach.shtml.
4. Kohonen, T. Sell-organized formation of topologically correct feature maps / T. Kohonen // Biological Cybernetics. − 1982. – № 43. − P. 59−69.
5. Golovko, V. A. Neural networks: training, organization, application. Book 4 Neurocomputers and their applications / V. A. Golovko ; ed.: A. I. Galushkin. – Moscow : Radiotechnika, 2001. − 256 p.
6. Khaikin, S. Neural networks: a complete course / S. Khaikin. – Moscow : Wiliams, 2006. − 1104 p.
7. Bengio, Y. Learning Deep Architectures for AI / Y. Bengio. − Now Publishers Inc, 2009. − 114 p.

Accepted 26.10.2021

UDC 681.5

CONTROLLER FUNCTIONS FOR ADAPTIVE COMPENSATION SYSTEM REACTIVE POWER

L. I. Vabishchevich[1], A. A. Klopotsky[2], A. V. Yarashevich[3]

[1] Ph.D in Engineering, Associate Professor of the Department of Automation of Technological Processes and Production, Brest State Technical University, Brest, Belarus
[2] Senior Lecturer, Department of Automation of Technological Processes and Production, Brest State Technical University, Brest, Belarus
[3] Ph.D in Engineering, Associate Professor, Associate Professor of the Department of Automation of Technological Processes and Production, Brest State Technical University, Brest, Belarus, e-mail: ya-v@tut.by

Abstract

The article is devoted to the construction of a controller algorithm as part of an adaptive reactive power compensation system.

To construct the structure of a system with a controller, a reactive power compensator circuit with an analog calculation of the capacitance of capacitors was selected.

The article reflects the following questions:

– the compensator of reactive power on urban electric networks by the automatic control system is presented, which made it possible to build a model in terms of the theory of automatic control;
– a graphical information model of the reactive power compensator with analog calculation of the capacitance of the capacitors is shown;
– a set of system parameters is selected for control and optimization by software;
– selected the numerical values of the parameters of the elements for building the model.

Keywords: controller algorithm, adaptive control system, reactive power compensation.

ФУНКЦИИ КОНТРОЛЛЕРА ДЛЯ АДАПТИВНОЙ СИСТЕМЫ КОМПЕНСАЦИИ РЕАКТИВНОЙ МОЩНОСТИ

Л. И. Вабищевич, А. А. Клопоцкий, А. В. Ярошевич

Реферат

Статья посвящена построению алгоритма контроллера в составе адаптивной системы компенсации реактивной мощности. Для построения структуры системы с контроллером была выбрана схема компенсатора реактивной мощности с аналоговым расчетом емкости конденсаторов. В статье отражены следующие вопросы:

– представлен компенсатор реактивной мощности на городских электрических сетях системой автоматического управления, что позволило построить модель с точки зрения теории автоматического управления;
– показана графическая информационная модель компенсатора реактивной мощности с аналоговым расчетом емкости конденсаторов;
– набор системных параметров выбирается для управления и оптимизации с помощью программного обеспечения;
– выбраны числовые значения параметров элементов для построения модели.

Ключевые слова: алгоритм контроллера, адаптивная система управления, компенсация реактивной мощности.

Introduction

The representation of a reactive power compensator on urban electrical networks by an automatic control system allows us to build a model of a reactive power compensator in terms of the theory of automatic control. To create a model, you can use the entire arsenal of software tools created for the study of automatic control systems (Matlab, Simulink, etc.).

Controller in the structure of an analog automatic control system

The reactive power compensator model will make it possible to investigate the inductive power compensation errors caused by a number of approximations adopted for constructing schemes for calculating the value of the compensating capacitance. First, this is the representation of the values of trigonometric functions $f = tg\ (\varphi)$ by the linear dependence $f = \varphi$ when expressing φ in radians for small values of the phase difference angle. Secondly, it is quantization according to the signal level by an analog-to-digital converter and, accordingly, a stepwise connection of the capacities of the compensating battery.

The model is based on the structural diagram of the reactive power compensator with analog determination of the capacitance to compensate for the inductive load [1]. The model avoids programmatic computation of $f = tg\ (\varphi)$ values. The last operation uses a rather complex algorithm of computational mathematics, which requires a significant time interval for implementation. In the structure of the automatic control system, this is represented as a pure delay link that degrades the quality indicators of the automatic control system.

The proposed block diagram of a reactive power compensator with a microprocessor-based controller included in the control loop is shown in Fig. 1.

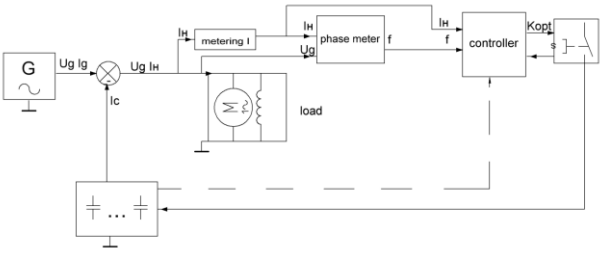

Figure 1 – Structural scheme

The controller only performs functions that require several cyclesoperation of the processor and does not introduce a significant signal delay into the automatic control system loop.

Generator *G* supplies the system load with sinusoidal voltage 220V 50Hz. The signals Ug, Ig are fed to the input of the comparison element. In this case, the comparison element performs the functions of vector algebra, creating vector sums of complexes of currents. The load changes the parameters of the current signal to $In = Ig - Ic$, where the capacitor current is created from the resonance condition of the currents of the inductive load and compensating capacitors.

The current meter generates a signal I_H, which with the signal Ug is fed to the phase meter, at the output of which the voltage f is proportional to the phase difference between the supply voltage and the load current.

The controller takes over the functions of a multiplier, amplifier and analog-to-digital converter. The multiplier unit multiplies the current and

doi.org/10.36773/1818-1112-2021-126-3-76-78

phase difference signals according to the formula for calculating the capacitance of the capacitors. Signal *C* at the output of the block determines the compensating capacitance. The amplifier scales the signal to the level required by the analog-to-digital converter to generate the code *K* for controlling the switching keys of the capacitors of the compensating battery.

The main stages of forming the control code are presented by the block diagram of the controller algorithm.

Switching in accordance with the *K* code will lead to an uneven load on the keys and operating capacitors, which will significantly reduce the reliability of the elements. In addition, with limited durability of elements, it is important to monitor their condition and take it into account when controlling commutation. For this purpose, a microprocessor controller was introduced into the control loop. The functions of the controller consist in analyzing the state of the triacs of the switch and capacitors, choosing the switching algorithm according to many criteria and informing about the loss of the device's performance. The *Kopt* key control signal is generated at the output of the controller.

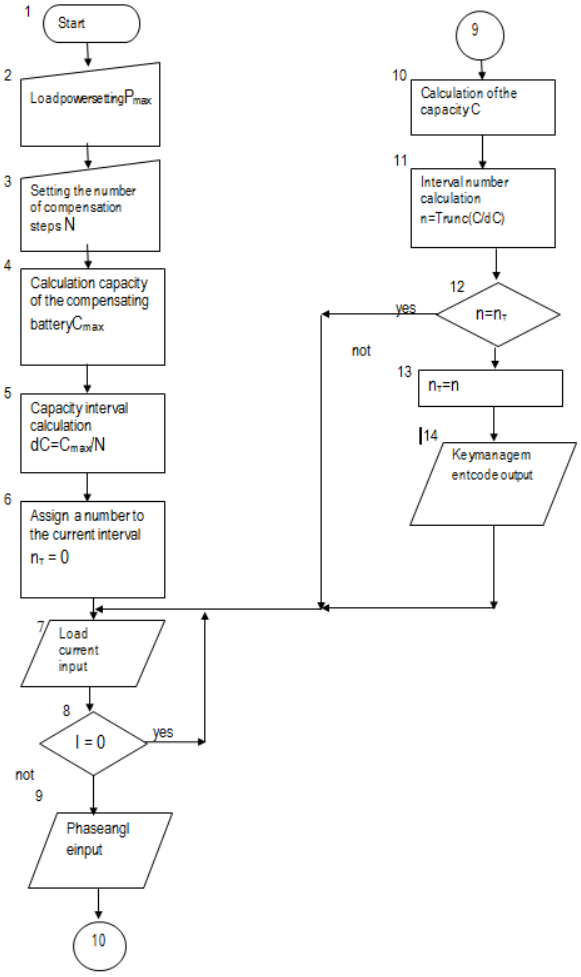

Block functions:

Block 2. Setting the load power. The load power determines the maximum current drawn from the network. The value of this current is used to calculate the total capacity of the compensating battery.

Block 3. Setting the number of compensation steps. The capacitor for compensation of inductive load is connected in steps. The number of stages is determined from economic and design requirements, as well as requirements for compensation accuracy. The seven-stage compensator can be realized with three capacitors controlled by a three-bit binary code.

Block 4. Calculation of the full capacity of the compensating battery. The initial data for the calculation are the maximum load current, determined by the power of the consumer and the voltage of the supply network, and the maximum angle of phase shift of voltage and current. This angle is selected from the statistically established one in real networks.

$$Cos\varphi_{max}=0{,}65:\ \varphi_{max} \approx 50^{o} \approx 0{,}87 rad.$$

Block 5. Calculation of the capacity interval. The capacity interval is determined by the total battery capacity and the number of control steps.

Block 6. Assigning the number of the current interval to the value zero. The number of the current interval is a multiplier with the capacity of the capacitor bank stage to determine the current compensation capacity. The current interval number is a binary discrete code for controlling the keys of the capacitor bank.

Block 7. Input of load current. The load current is obtained in the form of an analog signal by rectifying the output of the measuring current transformer. Input to the controller is made through the analog-to-digital converter block.

Block 9. Entering the phase angle. The phase angle is measured by a phase meter as an analog signal. Input to the controller is made through the analog-to-digital converter block.

Block 10. Calculation of the capacity of compensation. The initial data for the calculation are the load current and the phase angle of the voltage and current.

Block 11. Calculation of the number of the capacitance interval of the capacitor bank. The interval number is calculated as an integer part from dividing the calculated capacitance of the capacitor by the capacity of the section interval.

Block 12. Analysis: has the interval changed?

Block 13. Assigning a new value to the current interval number.

Block 14. Output of the number of the capacitor interval for controlling the switching keys of the capacitor bank.

Switching in accordance with the *K* code will lead to an uneven load on the keys and operating capacitors, which will significantly reduce the reliability of the elements. In addition, with limited durability of elements, it is important to monitor their condition and take it into account when controlling commutation. For this purpose, a microprocessor controller was introduced into the control loop. The functions of the controller consist in analyzing the state of the triacs of the switch and capacitors, choosing the switching algorithm according to many criteria and informing about the loss of the device's performance. The *Kopt* key control signal is generated at the output of the controller.

The switch block creates an electrical circuit for the current through the block of compensating capacitors.

The peculiarities of the functioning of the automatic control system of the reactive power compensator are determined by the random nature of the formation of the inductive component of the load. This uncertainty leads to uneven use of switch keys and capacitors of the compensating battery. Due to unevenness, the likelihood of loss of performance of the elements increases.

In such a situation, it is necessary to monitor the state of the switches and capacitors and ensure the uniformity of the load on the elements.

The random nature of the load forces us to build complex deterministic algorithms to ensure a uniform load of workable elements, which do not always give reliable error-free results. The task can be attributed to the synthesis of adaptive control systems. Adaptability involves tuning the system parameters to the optimal operating mode under conditions of random load changes and disturbing influences. This problem can be solved using a microprocessor controller in the loop of an automatic control system with an algorithm for generating commands according to artificial intelligence algorithms.

The controller performs a number of functions:

- control of the state of the key and accounting for the statistics of commutations;
- ensuring uniform loading of efficient capacitors and switches;
- assessment of the performance of the elements;
- taking into account the temperature of the capacitors;
- calculation of the priorities of elements to form the control code;
- informing the operator about the loss of system performance.

Parameters of elements for accounting for operability:

- key state *i - Ki* = 1 *(closed) or 0 (open);*
- the number of commands to close the key *i - ki, i* = 1 ... 7*;*
- the number of closures of the key *i - sii* = 1 ... 7*;*
- the average number of key closures *i - Scp* = Σ*si* / 7*;*
- the state of the capacitor *Ci* = 1 *(Uc* ≠ 0*) or* 0 *(Uc* = 0*) at Ki* = 1*;*
- condenser temperature *Ti* = 1 *(toC<Tmax) or 0 (to>Tmax);*

The main design ratios for choosing the numerical values of the model parameters are based on the following network parameters.

Maximum load current $I_{нmax}$ = 50 *A*. Power consumed in the network $P_{нmax}$ = 11 *kW*.

The number of control steps n = 7. The maximum error of the stepwise connection of the compensating power is 14%.

Maximum compensated phase shift of voltage and current

φ = 0.5 *rad* ($\varphi \approx 30^{o}$). In this case, $tg\varphi$ = 0.55. In this case, the error of the asymptotic representation is 10%.

To calculate the capacity of the capacitor bank, the following ratio is used.

$$C = 15\, I_{H}\varphi \ (\mu F)$$

The capacity of the capacitor bank is C = 15 * 50 * 0.55 = 412 μF. Then the capacity of one stage (capacitor) of the battery $C1$ = 412/7 = 58.9 ≈ 60 μF.

The main parameter for choosing capacitors is the value of the compensated reactive power Pc (var). This power can be calculated from the current in the compensating battery. From the vector diagram for the mode of full compensation of inductive power, $Ic / I = tg\varphi$ follows, where Ic is the capacitor current, I is the total current of the supply network, φ is the phase shift of the voltage and current in the network without reactive power compensation. For the maximum current I = 50 *A and* $\varphi = 30^{o} Ic$ = 50 * 0.55 = 27.3 *A.*

Compensation battery power at capacity C = 420 μF

$$Pc = Ic2 * Xc = Ic2 / 2\pi fC =$$
$$= 27.32 / (2\pi * 50 * 420 * 10\text{-}6) = 5650 \ (var).$$

Power per capacitor of one compensation stage

$$Pc1 = Pc / 7 = 0.8 \ (kvar).$$

The parameters of the signals of electronic elements in the structure of the ACS are determined by the choice of the element base for the implementation of circuits.

Conclusion

Analysis of the variety of control methods for reactive power compensation allows us to draw the following conclusions.

1. All methods are based on an indirect estimate of the value of the reactive power and do not provide the required cos φ of the network.
2. Assessment of the compensated power requires the study of specific characteristics of the load and technology of production processes.
3. Compensation control schemes require an individual approach to design and commissioning for a specific situation.
4. Circuits of control devices of compensators are not distinguished by simplicity and reliability.

Based on these conclusions, it can be concluded that the above disadvantages can be eliminated by using automatic control of reactive power compensation based on measuring the reactive power in the load or electrical parameters of the load, which can be used to calculate the value of the compensated reactive power.

Such a compensator must be built using a micro-processor controller to control the commutation of the compensating capacitors of the sectional battery.

To calculate the current capacity of the compensating capacitor, the value of the load current measured by the current transformer and the phase angle of the voltage and current from the electronic phase meter are used.

The control algorithm is developed in the form of a block diagram, which is the basis for programming the controller. The algorithm provides for the ability to vary the maximum load power and the number of capacitor bank sections. This uses the minimum number of I / O ports.

When choosing a controller, it is necessary to take into account the requirements of the algorithm, the shape of the input and output signals, the power requirements and the cost.

To build a model, a block diagram of a discrete automatic control system was obtained with the possibility of optimizing the parameters of elements to ensure a uniform load and taking into account the operability of the components.

References

1. Yaroshevich, A. V. Reactive power compensation scheme in apartment electric networks / A. V. Yaroshevich // Bulletin of the Brest State Technical University. Series: Physics, Mathematics, Informatics. – 2011. – № 5. – P. 66–67.

Accepted 26.10.2021

doi.org/10.36773/1818-1112-2021-126-3-76-78

UDC 621.387.143

THE RESEARCH INTO THERMAL AND ENERGY CHARACTERISTICS OF A PLASMATRON FOR OBTAINING HYDROGEN LOW TEMPERATURE PLASMA

A. I. Verameychyk[1], S. R. Onysko[2], M. I. Sazonov[3], V. M. Khvisevich[4]

[1] Ph.D in Physics and Mathematics, Associate Professor, Senior Research Associate of Brest State Technical University Testing Center, Brest, Belarus, e-mail: vai_mrtm@bstu.by
[2] Ph.D in Engineering, Dean of the Faculty of Mechanical Engineering of Brest State Technical University, Brest, Belarus, e-mail: osr@tut.by
[3] Doctor of Technical Sciences, Professor, Professor of the Department of Applied Mechanics of Brest State Technical University, Brest, Belarus
[4] Ph.D in Engineering, Associate Professor, Professor of the Department of Applied Mechanics of Brest State Technical University, Brest, Belarus, e-mail: vmhvisevich@bstu.by

Abstract
The article presents the results of experimental research of voltampere characteristics, thermal fluxes into the plasmatron elements, electrode erosion, thermal efficiency of a hydrogen plasmatron in the wide range of parameters. Has been developed an original construction of a plasmatron for obtaining hydrogen low-temperature plasma.

Key words: plasmatron, hydrogen, cathode, voltampere characteristic, heat flux, electrode.

ИССЛЕДОВАНИЕ ТЕПЛОВЫХ И ЭНЕРГЕТИЧЕСКИХ ХАРАКТЕРИСТИК ПЛАЗМОТРОНА ДЛЯ ПОЛУЧЕНИЯ ВОДОРОДНОЙ НИЗКОТЕМПЕРАТУРНОЙ ПЛАЗМЫ

А. И. Веремейчик, С. Р. Онысько, М. И. Сазонов, В. М. Хвисевич

Реферат
В статье представлены результаты экспериментальных исследований вольтамперных характеристик, тепловых потоков в элементы плазмотрона, эрозии электродов, теплового КПД водородного плазмотрона в широком диапазоне параметров. Разработана оригинальная конструкция плазмотрона для получения водородной низкотемпературной плазмы.

Ключевые слова: плазмотрон, водород, катод, вольт-амперная характеристика, тепловой поток, электрод.

Introduction

Currently, economically effective processes for the combined production of acetylene and ethylene from hydrocarbon raw materials, plasma-chemical processing of waste from various industries, etc. are widely used. Especially promising are considered the processes of using low-temperature hydrogen plasma [1–16]. In processes where combustion gases are used to supply energy, the efficiency of energy use is very low due to the fact that due to the presence of oxygen in the working mixture, a significant amount of resinous polymers is formed. This reduces the yield of target products and complicates the subsequent processing of gas cracking. These disadvantages can be eliminated if hydrogen heated to a temperature of (3000–4000) K is used as a coolant for pyrolysis of hydrocarbons. A DC or AC plasmatron of the required power can act as a hydrogen plasma generator [3, 4, 6–8]. The increase in the power and service life of such plasmatrons is largely determined by the success in the study of the thermal characteristics and erosion of electrodes. The following works are devoted to this kind of research [3–5, 9, 12–15, 17–20]. Cathode erosion occurs due to complex thermal, electrical, chemical and mechanical processes in the near-electrode area. The main emphasis in most studies of this problem is made on the experimental study of phenomena and empirical generalization of experimental data in order to create a substantiated mathematical model in the future and find rational methods for calculating the optimal designs of cathodes. It is known that the main factor determining the rate of erosion is the specific heat flux into the cathode [12–14, 17–19]. For thermionic electrodes, as a rule, it exceeds 50 kW/sm^2 and depends on the type of working gas, current strength, the nature of the electrode cooling, and other factors. If the arc burns in hydrogen, then the specific heat flux due to the high thermal conductivity of this gas is especially high, therefore, studies of heat fluxes into the elements of the plasmatron and the erosion of electrodes are relevant.

Description of the installation

The diagram of the plasmatron, its power supply and arc ignition are shown in Figure 1. The main elements of the plasmatron are the cathode (1), the igniting electrode (2) and the stepped anode (3). The cathode is made of a 10 mm long thoriated tungsten rod, soldered flush into a copper ring. Tungsten rods (3–10) mm in diameter were used in the experiments. The ignition electrode is made of copper in the form of a washer section with an inner diameter of d_1 = 16 mm. The tested copper stepped anodes had diameters d_2 = 8 mm and d_3 = 16 mm, length l_2 = (30–50) mm. The anode length $l = l_2+l_3$ varied from 90 mm to 150 mm. To reduce the erosion of the working surface of the anode, a solenoid wound from a copper tube (7) is installed. The axial magnetic field created by it (0,06–0,08) T provides such speeds of rotation of the closing radial section of the arc, at which the service life of the anode exceeds 1000 hours. The cathode, igniting electrode, anode and solenoid are intensively cooled with chemically purified water, which is supplied to the plasmatron cooling system under the pressure of (10–15)×10^5 Pa. To calculate the heat fluxes into the electrodes, the temperature of the water at the inlet and outlet of the plasmatron was determined using chromel-copel thermocouples with the recording of the EMP-109AI device readings.

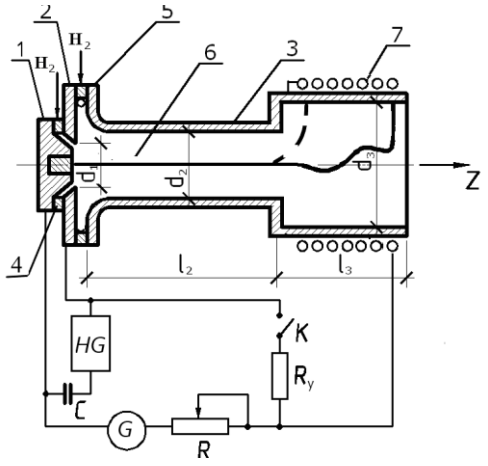

1 – cathode, 2 – ignition electrode, 3 – anode, 4,5 – insulators, 6 – arc, 7 – solenoid

Figure 1 – Plasmatron and power supply diagram

The hydrogen pressure before the flow meters at the plasma torch inlet was (4–8)×10^5 Pa. The gas consumption was measured with devices of the PV-1033 type, and its smooth adjustment was carried out by

automatic devices of the DMPK-100 type. Hydrogen was fed into the gap between the cathode and the ignition electrode through two tangential holes 1,2 mm in diameter located in a twist ring with an inner diameter of 50 mm (consumption 0,1–0,2 g/s). The second swirl chamber (5), located between the ignition electrode and the anode, was supplied with gas through four tangential holes 2,4 mm in diameter located in a swirl ring with an inner diameter of 64 mm. The total hydrogen consumption varied in the range of (0,9–1,2) g/s.

The plasmatron was powered from a power source with a rated current of 600 A and a voltage of 900 V. Since its external electrical characteristic is rigid, and the voltampere characteristic of the arc is falling, a variable step ballast resistance R is connected in series with the arc (for the purpose of its sustained burning). The plasmatron was ignited using a high-voltage high-frequency oscillator with a voltage applied to the ignition electrode (3). The resistance R_y = (10–20) Om is connected between the ignition electrode and the anode through the contactor. Such a circuit for connecting the oscillator to the electric power circuit of the plasmatron made it possible to exclude the ingress of HF voltage into the power supply circuit and thereby ensured a reliable protection of the rectifier from overvoltage. Solenoid (7) is connected in the power supply circuit in series with the arc.

Research of voltampere and thermal characteristics of the plasmatron

In accordance with the methodology [1–8, 16], investigations of the electric field strength of an arc burning in hydrogen were carried out. The results of experiments on the study of voltampere characteristics confirmed the need to maintain the high tangential velocity of hydrogen swirling and a smooth (nonseparated) transition from the swirl ring to the inner diameter of the electrode for the purpose of ensuring gas-dynamically stable arc burning. In the experiments, it was also found out that the arc in the plasmatron scheme under consideration burns with lower voltage pulsations compared to an arc with a self-adjusting length which burns in a cylindrical channel without a ledge.

Figure 2 shows the voltampere characteristics of a hydrogen arc burning in a plasmatron with different anode lengths.

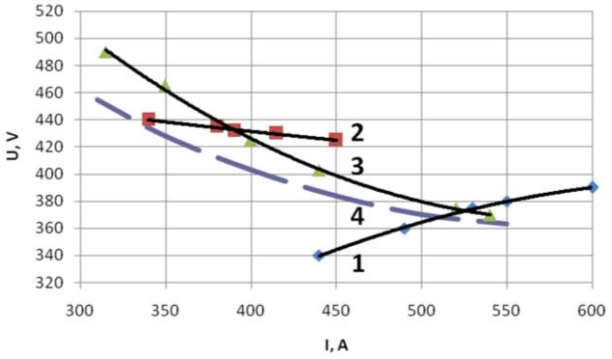

1 – l_2 = 30 mm; 2 – l_2 = 39 mm;
3 – l_2 = 50 mm; 4 – calculated curve
G_{H2} = 1 g/s, d_2 = 8 mm, p = 1,4×10^5 Pa

Figure 2 – Voltampere characteristics of the arc at different lengths

The experimental results showed that at a length $l_2 \le 30$ mm, the electrical characteristic is ascending (curve 1) and at a current of less than 520 A lies below the characteristic of an arc with a self-aligning length (curve 4), calculated by the formula:

$$U = 3190\left(\frac{G}{l}\right)^{0,4}\left(\frac{G}{d}\right)^{0,3}(pd)^{0,36}, \quad (1)$$

where d – inner diameter of the anode of constant cross-section, mm.

It can be surmised that at higher current values, curve 1 coincides with curve 4 on the assumption that the mechanism of formation of the current-voltage characteristic of an arc in hydrogen for a plasmatron with a stepped output electrode is similar to a cylindrical anode.

It should be noted that in the studied range of currents at $l_2 \le 30$ mm, the arc burns stably. Visual inspection of the inner surface of the anode showed that the arc shunting occurs only behind the ledge in the section of the electric discharge chamber with a diameter d_3. At l_2 = 50 mm, the voltampere characteristic of the arc (curve 3) practically coincides with the calculated curve 4, and the shunting zone, already near the ledge, captures some electrode surface with a diameter of d_2 = 8 mm; the electrode ledge undergoes noticeable erosion within a few hours of operation. Therefore, the length l_2 = 50 mm is more than the limiting one. With an increase in l_2 over 39 mm, the pulsation amplitudes of current and voltage increase, and the pulsation frequency also decreases. The data obtained testify to the possibility of achieving a high electrical efficiency of a plasmatron with a stepped shape of the output electrode.

Simultaneously with the study of the current-voltage characteristics of the arc, the study of heat fluxes into the elements of the plasmatron (cathode, anode and ignition electrode) was carried out. This made it possible to calculate the thermal efficiency of the plasmatron, the enthalpy and the average mass temperature of gas depending on the magnitude of the arc current, the anode length, and the methane content in hydrogen under pressure at the outlet of the plasmatron which equals 1,5×10^5 Pa.

Figure 3 shows the data on heat fluxes into the cathode when hydrogen is used as working gas.

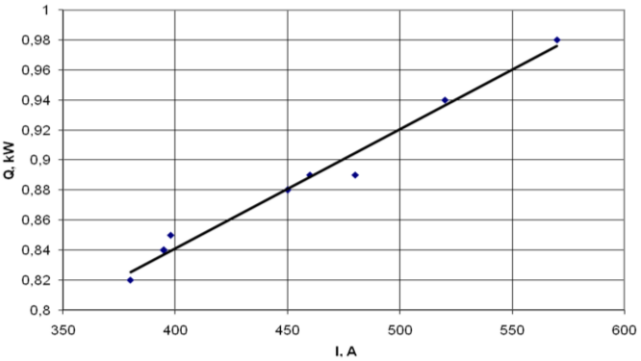

Figure 3 – Dependence of the heat flux into the cathode on the arc current in hydrogen at l_2 = 39 mm

Studies of heat fluxes into the cathode showed that when hydrogen was used as a working gas at equal currents and stable modes of arc burning (l_2 = 39 mm), they turned out to be lower than for nitrogen [15]. Somewhat unexpected results are obtained with an unstable mode (l_2 = 50 mm), when the current amplitude increases and the arc shunting frequency decreases. In this case, heat fluxes into the cathode in the range of current values under consideration increase by about 2 times (Figure 3). This is reflected in the rate of erosion of both the cathode and the anode.

Rapid destruction of the cathode in a hydrogen environment was found during the operation of the plasmatron in the non-self-sustained combustion mode, when the current pulsations reached a noticeable value, although the absolute value of the current didn't exceed several tens of amperes. At high currents (up to 600 A), but small (less than 10 %) high-frequency pulsations (several kHz), the degree of destruction was several times lower. A similar picture is observed in the case of an unstable arc burning mode caused by shunting on the ledge. In this case, each attachment spot moves chaotically along the tungsten surface passing from heated parts of the surface to colder ones. This leads to a decrease in thermo-emission and an increase in the electron auto-emission and, consequently, to an increase in heat fluxes into the cathode.

It was found out that in hydrogen the heat losses into the cathode practically do not depend on the diameter of the tungsten rod, soldered flush into the copper casing, which varied in the experiments within the range of (3–10) mm.

Figure 4 shows the heat fluxes to the anode depending on the arc current for a plasmatron with d_2 = 8 mm, d_3 = 16 mm, l_2 = 50 mm, l = 100 mm at a hydrogen consumption of 1,1 g/s in the operating range of currents they reach (48–64) kW. According to the estimates, heat losses in the area before the ledge do not exceed 10 kW, therefore, the main heat losses occur in the zone behind the ledge. With an increase in l, heat losses increase rapidly. They are mainly determined by convective heat exchange between the heated hydrogen flux and the anode wall. That is why, the thermal efficiency of the plasmatron is mainly determined by the heat loss behind the ledge, and in order to reach its maximum value, the length l should be no more than it is necessary for the zone of arc shunting.

doi.org/10.36773/1818-1112-2021-126-3-79-81

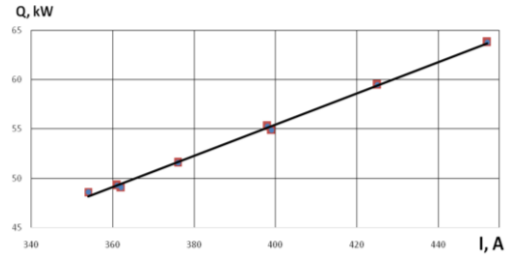

G_{H2} = 1 g/s, d_2 = 8 mm, d_3 = 16 mm,
l_2 = 50 mm, l = 100 mm

Figure 4 – Dependence of the heat flux into the anode on the arc current

The dependence of the thermal efficiency of the plasmatron on the value of the arc current at G_{H2} = 1 g/s, l_2 = 50 mm and different I values is shown in Figure 5. With an anode length close to the optimal (90 mm), the temperature of the jet at the plasmatron outlet reaches 3400 K, and thermal efficiency is (0,6–0,8). The dependence of the thermal efficiency on the current can be represented as:

$$\frac{1-\eta}{\eta} = 9{,}45\times10^{-5}\left(\frac{I}{G}\right)^{0,4}\bar{l}^{1,38}(pd)^{0,98}, \qquad (2)$$

WHERE $\bar{l} = \frac{l_2}{d_2} + \frac{l_3}{d_3}$, D_2 = 8 MM, D_3 = 16 MM.

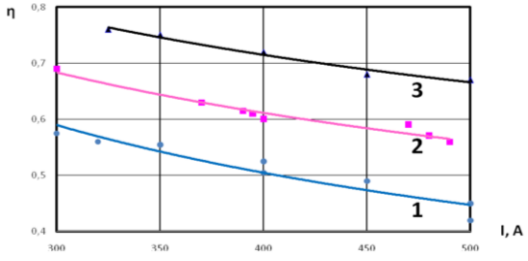

1 – l = 150 mm, 2 – l = 116 mm, 3 – l = 90 mm

Figure 5 – Dependence of the plasmatron thermal efficiency on the magnitude of the arc current

Electrode erosion studies.

Experimental studies of the influence of the rod diameter on the specific erosion of electrodes in a wide range of currents at I = (370 ± 30) A have been carried out.

The dependence of the cathode specific erosion on the rod diameter is given in Figure 6. The lowest value of specific erosion is observed for the rod diametre d_c = 5 mm and is no more than (2–4)×10^{-9} g/(A·s). The amount of erosion was determined by weighing the cathodes before and after the experiment. Inspection of the cathode surface after long-term operation showed that the value of its specific erosion with rod diameters of less than 5 mm increases due to the fact that the arc spot begins to capture a part of the copper ring, which is being intensively destroyed. In some experiments at d_c = 5 mm, the spot on the tungsten surface did not always stabilize; in this case, the amount of erosion increased several times. The increase in erosion at d_c > 5 mm is associated with a deterioration in heat transfer and an increase in the temperature of the tungsten surface in the region of the near-cathode spot. At d_c = 10 mm, the arc spot moved over an area with a diameter of about 6 mm, forming in some place's craters of up to 2 mm with a diameter and depth after (6–10) hours of the plasmatron operation. Evaluation of the cathode service life based on the obtained specific erosion showed that at current values of about 400 A, the continuous cathode service life will be at least 200 hours.

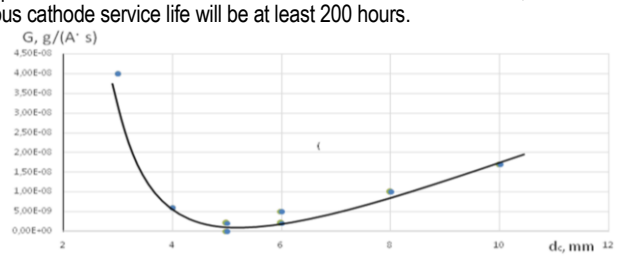

Figure 6 – Dependence of the cathode specific erosion on the tungsten rod diameter, at I = (370 ±30) A

Conclusion

Investigations of current-voltage characteristics, heat fluxes into the elements of the plasmatron, erosion of electrodes, thermal efficiency of the plasmatron for the generation of low-temperature hydrogen plasma have been carried out. On the basis of the developed technique, an original design of the plasmatron was developed. The obtained experimental results and engineering solutions can be used as initial data for designing industrial plasma installations of various capacity.

References

1. Zhukov, M. F. Applied dynamics of thermal plasma / M. F. Zhukov, A. S. Koroteev, B. A. Uryukov. – Novosibirsk : Nauka, 1975. – 299 p.
2. Dautov, G. Yu. Electric field strength in a vortex-stabilized arc / G. Yu. Dautov, M. I. Sazonov. – PMTF, 1967. – № 4. – P. 127–131.
3. Plasma torches. Research. Problems / M. F. Zhukov [et al.] ; ed. M. F. Zhukov. – Novosibirsk, 1995. – 293 p.
4. Veremeychik, A. I. Research of an electric arc in a helium flow in a high-current plasmatron / A. I. Veremeychik, M. I. Sazonov, D. L. Tsyganov // Instruments and experimental techniques. – 2006. – № 5. – P. 99–102.
5. Research of an electric arc in an argon flow / V. V. Batrak [et al.] // Bulletin of the Brest State Technical University. Mechanical engineering. – 2008. – № 4. – P. 26–28.
6. Zhukov, M. F. Electric arc generators of thermal plasma / M. F. Zhukov, I. M. Zasypkin, A. N. Timoshevsky. – Novosibirsk : Nauka, 1999. – 712 p.
7. Isakaev, M.-E. H. Development of a low-temperature plasma generator with an expanding channel and some of its applications : dis. … Dr. Tech. Sciences : 01.02.05; 05.16.01 / M.-E. H. Isakaev. – M., 2002. – 89 p.
8. Rutberg, Ph. G. Plasma / Ph. G. Rutberg [et al.] // IEEE Trans. Plasma Sci, 2002. – V. 30, № 4. – P. 1445–1448.
9. Investigation of thermochemical cathodes in arc plasmatrons / A. S. Anshakov [et al.] // Thermal physics and aeromechanics. – 2005. – T. 12, № 4. – P. 685–691.
10. Tumanov, Yu. N. Plasma, high-frequency, microwave and laser technologies in chemical-metallurgical processes / Yu. N. Tumanov. – M. : FIZMATLIT, 2010. – 968 p.
11. Brichkin, A. V. On the dynamics of electrode spots of an electric arc / A. V. Brichkin, A. V. Bolotov, T. V. Borisova // ZHTF. – 1966. – № 7. – P. 301.
12. Zhukov, M. F. Thermochemical cathodes / M. F. Zhukov, A. V. Pustogarov. – Novosibirsk : Institute of Thermal Physics. Academy of Sciences of the USSR, 1982. – 157 p.
13. Investigation of the erosion of electrodes in DC and AC plasmatrons / V. E. Kuznetsov [et al.] // Applied Physics. – 2019. – № 3. – P. 24–29.
14. Investigation of the erosion products of the copper electrode of the AC plasmatron / D. I. Subbotin [et al.] // Journal of Technical Physics. – 2017. – T. 87, no. 11. – P. 1637–1640.
15. Investigation of the erosion of the wave-frame cathode of the plasmatron for generating nitrogen plasma / A. I. Veremeychik [et al.] // Perspective materials and technologies: materials of the international symposium, Brest, May 27–31, 2019 / ed. V. V. Rubanik. – Vitebsk : VSTU, 2019. – P. 93–95.
16. Bublievsky, A. F. Criterion dependencies for non-flowing electric arcs in the channel / A. F. Bublievsky // IFZH. – 1997. – T. 70, № 1. –P. 99–104.
17. Kesaev, I. G. Cathodic processes of electric arc / I .G. Kesaev. – M. : Nauka, 1968. – 244 p.
18. Khoroshikh, V. M. Erosion of the cathode and the mass consumption of the cathode material in a stationary low-pressure arc / V. M. Khoroshikh // Physical engineering of the surface. – 2005. – T. 2. – № 4. – P. 184–199.
19. Aksenov, I. I. Investigation of the erosion of the cathode of a stationary vacuum arc / I. I. Aksenov [et al.]. – M. : Central Research Institute of Information and Technical and Economic Research on Nuclear Science and Technology, 1984. – 23 p.
20. High-Current Pulsed Vacuum-Arc Evaporator for Surface-Alloying Technologies / S. A. Popov [et al.] // IEEE Transactions on Plasma Science. – 2009. – V. 37. – № 8. – P. 1504–1510.

Accepted 26.10.2021

GEOECOLOGY

UDC 331.04

ECOLOGICAL FEATURES OF PILE WORKS IN CONSTRUCTION

V. P. Chernuk[1], V. P. Shcherbach[2], E. I. Shlyahova[3]

[1] Ph.D in Engineering, Associate Professor, Associate Professor of the Department of Construction Production Technology, Brest State Technical University, Brest, Belarus
[2] Associate Professor of the Department of Construction Production Technology, Brest State Technical University, Brest, Belarus
[3] Senior Lecturer of the Department of Construction Production Technology, Brest State Technical University, Brest, Belarus, e-mail: Katusha_bstu@mail.ru

Abstract
This article shows ecological features of pile works (provided with tables and figures) including pile works for driven piles. The most unfavorable features of pile works are noise and vibrations. Maximum permissible value of noise and vibrations are often exceeded during pile works. It causes growth of different illnesses, including neurological and mental. The article describes individual and collective ways to combat noise. It also shows noiseless and low noise types of pile works protected by patents of USSR and Republic of Belarus and utility models.

Keywords: pile works, features of works, noise, vibration, illnesses, maximum permissible values, individual and collective ways to combat noise, noiseless and low noise technologies, copyright certificates, patents, inventions and utility models.

ЭКОЛОГИЧЕСКИЕ ОСОБЕННОСТИ ПРОИЗВОДСТВА СВАЙНЫХ РАБОТ В СТРОИТЕЛЬСТВЕ

В. П. Чернюк, В. П. Щербач, Е. И. Шляхова

Реферат
В статье описаны экологические особенности производства свайных работ (с таблицами и цифрами), в том числе забивными способами. Наиболее неблагоприятными и проблематичными из них являются шум и вибрация, величина которых превышает предельно допустимые нормы по шуму и вибрации более чем в 2 раза, и они постоянно растут из года в год, а это является причиной множества разнообразных заболеваний людей, в том числе психических и невралгических. В этой связи рекомендованы индивидуальные и коллективные способы борьбы с шумом, а также представлены бес – и малошумные методы производства свайных работ, защищенные а.с. СССР и патентами РБ на изобретения и полезные модели.

Ключевые слова: свайные работы, особенности производства, шум, вибрация, болезни, предельно допустимые нормы, коллективные и индивидуальные средства защиты, бесшумные и малошумные технологии, авторские свидетельства, патенты, изобретения и полезные модели.

Introduction

Protecting the environment and protecting the health of workers are two of the most important issues facing the world today. Noise and vibration control, among others, are an integral part of them. The level of noise in a workplace and in the home might reach 90-100 dB, i.e. 1.5 times the maximum allowable noise standards, and it grows continuously from year to year by 1.5-2 dB, which is the cause of many human illnesses, including neurological ones. The incidence of neurological diseases is almost 80 %.

Noise in industrial and residential construction is particularly damaging, as it usually occurs in densely populated areas, as shown in [1.2]. About 41 % of the complaints of the population are related to noise and vibrations caused by diesel hammers, 12 % – to vibration hammers, vibration divers and copers, 17 % – to jackhammers, 7 % – to compressors and 23 % to other construction machines (excavators, cranes, cars, etc.). Approximately half of the public complaints about noise and vibration arising from construction work are psychological causes – impediments to rest, sleep, work and training. About two thirds (65 %) of complaints from the public are brought before the courts for compensation for moral damage, damage to health, and another third for material damage caused to residential buildings and structures adjacent to construction sites where construction works are being carried out. This is mainly due not only to the noise but also to the vibrations that accompany the construction of pile foundations due to piling equipment action.

In many Western European countries, such as France and the United Kingdom, pile works, operated with impact methods, are prohibited by law because of high levels of vibration and sound pressure and also to protect and preserve historical monuments, buildings and structures, as well as human health. This prompted many construction companies to switch to other impactless and quiet pile works and types of piles - from driven piles to filling and drilled piles (Strauss, Benoto, Franki, vibrotam, delta pile, and others) and the companies producing hammers for driven piles and copra adapt to production of machines with improved technological and technical characteristics.

Main part

As numerous studies have shown, noise and vibration can, to a greater or lesser extent, temporarily activate or permanently suppress certain psychological processes in the human body and lead to various neurological diseases. Physiopathological effects can occur in the form of hearing impairment and other analysers, such as the vestibular apparatus coordinating the functions of the cerebral cortex, the nervous and digestive system, the circulatory system and the heart. In addition, noise affects carbon, fat and protein metabolism in the body.

Vibration, in turn, acts on the central nervous system, gastrointestinal tract, organs of balance (vestibular apparatus), causes dizziness, numbness of limbs, joint disease. Long-term exposure to vibration leads to occupational disease, a vibrational disease that can only be effectively treated in the early stages and recovery is very slow, and under certain conditions irreversible processes may occur in the body, accompanied by total disability and impending disability.

Noise and vibration problems

The highest level of noise and vibration, and these are the associated adverse human exposure factors in the construction industry, as shown by the analysis, are created by machines and mechanisms, equipment and instruments of impact action.

The most unfavourable thanks to level of noise, sound and vibration, the degree of exposure is pile-driving equipment, especially diesel hammers (both rod and tubular), copra of any type (rail, tractor, road, excavator, bridge type), followed by vibration hammers and vibratory pile driver, rolling stock of rail transport as well as buses, trucks, cars and special vehicles, excavators and other earth-moving equipment, concrete mixers, concrete laying and other construction equipment.

For example, pile-driving machine equipped with a diesel hammer, at a distance of 15 m, the maximum sound pressure level reaches 100 Db or more, which has a detrimental effect on the health of the workers and surrounding peple, increases their fatigue and, consequently, reduces labour

doi.org/10.36773/1818-1112-2021-126-3-82-84

productivity. Levels of sound pressure for different ways of driving piles, measured by «Octave 101A» instrument, showed the following results:

Pile-driving with diesel hammers - 100 120 dB;

Vibration immersion of piles with vibratory pile driver - 80 100 dB;

Vibration with impact - 90 110 dB.

At the same time, the maximum allowable sound pressure levels, sound levels and equivalent sound levels for the most typical types of works are established by SanPiN 22.4/2.18.1032-2002 in the table. 1, almost 2.5 times lower than above mentioned. At the same time, the maximum allowable sound pressure levels (dB), sound levels (dBA) and equivalent sound levels (dBA) for the most typical types of works are given within octave bands with geometric mean frequencies of 31.5; 63; 125; 250; 500; 1000; 2000; 4000; 8000 Hz, because the human hearing system perceives sound oscillations in a frequency range of 16 to 20,000 Hz, and the area of the highest hearing sensitivity is in the region of 50,000 Hz, which is located in the octave band region. Oscillations up to 16 Hz (infrasound) and above 20,000 Hz (ultrasound) are not perceived by human ears. However, this does not mean that the effects of infrasound and ultrasound are not harmful to human beings.

In addition to the Republic's health standards for industrial noise GOST 12.1.003 also regulates sound and sound pressure levels in workplaces (tabl. 2).

Table 1 – Sound pressure limits, sound levels and sound equivalencies for the most typical occupations

Type of occupation	Sound pressure levels, dB, octave bands with geometric mean frequencies 31.5 - 8000 Hz	Sound levels and equivalent sound levels, dBA
Creative activity, management with increased requirements, design, study, teaching, medical activity, etc.	86-38	50
Focused, high-quality, administrative and managerial work	93-49	60
Operations and movement control	96-54	65
Focused and observational work	103-64	75
Work in permanent locations (except above)	107-69	80
Jobs in railway rolling stock	93/100 49/69	60/80
Jobs in buses, trucks and special vehicles	93/100 49/59	60/70

Note: Sound pressure levels, sound levels and equivalent sound levels for intermediate values in octave bands are between minimum 31.5 and maximum 8,000 Hz octave frequencies.

Table 2 – Allowable sound pressure levels, sound levels in workplaces, industrial premises and on the premises of enterprises

Workplaces	Sound pressure levels, dB, octave bands with geometric mean frequencies 63 - 8000 Hz	Sound levels, dBA
Design office facilities, experimental data processing laboratories	71 - 38	50
Control rooms, work rooms	79 - 49	60
Laboratory facilities for pilot work	94-70	80
Permanent workplaces and work zones in industrial premises and on the premises of enterprises	99-74	80

Note: see note to table. 1.

Noise abatement techniques

In general, human noise protection, including noise induced by pile works, is divided into personal and collective. Personal protective equipment:

- headphones that provide reasonable protection of the hearing. For example, VCNIOT headphones reduce the sound pressure level by 7÷38 dB in a frequency range of 125÷8000 Hz. Currently, the industry produces headphones of the Aria, Nautilus, Big, Traxon, etc.
- Noise-free inserts («Comfort-plus», MAX-1, Laser life, noise-free inserts (Byushi) etc.) inserted directly into the auditory canal of the outer ear. They are made of light rubber, elastic plastics, rubber, ebonite and ultrafine fibre. They lower the sound pressure level by 10÷15 dB.
- helmets are recommended for noise protection with a general level above 120 dBA. They hermetically cover the entire parotid region of the head and reduce the sound pressure level by 30 40 dB in the operating range of 125÷8000 Hz.

Means of collective protection:

- sound insulation - fences, panels, cabinets, screens, enclosures, fences and «green walls» preventing noise from one room to another or in the same room;
- sound absorption - the ability of a material or structure to absorb the energy of sound waves. These include linings, single-piece sound absorbers made of materials with sound absorption factor α>0.2. Sound-absorbing barriers are divided into 4 classes: fibrous-porous (felt, wool, acoustic plaster, ultra-thin glass or basalt fibre), membrane (PVC and other films, thin sheets of plywood or metal on trim), resonant (special structures based on the acoustic properties of the resonator), combined (devices using previous materials);
- silencers - adsorption, active, reactive, combined.

Collective protection measures such as:

- Removal or reduction of noise and vibration directly at the source, i.e. in piling equipment;
- Localization of noise and vibration sources in piling equipment;
- rational placement of piling equipment on the construction site;
- acoustic treatment of the auxiliary rooms for the staff servicing the installation;
- introduction of quiet and low-noise technological processes and equipment.

Mentioned in the last paragraph way, as the most promising and effective way to combat noise, must be discussed separately.

One of the most noiseless is the technology of pile works with predrilled large-diameter wells (larger than the diagonal of the cross-section of the pile), applied in dense and strong soils, where much noise is made during the process of drilling, followed by the filling of the grooves with a dirt mud. The method relates to drilling piles, is applicable and only possible in conditions of permafrost spread (Norilsk, Vorkuta, Yakutia and other regions) in the Far North of the Russian Federation and in areas of stable and rocky soils, including in Bashkortostan, in which piling is simply impossible.

Low noise method is the way in which piles are filled into small diameter wells (leading wells) pre-drilled in the ground, the diameter of which is equal to or less than 5 cm on the side of the square section of the pile. The conditions for the use of the method are the same as those for the noiseless ones, but the sound pressure level is reduced by half compared to the driven piles.

The low- and noiseless techniques used to immerse piles also include hydraulic submersion of the soil under the piles, as well as submersion of piles with sleeves and in thixotropic (clay) shirts. In these techniques, the dive force is reduced by 50-70%, which also reduces noise and vibration. In the development of these methods, the authors from BSTU proposed a number of technical developments of effective structures of driven piles and ways of their submersion by hydraulic and other methods protected by USSR patents (779507, 779508, 881201, 887725, 891840, 947278, 962447, 962454, 1004539, 1032102, 1135843, 1153010, 1157164, 1458500) RB patents on inventions (6032, 10518) and useful models (1682, 3603, 5228, 6882) and published in [3, 4]

The water-washing of a soil under high-pressure pumps or self-flow is used to facilitate immersion of hollow-shell piles, especially of large dimensions (cross-section and length) in unconnected (sand) and poorly connected (loamy and clay) soil, as well as for the high depth immersion and insufficient immersion capacity of the pile-driving equipment. This method is applicable if it doesn't cause slump of neighbouring buildings and structures.

The inventive method consists in washing the ground under the pile end. A water is suppled to the end of pile with a help tubes fixed on sides of a pile. As a result under the action of own weight and the weight of the hammer mounted thereon it immerses to the soil. At the last metre of immersion, the pile is stopped and the piling is finished in the usual way. Friction piles should be immersed with care, as the adhesion of the side surface of the pile to the ground is impaired. The effect of hydro-sweeping is that, under water pressure, the frontal resistance of the soil is reduced by erosion. In addition, the flow of water rises along the side surface of the pile, washing the soil and weighing its particles. As a result, ground resistance is reduced and the required pile loading is reduced too.

It is known that the fraction of resistance under the pile head is more than half the total immersion resistance, the rest (about 50%) is the friction on the side surface of the pile. Their ratio depends on the length and size of the cross-section of the pile (the longer the pile, the smaller the proportion of frontal resistance of the ground, and vice versa), the physical-mechanical properties of the soil and other parameters. In order to reduce friction (adhesion) of the pile against the ground, it is advisable to apply the coating of the side surface of the pile with materials having high antifriction properties and low friction coefficient. Such materials include clay (thixotropic) solutions and pastes, carbamide, furfurfurolanil, polyacrylamide and epoxy resins and coatings, and water as lubricant. The department of TSP has created a number of progressive inventions (RB patents on useful models 7573, 8601, 9781 and etc)

Several fairly simple and efficient hydraulic and self-lubricating structures of such piles are represented in figure 1, in which the reduction of the frontal and lateral resistance of the pile during immersion is due to the forced supply of water or the moulding into the friction zone and the destruction of the ground.

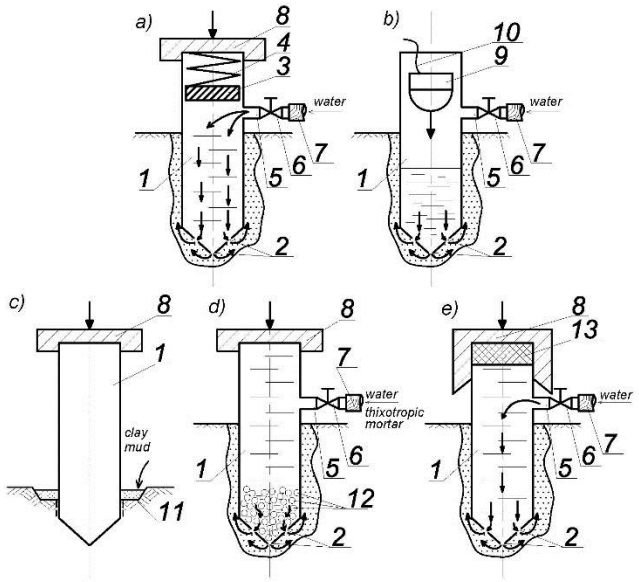

Figure 1. Efficient hydraulic washing (a, b, d, e) and self-lubricating piles (d, c): a) with spring-loaded disc; b) with floating cargo; c) with thixotropic moulding; d) - large-scale additions; e) with a resilient tie pad; 1 - pile; 2 - through holes; 3 - solid disc; 4 - compression spring; 5 - pipe; 6 - valve; 7 - hose; 8 - hose tip 9 - suspended weight; 10 - flexible thrust; 11- dibhole with thixotropic mortar; 12 - large-area rounded inclusions (boulders, pebbles); 13 - a resilient rubber pad.

Conclusion

Usage of individual and collective means of protection against noise and vibration, as well as noiseless and low-noise methods of pile works, washing the ground under the pile's, as well as coating of pile's lateral surfaces with anti-friction materials and lubricants makes it possible to reduce the noise level during the immersion of driven piles to permissible limit values, and also reduces the risk of occupational diseases at work.

References

1. Resource-saving foundations in rural construction sites / A. S. Krechin [et al.]. – Chisinau : Kartya Moldoveneaske, 1990. – 248 p.
2. Chernuk, V. P. Calculation, design and construction of pile foundations / V.P. Chernuk, P. S. Poyta. – Brest : Regional typography, 1998. – 216 p.
3. Chernuk, V. P. Production of pile works in special construction conditions / V. P. Chernuk, P. P. Ivasyuk. – Saarbrücken : LAP LAMBERT Academic Publishing, 2016. – 196 p.
4. Chernuk, V. P. Pile work technology in special construction conditions: textbook / V. P. Chernuk, E. I. Shlyahova. – Moscow : RUSAYNS, 2019. – 241 p.

Accepted 28.10.2021

doi.org/10.36773/1818-1212-2021-126-3-82-84

UDC 621.311.243(476)

ESTIMATION OF OPERATIONAL EFFICIENCY OF FIXED AND SOLAR TRACKING PV SYSTEMS IN BELARUS CLIMATE

A. P. Meshyk[1], K. A. Meshyk[2], M. V. Barushka[3], V. A. Marozava[4]

[1] *Ph.D in Engineering, Associate Professor, Head of the Department of Environmental Engineering, Brest State Technical University, Brest, Belarus, e-mail: omeshyk@gmail.com*
[2] *Master of Engineering Science, Teaching Assistant at the Department of Heat and Gas Supply and Ventilation of Brest State Technical University, Brest, Belarus, e-mail: krill3april@mail.ru*
[3] *Master of Engineering Science, Senior Lecturer of the Department of Foreign Languages, Brest State Technical University, Brest, Belarus, e-mail: borushko.marina@mail.ru*
[4] *Master of Engineering Science, Senior Lecturer of the Department of Descriptive Geometry and Engineering Graphics, Brest State Technical University, Brest, Belarus, e-mail: vmorozova-brest@mail.ru*

Abstract
The authors of the article estimate a feasibility of utilizing solar power facilities on the territory of Belarus. They calculate total values of solar radiation under ideal weather conditions and make conclusions about operational efficiency of fixed and tracking PV systems.

Keywords: Solar power facilities, PV system, installed capacity, Belarus, total solar radiation, fixed PV collector, single-axis tracker, two-axis tracker.

ОЦЕНКА ЭФФЕКТИВНОСТИ РАБОТЫ СТАЦИОНАРНЫХ И РЕГУЛИРУЕМЫХ ГЕЛИОСИСТЕМ В КЛИМАТИЧЕСКИХ УСЛОВИЯХ БЕЛАРУСИ

О. П. Мешик, К. О. Мешик, М. В. Борушко, В. А. Морозова

Реферат
В работе оценивается целесообразность применения гелиосистем для территории Беларуси. Установлены суммарные значения поступлений солнечного излучения в идеальных климатических условиях при стационарном размещении гелиоустановки, а также с динамическим стремлением к ортогональному закреплению воспринимающей поверхности по отношению к центру солнечного диска на базе одноосевого и двухосевого регулирования. Сделаны выводы о роли географического положения эксплуатируемых гелиосистем.

Ключевые слова: гелиосистемы, установленная мощность, Беларусь, солнечное излучение, стационарное расположение, одноосевое регулирование, двухосевое регулирование.

Introduction

A transfer from traditional sources of energy to renewable ones is quite reasonable due to the stable population growth and increasing consumption of energy. Alternative power resources are becoming more and more popular since they are inexhaustible, reduce our use of non-renewable potential of nature, and eliminate environmental damage caused by mining works and CO_2 emissions.

In Belarus solar industry seems the most promising kind of alternative energy among others. It is confirmed by the experience and implementation of the technology in neighboring countries with the climate features similar to Belarusian [1]. In accordance with the global distribution of solar radiation in different regions of the world the territory of our country receives 2655 kWh/m^2 of solar energy in the atmospheric boundary layer and 1184 kWh/m^2 on the underlying terrain, which actually correspond to the figures in Germany (2764 kWh/m^2, 1137 kWh/m^2, respectively) and Great Britain (2655 kWh/m^2, 1015 kWh/m^2, respectively). If we also take into account lower air temperatures in Belarus, we might assume even higher performance of solar power facilities here [2].

From 2000 till 2019 the total capacity of solar power plants increased 479 times and reached 587,134 MW [3]. Today, 108 solar plants in use generate electricity from solar radiation in Belarus. Their installed power capacity is increasing annually. In 2020 it reached 159 MW [4].

Some research that estimates the climate potential for developing solar industry in Belarus reveals that the potential here is 10% higher than in Poland or the Netherlands and it is 17% higher than in Germany, Belgium, Denmark, Ireland or Britain. Consequently, the climate factor cannot be regarded as a constraining one [1, 5, 6, 7, 8, etc.]. What can really restrict solar industry here is the cost efficiency of current solar panels available on the market and low electricity tariffs that do not allow the owners to return on their investment fast enough. Although, it is worth taking into consideration that the efficiency can be improved by implementing automated orientation of solar panels to the sun. It can be achieved with the use of an adjustment technology with single-axis and two-axis trackers [9].

Methods and Materials

This research uses meteorological data provided by Belhydromet (Republican center for hydrometeorology, control of radioactive contamination and environmental monitoring) in 2020-2021. These include hourly temperature fluctuations and wind regime in the area under study [10]. The universal assessment criterion is total solar radiation received in ideal clear sky weather. The authors of this research applied such methods of statistical processing of experimental data as regression analysis, time series analysis, spatial generalization of meteorological data, etc. Calculation was automated with the use of SunCalc and MS Excel applications.

Results and Discussion

Total solar radiation incident on an inclined surface is the sum of three components: beam, diffuse, and reflected radiation.

In general, this sum of solar radiation can be calculated with the following formula [11]

$$Q = S_{nakl} + D_{nakl} + R_{nakl}\,, \quad (1)$$

where S_{nakl} is the beam solar radiation incident on a tilted surface of a PV panel, W/m^2; D_{nakl} is the diffuse solar radiation incident on a tilted surface of a PV panel, W/m^2; R_{nakl} is the solar radiation reflected from underlying terrain and incident on a tilted surface of a PV panel, W/m^2.

The amount of beam radiation incident on an inclined surface depends on the amount of radiation reaching the surface orthogonal to the sun and the cosine of an incidence angle which changes during the day [12]

$$S_{nakl} = S_{ort} \cdot cos\theta, \quad (2)$$

where S_{ort} is the beam solar radiation incident on an orthogonal surface, W/m^2; θ is the angle of incidence of S_{nakl} on a PV collector, rad.

The amount of beam radiation incident on an orthogonally oriented surface is calculated here according to the adapted formula by Kastrov [2]

$$S_{ort} = S_0 - \frac{S_0 \cdot c}{c + sin\alpha}, \quad (3)$$

where S_0 is the solar radiation in the top atmosphere, W/m^2; α is the sun elevation angle, rad; c is the air transparency index.

The angle of sun rays incidence on a tilted surface θ allows us to assess the amount of beam radiation at a certain time. In order to calculate it foreign researchers use data about the sun declination angle around polar axis γ displaced from the south [13, 14, 15]. This angle represents the PV panel's azimuth declination. We apply the algorithmic approach to calculate the optimal orientation of a PV panel. That is why angle γ is displaced from the north as the sun's azimuth

$$cos\theta = sin\delta \cdot sin\varphi \cdot cos\beta + sin\delta \cdot cos\varphi \cdot sin\beta \cdot cos\gamma + cos\delta \cdot cos\varphi \cdot cos\beta \cdot cos\omega - cos\delta \cdot sin\varphi \cdot sin\beta \cdot cos\gamma \cdot cos\omega - cos\delta \cdot sin\beta \cdot sin\gamma \cdot sin\omega, \quad (4)$$

where δ is the geocentric declination, rad; φ is the latitude of location, rad; β is the incidence angle of a PV collector to the underlying surface, rad; γ is the sun's azimuth, rad; ω is the hour angle, rad.

We choose Brest and Vitebsk as geographic points to locate our PV systems as there is a big demand for electricity in the regions and to avoid losses of electricity during its transmission to large distances.

A PV panel is located effectively if its collector is mounted orthogonally to the sun at noon so as to receive the biggest possible share of direct beam radiation during the day. The angle directly depends on the panel's location and spatial characteristics of the sun at the point. We propose to make the adjustment of the PV system all the year round horizontally and both horizontally and vertically. It will allow us to assign the incidence angle of the PV system β as equal to the latitude of the location φ. In the case of single-axis trackers it is preferable to adjust the system daily β [14] when geocentric declination is as a correction factor,

$$\beta_{sut}^{n} = |\varphi - \delta|, \quad (5)$$

However, in the case of two-axis trackers it is not necessary to determine the incidence angle of the PV system as the beam radiation reaches the underlying surface orthogonally ($cos\theta = 1$).

The diffuse radiation incident on a titled surface is calculated with the following equation [16]

$$D_{nakl} = D_{gor} \cdot (0{,}55 + 0{,}434 \cdot cos\theta + 0{,}313 \cdot cos^2\theta), \quad (6)$$

where D_{gor} is the diffuse radiation incident on a horizontal surface, W/m^2.

In order to estimate the reflected radiation most experts apply the isotropic model [17]

$$R_{nakl} = Q_{gor} \cdot A_k \cdot (1 - cos\beta) \cdot 0{,}5, \quad (7)$$

where Q_{gor} is the total solar radiation incident on a horizontal surface, W/m^2; A_k is the albedo of the ground surface.

As a result, we estimated the intensity of total solar radiation incident on the surface of the PV collector randomly oriented in space. The calculation method was applied for solar power facilities with fixed orientation as well as for single-axis and two-axis trackers.

The maximum output capacity was calculated with the formula [18]

$$P_{sp} = K_w \cdot N_{sp} \cdot \eta_s \cdot Q \cdot ln\, 10^6 \cdot Q / T_{sp}, \quad (8)$$

where K_w is the coefficient of the solar panel CVC; N_{sp} is the number of solar panels ($N_{sp} \neq 1$ if medium-scale and large-scale trackers are used), items; η_s is the performance coefficient of the solar panel; Q is the total solar radiation, W/m^2; T_{sp} is the current temperature of the panel, °C.

We determined the total solar radiation in the following time periods:

1. January 2020-2021 (hourly determined radiation);
2. July 2020-2021(hourly determined radiation);
3. June 22nd, 2020 (minutely determined radiation).

The data about local air temperature and wind velocity necessary to determine a temperature regime of the PV panels were obtained from weather monitoring databases [10]. In order to facilitate calculation the values were averaged to hourly units. Actual duration of sunshine that changes every day was determined with SunCalc application.

We determined hourly peaks of all the radiation types from sunrise to sunset for each of the time periods under question. In order to optimize the results received we can provide aggregate number of the peaks for each day which are determined as follows

$$Q_m^n = Q_m^1 + Q_m^2 + \ldots + Q_m^{31}, \quad (9)$$

where Q_m^n is the total solar radiation obtained from the hourly determined peaks, kW/m^2; n is the number of the day; m is the number of the month.

For example, on January 1st, 2020 the duration of daylight in Brest was 7 hours 48 minutes. The sun rose at 9.35 a.m. and set at 5.23 p.m. The sun was at its zenith at 1.29 p.m. It is the time of maximum possible peak capacity in hourly units. As there is very little sunshine during the first few minutes after the sunrise and a few minutes before the sunset, we can ignore them. Therefore, we calculated the data from 10 a.m. to 5 p.m. This approach was used to calculate the total solar radiation in January and July 2020 and 2021 in Brest and Vitebsk. The calculation results are given in Table 1.

Table 1 – Total solar radiation per month

Month, year	Total solar radiation, kW/m^2					
	Fixed PV collector		PV with 1-axis tracker		PV with 2-axis tracker	
	Brest	Vitebsk	Brest	Vitebsk	Brest	Vitebsk
January 2020	64.45	48.37	111.88	87.13	127.74	104.70
January 2021	65.30	49.16	112.86	88.11	128.82	105.83
July 2020	348.19	333.65	401.97	400.81	428.47	432.68
July 2021	349.07	334.59	402.06	400.95	428.53	432.79

It is evident from the table that PV systems with two-axis tracker work much more efficiently than either fixed or single-axis ones. In winter two-axis trackers receive 1.14-1.2 times as much radiation as one-axis trackers and 1.97-2.17 times as much as the fixed ones depending on their geographic location. In summer, two-axis trackers receive 1.07-1.08 times as much radiation as one-axis trackers and 1.23-1.3 times as much as the fixed ones.

Under ideal weather conditions deviation in the calculation results in 2020 and 2021 is insignificant. It allows considering anticipated output capacity in advance. Maximum output capacity of the three PV collectors in the mentioned time periods are calculated with formula (8). The calculation results of the total output of the PV systems in Brest and Vitebsk are given in Table 2.

Table 2 – Total output capacity of PV collectors per month

Month, year	Total solar radiation, kW/m^2					
	Fixed PV collector		PV with 1-axis tracker		PV with 2-axis tracker	
	Brest	Vitebsk	Brest	Vitebsk	Brest	Vitebsk
January 2020	7.13	5.09	15.30	11.15	18.18	14.17
January 2021	7.24	5.19	15.47	11.31	18.37	14.36
July 2020	33.07	30.81	38.92	38.29	42.96	43.06
July 2021	33.16	30.91	38.92	38.29	42.96	43.06

The characteristic features of the solar radiation received appear to be different in these types of PV systems. To show the difference more vividly we calculated the radiation in minute units and separated it into beam radiation incident on a tilted surface S_{nakl}, and the sum of diffuse and reflected radiation $D_{nakl} + R_{nakl}$. We also took into account the maximum capacity of converter P_{sp}. The longest day of the year, June 22nd, 2020 was taken as an example of calculation. In our calculation we used actual duration of daylight. The summed up values are presented in Table 3.

Figures 1–3 show the parameters changing per minute if either a fixed PV panel or a single-axis tracker or a two-axis tracker is employed.

doi.org/10.36773/1818-1112-2021-126-3-85-87

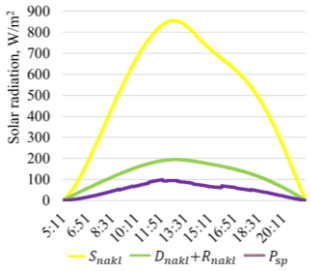

Figure 1 – Dynamic in solar radiation coming per minute and maximum capacity of a fixed PV system

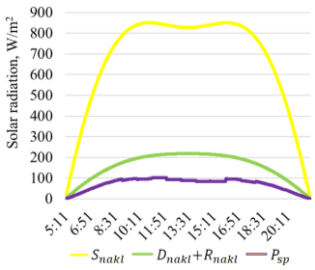

Figure 2 – Dynamic in solar radiation coming per minute and maximum capacity of a single-axis tracker

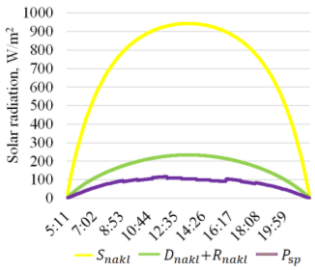

Figure 3 – Dynamic in solar radiation coming per minute and maximum capacity of a two-axis tracker

Table 3 – Summed up values per minute on June 22nd, 2020

Adjustment of PV system	S_{nakl}, W/m²	$D_{nakl} + R_{nakl}$, W/m²	P_{sp}, W/m²
Fixed PV collector	506.81	121.56	50.71
Single-axis tracker	664.56	155.46	71.18
Two-axis tracker	706.36	161.06	77.15

Conclusion

Climate conditions in Belarus are quite suitable to develop solar industry. The figures calculated in the research show an insignificant deviation although Brest and Vitebsk are situated quite far from each other. The deviation is more typical of summer. In winter the energy yield is better in Brest. But the total net generation reduces significantly as the angle of the sun elevation changes and the daylight shortens. The results obtained in the research confirm a sufficient power potential. However, in real life conditions it is necessary to take into account clouds as an important factor that can affect the energy generation. This factor is to be investigated in our further research where we are going to analyze cloudiness and use an algorithmic approach to operate PV systems according to the weather forecast [19].

This comparative analysis reveals that the PV systems with two-axis trackers are the most productive type of the three. They capture solar radiation 34.27% more effectively than the fixed PV systems and 7.73% more effectively than single-axis trackers.

References

1. Meshyk, O. P. Assessment of solar energy resources of the climate of Belarus / O. P. Meshyk, M. V. Borushko, V. A. Morozova // Bulletin of Brest State Technical University. Water management construction, heat power engineering and geoecology. – 2020. – № 2 (120). –P. 93–99. – DOI: https://doi.org/10.36773/1818-1212-2020-120-2.1-93-99.
2. Gremenok, V. F. Solar cells based on semiconductor materials / V. F. Gremenok, M. S. Kuznetsov, V. B. Tivanov. – Minsk : BSU, 2007. – 222 p.
3. Installed Capacity Trends [Electronic resource] / IRENA – International Renewable Energy Agency. – Access mode: https://www.irena.org/Statistics – Access date: 22.08.2021.
4. State cadastre of renewable energy sources [Electronic resource] / Ministry of Natural Resources of the Republic of Belarus. – Minsk, 2020. – Access mode: http://www.minpriroda.gov.by/ru/new_url_-19948904-ru/. – Access date: 22.08.2021.
5. Meshyk, A. Thermal Resources of the Climate of West Polesie, Belarus / A. Meshyk, M. Sheshka, M. Barushka // 7th International Congress on Energy and Environment Engineering and Management (CIIEM7) : Abstracs Book, Canary Islands, Spain, 17–19 July 2017 ; edited by ScienceKnowconferences. – Las Palmas (Spain), 2017. – P. 94–95.
6. Climate Resource Potential to Develop Solar Power in Belarus / A. Meshyk [et al.] // ICBTE 2020. 3S Web Conferences, 212 (2020) 01012. – DOI: https://doi.org/10.1051/e3sconf/202021201012.
7. Meshyk, O. P. Prospects for the development of solar energy in the Republic of Belarus / O. P. Meshyk, M. V. Borushko // Actual problems of Earth sciences: studies of transboundary regions: a collection of materials of the IV International scientific-practical conference assigned to 1000-anniversary of the city of Brest, September 12-14, 2019 / Brest State University named after A.S. Pushkin ; ed. A. K. Karabanova [et al.]. – Brest : BrSU, 2019. – Part 2. – P. 250–253.
8. Meshyk, O. P. Potential climatic resources for the development of solar energy in Belarus / O. P. Meshyk, M. V. Borushko, V. A. Morozova // Comprehensive approach to scientific and technical support of agriculture : materials of the International Scientific and Practical Conference dedicated to the memory of Ya. Bochkareva. – Part I. – Ryazan : RGATU, 2020. – P. 86–91.
9. The efficiency of solar systems (on the example of the climatic conditions of Belarus / O. P. Meshyk [et al.] // Actual scientific, technical and environmental problems of preserving the environment: collection of works of the IV International Scientific and Practical Conference dedicated to the 55th anniversary of the Brest State Technical University and the 50th anniversary of the Faculty of Engineering Systems and Ecology, Brest, October 7-8, 2021 / Brest State Technical University; editorial board: A. A. Volchek [et al.] ; scientific editor A. A. Volchak, O. P. Meshyk. – Brest : BrSTU, 2021. – P. 235–245.
10. Archive of meteorological observations [Electronic resource] / Belhydromet. – Access mode: http://www.pogoda.by/meteoarchive/#. – Access date: 22.08.2021.
11. Shakirov, V. A. Methodology for assessing the arrival of total solar radiation on inclined surfaces using long-term archives of meteorological data / V. A. Shakirov. – Systems. Methods. Technologies. – 2017. – № 4. – P. 115–121.
12. Calculation of the total radiation flux on the inclined plane of solar receivers under conditions of aerosol pollution of the atmosphere / B. I. Nazarov [et al.] // Reports of the National Academy of Sciences of Tajikistan. – 2015. – № 12. – P. 1111–1118.
13. Duffie, J. A. Solar engineering of thermal processes / J. A. Duffie, W. A. Beckman. – Fourth Edition. – Hoboken : John Wiley & Sons, 2013. – 928 p. – DOI: https://doi.org/10.1002/9781118671603.
14. Optimal Tilt Angle and Orientation of Photovoltaic Modules Using HS Algorithm in Different Climates of China / Mian Guo [et al.] // Applied Sciences. – 2017. – Volume 7, Issue 10. – DOI: https://doi.org/10.3390/-app7101028.
15. Mousavi Maleki, S. A. Estimation of Hourly, Daily and Monthly Global Solar Radiation on Inclined Surfaces: Models Re-Visited / S. A. Mousavi Maleki, H. Hizam, C. Gomes // Energies. – 2017. – Volume 10, Issue 1. – DOI: https://doi.org/10.3390/en10010134.
16. Samoilov, D. V. Creation and research of a thermal stabilization system for a greenhouse for the conditions of central Russia : Abstract of a dissertation for the degree of candidate of technical sciences [Electronic resource]. – Access mode: https://static.freereferats.ru/-_avtoreferats/01002979840.pdf. – Date of access: 22.08.2021.
17. Impact of solar panels on global climate / Aixue Hu [et al.] // Nature climate change. – 2016. – № 6. – P. 290–294. – DOI: https://doi.org/-10.1038/nclimate2843.
18. Obukhov, S.G. Choice of parameters and analysis of the effectiveness of the application of tracking systems for the Sun / S. G. Obukhov, I. A. Plotnikov // Bulletin of the Tomsk Polytechnic University. – 2018. – № 10. – P. 95–106.
19. Severyanin, V. S. Meteo-predictive regulation of the temperature regime of premises by automated heating systems / V. S. Severyanin, K. O. Meshyk // Bulletin of the Brest State Technical University. Water management construction, heat power engineering and geoecology. – 2019. – № 2. – P. 74–77.

Accepted 28.10.2021

UDC 621.9.08:004.514.62

RAIN SURFACE RUNOFF MODELING USING CELLULAR AUTOMATON

A. A. Volchak[1], D. A. Kostiuk[2], D. O. Petrov[3], N. N. Sheshko[4]

[1] Doctor of Geographical Sciences, Professor, Dean of the Faculty of Engineering Systems and Ecology, Brest State Technical University, Brest, Belarus; email: volchak@tut.by
[2] Ph.D in Engineering, Associate Professor of the Department of Electronic Computing Machines and Systems, Docent of Brest State Technical University, Brest, Belarus, email: dmitriykostiuk@gmail.com
[3] Ph.D in Engineering, Associate Professor of the Department of Electronic Computing Machines and Systems, Brest State Technical University, Brest, Belarus, email: polegdo@gmail.com
[4] Ph.D in Engineering, Associate Professor of the Department of Environmental Engineering, Brest State Technical University, Brest, Belarus, email: optimum@tut.by

Abstract

The numerical solution of a system of two-dimensional shallow water (Saint-Venant) differential equations in partial derivatives for modeling the dynamics of surface runoff using digital elevation models obtained by laser altimetry leads to a significant increase in the computational load on the computer.

The article offers a view on reasonable simplifications for the shallow water model, the two-dimensional cellular automaton for the modeling of rain surface runoff is proposed along with adequacy analysis of the calculations performed in their practical application.

Keywords: shallow water equations, rain surface runoff, cellular automaton.

МОДЕЛИРОВАНИЕ ДОЖДЕВОГО СТОКА ПРИ ПОМОЩИ КЛЕТОЧНОГО АВТОМАТА

А. А. Волчек, Д. А. Костюк, Д. О. Петров, Н. Н. Шешко

Реферат

Выполнение численного решения системы двумерных дифференциальных уравнений мелкой воды (Сен-Венана) в частных производных для моделирования динамики движения водных потоков по цифровым моделям рельефа, построенным на основе лазерного сканирования земной поверхности с высокой разрешающей способностью, приводит значительному повышению вычислительной нагрузки на ЭВМ.

В данной статье рассматриваются способы обоснованного упрощения модели движения воды по земной поверхности, предлагается один из вариантов применения клеточного автомата для моделирования дождевого стока и оценка адекватности выполняемых расчетов при их практическом применении.

Ключевые слова: уравнения мелкой воды, дождевой сток, клеточный автомат.

Introduction

Modeling of rainfall runoff is important as for predicting the regime of water supply to rivers, lakes, and reservoirs, so for preventing floods in urbanized areas. The significant improvement in the quality of 3D terrain models due to the development of remote sensing of the Earth's surface has led to increased requirements for the performance of hydraulic modeling software. The aim of the presented work is to review reasonable ways to simplify the model of water flow using digital models and to consider the features of using cellular automaton for such purposes with an analysis of the adequacy of the calculations performed.

Physically based hydraulic approach and ways to simplify it

The theoretical basis for rain surface runoff modeling is a physically substantiated calculation of water flows dynamics, which is described by a system of two-dimensional equations of shallow water (Saint-Venant) [1] having the following form[2, 3, 18]:

$$\frac{\partial U}{\partial t} + \frac{\partial F}{\partial x} + \frac{\partial G}{\partial y} = S \qquad (1)$$

$$U = \begin{pmatrix} h \\ hu \\ hv \end{pmatrix}; F = \begin{pmatrix} hu \\ hu^2 + gh^2/2 \\ huv \end{pmatrix}; G = \begin{pmatrix} hv \\ huv \\ hv^2 + gh^2/2 \end{pmatrix}; S = \quad (2) - (5)$$

$$S_{fx} = \frac{-n^2 u\sqrt{u^2+v^2}}{h^{4/3}}; S_{fy} = \frac{-n^2 v\sqrt{u^2+v^2}}{h^{4/3}} \qquad (6)$$

where t is time; x and y are horizontal coordinates; h is a water depth; u and v are depth-averaged projections of the water velocity vector onto the horizontal coordinate axes X and Y; g is acceleration of gravity; S_{0x} and S_{0y} are bottom slopes in the direction of the horizontal coordinate axes; S_{fx} and S_{fy} are friction slopes in the direction of the horizontal coordinate axes [2, 4, 18]; n is the Manning roughness coefficient; r is the rainfall intensity; f are water infiltration losses. If we neglect the inertial components in the equations conservation of momentum, then it is possible to obtain a diffusion approximation to describe the motion of water:

$$\frac{\partial U_d}{\partial t} + \frac{\partial F_d}{\partial x} + \frac{\partial G_d}{\partial y} = S_d \qquad (7)$$

$$U_d = \begin{pmatrix} h \\ 0 \\ 0 \end{pmatrix}; F_d = \begin{pmatrix} hu \\ gh^2/2 \\ 0 \end{pmatrix}; G_d = \begin{pmatrix} hv \\ 0 \\ gh^2/2 \end{pmatrix}; S_d = \quad (8) - (11)$$

Further simplification of the diffusion equations leads to a kinematic approximation of the description of the water motion:

$$\frac{\partial U_k}{\partial t} + \frac{\partial F_k}{\partial x} + \frac{\partial G_k}{\partial y} = S_k \qquad (12)$$

$$U_k = \begin{pmatrix} h \\ 0 \\ 0 \end{pmatrix}; F_k = \begin{pmatrix} hu \\ 0 \\ 0 \end{pmatrix}; G_k = \begin{pmatrix} hv \\ 0 \\ 0 \end{pmatrix}; S_k = \quad (13) - (16)$$

Since the river and surface runoff in conditions of a predominantly flat terrain (which, in particular, is typical for the Republic of Belarus) is characterized by a laminar flow, the use of the diffusion approximation

doi.org/10.36773/1818-1112-2021-126-3-88-91

for describing the movement of water in such conditions is permissible [18, 20].

Application of the cellular automaton to simulate water movement

The above equations can be solved numerically using the finite volume method and the implicit Euler difference scheme [5]. The finite volume method assumes covering the area of computations with a network of small contiguous polygonal cells and allows the researcher to decompose the solution of a two-dimensional problem into a set of interconnected one-dimensional problems to calculate the fluid flow through each side of discrete cells [3, 6].

For a wide class of fluid dynamics problems, including modeling of surface runoff, it is considered acceptable to replace the use of difference schemes for solving systems of partial differential equations with the use of a cellular automaton [7, 9 – 17]. The behavior of a cellular automaton (CA) is completely defined in terms of local dependencies as well as in a wide class of continuous dynamic systems defined by partial differential equations [8]. CA is a complex discrete dynamic system consisting of a finite number of elements called cells, the state of which changes synchronously over time according to a given set of rules [7, 8]. When using a digital elevation model in the form of a set of elevation marks located at the nodes of a regular rectangular mesh to simulate water runoff over the earth's surface, the mesh nodes are interpreted as the centers of independent discrete horizontal areas with a given height value, and the areas themselves (the bases of finite volumes) coincide with the cells of the cellular automaton.

Development of a cellular automaton for modeling rain runoff

The structure of the cellular automaton

Based on [17], a two-dimensional cellular automaton was created for simulating rain runoff, which is a set of $k_i \in K$ elements. The $k_i \in K$ placement coincides with the location of the square-shaped elements of the digital elevation model in the area on which liquid precipitation falls in the form of rain, while it is assumed that the accumulated water does not leave the DEM. Let us denote the set of elements of the cellular automaton located in the J. von Neumann neighborhood with respect to $k_i \in K$ as $k_j \in N^{k_i}$. The subset of $k_j \in N^{k_i}$ elements that can receive a non-zero volume of water by overflow from k_i will be denoted as $k_j \in N^{k_i}_{V_{ij}}$. The following attributes are defined for each k_i element of the cellular automaton (see Figure 1): z_i, Δx, A, n_i is the height (m), the length of the side (m), the area (m^2), and the Manning roughness coefficient of the appropriate DEM element, respectively; d_i is the depth of the water layer (m); $S_{ij} = (wl_i - wl_j)/\Delta x = \Delta wl_{ij}/\Delta x$ is the hydraulic slope between k_i and $k_j \in N^{k_i}$, where $wl_i = d_i + z_i$ and $wl_j = d_j + z_j$ are representing water height (m); $wl_{ij^{max}}$ is the maximum height of the water level among $k_j \in N^{k_i}$; $d_{ij} = wl_i - z_j$ is the effective water depth (m) for the k_i element in direction of $k_j \in N^{k_i}_{V_{ij}}$; $v_{ij} = [(d_{ij})^{2/3}\sqrt{S_{ij}}]/n_i$ is the speed of water stream (m/s) between k_i and $k_j \in N^{k_i}_{V_{ij}}$; $Q_{ij} = \Delta x \cdot d_{ij} \cdot v_{ij}$ is water discharge (m^3/s) between k_i and $k_j \in N^{k_i}_{V_{ij}}$; $Q_{ij^{max}}$ is water discharge (m^3/s) between k_i and the neighboring element with the maximum water height among $k_j \in N^{k_i}_{V_{ij}}$; $\Delta t_i = [(wl_i - wl_{ij^{max}}) \cdot A] / \square$ is the time period (s), during which the height of the water level in the k_i element will be equalized with the neighbor for which the height of the water level was previously determined equal to $wl_{ij^{max}}$ in the process of water flowing from the k_i element to all neighbors for which the $wl_i - wl_j \geq \delta$ condition is valid; $V^{out}_{ij} = Q_{ij} \cdot \Delta T$ is the volume of water transferred from k_i towards the direction of $k_j \in N^{k_i}_{V_{ij}}$, where ΔT is the step of time (s), defined for the cellular automaton at the current simulation iteration; $V^{out}_i = \sum V^{out}_{ij}$ is the total water volume (m^3), which leaves the k_i element in the direction of all $k_j \in N^{k_i}_{V_{ij}}$ at the current simulation iteration; $V_i = \sum V^{out}_{ji}$ is the total water volume (m^3), sourced from all $k_j \in N^{k_i}$ elements in the direction of k_i at the current simulation iteration.

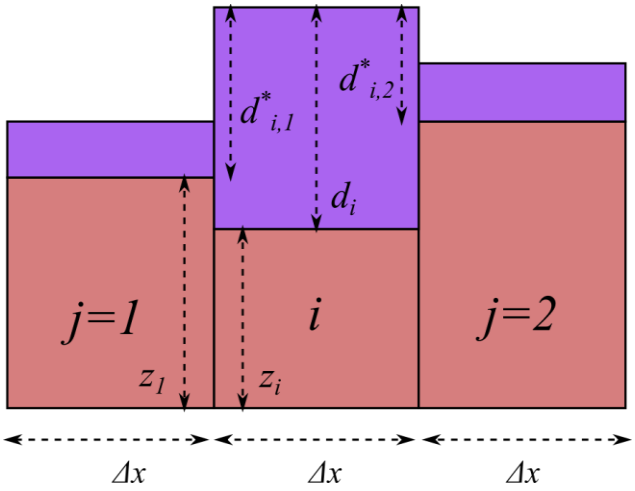

Figure 1 – The value of the effective water depth d_{ij} for the k_i element in the direction of the neighbors $k_j \in N^{k_i}_{V_{ij}}$.

The rule for changing the state of a cellular automaton

Before the start of the runoff simulation iterations, the water depth d_i for each $k_i \in K$ element it is set equal to the thickness of the water layer precipitated in 1 second. The rule of synchronous change in the state of $k_i \in K$ elements of the cellular automaton at each iteration of the simulation is described by the following sequence of steps:

1 The V^{out}_{ij} and V^{out}_i values are zeroed, Δt_i is set equal to ∞, $N^{k_i}_{V_{ij}} \equiv \emptyset$;
2 If the $d_i < \delta (\delta = 0{,}5 \cdot 10^{-3} m)$ condition is true, go to step 8;
3 Calculate $S_{ij} = (wl_i - wl_j)/\Delta x = \Delta wl_{ij}/\Delta x$ for $k_j \in N^{k_i}$;
4 The $k_j \in N^{k_i}$ elements, for which the $S_{ij} > \delta$ condition is true, are included into the $N^{k_i}_{V_{ij}}$ set;
5 Calculate $\Delta t_i = [(wl_i - wl_{ij^{max}}) \cdot A] / \square$;
6 Accept the $\Delta T = min(\Delta t_i)$ value – find minimal Δt_i among all set of $k_i \in K$;
7 Calculate $V^{out}_{ij} = Q_{ij} \cdot \Delta T$ and $V^{out}_i = \sum V^{out}_{ij}$;
8 Calculate $V_i = \sum V^{out}_{ji}$;
9 Decrease d_i with the V^{out}_i / A value;
10 Add the total of V_i / A and the thickness of precipitated water layer, which precipitated during the ΔT time interval, to d_i.

Analysis of the adequacy of the proposed model

The analysis of the adequacy of the proposed method for modeling rainfall runoff was carried out based on the execution of the scenario of rainfall in an urbanized area (see Figures 2 and 3) given in [19, p. 99] under the title "Test 8A: Rainfall and point source flow in urban areas". According to the scenario, liquid precipitation occurs on an urban terrain with an area of 0.388 km^2 with an intensity of 400 mm/h during 3 minutes, then, 16 minutes after the end of the rain from a point source, water begins to flow for 35 minutes with a peak water discharge of 5 m^3/s, and after 17 minutes no water runoff from the modeling site beyond its boundaries occurs. The horizontal resolution of the provided digital elevation model is 2 m, the Manning roughness coefficient of the DEM elements representing paved areas of the territory (roads and sidewalks) is 0.02, and the roughness of the rest of the area is 0.05.

Figure 2 – General view of a section of an urbanized territory used in the scenario of modeling rain runoff (there are no buildings on the digital elevation model)

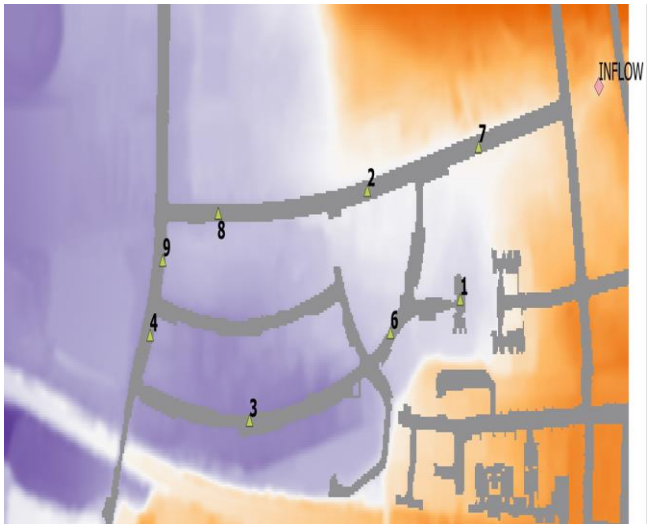

Figure 3 – Image of a digital elevation model for a scenario of rainfall runoff modeling: the control points for measuring the height of the water level are indicated by numbers, the mark "INFLOW" is the location of a point source of water inflow [19, p. 99]

With the help of the software implementation of the proposed cellular automaton, a simulation of rain runoff with a duration of 100 minutes was carried out according to the scenario described in [19]. The results of measuring the height of the water level at control points No. 1 and No. 2 are shown in Figures 4 and 5. For comparison, the figures show the graphs of changes in the water depth at these points, obtained by the authors of the test scenario using foreign software for hydraulic modeling, based both on the solution two-dimensional shallow water equations without simplifications, and on the solution of simplified diffusion equations (in this case, the RFSM EDA software package was used [20]).

The Pearson correlation coefficient was used as a quantitative characteristic of the differences between the results of the cellular automaton operation and the reference software. The correlation of the obtained values of the water level height with the results of solving the shallow water equations was 0.873 and 0.782 for control points No. 1 and No. 2, respectively, and the correlation with the solution of simplified diffusion equations was 0.943 and 0.913 for the same control points, respectively.

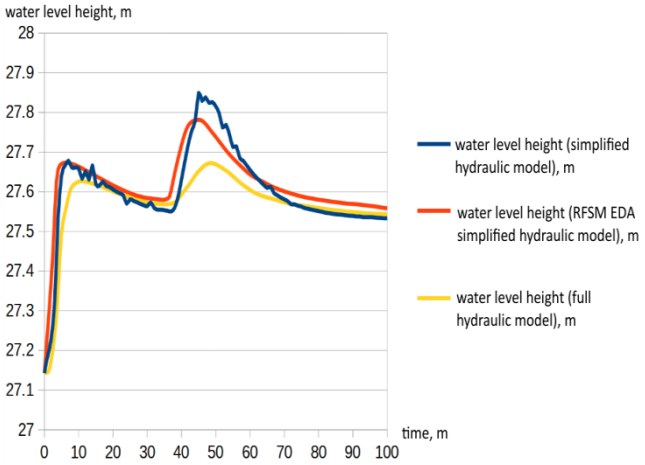

Figure 4 – Simulation results of the water level height change at the control point No. 1

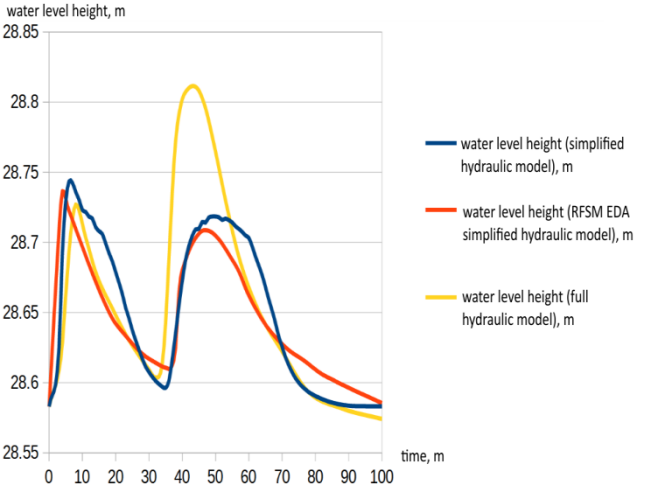

Figure 5 – Simulation results of the water level height change at the control point No.2

Conclusion

Considering the correspondence between the results of the analysis of water movement using a high-resolution digital elevation model using mathematical methods with varying degrees of simplification of the ongoing physical processes, it is possible to note noticeable differences when calculating the dynamics of transient processes between the complete and simplified hydraulic models. Despite these differences, a simplified hydraulic model implemented using a cellular automaton makes it possible to adequately assess not only the final picture of water spreading over the terrain [21, 22, 23], but also the time of the end of the process of water movement, which can be important when forecasting floods in an urbanized area.

References

1. Kivva, S. L. Two-dimensional modeling of rainfall and sediment transport in small catchments / S. L. Kivva, M. I. Zheleznyak // Applied Hydromechanics. – 2002. – T. 4 (76), № 1. – P. 34–43.
2. Nikishov, V. I. From open flow hydraulics to hydromechanics of river systems / V. I. Nikishov // Applied hydromechanics. – 2007. – T. 9, № 2–3. – P. 103–121.
3. Costabile, P. Comparative analysis of overland flow models using finite volume schemes / P. Costabile, C. Costanzo, F. Macchione // Journal of Hydroinformatics. – 2012. – Vol. 14, № 1. – P. 122–135.
4. Karepova, E. D. Simulation of unsteady water movement in the lower bank of the Boguchanskaya HPP / E. D. Karepova, G. A. Fedorov // Computational technologies. – 2008. – T. 13, № 2. – P. 28–38.

doi.org/10.36773/1818-1112-2021-126-3-88-91

5. Baranov A. V. Hydrological module in the software package "Nymph" / A. V. Baranov [et al.] // Supercomputing and mathematical modeling. Proceedings of the XVII International Conference, Sarov, October 15–19, 2018 / Ed. R. M. Shagalieva / FSUE RFYATs-VNIIEF. – Sarov : FSUE RFYATs-VNIIEF, 2019. – P. 33–37.
6. Smirnov, E. M. The finite volume method as applied to problems of hydro-gas-dynamics and heat transfer in areas of complex geometry / E. M. Smirnov, D. K. Zaitsev // Scientific and technical statements of St. Petersburg State Technical University. – 2004. – T. 2, № 36. – P. 70–81.
7. Dottori, F. A 2d flood inundation model based on cellular automata approach / F. Dottori, E. Todini // XVIII International Conference on Water Resources, Barcelona, Spain, June 21–24, 2010 / International Centre for Numerical Methods in Engineering. – International Centre for Numerical Methods in Engineering, 2010.
8. Toffoli T. Cellular automata machines: trans. with. English / T. Toffoli, M. Margolus. – M .: Mir, 1991 . – 280 p.
9. Cellular automata for simulating lava flows: A method and examples of the Etnean eruptions / D. Barca [et al.] // Transport Theory and Statistical Physics. – 1994. – Vol. 23, № 1–3. – P. 195–232.
10. Di Gregorio, S. An empirical method for modeling and simulating some complex macroscopic phenomena by cellular automata / S. Di Gregorio, R. Serra // Future Generation Computer Systems. – 1999. – № 16. – P. 259–271.
11. Pyroclastic flows modeling using cellular automata / M. V. Avolio [et al.] // Computers & Geosciences. – 2006. – № 32. – P. 897–911.
12. Developing an effective 2-D urban flood inundation model for city emergency management based on cellular automata / L. Liu [et al.] // Nat. Hazards Earth Syst. Sci. – 2015. – № 15. – P. 381-391.
13. A Cellular Automata Fast Flood Evaluation (CA-fffé) Model / B. Jamali [et al.] // Water Resources Research. – 2019. – № 55. – P. 4936–4953.
14. Cirbus J. Cellular Automata for the Flow Simulations on the Earth Surface, Optimization Computation Process / J. Cirbus, M. Podhoranyi // Appl. Math. Inf. Sci. – 2013. – Vol. 7, № 16. – P. 2149–2158.
15. Application of cellular automata approach for fast flood simulation / B. Ghimire [et al.] // CCWI 2011: Computing and Control for the Water Industry, Exeter, UK, September 5–7, 2011 / University of Exeter. – University of Exeter, 2011.
16. A weighted cellular automata 2D inundation model for rapid flood analysis / M. Guidolin [et al.] // Environmental Modelling & Software. – 2016. – № 84. – P. 378–394.
17. Development of a diffusive wave shallow water model with a novel stability condition and other new features / M. Jahanbazi [et al.] // Journal of Hydroinformatics. – 2017. – Vol. 19, № 3. – P. 405–425.
18. Néelz, S. Desktop review of 2D hydraulic modelling packages / S. Néelz, G. Pender. – Bristol : Environment Agency. – 2009. – 63 p.
19. Néelz, S. Benchmarking the latest generation of 2D hydraulic modelling packages / S. Néelz, G. Pender. – Bristol : Environment Agency. – 2013. – 194 p.
20. A highly efficient 2D flood modelling with sub-element topography / S. R. Jameison [et al.] // Proceedings of the ICE – Water Management. – 2012. – Vol. 165, № 10. – P. 581–595.
21. Petrov, D. O. Algorithm for calculating the boundaries of the flooded area for a river network with modeling the propagation of water using a raster representation of the relief / D. O. Petrov, A. A. Volchek, D. A. Kostjuk // BSUIR reports. – 2016. – № 5 (99). – P. 73–78.
22. A system for calculating and visualizing a flood zone based on a cellular automaton / D. O. Petrov [et al.] // Collection of materials of the international scientific and practical conference dedicated to the year of science in the Republic of Belarus: in 2 parts, Brest, September 25–27, 2017 / Institute of Nature Management of the National Academy of Sciences of Belarus, BrSU A. S. Pushkin, BrSTU ; editorial board: A. K. Karabanov [et al.] ; scientific. ed. A. K. Karabanov, M. A. Bogdasarov. – Brest : BrSU, 2017. – Part 1. – P. 145–148.
23. Petrov, D. O. Evaluation of the adequacy of the use of geometric methods for constructing a flood zone for flood plain rivers / D. O. Petrov, A. A. Volchek // Tourist and natural potential of water bodies of the Belarusian-Polish border area: materials of scientific-practical conference, Brest, October 30–31, 2020 / Ch. Ed. N. V. Mikhalchuk. – Brest : Alternative, 2020. – P. 127–130.

Accepted 26.10.2021

UDC 556.5

STATISTICAL ASSESSMENT OF THE RUNOFF TIME SERIES HOMOGENEITY OF THE RIVERS IN BELARUS

A. A. Volchak[1], S. V. Sidak[2], S. I. Parfomuk[3]

[1] Doctor of Geographical Sciences, Professor, Dean of the Faculty of Engineering Systems and Ecology, Brest State Technical University, Brest, Belarus; email: volchak@tut.by
[2] Assistant of the Department of Informatics and Applied Mathematics Brest State Technical University, Brest, Belarus; e-mail: harchik-sveta@mail.ru
[3] Ph.D in Engineering, Associate Professor, Head of the Department of Informatics and Applied Mathematics Brest State Technical University, Brest, Belarus; e-mail: parfom@mail.ru

Abstract

The article considers the need to evaluate the homogeneity of hydrological series using several statistical criteria, since the effectiveness of methods for testing homogeneity depends on the distribution of data. In addition to the officially recommended statistical parametric Student and Fisher criteria for this purpose, the Buishand tests, the standard normal homogeneity test and the nonparametric Pettitt test were tested to assess the homogeneity of the time series of the runoff of rivers in Belarus. Based on the application of tests for series of different types of runoff, the classification of the studied series is carried out depending on the number of tests confirming the homogeneity hypothesis.

Keywords: river runoff, homogeneity, points of decomposition, statistical criteria, classes of homogeneity.

СТАТИСТИЧЕСКАЯ ОЦЕНКА ОДНОРОДНОСТИ ВРЕМЕННЫХ РЯДОВ СТОКА РЕК БЕЛАРУСИ

А. А. Волчек, С. В. Сидак, С. И. Парфомук

Реферат

В статье рассмотрена необходимость оценивания однородности гидрологических рядов с использованием нескольких статистических критериев, поскольку эффективность методов тестирования однородности зависит от распределения данных. Кроме официально рекомендуемых для этих целей статистических параметрических критериев Стьюдента и Фишера, для оценки однородности временных рядов стока рек Беларуси апробированы тесты Буишанда, стандартный нормальный тест на однородность и непараметрический тест Петтитта. На основании применения тестов для рядов различных видов стока проведена классификация исследуемых рядов в зависимости от количества тестов, подтверждающих гипотезу однородности.

Ключевые слова: речной сток, однородность, точки разладки, статистические критерии, классы однородности.

Introduction

Statistical analysis of hydrological time series is a fundamental step that must be performed before any action on modeling hydrological processes. An important issue in the study of the statistical structure of hydrological series is the choice of a method for processing the available hydrological information. To effectively apply the methods of mathematical statistics and probability theory to the series of hydrological characteristics, it is necessary to assess the adequacy of the time series to the required prerequisites of the mathematical apparatus used. The main requirements are the homogeneity and stationary of the sample, i.e. it is necessary that all random variables of the sample are from the same distribution of the general population, and the key sample parameters (mean, variance) are invariant in time [1].

The presence of points of decomposition (years of deviation from the homogeneity of observations) in the hydrological time series, reflecting both changes in the behavior of runoff-forming factors and the itself, is the main indicator of changes in the degree of impact of anthropogenic load and climate on the process of runoff formation. In case of violation of the homogeneity and stationary of the hydrological time series, the previously performed calculations of the main hydrological characteristics become unreliable, which results in a change in the degree of vulnerability of hydraulic structures, the inability to assess the risk of dangerous hydrological phenomena, etc. In this regard, the detection of such points of decomposition should be considered as the very first and key step in the analysis of the variability of hydrological processes.

According to the technical code of established practice, for the quantitative assessment of the homogeneity of hydrological series, it is recommended to use the criteria of sharply deviating extreme values in the empirical distribution (the Smirnov-Grubbs and Dixon criteria), the homogeneity of sample variances (the Fisher criterion) and sample averages (the Student's criterion) [2]. The peculiarity of the application of the Smirnov-Grubbs and Dixon criteria is that they are applicable for the conditions of a normal symmetric distribution law of the general population and the absence of autocorrelation. However, the empirical distributions of hydrological characteristics, in particular extreme runoff, may have an asymmetry, and often in time series there may be a statistically significant autocorrelation between adjacent members of the series (r(1)) [3, 4].

Specialists of the State Hydrological Institute (Russia) have developed generalized Fischer and Student criteria that are calculated for series that have an intra-row or inter-row connection [5]. These criteria are included in regulatory documents, which provided them with a mandatory status and wide use in hydrological research. However, it is proved in [6] that the generalized Student and Fisher criteria have much more disadvantages than advantages and are not acceptable for assessing the homogeneity and stationary of hydrological series. It is also worth noting that the WMO Guidelines on hydrological Practice do not recommend the use of these criteria in hydrological studies [7]. The main disadvantage of parametric criteria is due to the fact that the classical results ensure the correctness of the application of these criteria only when the assumption that the analyzed samples belong to the normal distribution law is fulfilled, since only for this situation are the distributions of the statistics of the considered parametric criteria or the percentage point table known and runoff does not always meet these requirements [8].

In this regard, a combined approach is used in this work: in addition to the standard tests (Student, Fisher), three additional tests for homogeneity are applied. All three tests can be used to determine the points of decomposition, if there is a violation of homogeneity. Two parametric tests – Buishand Range Test (BHR) and Standard Normal Homogeneity Test (SNH) and one nonparametric test – Pettitt's Test (PT) were used.

The purpose of the study is to test and compare methods for assessing the homogeneity of the series of different types of runoff on the example of rivers in Belarus.

To achieve this goal, the following tasks have been solved:

1) Analysis of the homogeneity of the runoff series of the rivers of Belarus using the Fischer and Student criteria;
2) Testing of BHR, SNH, PT tests to assess the homogeneity of the river runoff in Belarus, determining the points of decomposition in the runoff time series;
3) Classification of the studied series by the number of tests confirming the homogeneity hypothesis.

doi.org/10.36773/1818-1112-2021-126-3-92-95

Initial Data

The study used the observation data of the State Institution "Republican Center for Hydrometeorology, Control of Radioactive Contamination and Environmental Monitoring" of the Ministry of Natural Resources and Environmental Protection of the Republic of Belarus for the current hydrological stations for the period of instrumental observations published in the materials of state cadasters. The assessment of the stationary and homogeneity of the river runoff series was performed for 6 hydrological stations of the largest rivers of Belarus: the Pripyat River at the Mozyr station, the Neman River at the Grodno station, the Western Dvina River at the Vitebsk station, the Berezina River at the Bobruisk station, the Dnieper River at the Orsha station, and the Dnieper River at the Rechitsa station. The 70-year period (1948-2017) was chosen as a representative period. The gaps in the data series were restored using the computer software complex "Hydrolog" [9].

Research Methods

The calculated value of the Student's criterion statistics (C*t*) is determined by the formula:

$$Ct = \frac{\overline{Q_1} - \overline{Q_2}}{\sqrt{n_1 \cdot \sigma_1^2 + n_2 \cdot \sigma_2^2}} \cdot \sqrt{\frac{n_1 \cdot n_2 \cdot (n_1 + n_2 + 2)}{n_1 + n_2}} \quad (1)$$

where $\overline{Q_1}$, $\overline{Q_2}$, σ_1^2, σ_2^2 – average values and variances of two consecutive samples, respectively, n_1, n_2 – sample volumes.

To assess the homogeneity according to the Student's criterion, it is necessary to compare the calculated values of Ct obtained by the formula (1) and the critical values of the statistics t_{cr} at a given significance level [10]. As a rule, the significance level is set to 5%, which is equivalent to accepting the null hypothesis about the equality of the average two samples of the time series with a probability of 95%. If $Ct > t_{cr}$, then the hypothesis of homogeneity for the two parts of the series is rejected. Accordingly, a number of the considered hydrological characteristics are recognized as heterogeneous.

To estimate the homogeneity of the variances of two consecutive parts of the series, the value of the Fisher statistics F is used:

$$F = \sigma_1^2/\sigma_2^2 \text{ when } \sigma_1^2 > \sigma_2^2. \quad (2)$$

If the calculated value of the criterion statistics is $F < F_{cr}$ at given degrees of freedom, then the hypothesis of homogeneity of variances is accepted at a given significance level α [10].

All additional tests for the study of homogeneity (BHR, SNH, and PT) are determined by the null hypothesis that the data are independent and equally distributed; while the alternative hypothesis indicates that the data is considered heterogeneous with the presence of a point of decomposition. The choice of these tests for an additional study of the homogeneity of hydrological series is based on the following: the PT test is used for any type of distribution of sample data; the SNH test is more sensitive to detecting points of decomposition at the beginning and end of the time series. Despite the fact that the properties of the BHR test are mainly studied for a normal distribution, this test, like the PT test, can be applied to any type of data distribution.

The Buishand Range Test is based on adjusted partial sums or cumulative deviations from the average [12]:

$$S_0^* = 0,\ S_k^* = \sum_{t=1}^{k}(Q_t - \overline{Q}),\quad k = \overline{1, n}, \quad (3)$$

where S_k^* – cumulative deviation, Q_t – observed data on river runoff, $\overline{Q} = \frac{\sum_{k=1}^{n} Q_k}{n}$ – sample average, n – sample volume.

Adjusted partial amounts (S_k^{**}) are calculated by the formula:

$$S_k^{**} = \frac{S_k^*}{\sigma_Q},\quad k = \overline{0, n}, \quad (4)$$

where $\sigma_Q = \sqrt{\frac{1}{n-1}\sum_{t=1}^{n}(Q_t - \overline{Q})^2}$ – standard deviation.

Outlier-sensitive Statistics $\widetilde{Q}$ is calculated by the formula:

$$\widetilde{Q} = \max_{0 \le k \le n} |S_k^{**}|. \quad (5)$$

If $\frac{\widetilde{Q}}{\sqrt{n}} < \widetilde{Q}_{kp}$ then the null hypothesis is accepted. Otherwise, the series is homogeneous.

The Standard Normal Homogeneity Test [13] compares the average values of the data for the first k years with the data for the last (n-k) years using the T_k statistics:

$$T_k = k\overline{z_1} + (n-k)\overline{z_2},\ \ k = \overline{1, n-1}, \quad (6)$$

where

$$\overline{z_1} = \frac{1}{k}\sum_{i=1}^{k}\frac{Q_i - \overline{Q}}{s},\ \ \overline{z_2} = \frac{1}{n-k}\sum_{i=k+1}^{n}\frac{Q_i - \overline{Q}}{s},\ \ s = \frac{\sum_{i=1}^{n}(Q_i - \overline{Q})^2}{n-1}. \quad (7)$$

If the statistics $T_0 = \max_{1 \le k \le n-1} T_k$ is greater than the critical value [14], then the null hypothesis about the homogeneity of the series is rejected. For the maximum value of T_k the number k corresponds to the year of the homogeneity violation.

The Pettitt's Test. Statistics U_k for the calculation of which the ranks r_i of the hydrological quantities Q_i, $i = \overline{1, n}$ are used, is calculated by the formula:

$$U_k = 2\sum_{i=1}^{k} r_i - k(n+1),\ \ k = \overline{1,n}, \quad (8)$$

Next, we calculate the statistics $U_0 = \max_{1 \le k \le n} |U_k|$. The statistical significance of the fracture point is checked by comparing the value of U_0 with the critical value [15].

Results and Discussion

To assess statistical homogeneity in terms of variances and averages, respectively, according to the Fisher and Student criteria, the time series is divided into two or more consecutive samples of the same or different length, and it is desirable to associate the boundaries of the partition with the dates of the alleged violation of stationary. In this regard, the verification of homogeneity according to these criteria was carried out in two stages: the first stage – the entire period of the study was divided into two shorter ones: 1948-1965 and 1966-2017 (division is due to mass reclamation works in 1965); the second stage is the division into the periods 1948-1987 and 1988-2017 (division is due to the fact that 1988 corresponds to the beginning of an intensive increase in average annual air temperatures on the territory of Belarus [16]). The results of the study of the series of average annual, maximum and minimum river runoff rates for homogeneity according to the Student and Fisher criteria are presented in Table 1.

Table 1 – The results of checking for the time series homogeneity of different types of river runoff using the Student and Fisher criteria

River – Station	Annual		Maximum spring		Minimum summer-autumn		Minimum winter	
	Ct	*F*	*Ct*	*F*	*Ct*	*F*	*Ct*	*F*
	(1948-1965) – (1966-2017)							
Pripyat – Mozyr	-3.05 (-)	1.11	0.48	1.23	-3.38 (-)	1.77	-2.61 (-)	3.00 (-)
Neman – Grodno	0.08	1.97	2.96 (-)	5.62 (-)	-1.46	1.02	-0.47	1.33
Western Dvina – Vitebsk	0.10	1.36	3.33 (-)	2.01	1.29	2.83 (-)	-1.41	2.01
Berezina –Bobruisk	0.47	2.29 (-)	3.58 (-)	7.71 (-)	-2.47 (-)	1.53	-2.32 (-)	1.29
Dnieper – Orsha	-0.18	1.31	4.97 (-)	3.76 (-)	-1.24	1.02	-2.52 (-)	5.15 (-)
Dnieper –Rechitsa	0.26	0.45	4.03 (-)	0.17	-1.07	1.01	-2.74 (-)	1.53
	(1948-1987) – (1988-2017)							
Pripyat – Mozyr	-1.16	1.21	2.51 (-)	2.66 (-)	-1.07	1.00	-1.44	4.34 (-)
Neman – Grodno	0.88	1.31	3.00 (-)	7.70 (-)	1.11	1.17	-2.16 (-)	1.34
Western Dvina – Vitebsk	-1.82	1.20	2.65 (-)	1.36	-0.44	1.34	-3.85 (-)	2.63 (-)
Berezina –Bobruisk	-0.17	1.07	3.50 (-)	9.44 (-)	-1.43	1.08	-3.19 (-)	1.25
Dnieper – Orsha	-2.14 (-)	1.45	3.56 (-)	2.43 (-)	-3.73 (-)	2.00	-4.34 (-)	3.41 (-)
Dnieper –Rechitsa	-1.13	1.04	3.45 (-)	6.63 (-)	-2.16 (-)	2.02	-4.85 (-)	1.36

Note: (-) – the series is inhomogeneous.

The results obtained in Table 1 show that the use of only the Student and Fisher tests in most cases does not allow us to make an unambiguous decision about the homogeneity of the hydrological series. This result is quite predictable, since the tests are based on a comparison of different sample parameters. This justifies the need to use more tests to check the homogeneity of the series.

The results of checking the runoff series for homogeneity by SNHT, BHR, PT tests are presented in Table 2.

Table 2 – The results of the analysis of time series of river runoff for homogeneity using the BHR, SNHT, PT tests

Test / River – Station	BHR		SNHT		PT	
	$\widetilde{Q}/\sqrt{n}$	point of decom com-po-sition	T_0	point of decom com-po-sition	U_0	point of decom com-po-sition
	Annual runoff					
Pripyat – Mozyr	1.29	1968	8.09		457	1968
Neman – Grodno	0.59		3.61		258	
Western Dvina – Vitebsk	1.19		5.63		485	1984
Berezina – Bobruisk	0.55		5.64		226	
Dnieper – Orsha	1.28	1984	6.51		525	1984
Dnieper – Rechitsa	0.61		6.61		350	
	Maximum spring runoff					
Pripyat – Mozyr	1.49	1981	8.90	1981	534	1983
Neman – Grodno	1.58	1971	11.32	1970	641	1988
Western Dvina – Vitebsk	1.8	1971	14.63	1970	584	1971
Berezina – Bobruisk	1.88	1971	15.71	1971	678	1987
Dnieper – Orsha	2.19	1970	21.75	1970	747	1972
Dnieper – Rechitsa	1.95	1970	17.24	1970	700	1987
	Minimum summer-autumn runoff					
Pripyat – Mozyr	1.56	1967	11.94	1967	555	1968
Neman – Grodno	0.85		3.43		298	
Western Dvina – Vitebsk	0.83		4.16		260	
Berezina – Bobruisk	1.29	1972	9.49	1961	473	1972
Dnieper – Orsha	1.78	1983	12.78	1983	672	1981
Dnieper – Rechitsa	1.28	1979	6.04		453	1976
	Minimum winter runoff					
Pripyat – Mozyr	1.41	1969	9.25	1969	638	1969
Neman – Grodno	1.28	1992	7.11		499	1992
Western Dvina – Vitebsk	1.86	1988	14.31	1989	593	1988
Berezina – Bobruisk	1.46	1987	8.86	1990	524	1985
Dnieper – Orsha	2.14	1980	18.42	1980	757	1981
Dnieper – Rechitsa	2.09	1978	18.51	1990	764	1977

The final results obtained during the analysis for homogeneity of various types of runoff time series using five tests are presented in Figure 1. The obtained diagrams show the number of tests that reject the null hypothesis of data homogeneity for the studied hydrological series at the significance level of 5 %.

According to the results of checking the homogeneity of hydrological series for five tests, the studied series are classified depending on the number of tests that accept the hypothesis of data homogeneity at the significance level of 5% according to the following rules:

- Data series belongs to class A, if the null hypothesis is accepted by all tests or rejected by one of five tests at a 5% significance level;
- Data series belongs to Class B if two or three tests reject the null hypothesis of data homogeneity;
- Data series belongs to Class C if four or five tests reject the null hypothesis of data homogeneity at the 5% significance level.

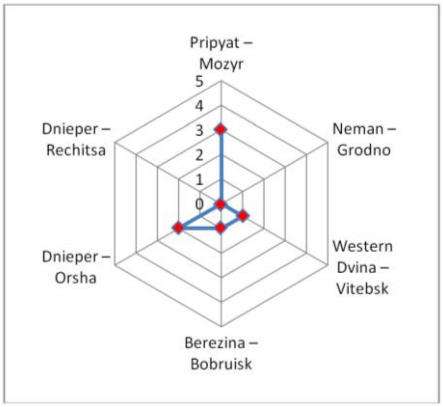

a

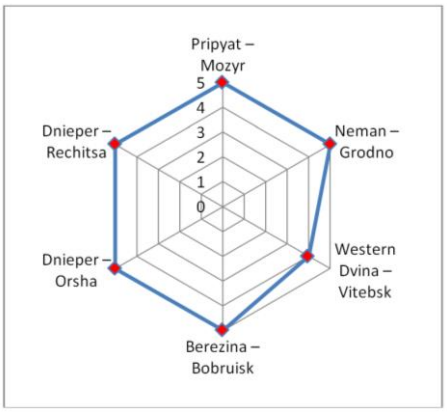

b

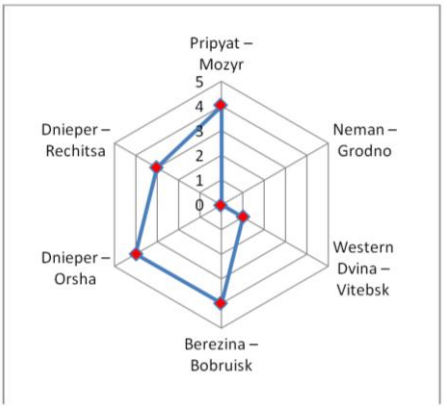

c

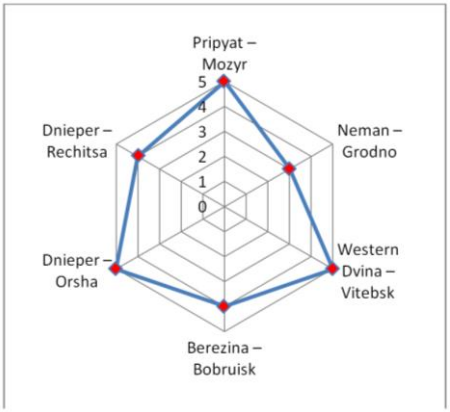

d

Figure 1 – The number of tests rejecting the null hypothesis of data homogeneity for the series of average annual runoff (a), maximum spring runoff (b), minimum summer-autumn runoff (c), minimum winter runoff (d)

doi.org/10.36773/1818-1112-2021-126-3-92-95

As a result of checking the series of river runoff for homogeneity, we came to the result: all the studied series of maximum runoff belong to class C (the points of decomposition in these series fall on the period 1970-1988); the series of annual runoff for the Pripyat River at the Mozyr station (with the point of separation in 1968) and the Dnieper River at the Orsha station (with the point of decomposition in 1984) belong to class B, the rest of the studied annual runoff series belong to class A; the range of the minimum winter runoff the Neman River at the Grodno station belongs to class B (with the point of decomposition in 1992), all the other studied rows of the minimum winter runoff belong to class C (the points of decomposition in these rows fall on the period 1969-1992); the rows of the minimum summer-autumn runoff for the Berezina River at the Bobruisk station, the Dnieper River at the Orsha station, and the Pripyat River at the Mozyr station belong to Class C, the Dnieper River at the Rechitsa station belongs to Class B, others belong to Class A.

Conclusion

The BHR, SNHT, and PT tests used in this study allow us to draw more reasonable conclusions about the homogeneity and points of decomposition of the hydrological series. The general conclusion from the statistical analysis of the homogeneity of the series of different types of river runoff in Belarus for the period 1948-2017 is that all the series of the maximum runoff and most of the series of the minimum winter runoff for the studied channels do not meet the conditions of homogeneity. Most of the annual runoff series are characterized by homogeneity, the minimum summer-autumn runoff series belong to different classes of homogeneity. The results of the analysis of the homogeneity of the samples of the series as a whole indicate significant changes in the formation of the water content of the rivers of Belarus, mainly in the period from the 1970s to the 1990s.

In this study, only statistical methods for estimating homogeneity are considered. However, all series belonging to Class B should be subjected to critical analysis before further use of the series, for example, for modeling. Such an analysis can serve as hydro-genetic methods for assessing homogeneity, which take into account the physical conditions of the formation of river runoff.

The work was carried out with the support of the BRFFI (grant no. X20M064)

References

1. Sikan, A. V. Methods of statistical processing of hydrometeorological information / A. V. Sikan. – St. Petersburg : RSHMU, 2007. – 278 p.
2. Calculated hydrological characteristics. The order of definition. Technical Code of Established Practice. TCP 45-3. 04-168-2009(02250) // Minsk : RUE "Stroytechnorm", 2010. – 55 p.
3. Volchek, A. A. Assessment of changes in the runoff of the Vilia River on the territory of Belarus / A. A. Volchek // Hydrometeorology and ecology. – 2016. – No. 4. – P. 32–62.
4. Volchek, A. A. Accounting for the distribution of maximum values of river runoff during the restoration of historical and cultural values / A. A. Volchek, S. V. Sidak // Restoration of historical and cultural objects as the preservation of the cultural heritage of the Republic of Belarus: a collection of articles of a scientific and technical seminar, Brest State Technical University, Brest, September 30, 2020 / editor: E. A. Tur [et al.]. – Brest: BrSTU Publishing House, 2020. – P. 35–39.
5. Rozhdestvensky, A. V. Synthesis of homogeneous criteria student's t test and Fisher to the case of correlated in time and space hydrological characteristics / A. V. Rozhdestvensky, A. V. Saharuk // Trudy GGI. – 1981. – Vol. 282. – P. 51–71.
6. Gorbachev, L. A. Evaluation of the homogeneity and stationarity of the series of annual runoff of rivers in Ukraine / L. A. Gorbachev, B. F. Khristyuk // Hydrology, hydrochemistry and Hydroecology. – 2014. – Vol. 1 (32). – P. 22–31.
7. Guide to hydrological practice. Volume II. Water resources management and the practice of applying hydrological methods / WMO No. 168. – Geneva, 2021. – 808 p.
8. Application of Homogeneity Tests: Problems and Solution / B. Y. Lemeshko [et al.] // Analytical and Computational Methods in Probability Theory. First International Conference, ACMPT 2017, Moscow, Russia, October 23-27, 2017 / Proceedings Editors: Vladimir Rykov, Nozer D. Singpurwalla, Andrey M. Zubkov (Eds.). – Cham : Springer, 2017. – P. 461–475.
9. Volchek, A. A. Automation of hydrological calculations / A. A. Volchek // Water management construction and environmental protection: Proceedings of the international scientific and practical conference on problems of water management, industrial and civil construction and economic and social transformations in the conditions of market relations / Brest polytechnic Institute. – Biberach-Brest-Nottingham, 1998. – P. 55–59.
10. Recommendations on statistical methods for analyzing the homogeneity of spatio-temporal fluctuations of river runoff. – Leningrad : Hydrometeoizdat, 1984. – 78 p.
11. Taxak, Arun Kumar. Long term spatial and temporal rainfall trends and homogeneity analysis in Wainganga basin, Central India / Arun Kumar Taxak, A. R. Murumkar, D. S. Arya // J. Weather and Climate Extremes. – 2014. – № 4. – P. 50–61.
12. Buishand, T. A. Some methods for testing the homogeneity of rainfall records / T. A. Buishand // Journal of Hydrology. – 1982. – № 58. – P. 11–27.
13. Alexandersson, H. A. A homogeneity test applied to precipitation data / H. A. Alexandersson // International Journal of Climatology. – 1986. – № 6. – P. 661–675.
14. Khaliq, M. N. On the critical values of the standard normal homogeneity test (SNHT) / M. N. Khaliq, T. B. M. J. Ouarda // International Journal of Climatology. – 2007. – № 27. – P. 681–687.
15. Pettitt, A. N. A Non-parametric Approach to the Change-point Problem / A. N. Pettitt // Journal of the Royal Statistical Society. Series C (Applied Statistics). – 1979. – № 28 (2). – P. 126–135.
16. Climate change in Belarus and their consequences / V. F. Loginov [et al.] / National Academy of Sciences of Belarus, Institute for Problems of Natural Resources Use and Ecology. – Minsk : Tonpik, 2003. – 330 p.

Accepted 26.10.2021

ECONOMICS

UDC 332.1

INNOVATIVE TECHNOLOGIES IN MANAGEMENT MUNICIPAL SOLID WASTE IN THE REPUBLIC OF BELARUS

S. A. Bunko[1], V. V. Zazerskaya[2]

[1] PhD in Economics, Deputy Dean of Faculty of Economics, Brest State Technical University, Brest, Belarus, e-mail: swetlanabunko@mail.ru
[2] PhD in Economics, Associate Professor, Dean of Faculty of Economics, Brest State Technical University, Brest, Belarus, e-mail: zazerskaya@mail.ru

Abstract

The article is devoted to the problems of solid municipal waste management in the Republic of Belarus. The importance of finding innovative approaches to waste management due to the growing environmental, economic and social problems in society with an increase in the volume of generated waste is justified. The damage caused by the accumulation of municipal solid waste from the socio-economic system was systematized.

The article considers trends in waste management in the world, analyses the experience of using innovative solutions in the field of solid municipal waste management in the context of administrative-economic, organizational-technical and information-educational tools. Priority directions for the development of innovative technologies in the field of solid municipal waste management in the Republic of Belarus have been identified.

Keywords: municipal solid waste, waste management, sustainable development, ecological consciousness.

ИННОВАЦИОННЫЕ ТЕХНОЛОГИИ В УПРАВЛЕНИИ ТВЕРДЫМИ КОММУНАЛЬНЫМИ ОТХОДАМИ В РЕСПУБЛИКЕ БЕЛАРУСЬ

С. А. Бунько, В. В. Зазерская

Реферат

Статья посвящена проблемам управления твердыми коммунальными отходами в Республике Беларусь. Обоснована важность поиска инновационных подходов к управлению отходами ввиду нарастания экологических, экономических и социальных проблем в обществе с ростом объемов формируемых отходов. Систематизирован ущерб, наносимый накоплением твердых коммунальных отходов социально-экономическим системам.

В статье рассмотрены тренды обращения с отходами в мире, выполнен анализ опыта использования инновационных решений в сфере управления твердыми коммунальными отходами в разрезе административно-экономических, организационно-технических и информационно-образовательных инструментов. Определены приоритетные направления развития инновационных технологий в сфере обращения с твердыми коммунальными отходами в Республике Беларусь.

Ключевые слова: твердые коммунальные отходы, управление отходами, устойчивое развитие, экологическое сознание.

Introduction

In 2015, the world community reaffirmed its commitment to sustainable development by adopting the 2030 Agenda (Agenda 2030). With the signing of the document, the United Nations member States had undertaken to ensure sustained and sustained economic growth, social integration and environmental protection for the benefit of partnership and peace. In order to specify the goals of Agenda 2030, document [1] was developed, which includes 17 Sustainable Development Goals (SDGs). Each country planned to achieve the goals set for the world community and set priorities and targets based on its own level of development.

The Republic of Belarus, despite some differences in terminology, also adhered to the principles of sustainable development. The socio-economic development policy and forecast documents under development included quantitative indicators and qualitative characteristics of the environmental component, but that was not reflected in the title.

Since the programme documents do not define socio-economic development, we will consider it as a process of managed change in various areas of life, aimed at achieving sustainable economic growth, a high degree of employment and, on this basis, raising the standard of living of the population with the least damage to natural resources. Such an understanding of socio-economic development in relation to Belarus was made possible by the study of the goals of socio-economic development stated in the legislative documents and the prevailing ideas about development as "a characteristic of qualitative changes in objects, the emergence of new forms of being, innovations and innovations associated with the transformation of their internal and external ties" [2].

Belarus until 2030, according to which one of the development priorities is the green transition to inclusive and sustainable growth based on the requirements of the Responsible Consumption and Production TsUR-12. We can say that in Belarus Agenda 2030 is embedded in the system of state planning and forecasting documents and the "green economy" is one of the priorities of the country's development. This goal has many sub-goals, the most relevant is a significant reduction in the volume of waste by taking measures to prevent its generation, reduction, recycling and reuse by 2030.

These objectives require the participation of various stakeholders, including producers, consumers, researchers, scientists, the media, development cooperation institutions and others. Such participation in Belarus was realized through the creation of a partnership group under the Sustainable Development Council, consisting of representatives of the above groups [3]. In this article we will consider the results Belarus has achieved on this path; priority goals of development and possibilities of using innovative technologies in the field of solid municipal waste management (MSW) in the Republic of Belarus.

Results and discussion

Among the goals of sustainable development, waste management occupies a special place, since MSW causes significant economic, social and environmental damage to socio-economic systems, the main types of which are identified by us and are given in Table 1.

doi.org/10.36773/1818-1112-2021-126-3-96-99

Table 1 – Damage to MSW socio-economic systems

Type of damage	Components
Economic	a) extraction from the turnover of land allocated for the arrangement of landfills: – reduction of land for possible economic use or human habitation; – construction costs of landfills; – costs of land restoration after use as landfills; b) extraction of resources from the turnover: – reduction of material resources due to their unsustainable use; – high waste delivery costs due to the remote location of landfills from settlements
Social	– increasing morbidity and mortality of the population; – reducing life expectancy; – reduction of the working population; – increased costs of temporary disability sheets;of full or partial disability payments
Ecological	– costs of environmental monitoring
	– costs of rehabilitation activities

Note: compiled by the author on the basis of [4, 5, 6, 7]

According to Agenda 2030, the governments of the countries that signed this document committed themselves to take measures to reduce all types of damage caused by MSW. The Republic of Belarus has also significantly increased its attention in recent years to problems in the area of responsible consumption and production. As a result, there is an increase in the collection of WTO resources (from 2010 to 2020 from 328.4 thousand tons to 1018.7 thousand tons (or 210%). As a result, the share of processed municipal solid waste in the total amount of its generation is increasing. In the period from 2016 to 2020 alone, their share increased from 15.8 to 25 % (Figure 1).

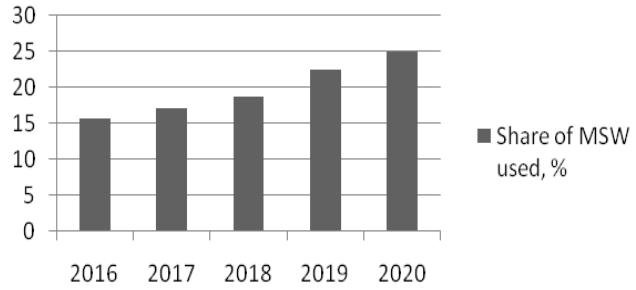

Figure 1 – Dynamics of the share of MSW used for 2016-2020 years,%

Note: proprietary development based on [8]

However, one cannot fail to note the negative dynamics of indicators related to waste generation. So, Figure 2 shows that if until 2019 there was a barely noticeable trend towards a decrease in the total volume of MSW formed, then in 2020 there was a rather sharp jump from 3784 thousand tons to 4070.4 thousand tons or by 7.56 %.

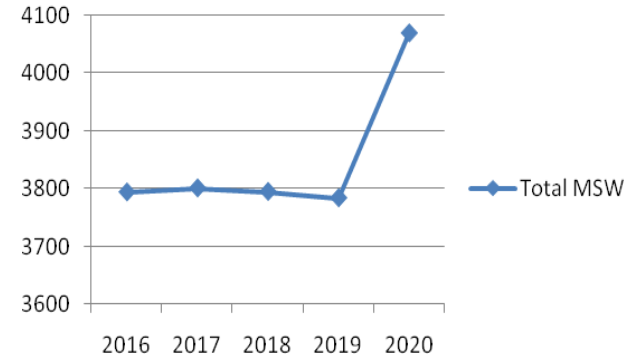

Figure 2 – Dynamics of municipal solid waste generation in 2016-2020 years

Note: proprietary development based on [9]

A negative trend is also noted in the dynamics of MSW per capita: if from 2016 to 2019 stabilization is observed at the level of 402 kg/person. (which corresponds to the European average), in 2020 there was a jump to the level of 433.9 kg or 8% (Figure 3).

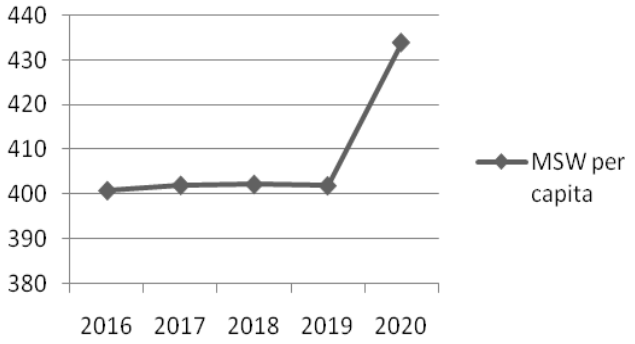

Figure 3 – Dynamics of MSW formation per capita for 2016-2020, kg/person.

Note: proprietary development based on [9]

The growth rate is even higher for MSW per unit of GDP expressed in international dollars. If for the period from 2016 to 2019 there was a downward trend (for this period there was a decrease of 7.8%), then as a result of a jump in 2020, the volume of MSW per unit of GDP increased by 8.65% and exceeded the level of 2016 (Figure 4).

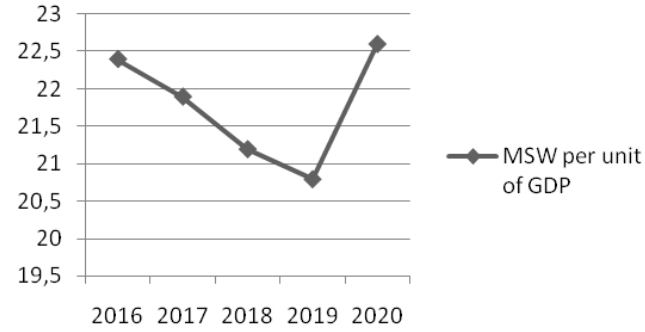

Figure 4 – Dynamics of MSW formation per unit of GDP for 2016-2020 years, kg/thousand international dollars.

Note: proprietary development based on [9]

The statistics we have provided show that efforts to increase waste use do not even offset the growth in waste generation. It is also important to analyse not only the proportion of secondary waste used, but also which waste management approaches are used in general. In world practice, considerable experience has been gained in the field of waste management. So, at the level of the European Union, there is a general waste management policy, the tools of which are taxes on primary raw materials, the principles of eco-design of products, requirements for the recycling of vehicles and much more. The experience of foreign countries shows that waste prevention and reuse are priority approaches, since the division of waste into useful components used as secondary raw materials in enterprises allows not only to benefit financially from garbage, but also to clean the environment.

The methods of use of the generated municipal waste can be conditionally divided into the following three groups:

1. Processing (recycling) – the return of individual MSW components to commercial circulation by separating them from the total mass and transferring them to use as raw materials for production of products.
2. Composting – use of the organic part of MSW after its biological treatment (decomposition of organic substances) with the help of various microorganisms;
3. Incineration - use of mixed MSW or calorific fractions separated from them to obtain thermal and/or electrical energy.

Unused MSW shall be buried in specially equipped places (in the field) taking into account environmental protection requirements.

The use of existing approaches to MSW management in Belarus as of 2020 is presented in Figure 5.

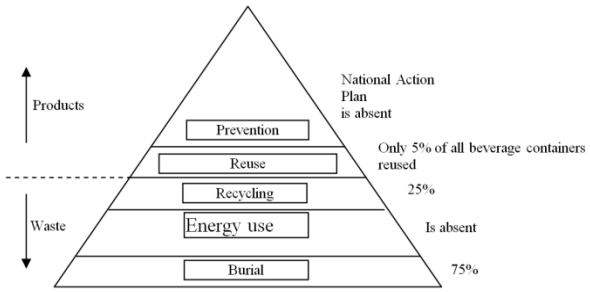

Figure 5 – MSW management approaches and their use in the Republic of Belarus

Note: proprietary development based on [10]

As we see, the main approach in Belarus is burial, there is no energy use, as well as the National Action Plan to prevent the formation of MSW, which cannot be evaluated positively.

The use of these groups of methods varies considerably among countries, due to both the general level of socio-economic development and a number of other factors, and the characteristics of different countries.

Quantitative data on the use of secondary material resources (BMP) collection, composting and MSW combustion in the countries of the European Union and the Republic of Belarus as of 2017 are presented in Figure 6.

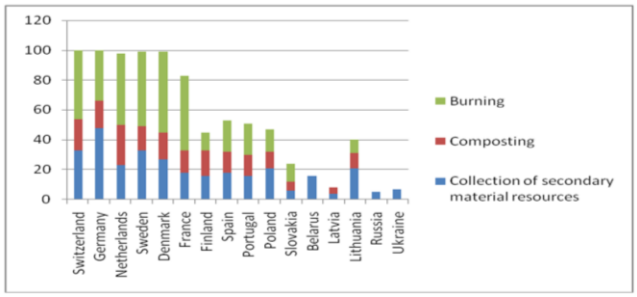

Figure 6 – Methods of MSW use in the countries of the European Union and the Republic of Belarus,%

Note: proprietary development based on [10]

As shown in Figure 6 in the EU countries at present, the priority approach to MSW management is to involve them in industrial processing and recycling. This approach initially began to be implemented forcibly in countries with a small area and a high population density. To implement the approach, the concept of "Wastetoenergy" ("waste - into energy") was developed, according to which waste is considered a source of renewable energy. As a result, emphasis was placed on thermal processing of MSW, primarily on combustion for energy production.

However, practice has shown that the construction of incinerators is not a solution to the MSW problem. First, incineration of unprepared, unsorted MSW is the most costly and environmentally unsafe option to solve the waste problem. When burning MSW, hazardous wastes (fly ash, a mixture of gases) are formed, which with atmospheric precipitation return to the surface of the earth, contaminating the soil and water. Direct energy utilization of MSW excludes their use as secondary material resources (BMP), which is not economically feasible.

Due to the impossibility of solving the problem of waste only by burning it, the so-called "compost" concept was developed. Its proponents assumed that up to 70% of MSW is a biodegradable fraction, therefore they can be fermented to produce a product for agricultural use, provided that it does not contain heavy metals and other contaminants, including mechanical ones; compost improves soil structure, moisture content, reduces erosion. However, the use of such a method has a number of limitations, special requirements for the temperature and humidity of landfills, and on its basis it is also impossible to completely solve the problem of waste disposal.

As a result, the concept of integrated MSW processing was widespread, in which the justification for the use of combination technological solutions was given, based on sorting. According to the concept, it is impossible to use one particular method or technology to process the entire generated mass of MSW, otherwise this leads to a deterioration in economic indicators, an increase in costs, an increase in the negative impact of technology on the environment, which ultimately does not solve the problem of waste. That is, for a long time, waste was managed in relation to waste generated after the sale of various goods. However, the possibilities of waste management are much wider and it is necessary to use innovative technologies and solutions in this area based on a combination of administrative-economic, organizational-technical and information-educational tools.

Administrative and economic instruments include measures related to improving legislation in the field of waste management, the formation of a system of incentives for the population for environmentally responsible behavior (financial incentives, a system of fines and restrictions, the development of business incentives (financial, tax incentives).

By organizational and technical we will mean tools aimed at introducing new technologies and improving infrastructure at all stages of the waste management life cycle: prevention, collection, transportation, sorting and disposal and recycling of MSW. These include the introduction of resource-saving technologies, information systems for managing the waste management system, the organization of training of qualified personnel for the field of MSW circulation management, the expansion of the use of secondary raw materials and the introduction of innovative technologies for their processing and recycling. As practice has shown, the use of public-private partnerships is also effective [11].

Information and educational tools are understood as a set of measures aimed at the formation of guidelines for environmental responsibility of the population, popularization of behaviors, education of environmental culture, and the development of environmental marketing. It is necessary to form a conscious attitude among the population to waste collection, to hold conversations with children, starting from kindergarten and school, to form a careful attitude to nature at an early age.

The above-mentioned tools affect the efficiency of waste management at various stages of the waste management life cycle: prevention, collection, transportation, sorting, processing and disposal (Table 2).

Table 2 – Effectiveness of circulation management tools of MSW

Tools	Degree of impact at stages of MSW circulation life cycle				
	preventing	collection	transportation	sorting	disposal and processing
Administrative and economic	H	H	A	L	H
Organizational and technical	M	H	M	M	M
Information and education	H	H	M	A	L

Note: a) H – high, MC – medium, L – low, A – absent; b) proprietary development based on [12]

Belarus has recently adopted a number of legislative documents regulating economic relations in the field of MSW circulation [13-16]. It seems to us that it is extremely important to adopt a decree outlining measures for 2020-2023 to gradually reduce the use of polymer packaging. In addition to prohibiting measures, this document also provides for the introduction of incentive measures for the production of biodegradable packaging; and the use of new types of compensation for producers using eco-packaging in the production of products intended for sale in Belarus, produced using at least 30% of secondary resources.

From the point of view of developing the infrastructure of the waste management industry in Belarus, significant efforts are also being made: waste processing plants are being put into operation, the number of container sites for separate garbage collection is constantly increasing. In addition, Belarus pays great attention to the development of biodegradable materials: a biodegradable film made of polylactide, as well as a biodegradable packaging material - paper with various properties [17]. However, steps should be taken to encourage the development of other types of environmentally friendly packaging, since none of the existing biodegradable plastics is completely safe [18].

In our opinion, in addition to the actual growth in the volume of production and consumption waste, the problem of waste is acute, which is impossible or extremely difficult to process. Thus, in this area, States have two tasks: reducing the actual amount of waste generated, reducing

doi.org/10.36773/1818-1112-2021-126-3-96-99

the proportion of non-decomposable waste and waste that cannot be recycled [19]. In our view, these problems require:

- firstly, the awareness of the need for separate garbage collection by the population. To this end, information and educational influence on the population forming environmental consciousness is used in world practice;
- secondly, the need to train the population in the correct sorting of waste. In addition to the issues of the availability of containers for separate garbage collection, in this direction there are problems of low public awareness of the possibility of recycling certain types of plastic. Improper collection of plastic waste leads either to the need for additional sorting, or to unsuitability for recycling. Studies in this area have shown that only about 25% of consumers are well versed in environmental signs. Most respondents know about environmental labeling and the need for its application by manufacturers, but do not know how to recognize and interpret it [20].
- In Belarus, the solution of problems in the sphere of MSW circulation, we believe, can significantly accelerate the use of information and educational tools by creating an environmental consciousness of the population, both collective and individual, the development of environmental marketing at all levels.

Collective ecological consciousness is understood by us as the commonality of views on the strategy of attitude to nature, due to the level of understanding of the natural environment as an integral part of man and humanity as a whole [19, 21]. The interpretation of the forms and content of the relationship between man and nature common to any social structure creates opportunities for following the common goals of organizing and implementing the impact on objects and phenomena of nature and the general adoption of all regulatory and legal regulations that determine such impact.

Individual ecological consciousness is considered by us as the result of individual concrete experience of interaction with nature, knowledge about nature and the external environment obtained in the process of learning, and models of ecological consciousness and ecological behavior imposed by society, formed on the basis of personal psychological characteristics [19, 22].

Currently, the world practice has already accumulated considerable experience in the system management of the formation of ecological consciousness of the population and business through the creation of unified information portals, the creation of environmental education centers, the development and implementation of mass information and education programs, street advertising that can be used in Belarus. In addition, we consider it important to develop understandable, easily memorable symbols to indicate information on the package about the possibility or impossibility of its processing.

Conclusion

On the basis of the above, it can be said that in recent years Belarus has taken significant steps to solve problems of waste management, primarily on the basis of organizational, technical and administrative-economic instruments. In order to achieve the intended goals of sustainable development in the sphere of MSW circulation management, in our opinion, it seems advisable to more actively use innovative information and educational tools of environmental marketing:

- Strengthening of motivation of producers to use of eco-friendly packing;
- Encouraging producers, in addition to the application of standardized symbols for ecological packaging, to post visible information to consumers about the possibility or impossibility of its disposal and processing;
- Purposeful activity on formation of ecological consciousness not only producers, but also society as a whole.

References

1. Transformation of our world: an agenda for sustainable development until 2030 [Electronic resource]. – Access mode: https://docs.cntd.ru/document/420355765. – Date of access: 02.03.2021.
2. Big encyclopedic dictionary: philosophy, sociology, religion, esotericism, political economy / V. L. Abushenko [et al.] ; main scientific ed. and comp. S. Yu. Solodovnikov. – Minsk : Minsk factory of color printing, 2002. – 1008 p.
3. Bunko, S. A. Development of ecological marketing in the context of sustainable development of the Republic of Belarus / S. A. Bunko // Economic science today: collection of articles. scientific. Art. / BNTU. – Minsk, 2021. – Issue. 13. – P. 103−111.
4. Zhulay, E. A. Types of environmental harm and methods of its compensation [Electronic resource] / E. A. Zhulay, E. G. Cherkashina. – Access mode: https://cyberleninka.ru/article/n/vidy-ekologicheskogo-vreda-i-sposoby-ego-vozmescheniya. – Date of access: 09/04/2021.
5. Zazerskaya, V. V. Economic growth in conditions of sustainable development / V. V. Zazerskaya // Innovations: from theory to practice: collective monograph ; under scientific ed. A. M. Omelyanyuk [et al.]. – Brest : BrSTU, 2019. – Subsection 5.4. – P. 254–262.
6. Druzhinina, E. O. Export of "environmental problems" and its socio-ecological consequences / E. O. Druzhinina, N. V. Potapova // Problems of accounting methodology, control and analysis: international collection of scientific works, issue 2 (20). – Zhitomir, 2011. – P. 176–193.
7. Shchetkina, M. A. Implementation of the Sustainable Development Goals in Belarus: Agenda until 2030 / M. A. Shchetkina, A. N. Danilov // Journal of the Belarusian State University. Sociology. – 2019. – No. 1. – P. 4–11.
8. Waste management [Electronic resource]. – Access mode: https://www.belstat.gov.by/. – Access date: 05.03.2021.
9. Waste generation [Electronic resource]. – Access mode: https: //www.belstat.gov.by.– Access date: 05.03.2021.
10. On the approval of the National strategy for the management of municipal solid waste and secondary material resources in the Republic of Belarus for the period up to 2035 [Electronic resource]. – Access mode: https://pravo.by/upload/docs/op/C21700567_1501880400.pdf. – Access date: 03/05/2021.
11. Zazerskaya, V. V. Development of public-private partnership in housing and communal services [Electronic resource] / V. V. Zazerskaya // Innovative economy in the context of globalization: modern trends and prospects : materials of the International Scientific and Practical Conference, Minsk, 25–26 April 2013. – Minsk : MITSO, 2013. – P. 25–26.
12. Review of technologies and solutions for improving the system of solid municipal (household) waste management in Moscow [Electronic resource] / Agency of innovations in Moscow. – Access mode: https://innovationmap.innoagency.ru. – Access date: 09/05/2021.
13. On waste management [Electronic resource]: Law of the Republic of Belarus of 20.07.2007 No. 271-3 // ConsultantPlus: Belarus / YurSpektr, National Center for Legal Information. Republic of Belarus.
14. On the gradual reduction in the use of polymer packaging: resolution of the Council of Ministers of the Republic Belarus from 13 Jan. 2020 № 7 // ConsultantPlus: Belarus / YurSpektr, National Center for Legal Information. Republic of Belarus.
15. Environmental protection and nature management. Waste. Waste management rules [Electronic resource]: Technical Code of TCH established practice 17.11-08-2020. – Access mode: https://vtoroperator.by/content/tkp-1711-08-2020-pravila-obrashcheniya-s-kommunalnymi-otkhodami. – Access date: 09/05/2021.
16. Code of the Republic of Belarus on Administrative Offenses dated 06.01.2021 No. 91-3 [Electronic resource] // ConsultantPlus: Belarus / YurSpektr, National Center for Legal Information. Republic of Belarus.
17. All about biodegradable plastics. World market of biopolymers [Electronic resource]. – Access mode: https://ect-center.com/blog/-biodegradable-polymers. – Access date: 12.10.
18. Makaruk, O. E. Technoparks in regional innovation systems: problems of efficiency assessment / O. E. Makaruk // Bulletin of Brest State Technical University. Economics. – 2018. – No. 3. – P. 107–111.
19. Bunko, S. A. Ways to achieve the goals of sustainable development of the Republic of Belarus in the field of waste management / S. A. Bunko // Actual problems of modern economic systems – 2020 : collection of articles of the International Scientific and Practical Conference, Brest, 27 November 2020 / BrSTU ; editorial board: A. G. Prorovskiy [et al.]. – Brest : BrSTU, 2020. – P. 29–33.
20. How do buyers choose eco-products? [Electronic resource] / Ecological Union of St. Petersburg. – Access mode: http://ecounion.ru. – Access date: 12.10.
21. Medvedev, V. I. Environmental consciousness: textbook. allowance / V. I. Medvedev, A. A. Aldasheva. – M. : Logos, 2001. – 384 p.
22. Begidova, S. N. The structure of ecological consciousness [Electronic resource] / S. N. Begidova, I. V. Makrushina. – Access mode: https://cyberleninka.ru/article/n/struktura-ekologicheskogo-soznaniya. – Access date: 10/22/2020.

Accepted 25.10.2021

UDC 338.24: 658

DEFINITION OF CONDITIONS FOR SUSTAINABLE DEVELOPMENT OF THE ENTERPRISE

I. M. Garchuk

PhD in Economic, Head of the Department of Management, Brest State Technical University, Brest, Belarus, e-mail: garchuk_im@mail.ru

Abstract

The sustainable development of the national economy directly depends on the sustainable development of all industries, which, in turn, are formed from the development of each, separately taken enterprise - the main reproductive link. Under the influence of the factors of the business environment, the enterprise faces many tasks, the most important of which is the restructuring of the management system with a focus on sustainable development. In this regard, it becomes necessary to determine the conditions and assess the degree of sustainable development of the enterprise. The article examines the content of the category "sustainable development of an enterprise", methods for assessing the effectiveness of sustainable development management processes and provides the methodological foundations of the management system for sustainable development of an enterprise.

Keywords: sustainable development of an enterprise, management processes, category, management system, approaches, assessment of the effectiveness of management processes.

ОПРЕДЕЛЕНИЕ УСЛОВИЙ УСТОЙЧИВОГО РАЗВИТИЯ ПРЕДПРИЯТИЯ

И. М. Гарчук

Реферат

Устойчивое развитие национальной экономики напрямую зависит от устойчивого развития всех отраслей, которые, в свою очередь, складываются из развития каждого, отдельно взятого предприятия – основного воспроизводственного звена. Под воздействием факторов деловой среды перед предприятием стоит множество задач, важнейшими из которых является перестройка системы управления с ориентацией на устойчивое развитие. В этой связи возникает необходимость определения условий и оценки степени устойчивого развития предприятия. В статье рассматривается содержание категории «устойчивое развитие предприятия», методики оценки эффективности процессов управления устойчивым развитием и приведены методологические основы системы управления устойчивым развитием предприятия.

Ключевые слова: устойчивое развитие предприятия, процессы управления, категория, система управления, подходы, оценка эффективности процессов управления.

Introduction

The concept of sustainable development of the economy largely presupposes the observance of the balance of the economy, the environment and the social sphere, as well as the solution of problems, taking into account the subsequent prospects for future generations. Any system in the course of its life can be either in a stable or in an unstable state, therefore the concept of sustainable development can be applied not only in relation to individual countries and regions, but also to enterprises. Under the conditions of the planned economic system, the sustainable development of the enterprise was achieved mainly due to external factors: administrative reorganization of production, additional economic support, replacement of the director, adjustments to plans [1]. The market economy presupposes a different mechanism for ensuring the sustainable development of an enterprise, therefore, the issues of improving the theory and practice of managing the sustainable development of an enterprise are of great practical importance. unified decimal classification

Sustainable development of the enterprise

Sustainable development of enterprises is a guarantee of quality and compliance with requirements related not only to the production of products, but also to all types of activities of enterprises. Often, only development factors are singled out in the form of changes in the external and internal conditions of life of the macroeconomic processes of the market environment, the state of the property and intellectual potential of enterprises. However, the development in the system should be considered as self-movement, which is expressed by the law of development: each system seeks to achieve the greatest total potential during the passage of all stages of the life cycle.

The problems of sustainable development of enterprises in general, individual industrial sectors, regional territories and other economic systems were studied by such domestic and foreign scientists as V. F. Medvedev, R. S. Sedegov, O. A. Vysotsky, L. N. Nekhorosheva, A. S. Pelikh, S. S. Polonik, S. A. Kasperovich, V. I. Kudashov and others.

These problems are reflected in publications of Russian and foreign authors such as L. I. Abalkin, A. A. Ambartsumov, Yu. P. Anisimov, V. M. Bautin, AM Bukreev, V.P. G. Zakshevsky, E. M. Korotkov, R. Kaplan, D. Norton, T. I. Ovchinnikov, A. N. Polozov, M. Porter, T. V. Sukhorukova, G. I. Tamoshina, G. Hamel , L. I. Churikov, A. D. Sheremet, J. Schumpeter and others. However, despite the significant scientific contribution and accumulated experience, the problem of sustainable development of enterprises has not been comprehensively and systematically studied.

The concept of sustainable development of industrial socio-economic systems, which includes enterprises, is a new management system that uses monitoring of continuous measurement, analysis and adjustment of processes and management procedures in a given direction and speed of development. The ambiguity of solving the emerging problems of sustainable development makes it necessary to conduct research to substantiate theoretical and methodological approaches to assessing the economic efficiency of management processes.

The most important task of ensuring the sustainable development of the enterprise is the development of appropriate organizational and economic mechanisms that are adequate to modern global, socio-cultural, economic, political, technological challenges of our time.

Most often, the concept of "sustainable development" is considered in relation to a country, region, region, city, which is understood as long-term planning, covering institutional, legal, environmental, financial and economic aspects, and does not jeopardize the ability of future generations to satisfy their own needs [2; 3].

Changes in the structure of economic ties, a serious transformation of the system of centralized sectoral management led to the transfer of a significant part of the responsibility for solving development problems to the enterprise as the main economic entity [4].

Currently, the role of the enterprise is being rethought, there is an awareness of its institutional role as a subject of concentration and reproduction of resources, the formation of future needs and trends, necessary and sufficient conditions are identified that ensure its stability and further development.

doi.org/10.36773/1818-1112-2021-126-3-100-102

In accordance with one of the approaches to the essence of the concept of "sustainable development of an enterprise" it means socially oriented development throughout the entire life cycle of an enterprise [5; 6; 7].

N.P. Mytskikh considers the achievement of sustainable development of an enterprise through the use as the main elements of products or technological processes of newly created, previously considered inaccessible or irrational for the use of sources and types of resources [8].

We should agree with the studies of E.N. Kucherova, who considers the sustainable development of the enterprise from the point of view of the functioning of the enterprise, in which the operational, current and strategic plans of the organization's activities are carried out [9].

A number of scientists equate sustainable development of an enterprise with the concept of "sustainable operation" and are very often considered synonymous. However, in our opinion, the identification is not very correct, since organizations can function steadily, but not develop [10; 11; 12; 13; 14].

Another opinion is the understanding of sustainable development of an enterprise as economic stability and comparing it with the financial state, in which the fact of unprofitableness plays a major role, and bankruptcy is considered as one of the institutions designed to ensure the functioning of sustainable organizations [15; 16; 17]. However, the sustainable development of the enterprise includes, in addition to the development of finance, a number of other functions: production, marketing, procurement, sales and others.

Some authors adhere to the approach that the sustainable development of an enterprise is ensured by the degree of its reaction to external influences [18; 19; 20]. An enterprise in conditions of instability and the impact of the external environment can suspend its development program, and sustainable development is a consequence of management decisions.

M. K. Aristarkhova, R. A. Shepel believe that sustainable development is the result of the innovative activity of an enterprise [21; 22]. They highlight the basic principles of sustainable development: readiness to innovate, flexibility, interest in the results of innovation, innovative receptivity of personnel, continuity of innovation and optimal development. At the same time, innovation alone is not enough for the sustainable development of organizations, since innovation is only one of the key tools for achieving sustainable development.

The performed analysis of the main approaches to defining the essence of sustainable development of an enterprise made it possible to propose the author's interpretation of the concept of "sustainable development of an enterprise" - this is such a development of an enterprise management system when, under the influence of the indicators of the business environment, the needs and expectations of stakeholders, it is able to achieve the set strategic, current and operational indicators [23]. This interpretation assumes that sustainable development is a process of long, continuous, balanced socio-economic development and it is possible only if the indicators characterizing the management processes increase over a certain period of time. The higher the actual level of indicators of management processes in comparison with the previous one, the more reliably the sustainable development management system of the enterprise functions.

The methodological foundations of the management system for sustainable development of an enterprise in accordance with the requirements of international standards ISO 9004 include:

- choice of the management level (operational, current, strategic);
- determination of the goals of the interested parties (strategic, current, operational);
- achieving high quality management of the organization:
- setting goals for achieving goals;
- definition of management functions;
- stable integration with other control systems;
- change and monitoring of sustainable development;
- forecasting sustainable development in the medium term;
- development of management measures and procedures;
- provision of the necessary resources;
- evaluation of the effectiveness of the proposed measures [24].

The totality of the proposed measures allows to ensure the development of an integrated management system for the sustainable development of the enterprise. The sustainable development system consists of three subsystems:

- an operational subsystem for managing the sustainable development of an enterprise;
- the current subsystem of sustainable development management of the enterprise,
- a strategic subsystem of sustainable development of the enterprise.

Each of the subsystems included in the sustainable development management system of the enterprise includes a group of management functions that ensure the implementation of all tasks, processes and procedures for managing this production system.

One of the directions for ensuring the sustainable development of an enterprise is the efficiency of management, in connection with which there is a need for an objective and effective tool for assessing management. Analysis of scientific and practical publications on management issues led to the conclusion that there is practically no research on the problems of assessing the effectiveness of management processes.

One of the approaches to assessing the effective development of an enterprise is based on determining the following indicators: achieving sustainable rates of economic growth of the main activity of the enterprise, making a profit sufficient for self-financing of economic development and ensuring its sustainable growth in dynamics. At the same time, the author uses the category of sustainability in relation to the set goals: the construction of a goal tree, which shows the ways to achieve the set general goal through subgoals [20].

T. V. Kasaeva, E. S. Gruznevich to assess the implementation of sustainable development strategies use an approach based on the application of a system of balanced indicators, in accordance with which the organization is considered as a combination of four aspects: finance, customers and marketing, internal business processes , personnel and development, which will make it possible to translate the strategy being implemented into a set of specific interrelated indicators with the possibility of presenting causal relationships between subgoals within the framework of the chosen strategic goal [25].

A. V. Abchuk considers income, profit and profitability as examples of calculations of effective management; the coefficients of efficiency of the organization's activity and calculations of the optimal use of resources [26].

The conducted studies have shown that the existing methods developed by researchers are most often based on the dynamics of existing indicators that do not affect strategic goals and their management processes, which made it possible to consider this problem within the framework of this study.

Sustainable development of the enterprise is ensured with the coordinated functioning of the constituent elements of the management system and is based on information support for the management decision-making process. In accordance with the theory of measuring the manageability of an enterprise's economic activity, the field of manageability by the sustainable development of an enterprise can be represented in the range from 0 to 1,0 (or from 0 to 100 %) in the form of six areas of work:

- zone of natural deviations (100–80 %);
- stabilization zone (80–60 %);
- sanitation zone (60–40 %);
- restructuring zone (40–20 %);
- crisis zone or crisis zone (20–0 %);
- bankruptcy zone (0 %) [27].

The sustainable development of an enterprise is maintained if the values of the indicators of management processes are in the range from 100% to 80%, i.e. all functions of management of sustainable development of the enterprise work effectively. In this controllability zone, all departments of the enterprise, as well as all managers, are set up to address the issues of sustainable development of the enterprise and work in accordance with the requirements of ISO 9004: 2010 standards.

With a controllability level equal to 70%, the management system loses its stability, that is, the organization's management needs to urgently make decisions to improve the efficiency of management processes. However, the modes of sustainable development of the enterprise are also possible in other control zones. If the level of controllability is 60% and the responsible employees participating in the management processes have chosen a rational rate of development of the indicators of management processes, that is, their increase per unit of time is constantly and progressively implemented, then this mode of enterprise development is also stable.

Conclusion

The analysis of domestic and foreign literature on sustainable development of enterprises showed that there is no definite concept of sustainable development of an enterprise, research in this area is being conducted quite intensively, but the attention of scientists is mainly focused on its financial and economic aspects. In industrialized countries, the problems of sustainable development of an enterprise are considered in connection with a possible crisis and competitiveness.

In this regard, the author's interpretation of this concept is proposed as the development of an enterprise management system, when, under the influence of the indicators of the business environment, the needs and expectations of stakeholders, it is able to achieve the set strategic, current and operational indicators. The novelty of this definition lies in establishing the basis for improving the results of the organization's activities: planning, measuring, analyzing, evaluating, as well as taking into account the factors of the business environment and the needs of interested parties. It has been determined that sustainable development occurs when the actual level of indicators of management processes becomes higher than the previous ones or the reporting level for the past period of time.

The implementation of the methodology for assessing the effectiveness of enterprise management processes and the fulfillment of the requirements of the ISO 9004: 2010 quality standards make it possible to achieve a sustainable development zone with a management level of the enterprise equal to 90% or more.

References

1. Krupenchenko, V. R. Construction management: textbook for universities / V. R. Krupenchenko. – M. : Stroyizdat, 1986. – 343 p.
2. National strategy for sustainable socio-economic development of the Republic of Belarus for the period up to 2030 [Electronic resource] / Scientific Research Institute of Economics. – Minsk, 2015. – Access mode: http://srrb.niks.by/info/program.pdf/ – Access date: 05.12.2018.
3. Report of the World Commission on Environment and Development: Our Common Future [Electronic resource]. – Access mode: http://www.un-documents.net/our-common-future.pdf/ – Date of access: 11/16/2018.
4. Sustainable and effective functioning of enterprises: problems and ways of achieving / V. I. Kudashov [et al.]. – Minsk : Minsk Institute of Management, 2007. – 406 p.
5. Afanasyeva, O. V. Research of theoretical aspects of sustainable development of an enterprise in modern science / O. V. Afanasyeva // Integration of education. – 2007. – No. 1. – P. 127–131.
6. Baranovsky, A. G. Sustainable development of the agro-industrial complex and its regulation / A. G. Baranovsky // Problems of economics: collection of scientific articles / Belarusian Agricultural Academy. – Gorki, 2017. – No. 2. – P. 3–13.
7. Kasperovich, S. A. Sustainable development of an enterprise as a factor of intensive economic growth / S. A. Kasperovich, M. V. Rogova // Proceedings BSTU. Series 5, Economics and Control. – 2011. – No. 7. – P. 263–267.
8. Mytskikh, N. P. Innovative strategies in the state anti-crisis regulation of the economy: study guide / N. P. Mytskikh, V. A. Mytskikh, M. A. Slonimskaya. – Minsk : Academy at the President of the Republic of Belarus, 2007. – 247 p.
9. Kucherova, E. N. Theoretical foundations of the development of a mechanism for sustainable development of the enterprise / E. N. Kucherova // Topical issues of modern science. – 2009. – No. 6–2. – P. 91–101.
10. Bakanov, M. I. Theory of economic analysis : textbook for students of economic specialties / M. I. Bakanov, M. V. Melnik, A. D. Sheremet ; ed. M. I. Bakanova. – Ed. 5th, rev. and add. – M.: Finance and statistics, 2008. – 536 p.
11. Kovalev, V. V. Financial management: theory and practice / V. V. Kovalev. – 2nd ed., rev. and add. – M. : Prospect, 2007. – 1024 p.
12. Savitskaya, G. V. Analysis of the economic activity of the enterprise: textbook / G. V. Savitskaya. – 5th ed., rev. and add. – M. : Infra-M, 2009. – 536 p.
13. Grachev, A. V. Financial stability of the enterprise: criteria and methods of assessment in a market economy: textbook / A. V. Grachev. – M. : Business and Service, 2008. – 358 p.
14. Vakhromov, E. N. Assessment of sustainable development and functioning of the enterprise: factors, criteria, features / E. N. Vakhromov, D. Yu. Markaryan // Bulletin of Astrakhan State Technical University. – 2008. – No. 4 (45). – P. 52–62.
15. Korotkov, E. M. Anti-crisis management: textbook / E. M. Korotkov. – 2nd ed., add. and rev. – M. : Infra-M, 2010. – 620 p.
16. Korobkova, Z. V. The economic mechanism of sustainable development of an enterprise in the conditions of growing economic globalization / Z. V. Korobkova // Functioning of enterprises in the Russian economy: problems and solutions: collection of scientific articles / ed. V. V. Titov, V. D. Markova. – Novosibirsk : IEOPP SO RAN, 2006. – P. 57–68.
17. Sheremet, A. D. Methods of financial analysis of the activities of commercial organizations / A. D. Sheremet, E. V. Negashev. – 2nd ed., Rev. and add. – M. : Infra-M, 2008. – 208 p.
18. Koryakov, A. G. Methodological issues of sustainable development of enterprises / A. G. Koryakov // Issues of Economics and Law. – 2012. – No. 4. – P. 110–114.
19. Mikhalev, O. V. Economic stability of economic systems: methodology and practice of research and applied analysis: monograph / O. V. Mikhalev. – SPb. : Publishing house of the St. Petersburg Academy of Management and Economics, 2010. – 200 p.
20. Ryabov, V. M. Sustainable development of industrial enterprises in modern conditions / V. M. Ryabov // Science Vector of TSU. – 2011. – No. 4 (18). – P. 271–273.
21. Aristarkhova, M. K. Assessment of the impact of events on the development of the enterprise / M. K. Aristarkhova, A. N. Ponomareva // Russian Journal of Entrepreneurship. – 2007. – Volume 8, No. 10. – P. 105–110.
22. Shepel, R. A. Formation of mechanisms for sustainable development of innovation-oriented industrial enterprises: abstract of thesis ... candidate of economic sciences: 08.00.05 / R. A. Shepel ; [Place of protection: Russian State Social University]. – Moscow, 2009. – 28 p.
23. Garchuk, I. M. The use of innovative technologies of effective management to achieve sustainable development of the organization / I. M. Garchuk // Innovations: from theory to practice: VI International scientific-practical Conference, Brest, 5–7 October, 2017 : collection of scientific articles / Brest State Technical University ; editorial board: P. S. Poyta [et al.]. – Brest : Alternative, 2017. – P. 26–30.
24. Management to achieve sustainable organizational success. Quality Management Approach : STB ISO 9004-2010. – Instead of STB ISO 9004-2001; entered 20.05.2010. – Minsk : Gosstandart, 2010. – 45 p. – (State standard of the Republic of Belarus).
25. Kasaeva, T. V. Development of a mechanism for assessing the implementation of the sustainable development strategy of a commercial organization / T. V. Kasaeva, E. S. Gruznevich // Bulletin of the Vitebsk State Technological University. – 2014. – Issue. 26. – P. 196–205.
26. Abchuk, V. A. Management: textbook / V. A. Abchuk. – SPb. : Soyuz, 2002. – 463 p.
27. Vysotsky, O. A. The theory of measuring the controllability of economic activities of enterprises / under scientific. ed. R.S. Sedegova. – Minsk : Law and Economics, 2004. – 396 p.

Accepted 25.10.2021

doi.org/10.36773/1818-1112-2021-126-3-100-102

UDC 69.003.13

METHOD FOR SELECTING A COST-EFFECTIVE OPTION OF THE SEQUENCE OF CONSTRUCTION OF BUILDINGS AND STRUCTURES IN A COMPLEX

A. N. Kochurko[1], L. G. Sryvkina[2]

[1] PhD in Economics, Associate Professor, Associate Professor of the Department of Economics of Construction and Organization of Building Works, Brest State Technical University, Brest, Belarus, e-mail: ankochurko@gmail.com
[2] Senior Lecturer of the Department of Economics of Construction and Organization of Building Works, Brest State Technical University, Brest, Belarus, e-mail: lgsryvkina@mail.ru

Abstract

When developing a justification for investment in the construction of facilities in accordance with regulatory documents, alternative studies and calculations should be carried out in order to determine the effectiveness of investments.

This article offers a method for assessing the economic efficiency of options for the sequence of construction of a complex of buildings and structures. The method is based on the income approach (the net income generated by the complex of facilities is calculated) and on the cash flows discounting. At the same time, the economic effects for the investor are taken into account: effects from the reduction of discounted costs at the stage of construction of the complex, and effects in the field of operation of individual buildings and structures for the period of the calculation horizon.

Keywords: pre-design stage, construction organization project, complex of buildings and structures, construction phase, sequence of construction, financing schedule, discounted costs.

МЕТОДИКА ОЦЕНКИ ЭКОНОМИЧЕСКОЙ ЭФФЕКТИВНОСТИ ВАРИАНТОВ ОЧЕРЕДНОСТИ ЗАСТРОЙКИ КОМПЛЕКСА ЗДАНИЙ И СООРУЖЕНИЙ

А. Н. Кочурко, Л. Г. Срывкина

Реферат

При разработке обоснования инвестиций в строительство объектов в соответствии с нормативными требованиями должны выполняться альтернативные проработки и расчеты по определению эффективности инвестиций.

В данной статье предлагается методика оценки экономической эффективности вариантов очередности застройки комплекса зданий и сооружений, основанная на доходном подходе (рассчитывается чистый доход, приносимый комплексом объектов) и дисконтировании денежных потоков. При этом учитываются экономические эффекты от сокращения дисконтированных затрат на стадии возведения комплекса, экономический эффект в сфере эксплуатации отдельных зданий и сооружений, введенных за период горизонта расчёта, для инвестора.

Ключевые слова: предпроектная стадия, проект организации строительства, комплекс зданий и сооружений, очередь строительства, последовательность застройки, график финансирования, дисконтированные затраты.

Introduction

The pre-design stage in accordance with the Decree [1] is part of the life cycle of most construction projects. It serves to substantiate the decision to implement an investment project in terms of its necessity, technical feasibility, economic benefits, and environmental impact. At the same time, TCP 45-1.02-298-2014 indicates the need at this stage to carry out alternative studies and corresponding calculations of the investment efficiency for the full life cycle of the project (pre-investment, investment, operational and liquidation stages), to determine, if necessary, the sequence of construction, to make proposals on the organization and duration of construction [2].

Variant studies should cover all decisions: space-planning, constructive, organizational and technological decisions, and also take into account the social and environmental consequences of the construction and operation of the facility. It should be noted that it is rather problematic to take into account the full life cycle of the project in the calculations of the investment efficiency due to the lack of information on the operational stage [3].

When implementing an investment project, which includes a complex of buildings and structures, an important role in determining the efficiency of investments is played by the choice of the optimal sequence for the construction of its individual parts. The investor (customer, developer), when determining the order of construction, takes into account the sources and conditions for financing the construction of individual phases and start-up complexes, basic technological solutions for production facilities, decisions of the general layout and the possibility of organizing construction sites for the residential complexes (quarters, housing estates).

Changing the sequence of development entails changes in the schedule of capital investment distribution. The economic effect is achieved from the implementation of a more rational financing schedule and, as a result, a reduction in discounted costs.

The aim of this study is to develop an algorithm for the choice of an optimal option of the sequence of development of a complex consisting of several buildings and structures, which will maximize the net present value (NPV) for the investor.

The state of research in the area under consideration

In the 80s, a significant amount of research was carried out, a regulatory framework [4, 5, 6] and software were developed to determine the optimal sequence of development and calculate the cost efficiency of Construction Organization Project (COP).

The basis for determining the comparative effectiveness of design solutions for organizing the construction of production facilities was the Instruction [7], in accordance with which the best option is considered to give the minimum value of the reduced costs. At the same time, the effect of reducing the duration of construction was taken into account.

When comparing the options for the order of development of housing estates with urban planning complexes, the volume of work in progress for engineering equipment of the territory was taken as the basis for comparison [5, p. 16]. For each urban planning complex, the communications necessary for putting the buildings of this complex into operation were determined, considering that this site was commissioned first. The lengths of the networks and the roads were used to calculate the cost of engineering equipment for it. The first construction phase was the site for which the unit costs for engineering equipment per 1 m^2 of residential area were the lowest. Then, this site was excluded from consideration (it was assumed that engineering networks were laid to it) and the calculations were repeated for the remaining sites.

Today the economic system and project management methods have changed, which makes it impossible to apply previously developed algorithms. At the same time, there is a revival of interest in solving the problem of determining the optimal sequence of construction of buildings and

structures within the complex. There are two main approaches to solve this problem:

1. Choosing the best option for the sequence of construction in terms of organizational criteria, for example, reducing breaks between works, minimizing the number of workers, reducing the total duration of construction (Bolotin S.A., Velichkin V.Z., Chelnokova V.M., Morozova T F., etc.).
2. Choosing the best of the pre-developed options of sequence in terms of cost efficiency criteria.

Examples of the implementation of the first approach:

- formation of a schedule of the flow development of the territory using the method of undefined resource coefficients [8]. The method makes it possible to solve the problem of incompleteness of the initial data on the duration of work at the early stages of planning the development of the territory by urban planning complexes. Resource coefficients are values that are inversely proportional to the number of resources required to perform some work. To solve the problem, classical linear programming algorithms are used. Maximizing the objective function allows you to reduce organizational breaks between works;
- application of the branch and bound method in solving the problem of organizing residential quarter development [9]. As an objective function, the minimum duration of construction of all buildings of the quarter, a minimum of downtime for teams of workers, or a minimum of the duration of the work of teams on a quarter development can be used. Limitations - the deadlines for the construction of individual buildings and the entire complex, the total downtime of teams, the methods of flow organization of work on individual buildings and the complex as a whole (flow organization by the critical path method, by the rank method, by the continuous labor and technical resources employment method, by the continuous development of work fronts method);
- joint use of BIM-modeling programs (such as Revit) and project management programs (Project Expert, Microsoft Project) to determine the optimal sequence of construction of buildings included in the urban planning complex [10];
- breakdown of projects for Integrated Development of the Territory into urban planning complexes (several residential buildings provided with social infrastructure, landscaping and greening) and scheduling of flow construction [11, 12, 13]. At the initial stage, variants of matrices of the flow organization of work for individual facilities are calculated using the basic methods [14]. The corresponding object flows are formed. Then the matrices of complex flows of the following main types are calculated: Complex Compacted Flow, Complex Aggregated Flow, Complex Combined Flow. The variants are analyzed and the most appropriate for the construction conditions is determined;
- application of a heuristic algorithm for enumerating resource profiles for peak loads based on statistical modeling methods [15]. As a result, the resource peak (the maximum number of workers) and the corresponding area of temporary buildings are reduced. The economic effect is calculated as a reduction in the cost of temporary buildings.

Thus, when using the first approach, options are determined that are optimal from the point of view of organizational criteria, that is, from the point of view of a contractor or developer carrying out construction on their own. In practice, the interests of the investor and the contractor may differ significantly, and the investor will not choose finance options that are not optimal for him. Therefore, at the stage of development of predesign documentation and COP, it is advisable to make decisions that are effective primarily for the investor, and at the stage of organizational and technological design, when the contractor develops a Work Production Project - effective for the contractor, within the framework of COP decisions and the terms of the construction contract. Accordingly, it becomes necessary to develop different techniques for different stages of organizational and technological design.

When implementing the second approach, dynamic criteria of cost efficiency (on a discounted basis) are applied, classical calculations of the net present value, the profitability index are performed to select the best schedule option from the presented ones. At the same time, the described algorithms [16] use a somewhat simplified approach that does not take into account the differences between commercial and non-commercial facilities. Hence, it becomes necessary to concretize the methods for calculating the indicators of cost efficiency.

Assessment of the cost efficiency of options for the sequence of construction of a complex of buildings and structures in the development of pre-design and design documentation

Variants of technological and organizational solutions during their implementation do not affect the area of operation of the commissioned ed facilities. Therefore, the costs of their implementation are determined only in one area - the sphere of construction production. As for design solutions, the comparison of organizational and technological options should be carried out subject to certain conditions that ensure their comparability. These conditions include: compliance with work technology, high-quality performance of work, comparable working conditions.

The design of alternative construction schedules should be carried out under the following conditions:

- the option with the maximum duration does not exceed the prescribed or standard term for the construction of the complex;
- if it is possible to fulfill the above organizational and technological conditions, the sequence of construction of buildings in the flow is taken from longer in terms of construction duration to shorter ones. This allows you to reduce organizational breaks between the stages of building construction (underground, aboveground part, finishing and special works, installation of equipment);
- it is assumed that investment costs are incurred at the beginning of each considered time period, and investment results are obtained at the end of the period;
- when determining the duration of the construction of facilities in the schedules, one should proceed from at least two-shift work when using the main construction machines, without using - on average, 1.5 shifts, taking into account the regulatory requirements [17];
- the calculation horizon for economic comparison is taken as the duration of the construction of a complex of buildings, structures according to the option with a longer duration (except for cases of the same duration for options).

The main goal of the investor (customer, developer) will be the receipt of the maximum income, expressed in the growth of the net present value (NPV), which is the total difference between discounted income cash flows and discounted outcome cash flows (investments) for the entire considered period of the project (calculation horizon).

Thus, the economic effect for the investor (E_{inv}) from the choice of the option of organizational decisions is calculated as the difference between the NPV values of the best ($NPV_{inv}^{\min}$) and other options ($NPV_{inv}^{\max}$).

The economic effect of using a more profitable organizational solution includes:

- economic effect at the construction stage due to the reduction in discounted capital costs (E_{inv}^{C}), rubles;
- economic effect at the stage of operation, due to income from the use of the object for the period from the commissioning of a particular building to the end of the calculation horizon (E_{inv}^{O}), rubles:

$$E_{inv} = NPV_{inv}^{\min} - NPV_{inv}^{\max} = E_{inv}^{C} + E_{inv}^{O} \quad (1)$$

In accordance with the legislation [18], a construction object may consist of one or more buildings, structures and their parts, engineering and transport communications and other real estate objects.

As part of a construction object, design documentation can identify construction phases and start-up complexes.

The construction phase is a part of a main-purpose facility, which can be independently operated and ensure, among other things, the safety of its functioning, product release, production of work, provision of services.

If the object is a complex of buildings, structures, then, taking into account their purpose and the degree of autonomy of functioning after commissioning, the following options are possible:

- during the construction of a complex of buildings, structures, including residential, public, retail, administrative and other buildings for cultural and domestic purposes, each building with the infrastructure necessary for its functioning is a separate completed construction phase, which can generate income for the period from its commissioning into operation until the end of the calculation horizon;
- during the construction of a complex of industrial buildings and structures, representing a single property complex of the enterprise, the following options are possible:

1) the construction is carried out without the allocation of phases or start-up complexes, then when comparing the options according to the described method:

doi.org/10.36773/1818-1112-2021-126-3-103-107

- ✓ for an option with a shorter construction duration, income is taken into account from the moment the complex is put into operation according to this option until the end of the calculation horizon;
- ✓ for an option with a maximum duration equal to the calculation horizon, income is not taken into account;

2) the construction is carried out in several construction phases (start-up complexes) with the commissioning of each of them separately, after which the receipt of income from the commissioned phase begins until the end of the calculation horizon.

The economic effect of reducing discounted costs at the stage of construction of the complex:

$$E_{inv.}^{C} = \sum_{i=1}^{n^{I}+1} PV_{i}^{Inv^{I}} - \sum_{i=1}^{n^{II}+1} PV_{i}^{Inv^{II}} = \\ = \sum_{i=1}^{n^{I}+1} \frac{Inv_{i}^{I}}{\left(1+R_{inv}^{calc}\right)^{i-1}} - \sum_{i=1}^{n^{II}+1} \frac{Inv_{i}^{II}}{\left(1+R_{inv}^{calc}\right)^{i-1}} \quad (2)$$

where I and II – indices of the corresponding options;

i – number of the calculation period;

Inv_i – amount of capital investments (cash outflow, investment costs), mastered in the i-th calculation period of construction (month), rubles;

n – number of calculation periods during the calculation horizon;

$\boldsymbol{R}_{inv}^{calc}$ – real discount rate for the calculating period for the investor.

If the compared options for the construction of a complex of buildings and structures have the same duration, then the economic effect can be achieved from a more rational financing schedule and, as a consequence, a reduction in discounted costs.

If the duration of the construction of a complex of buildings and structures for both options is the same ($n^{I} = n^{II}$) and construction for both options is carried out without allocation of construction phases, then $E_{inv}^{O} = 0$.

If the duration of the construction of a complex of buildings and structures for both options is the same ($n^{I} = n^{II}$), the number of construction phases is the same ($m^{I} = m^{II}$) and the duration of the construction of phases is the same ($n_{j}^{I} = n_{j}^{II}$) for all $j = 1, 2 \ldots m$, then $E_{inv}^{O} = 0$.

The real discount rate for the calculating period for the investor is determined by the formula [19]:

$$R_{inv}^{calc} = \frac{R_{inv} \cdot t_{calc}}{360} \quad (3)$$

where t_{calc} – duration of the calculation period, days;

$\boldsymbol{R}_{inv}$ – annual real discount rate:

$$R_{inv} = \frac{r - in}{1 + in} \quad (4)$$

where in – inflation rate;

r – nominal weighted average discount rate:

$$r = r_{e} \cdot \alpha_{e} + r_{d} \cdot (1 - \alpha_{e}) \quad (5)$$

where r_e, r_d, – nominal interest rates of the investor's equity capital and debt capital;

α_e – share of equity in the total volume of capital investments.

The nominal interest rate r_e is calculated as follows:

- when financing the construction of commercial facilities, it is taken in accordance with the value of the return on invested equity capital:

$$r_{e} = \frac{NP^{r}}{E^{r}} \quad (6)$$

where NP^{r} – net profit for the reporting period, rubles;

E^{r} – equity in the reporting period, rubles;

- when financing the construction of non-commercial residential buildings by individuals, it is taken equal to the nominal interest rate on a long-term deposit r_{ld} or long-term government and bank bonds r_{lb};
- when financing the construction of non-commercial facilities by the state, it is taken to be equal to the standard coefficient of investment efficiency, determined by the ratio of net profit to invested capital on average per year.

The r_e value must not be lower than the refinancing rate of the National Bank of the Republic of Belarus.

If the planned share of equity capital in the total capital investment α_e is unknown, then the nominal weighted average discount rate for the investor r when financing commercial objects is equal to the return on invested total capital:

$$r = \frac{NP^{r}}{IC^{r}} \quad (7)$$

where IC^{r} – total amount of investor's capital in the reporting period, rubles.

When the construction phase is put into operation during the calculation horizon, the investor will receive additional income for this period. The economic effect of the investor in the area of operation from the functioning of the facility for the period of early commissioning is determined by the following formula:

$$E_{inv}^{O} = \sum_{i=n_{h}^{I}+1}^{n^{I}+1} PV_{hi}^{NI^{I}} - \sum_{i=n_{h}^{II}+1}^{n^{II}+1} PV_{hi}^{NI^{II}} = \\ = \sum_{i=n_{h}^{I}+1}^{n^{I}+1} \frac{NI_{hi}^{I}}{\left(1+R_{inv}^{calc}\right)^{i}} - \sum_{i=n_{h}^{II}+1}^{n^{II}+1} \frac{NI_{hi}^{II}}{\left(1+R_{inv}^{calc}\right)^{i}} \quad (8)$$

where h – index of the construction phase;

i – numbers of calculation periods in which net income is received, in the range from the moment of commissioning the h-th construction phase of the object according to the option to the moment of the end of the calculation horizon;

n_h – the moment of commissioning the h-th construction phase, calc. periods;

NI_{hi}^{II} is the investor's net income from the operation of the h-th construction phase in the i-th calculation period, rubles / calc. period.

When determining net income, the following options can be distinguished, depending on the purpose of real estate objects:

1) commercial objects:
- income can be received only after the commissioning of the entire complex of buildings and structures (the object as a whole);
- income can be received after the commissioning of a separate construction phase (part of the object that can be independently operated and generate income);

2) non-commercial objects:
- net income of a commercial investor (except for the state) after the commissioning of each construction phase (for example, a residential building with infrastructure);
- net income of the investor (state) after the commissioning of each construction phase (administrative building, school, etc. with infrastructure).

The net income for the option will be determined on an accrual basis as the construction phases are accepted into operation within the calculation horizon.

The investor's net income for commercial objects is determined as follows according to [19]:

$$NI_{hi} = NP_{hi} + DE_{hi} \quad (9)$$

where NP_{hi} is the net profit from the operation of the h-th phase as part of the construction object for the i-th calculation period, rubles / calc. period;

DE_{hi} – corresponding depreciation expenses, rubles / calc. period.

$$NP_{hi} = R_{o}^{calc} \cdot EC_{hi} \quad (10)$$

where $\boldsymbol{R}_{o}^{calc}$ is the real profitability of objects in terms of net profit for the calculating period;

EC_{hi} – the estimated cost of the j-th building, structure as part of the h-th construction phase, rubles.

You can take the real profitability of the object in terms of net profit at the level of the real discount rate for the investor (formula (3)).

Depreciation expenses for the *h*-th construction phase in the *i*-th calculation period:

$$DE_{hi} = \left(\sum_{j=1}^{N_h^b} \frac{EC_{jh}^b}{T_{jh}^b} + \sum_{j=1}^{N_h^{eq}} \frac{EC_{jh}^{eq}}{T_{jh}^{eq}} \right) \cdot \frac{t_{calc}}{360} \quad (11)$$

where, EC_{jh}^b, EC_{jh}^{eq} is the estimated cost of construction and installation work of the *j*-th building (structure, infrastructure element) in accordance with the consolidated estimate, or the *j*-th unit of equipment, respectively, rubles; ,

T_{jh}^b, T_{jh}^{eq} is the standard service life of the *j*-th building (structure, infrastructure element) or the *j*-th type of equipment as part of the *h*-th construction phase, respectively, years;

N_{jh}^b, N_{jh}^{eq} – the number of buildings, structures, types of equipment, respectively, in the *h*-th construction phase.

Investor's net income (except for the state) from the operation of a non-commercial residential building:

$$NI_{ji} = I_{ji}^A + D_{ji}^{CR} \quad (12)$$

where I_{ji}^A – is the alternative income from the operation of the *j*-th building for the *i*-th calculation period, rubles / calc. period;

D_{ji}^{CR} – deductions for capital repairs for the *j*-th building in the *i*-th calculation period, rubles / calc. period.

We consider deductions D_{ji}^{CR} as expenses that will lead to an increase in the value of the complex of buildings in the future, which is tantamount to earning income.

An investor's alternative income for non-commercial residential buildings is defined as savings in rental costs for similar residential buildings:

$$I_{ji}^A = RR_j \cdot S_j^t \cdot \frac{t_{calc}}{30} \quad (13)$$

Where RR_j is the rental rate for the *j*-th building, rubles / m²·month;

S_j^t – the total area of living quarters in the *j*-th building, m².

For residential buildings that are built without the participation of state budget funds (at the expense of future apartment owners), the rental rate is taken at the level of the market weighted average in the region according to the Internet.

For residential buildings under construction at the expense of the budget funds, the rental rate is determined as the base rate of payment for the use of public rental housing:

$$RR_j^{st} = 0,2 \cdot BV \cdot C_{im} \quad (14)$$

where BV is the base value, rubles;

C_{im} – is a coefficient determined by the regional executive committees and the Minsk city executive committee, taking into account the degree of improvements and the district where the residential premises are located.

Deductions for major repairs for the *j*-th residential building in the *i*-th calculation period:

$$D_{ji}^{CR} = d_j^{CR} \cdot S_j^t \cdot \frac{t_{calc}}{30} \quad (15)$$

where d_j^{CR} – is the standard of deductions for capital repairs for the *j*-th building, rubles / m² month.

The investor's (state's) net income from the operation of a non-commercial facility is calculated using the following formula according to [19]:

$$NI_{ji} = E_{ji}^n + D_{ji}^{CR} \quad (16)$$

where E_{ji}^n is the normative effect from the use of the ***j***-th object (construction phase) in the ***i***-th billing period (a non-commercial object brings a social or environmental effect that can be expressed in monetary terms), rubles / calc. period: ,

$$E_{ji}^n = R_{inv}^{calc} \cdot EC_j \quad (17)$$

where R_{inv}^{calc} is the real discount rate for the accounting period for the investor, in accordance with formulas (3) and (4);

EC_j – the estimated cost of construction of the ***j***-th object, rubles.

Conclusion

The method has been developed for assessing the cost efficiency of options for the sequence of construction of a complex of buildings and structures, based on an income approach (the net income brought by a complex of facilities is calculated) and discounted cash flows.

This takes into account the economic effects of reducing discounted costs at the stage of construction of the complex, and the economic effects in the field of operation of individual buildings and structures, commissioned over the period of the calculation horizon, for the investor. This technique is currently relevant and complies with the rules for the development of business plans for investment projects [20].

References

1. On measures to improve construction activities [Electronic resource]: Decree of the President of the Republic of Belarus, January 14, 2014, No. 26 // ETALON-ONLINE / National Center for Legal Information of the Republic of Belarus. – Minsk, 2021.
2. Construction. Pre-design (pre-investment) documentation. Composition, order of development and approval: TCP 45-1.02-298-2014 * (02250). – Entered 20.07.2014. – Minsk : Ministry of Architecture and Construction of the Republic of Belarus, 2019. – 52 p.
3. Kochurko, A. N. The analysis of approaches to assessment of efficiency of alternatives of implementation of investment projects at the predesign stage / A. N. Kochurko, L. G. Sryvkina // Vestnik BrSTU. – 2019. – No. 1. – P. 112–117.
4. Recommended practice for planning and organization of nonindustrial construction when developing cities using urban development complexes / TsNIIPgradostroitelstva. – Moscow : Stroyizdat, 1988. – 128 p.
5. A guide for the development of construction organization plans and work execution plans for civil construction (to SNiP 3.01.01-85) / TsNIIOMTP. – Moscow : Stroyizdat, 1989. – 160 p.
6. Development of construction organization plans and work execution plans for industrial construction: manual to SNiP 3.01.01-85 "Organization of construction production" / TsNIIOMTP. – Moscow : Stroyizdat, 1990. – 238 p.
7. Guidelines for the determining return on capital investments in construction: SN 423–71. – Moscow : Stroyizdat, 1979. – 41 p.
8. Interactive formation of a schedule of flow development of an urban planning complex / S. A. Bolotin [et al.] // Organization of Construction Production : proceedings of the 3rd All-Russian Scientific Conference, St. Petersburg, 10–11 February, 2021 / Saint Petersburg State University of Architecture and Civil Engineering. – St. Petersburg : SPbGASU, 2021. – P. 3–17.
9. The branch and bound method applied to the construction of residential quarters / V.Z. Velichkin [et al.] // Vestnik MGSU. – 2021. – Vol. 16 (1). – P. 91–104.
10. Bolotin, S. A. Scheduling of a complex development using Revit and Microsoft Project / S/ A. Bolotin // BIM in Construction and Architecture : proceedings of the 2nd International Scientific Conference, St. Petersburg, May 15–17, 2019 / Saint Petersburg State University of Architecture and Civil Engineering. – St. Petersburg : SPbGASU, 2019. – P. 53–58.

doi.org/10.36773/1818-1112-2021-126-3-103-107

11. Chelnokova, V. M. Substantiation of the breakdown of projects for the integrated development of territories into urban-planning complexes / V. M. Chelnokova, A. B. Gurevich // Architecture – Construction – Transport : proceedings of the 73rd scientific conference of professors, lecturers, researchers, engineers and post-graduate students of the university, St. Petersburg, October 4–6, 2017: in 3 parts / Saint Petersburg State University of Architecture and Civil Engineering. – Part I. – St. Petersburg : SPbGASU, 2017. – P. 90–93.
12. Chelnokova, V. M. Method of scheduling flow construction of facilities with their subsequent combination into complexes / V. M. Chelnokova, Yu. S. Vinokurova, E. P. Kondra // Architecture – Construction – Transport : proceedings of the 74th scientific conference of the staff and post-graduate students of the university, St. Petersburg, October 3–5, 2018: in 2 parts / Saint Petersburg State University of Architecture and Civil Engineering. – Part I. – St. Petersburg : SPbGASU, 2018. – P. 71–74.
13. Chelnokova, V. M Organization of complex development of populated areas / V. M Chelnokova // Petersburg School of Flow Organization of Construction : proceedings of 1st All-Russian Scientific Conference, St. Petersburg, February 19-20, 2018 / Saint Petersburg State University of Architecture and Civil Engineering; total. ed. E. B. Smirnova. – St. Petersburg : SPbGASU, 2018. – P. 11–16.
14. Afanasyev, V. A. Models of flow organization of work: textbook / V. A. Afanasyev, T. F. Morozova. – St. Petersburg : SPbSPU, 2002. – 37 p.
15. Morozova, T. F. Organization of quarters' line building by social, cultural and communal facilities / T. F Morozova, N. N Bokovaya, Xia Jiaming // Construction of Unique Buildings and Structures. – 2013. – No. 1 (6). – P. 36–46.
16. Mishina, O. O. Analysis of the economic efficiency of the project with different options for the construction of the objects in the composition of the complex [Electronic resource] / O. O. Mishina, R. G. Abakumov, I. P. Avilova // Innovative Economy: Prospects for Development and Improvement. – 2018. – No. 3 (29). – P. 105–111. – Access mode: https://cyberleninka.ru/article/n/analiz-ekonomicheskoy-effektivnosti-proekta-pri-raznyh-variantah-ocherednosti-stroitelstva-obektov-v-sostave-kompleksa. – Date of access: 09.04.2021.
17. Standards for the duration of construction of buildings, structures and their complexes. Basic provisions: TCP 45-1.03-122-2015 * (33020). – Entered 01.01.2016. – Minsk : Ministry of Architecture and Construction, 2018. – 15 p.
18. On architectural, urban planning and construction activities in the Republic of Belarus [Electronic resource]: Law of the Republic of Belarus, July 5, 2004, No. 300-Z // ETALON-ONLINE / National Center for Legal Information of the Republic of Belarus. – Minsk, 2021.
19. Construction economics. Course and diploma design: textbook / A. N. Kochurko [et al.]. – Minsk : Grevtsov Publishing House, 2012. – 396 p.
20. Rules for the development of business-plans for investment projects [Electronic resource]: Resolution of the Ministry of Economy of the Republic of Belarus, August 31, 2005, No. 158 // ETALON-ONLINE / National Center for Legal Information of the Republic of Belarus. – Minsk, 2021.

Accepted 25.10.2021

UDC 658.5

STABILIZATION OF LOGISTICS FUNCTIONS IN THE RISK MANAGEMENT OF REGIONAL LOGISTICS SYSTEMS ON THE PRINCIPLES OF THE INTERNATIONAL STANDARD

V. V. Nebelyuk[1], E. L. Shishko[2]

[1] Master of Economics, Senior Lecturer of the Department of Economic Theory and Logistics, Brest State Technical University, Brest, Belarus, e-mail: vvnebelyuk@bstu.by
[2] Master of Economics, Postgraduate, Senior Lecturer of the Department of Economic Theory and Logistics, Brest State Technical University., Brest, Belarus, e-mail: aljonaschischko@mail.ru

Abstract

The issues of stabilization of logistics functions in the risk management of regional logistics systems are based on the principles of the international standard. Logistics functions are presented as special management functions.

The stages and components of the monitoring system of the logistics functions of the organization are identified. Attention is paid to the issues of stabilization of the logistics functions management system in accordance with the new requirements and conditions of the international standard ISO 9004:2018 series.

The article substantiates the procedure for diagnosing logistics functions as a means of self-assessment in the management of the organization and measuring the parameters of production and economic activity with the prospect of stabilizing the logistics functions «procurement» and «implementation», as well as risk management in regional logistics systems.

Keywords: international standard, logistics functions "procurement" and "implementation", stabilization, risk-management, monitoring, measurement.

СТАБИЛИЗАЦИЯ ЛОГИСТИЧЕСКИХ ФУНКЦИЙ В РИСК-МЕНЕДЖМЕНТЕ РЕГИОНАЛЬНЫХ ЛОГИСТИЧЕСКИХ СИСТЕМ НА ПРИНЦИПАХ МЕЖДУНАРОДНОГО СТАНДАРТА

В. В. Небелюк, Е. Л. Шишко

Реферат

Вопросы стабилизации логистических функций в риск-менеджменте региональных логистических систем опираются на принципы международного стандарта. Логистические функции представлены как специальные функции управления.

Выявлены этапы и составляющие системы мониторинга логистических функций организации. Внимание уделяется вопросам стабилизации системы управления логистическими функциями согласно новым требованиям и условиям международного стандарта серии ISO 9004:2018.

Обоснована процедура диагностики логистических функций как средство самооценки в управлении организации и измерения параметров производственно-хозяйственной деятельности с перспективой стабилизации логистических функций «закупки» и «реализация», а так же управления рисками в региональных логистических системах.

Ключевые слова: международный стандарт, логистические функции «закупки» и «реализация», стабилизация, риск-менеджмент, мониторинг, измерение.

Introduction

The paper suggests approaches to solving the problems of managing the sustainable development subjects of the regional logistics system. The practice of mastering the modern logistics concept is presented. The approaches that ensure the improvement of the risk management system in regional logistics systems are demonstrated based on the principles of the international standard. The tools that will provide a timely «targeted» response to changes in the business environment are presented. The proposed practice will allow for the stabilization of the logistics functions of the enterprise, which is associated with the loss of stability and risk management in regional logistics systems.

International quality management standards and the practice of mastering a new logistics concept

International standards of the quality management system form the principles of modern management. IS QMS is based on fundamental certification models:

1) ISO 9001 – Quality assurance model at the development stages (during production, design, installation and maintenance);
2) ISO 9002 – Quality assurance model at the production and installation stages;
3) ISO 9003 – Quality assurance model at the stage of control and testing of finished products.
4) ISO 9004 – 2008 «Management for achieving the sustainable success of the organization».
5) ISO 9004 – 2018 «Quality management. The quality of the organization. A guide to achieving the sustainable success of an organization».

Special attention is currently being paid to the ISO 9004 series. It regulates the management of sustainable socio-economic development (MSSED) of business entities. The management process is considered as the activity of management entities united in a system (line and functional managers, other management personnel); activities aimed at achieving the goals of the team and covering all eight special management functions (SMF):

1) organization policy;
2) human resource management;
3) production management;
4) marketing function;
5) *the implementation function* is assigned to sales managers;
6) *procurement function* – assigned to supply managers;
7) financial management;
8) the function of the quality management system (QMS).

The logistical aspect of management is to answer the question: «where it is more profitable to interact on business operations» - within the company or with the help of the market. The development of network structures in the interests of cooperation between suppliers and partners in the field of procurement and implementation creates innovative business models.

The authors formulate a view on the logistics functions of the organization as special management functions (SMF) «implementation» and «procurement». The processes of managing logistics functions involve work in two directions: 1) monitoring and evaluation of the sustainability of management in the field of «procurement» and 2) monitoring and evaluation of the sustainability of management in the field of «implementation».

doi.org/10.36773/1818-1112-2021-126-3-108-111

Management of the sustainable development of a production organization covers eighteen management functions. They include: 1) special management functions (SMF), 2) common (general) management functions (CMF), SMF and CMF at three levels of management – strategic, current, operational.

For measurement purposes the level of manageability of logistics functions (LM LF), the authors applied the «Theory of measuring the manageability of economic activities of enterprises» by Professor O. A. Vysotsky. The LM LF measurement is performed simultaneously in the «procurement» and «implementation» areas. For this purpose, the main characteristics of the organization's management processes in the «starting conditions» are determined.

When conducting LF diagnostics, the authors use an *express analysis of the organizational structure* of management. The analysis allows to develop a program for managing the economic system and evaluate: 1) special and basic management functions; 2) the work of specialists who are responsible for the successful development of the enterprise; 3) the work of the functional and technical subsystem in the analyzed time period.

For the analysis, groups of experts are identified who should be interviewed in order to measure the special and common management functions of the organization (SMF and CMF). The content and stages of diagnostics of the logistics functions of the organization are presented in Table 1.

Table 1 – Stages of logistics management diagnostics and the content of work

Diagnostic directions	Content	Sources of information
Stage 1: Diagnostics of the control object		
OSM (organizational structure of the enterprise management)	Express analysis of the organizational structure of management based on the analysis of the staffing table. Analysis of the procedure for making managerial decisions in the field of logistics.	Information about the production and organizational structure of the enterprise; staffing table; expert survey.
Stage 2. Measurement of the overall management functions of the organization that form the management of sustainable development		
CMF (common management functions of the organization)	Preparation of the questionnaire. Measurement of the level of manageability by the main management functions in the field of logistics.	A survey of the organization's experts in the field of planning and control.
Stage 3. Measurement of the processes of managing the logistics functions of the organization		
L SMF (logistics special management functions)	Preparation of the questionnaire. Analysis of the level of development of special functions «Procurement» and «Implementation» in the organization's management processes.	Survey of the organization's experts in the field of logistics «Procurement» and «Implementation».
Stage 4. Determining the corrective effect for stabilization of the logistics functions «procurement» and «implementation»		
Dynamics of LM LF (the level of manageability of logistics functions)	Measurement of the level of manageability by the sustainable development of the LF. Determination of vectors of development forces for each LF for stabilization.	Analytical work: determination of the control zones of the LF.
Results: design of passports of the "Procurement", "Implementation" process and maps of procedures of related subprocesses		

Source: personal development

This diagnosis is based on: a) analysis of the staffing table and functional responsibilities of logistics specialists; b) the theory of measuring the manageability of the economic activity of the organization by Professor O. A. Vysotsky; c) the feedback law and its role in management, according to the MS QMS of the ISO 9004 series. This diagnosis allows to reduce the uncertainty of the business environment – to compensate for the negative impact in the field of risk management.

Risk management in regional logistics systems. Experimental implementation of the author's model of diagnostics of manageability of logistics functions in the regional system (Brest region)

Based on the conducted research, it was revealed that in the Brest region, as a transit region, the risks of providing logistics services «procurement» and «implementation» fell into the zone of critical risk with negative consequences. The level of controllability (LC) of the event is 16%, the probability of occurrence – 77%, the time of occurrence – 23%. This indicates a low degree of event manageability, a lack of time for decision-making. As a result, there is a high probability of a critical risk with negative consequences. The solution to this problem is prevention of risk, which contribute to the transition of a critical risk with negative consequences to an acceptable or permissible risk zone, or a critical risk with positive consequences (Drawing 1).

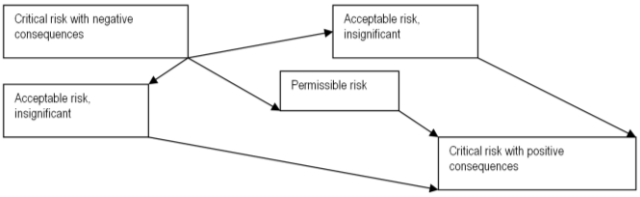

Drawing 1 – *Possible ways of risk transfer*

Source: personal development

According to the authors, a positive result in risk management in regional logistics systems (RLS) is achieved through increasing the level of event manageability. Diagnostics of management processes is necessary to stabilize management functions in the field of «procurement» and «implementation».

«Procurement» management is the first logistics subsystem that needs to be diagnosed. The measurement of the levels of «procurement» management was carried out by the authors through the assessment of the common management functions (CMF): 1) planning, 2) organization (decision-making), 3) motivation(stimulation), 4) control (monitoring), 5) accounting, 6) analysis (evaluation), 7) coordination (adjustment). This is a group of functions called the «Quality Loop».

Six experts who know the procurement management processes and have their own performance assessments (their own opinion) were selected for the diagnosis. The experts worked with the questionnaire and evaluated the effectiveness of procurement management in the regional logistics system (radar) through the CMF on a 10-point scale. After filling out the questionnaires, the experts calculated the average scores for all indicators and determined the starting zones of manageability of «purchases» (table 2).

Table 2 – Processing of expert assessments and calculation of manageability levels by the logistics function «procurement» in the regional logistics system

Common management functions	Estimation in points										Definition *LM*, %
	1	2	3	4	5	6	7	8	9	10	
1	2	3	4	5	6	7	8	9	10	11	12
1. Planning *LM* 1					+	+++		++			65
2. Organization, decision-making *LM* 2							+	+	++ ++		85
3. Motivation, stimulation *LM* 3			+	+	+	+	+	+			55
4. Control, monitoring *LM* 4					+	++	+	++			46
5. Accounting *LM* 5						+	++	++	+		65
6. Analysis and evaluation *LM* 6				+		+++ ++					56
7. Coordination, correction *LM* 7				++ +	++	+					46
Generalizing level of manageability *LM* = ($\sum LM_1 ... LM_7$) / 7											59

Source: personal development based on the present data

The level of manageability of the logistics function «procurement» in the regional logistics system of the Brest region is 59%. Based on Table 2, a schedule for determining the «procurement» manageability zones is compiled (Drawing 2).

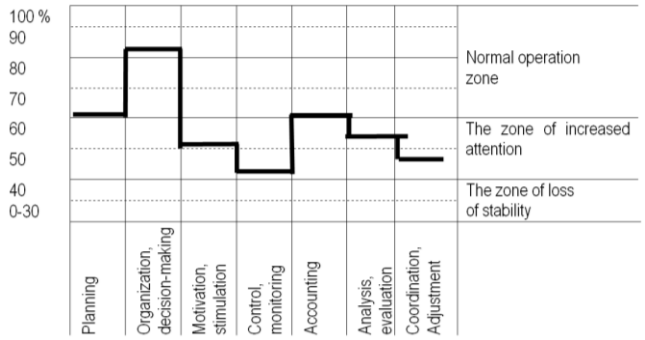

Drawing 2 – Graph of controllability zones

At this stage of material flow management, it becomes necessary to make decisions on coordinating the interests of supplier and consumer enterprises. To do this, it is necessary to create a flexible system of centralized regulation and control.

The controling and monitoring functions are close to the «loss of stability» zone and require stabilization. Next, the authors present the analytical tool «logistics barometer», it contributes to the removal of the OFU from the zone of increased attention to the zone of normal operation (Drawing 3).

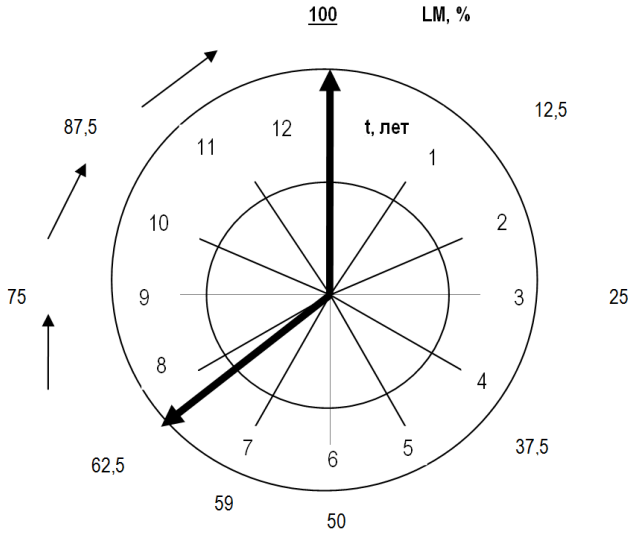

Drawing 3 – Determination of the time of withdrawal of the main control functions from the zone of increased attention to the zone of normal operation

Source: personal development based on the present data

It is known that «procurement» is the process of movement of stock, materials, spare parts and components from the procurement market to the warehouses of the enterprise. «Procurement» management is the planning, organization and control of providing the main production with the necessary material and technical resources in a certain time mode with minimal total costs.

To calculate the time intervals of stabilization of each of the main functions: planning, organization and decision-making, motivation and stimulation, control and monitoring, accounting, analysis and evaluation, coordination, adjustment, we use the formula:

$$LM\,\Delta t = LM\,\Delta t3 - LM\,\Delta t0, \quad (1)$$

where, $LM\,\Delta t$ – interval indicator,

$LM\,\Delta t3$ – final indicator,

$LM\,\Delta t0$ – the indicator of the function in the starting conditions.

According to the general accounting system, the authors took a year as a unit of time, the period of stabilization of the main functions of the procurement department was 4,2 years.

According to the results of diagnostics, the average levels of controllability of each CMF at the initial stage differ. To know what forces to apply to the development of each function, the vectors of forces of development (VFD) were calculated CMF «procurement» (table 3).

Table 3 – VFD of the main functions of procurement management, %

Name of the indicator	Indications *LM* on t_0	Stage 1		Stage 2		Stage 3		Stage 4	
		LM (Δt_1)	*LM* (t_1)	*LM* (Δt_2)	*LM* (t_2)	*LM* (Δt_3)	*LM* (t_3)	*LM* (Δt_4)	*LM* (t_4)
1	2	3	4	5	6	7	8	9	10
1. Planning	46	13,5	59,5	13,5	73	13,5	86,5	13,5	100
2. Organization, decision-making	65	8,75	73,75	8,75	82,5	8,75	91,25	8,75	100
3. Motivation, stimulation	46	13,5	59,5	13,5	73	13,5	86,5	13,5	100
4. Control, monitoring	85	3,75	88,75	3,75	92,5	3,75	96,25	3,75	100
5. Accounting	55	11,25	66,25	11,25	77,5	11,25	88,75	11,25	100
6. Analysis and evaluation	65	8,75	73,75	8,75	82,5	8,75	91,25	8,75	100
7. Coordination, adjustment	56	11	67	11	78	11	89	11	100

Source: personal development based on the present data

Management of *«implementation»* is the final function of logistics, it aims to form an optimal logistics distribution network. This requires close interaction of related services with each other: marketing, sales, procurement and finance services.

To measure the levels of «implementation» management in the logistics system (Brest Region), a similar work was carried out: based on expert assessments, the levels of manageability of general distribution management functions in the regional logistics system were calculated; the initial distribution manageability zones in the regional logistics system were determined.

As a result, it was revealed: the largest amount of work needs to be carried out regarding the main functions in the field of «procurement»: 1) planning, 2) motivation and stimulation, 3) accounting – it is necessary to provide an increase of 50 %. The use of vectors of development forces for 4 years will increase the controllability levels of all OFU LF to 100 % – the zone of normal operation mode. Thus, due to the proper performance of the main functions in the field of «procurement» and «implementation», the logistics functions of the regional logistics system are stabilized.

Conclusion

The conclusions and recommendations made based on the results of the study will allow the subjects of regional logistics systems to increase the efficiency of logistics activities. Tools for managing the level of socio-economic development (LM SE) of subjects (RLS) in the field of logistics are proposed.

The theoretical significance of the research results lies in the fact that the conclusions and recommendations are aimed at solving the scientific problem – determination of methods of analysis and measurement of logistics function management processes. They expand the understanding of the need to assess the level of risk management in logistics systems as an indicator of their effectiveness and as a tool for tracking the dynamics of system development.

The authors draw attention to the need to follow the principles of achieving sustainable success in the field of logistics, according to the ISO 9000 QMS: identify short-term (from a month) and long-term (up to 5 years) risks associated with the organization's activities and form a general strategy for reducing them; provide an opportunity for managers and employees of the organization to «learn lessons» and exchange experience to maintain the viability of the organization; develop and maintain processes of innovation and improvement of methods of sustainable risk management in regional logistics systems in a workable state.

doi.org/10.36773/1818-1112-2021-126-3-108-111

References

1. Vysotsky, O. A. Theory of measurement of manageability of economic activity of enterprises / under the scientific editorship of R. S. Segedova. – Minsk : Law and Economics, 2004. – 396 p.
2. Vysotsky, O. A. Fundamentals of sustainable development of a production organization / O. A. Vysotsky, I. M. Garchuk, N. S. Danilova ; under the scientific editorship of V. F. Medvedeva ; Brest State Technical University. – Minsk : Law and Economics, 2015. – 258 p. – (Series "Higher School of Business").
3. Vysotsky, O. A. Innovative technologies of effective management control systems sustainable socio-economic development of the organization // Bulletin of the Brest state technical University. Economy. – 2018. – No. 3. – P. 3–10.
4. Deming, E. Out of the crisis: A new paradigm for managing people, systems and processes / Edwards Deming ; Trans. from English.: Yu. Adler, V. Shpered, N. V. Velichko. – M.: Alpina Business Review, 2007. – 147 p.
5. Nebelyuk, V. V. Innovative support of the system of sustainable management of socio-economic development of the organization / V. V. Nebelyuk // Economics and management: social, economic and engineering aspects : collection of scientific. articles of the II International scientific-practical conference, Brest, December 5–6, 2019 / redkol.: V. Zazerskaya [et al.]. – Brest : BrSTU, 2019. – P. 160–165.
6. Neave, G. R. Dr. Deming space: Principles of sustainable of business / Henry R. Neave ; Trans. from English. – M. : Alpina Business Review, 2005. – 370 p.
7. On the State program of Innovative Development of the Republic of Belarus for 2016-2020 (as amended. Decrees of the President of the Republic of Belarus dated 25.07.2017 No. 258, dated 30.11.2017 No. 428). [Electronic resource]. – Minsk, 2017. – Access mode: http://naviny/org/2014/06/20/by2375.htm/ – Date of access: 23.05.2021.
8. Quality management systems. International standard ISO 9001:2015 series [Electronic resource]. – Access mode: http://iso-management.com/wp-content/uploads/2015/12/ISO-9001-2015.pdf/ – Access date: 20.05.2021.
9. Shishko E. L. The use of simulation modeling in risk assessment in the logical system of the region / E. L. Shishko // Logistics audit of transport and supply chains: Materials of the International scientific and practical conference, April 26, 2018 / Editor-in-chief O. Y. Smirnova. – Tyumen : TIU, 2018. – P. 441–449.
10. Shishko, E. L. Competitiveness of enterprises and external macroeconomic risks / / L. P. Zenkova, E. L. Shishko // Science and Innovation. – Minsk, 2020. – No. 7. – P. 61–66.
11. Shishko, E. L. Conceptual approaches to modeling the development of regional logistics systems / E. L. Shishko // Scientific and practical journal "Consumer cooperation". – 2019. – № 2 (65). – P. 30–36.
12. Shishko, E. L. Methodological issues of determining the logistics system of the Brest region / E. L. Shishko // Bulletin of the Brest State Technical University. Series: Economics. – 2020. – No. 3. – P. 112–115.
13. Shishko, E. L. Regional logistics system: a conceptual approach / E. L. Shishko // Actual problems of science of the XXI century: collection of scientific articles of young scientists. – 2019. – No. 8. – P. 63–71.
14. Shishko, E. L. Regional aspect of logistics system sustainability / E. L. Shishko // Bulletin of the BSEU. – Minsk : BSEU, 2020. – No. 4. – P. 23–31.
15. Shishko, E. L. The role of digitalization in the sustainable development of society / E. L. Shishko // Bulletin of the Brest State Technical University. Series: Economics. – 2020. – No. 3. – P. 107–111.
16. Shishko, E. L. The state and prospects of development of the regional logistics system / E. L. Shishko // Bulletin of the Brest State Technical University. Economics series. – 2019. – No. 3. – P. 100–104.
17. Shishko, E. L. Strategies for the formation of supply chains in production / E. L. Shishko // Economic science today: collection of scientific articles / BNTU. – Minsk. – 2018. – No. 7. – P. 314–320.
18. Shishko, E. L. Theoretical foundations of risk management in the logistics system at the enterprise / E. L. Shishko // Bulletin of the Brest State Technical University. Economics series. – 2018. – No. 3. – P. 133–136.
19. Zenkova, L. P. Institutional reserves for improving the competitiveness of enterprises and regions of Belarus / L. P. Zenkova, E. L. Shishko // Efficiency of using resources of innovative competitive economic development: monograph ed. M. I. Plotnitsky. – Minsk : Misanta, 2019. – P. 135–145.
20. Shishko, E. L. Risks in logistics systems: a regional aspect / E. L. Shishko, L. P. Zenkova. – Minsk : IVC of the Ministry of Finance, 2020. – 195 p.
21. Shishko, E. L. Risk management as a strategic direction in the innovative development of the regional logistics system / E. L. Shishko // Innovations: on theory to practice: a collective monograph; under scientific ed.: A. M. Omelianyuka [et al.]. – Brest : BrSTU, 2019. – P. 192–196.

Accepted 25.10.2021

UDK 338.12

INVESTMENT PRIORITIES DURING THE PANDEMIC

A. G. Prarouski

PhD in Economics, Associate Professor, Head of the Department of World Economy, Marketing, Investments
Brest State Technical University, Brest, Belarus, e-mail: agprorovskij@g.bstu.by

Abstract

The work analyzes investment activity in the context of the COVID-19 pandemic that caused the global economic crisis. It is concluded that the pandemic has become a catalyst for the digitalization of the world economy. Both countries and businesses that quickly adapt to new conditions will be the leaders of the new economic cycle. Investments lead to the fact that enterprises acquire fixed assets. Capital investments are of a long-term nature, which allows companies to earn income for many years by adding or improving production capacities and increasing operational efficiency.

Additional or improved fixed assets increase labor productivity, making enterprises more productive and efficient. As labor becomes more efficient, increasing efficiency across the country leads to an increase in gross domestic product.

Investment processes in the world economy are currently undergoing significant changes. This is due to such factors as: changes in the US investment policy, the end of the next economic cycle, trade wars in the global economy, the spread of the COVID-19 coronavirus.

Keywords: investment, innovation, foreign direct investment.

ИНВЕСТИЦИОННЫЕ ПРИОРИТЕТЫ ВО ВРЕМЯ ПАНДЕМИИ

А. Г. Проровский

Реферат

В работе анализируется инвестиционная активность в контексте пандемии COVID-19, вызвавшей глобальный экономический кризис. Делается вывод о том, что пандемия стала катализатором цифровизации мировой экономики. Как страны, так и предприятия, которые быстро адаптируются к новым условиям, станут лидерами нового экономического цикла. Инвестиции приводят к тому, что предприятия приобретают основные средства. Капитальные вложения носят долгосрочный характер, что позволяет компаниям получать доход в течение многих лет за счет добавления или улучшения производственных мощностей и повышения операционной эффективности. Дополнительные или усовершенствованные основные средства повышают производительность труда, делая предприятия более производительными и эффективными. По мере того как рабочая сила становится более эффективной, повышение эффективности по всей стране приводит к увеличению валового внутреннего продукта. Инвестиционные процессы в мировой экономике в настоящее время претерпевают значительные изменения. Это связано с такими факторами, как: изменения в инвестиционной политике США, окончание следующего экономического цикла, торговые войны в мировой экономике, распространение коронавируса COVID-19.

Ключевые слова: инвестиции, инновации, прямые иностранные инвестиции.

Introduction

Forecasts about overcoming the crisis caused by the coronavirus pandemic in the world economy in 2021 are not justified. Against the background of new waves of the pandemic, the initial forecasts of a full-fledged recovery of the world economy from the crisis in 2021 are not justified until the factors that negatively affected the world economy in 2020 are eliminated. Experts expect an acceleration of global economic growth in 2021, which will be facilitated by a decrease in the intensity of the pandemic as mass vaccination and the preservation of stimulating monetary and fiscal policies in the world's largest economies. The weakening of social isolation measures and the improvement of external conditions will be key factors in strengthening consumer and investment demand.

Foreign direct investment

In 2020, the global volume of foreign direct investment (FDI) amounted to only 859 billion US dollars, while in 2019 it was at the level of 1.5 trillion dollars. There have not been such low investment investments since the early 1990s. This year's figures are 30% lower even than in 2009, when the world was in a state of global financial crisis.

The least popular among investors this year were rich countries, where FDI flows fell by 69% - to about $ 229 billion. Investments in the United States decreased by 49% and amounted to $ 139 billion.

Developing countries received 12% less investment money this year compared to the previous year. Thus, the share of developing countries in world FDI has reached 72% - this is the highest figure in history. At the same time, China led the ranking of the largest recipients of FDI.

As for the countries with economies in transition, the inflow of foreign direct investment there fell sharply by 77% - to about $ 13 billion. This is the lowest level of inflow to the region since 2002. At the same time, investment projects in Russia suffered the most due to the COVID-19 crisis. FDI to this country decreased from $ 32 billion in 2019 to $ 1.1 billion in 2020. In addition to the pandemic, there were other factors. Thus, weak international demand for crude oil and the April 2020 conflict with other major producers related to its prices undermined investors interest in the oil sector.

Many of the jobs cut due to the pandemic depend on the investments and operations of multinational corporations (TNCs), their buyers and suppliers in global value chains. New FDI in 2019 created almost 80,000 new jobs every month in OECD countries and more than 100,000 in developing countries. The decline in FDI in new industries in 2020 reduced the potential job creation by almost 50%, which means that up to 500,000 jobs that could be expected to be created in the first five months of 2020 have not materialized. Even before the pandemic, FDI into the economy of the Republic of Belarus rarely exceeded $ 2 billion per year (Figure 1) [2].

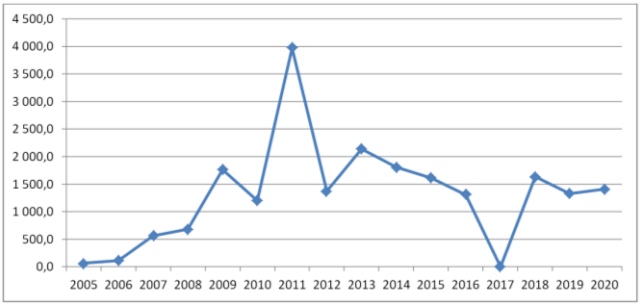

Figure 1 – Foreign direct investment on a net basis, million US dollars [2]

doi.org/10.36773/1818-1112-2021-126-3-112-114

In the OECD countries, new private investment in infrastructure and services protected these economies from a serious drop in GDP, job losses and even a slight recovery in employment in June and July 2020.

At the same time, developing countries have suffered from a sharp decline in FDI in infrastructure, automotive, consumer electronics, textiles and business services, which has made it difficult to create jobs. These sectors tend to be massive job creators and received large investments before the pandemic. Job creation due to FDI has remained low in developing countries since March 2020. Countries with attractive agri-food and communication sectors are experiencing the crisis with less damage, since FDI in these sectors, which create jobs, increased during the crisis.

The crisis forced foreign investors to curtail their activities in the host countries, which negatively affected jobs, income and livelihoods. Some foreign firms were able to protect their workforce from such an impact, but many had to lay off employees or reduce working hours. Foreign firms believe that the reduction of staff during the crisis will lead to significant losses of competitiveness and prevent rapid growth after the crisis.

The priority for companies operating during the pandemic is to protect the health and safety of employees, as well as reduce their exposure to Covid-19 in the workplace. This can be particularly difficult in sectors such as the garment industry, construction, or healthcare.

Foreign firms managed to adapt their way of action to the new business and work realities created by the crisis relatively better than their domestic counterparts: 30% of foreign firms surveyed by the World Bank in 2020 started or increased their online activity compared to 25% of their domestic competitors. Similarly, almost 50% of foreign companies have either started or expanded remote work, while only 27% of local firms have done so.

Unlike domestic enterprises, TNCs should take into account the differences in approaches to overcoming the pandemic in the different countries in which they operate. Which can be a difficult task for companies that use uniform global management.

TNCs can become leaders in the development and implementation of new telecommunications technologies in business processes. This will allow them not only to survive during the pandemic, but also to gain a competitive advantage.

The digital economy is gaining momentum, and remote jobs, telecommunications educational technologies, e-commerce, esports and telemedicine are all accelerated by the pandemic. As soon as the crisis subsides, there will be some technological return to its doc-like state. However, most of the digital acceleration will be permanent, and hybrid models will become permanent practices.

From a macro point of view, digital platforms are characterized by low costs and a business scaling effect. This creates winner-takes-all markets that favor global champions. In addition, the "light asset" business model, in which technology is increasingly replacing capital and labor, indicates an improvement in the free cash flow margin and an increase in the return on investment. This will allow many companies to increase their dividends and share repurchases, while maintaining overall payout ratios significantly higher than historical norms.

Digitalization, automation and globalization significantly reduce transaction costs and increase the efficiency of business processes, which will lead to a significant increase in capitalization with increased investor interest.

The year 2020 was deeply transformational and the shock from COVID became a catalyst for the digitalization of the economy. This radical transition is particularly beneficial for business models with a light asset in the technology, medical and communications sectors, but will also accelerate the development of a number of industries, including education, telemedicine, e-commerce and esports.

For investors, the COVID shock is best viewed as a forced experiment, forcing most of the economy to go online, to the digital sphere, and offering an opportunity to assess what works and what does not. The pandemic has significantly accelerated the introduction of remote activities, such as work, study, shopping, and consulting with a doctor.

With the COVID shock, the digital business is thriving and gaining an increasing market share. Even before the pandemic, the digital economy was growing more than four times faster than the rest of the economy. Other critical factors include massive improvements in technological equipment, cloud computing, the ongoing adoption of 5G, and exponential growth in AI efficiency.

In the period from 1960 to 2000, the share of full-time workers working at home never exceeded 3.5%. Over the two decades since 2000, this share has slowly but steadily grown to 5.5%, and in 2020 it may reach 37%.

This year, the rapid transition to remote work was provided by two conditions. Firstly, the capabilities of technological equipment, broadband communication in residential premises, cloud services and video conferencing capabilities. Secondly, the economy now revolves around services, not production, which has allowed most companies to participate in the experiment on remote work opportunities.

Economists are feverishly collecting data to make sense of this year's experiment, and so far the productivity data looks mixed. Whatever it was, it is clear that the nature of the work has changed a lot. To begin with, many employees have changed fixed hours from 9 to 18 hours to fragmented "Swiss cheese" schedules, while working hours are becoming more flexible, night email traffic is growing rapidly, the division of weekdays into weekends is almost disappearing,and business trips are plummeting.

Remote work at Microsoft was the subject of a July study in the Harvard Business Review, which showed that meetings were getting shorter, but there were more of them, so that the total meeting time actually increased by 10% overall. The analysis showed that more connections were planned to compensate for the lack of informal discussions. Employees worked an average of four hours more per week, as the "night shift" appeared and work on weekends increased, and managers bear the brunt of the transition to remote work.

These results were confirmed by a July study by the Harvard Business School. It covered a large number of firms and found that compared to the pre-pandemic level, the number of meetings per one person increased by 13%, while the average duration of meetings decreased by 20%. It also turned out that the average working day increased by 8% (50 minutes).

The tourism sector, including business, has seriously sagged. And there will not be a full recovery in the near future, firms expect to reduce their annual travel expenses by 30%. This large-scale reduction in travel costs not only suggests a sluggish and potentially protracted recovery for the travel, accommodation and transport industries, but also indicates that firms are counting on a shift from face-to-face meetings to cheaper virtual meetings

In the field of educational technologies, there is a need to make online learning more effective. In mid-April, at the peak of the global pandemic, 192 countries closed all their educational institutions (six countries partially closed them). According to UNESCO, this has affected a staggering 1.6 billion students and schoolchildren worldwide (90% of the total number of students). Those countries that will not be able to organize the educational process in the conditions of a pandemic, and these are the poorest countries in the world, will receive the effect of a "lost generation" and an even greater decrease in the competitiveness of their economies.

The good news is that education is rapidly moving beyond " chalk and talk", and Edtech companies are not only offering independent e-learning, but are also increasingly focusing on artificial intelligence-based learning, mixed reality tools (using AR and VR), gamification and educational bots (programs that can interact with users). Such advanced learning technologies are at the epicenter of deep innovation, and global revenues are projected to increase by an average of 25% over the next five years. Growth is expected to be particularly strong in higher and secondary education, as well as in corporations (including healthcare) and government agencies (for example, in the field of military training).

In order to ensure the stable functioning of the Belarusian economy, it is extremely necessary to achieve a positive balance of foreign trade. However, we are not able to ensure a steady excess of exports over imports (Figure 2).

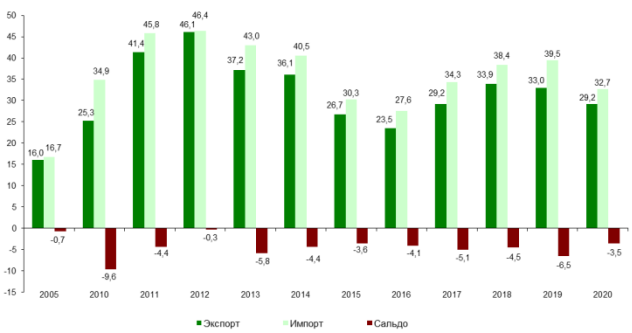

Figure 2 – Turnover of foreign trade in goods of the Republic of Belarus, million US dollars [2]

To change the structure of the Belarusian economy, it is necessary to advance the development of knowledge-intensive and innovative industries. A lot is being done in the republic for the development of innovative activity, but the innovativeness of GDP (Figure 3) lags behind the similar indicator of highly developed countries (3%).

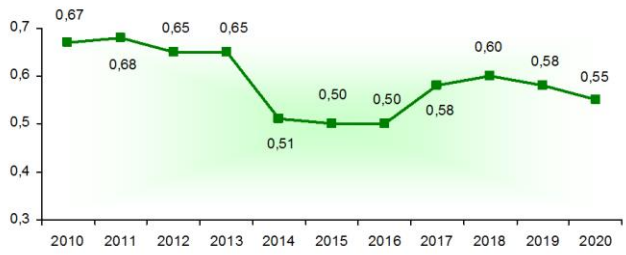

Figure 3 – Innovation of the economy of the Republic of Belarus [2]

Economic growth is primarily driven by consumer spending and capital expenditures of enterprises. As enterprises invest in their development to increase production volumes, they hire more employees and increase wages. All these activities lead to economic growth, measured by the gross domestic product - the total volume of production of goods and services for the country in a given period.

How investments are related to economic growth.

Investments lead to the fact that enterprises acquire fixed assets. Capital investments are of a long-term nature, which allows companies to earn income for many years by adding or improving production capacities and increasing operational efficiency.

Additional or improved fixed assets increase labor productivity, making enterprises more productive and efficient. As labor becomes more efficient, increasing efficiency across the country leads to an increase in gross domestic product.

Investment processes in the world economy are currently undergoing significant changes. This is due to such factors as: changes in the US investment policy, the end of the next economic cycle, trade wars in the global economy, the spread of the COVID-19 coronavirus.

The sources of investment are:

1. Funds of enterprises, mainly retained earnings and depreciation. But the low profitability of Belarusian enterprises (Figure 2) does not allow accumulating a large amount of financial resources for investment. Belarusian enterprises also cannot apply massively accelerated depreciation methods due to the small difference between the cost and the price. An increase in depreciation charges will lead to an even greater decrease in profitability and, even, the need to raise the price of manufactured products.
2. State financial resources. The state remains a powerful investment resource for the economy, but the accumulated debt obligations and the need to maintain a balanced state budget limit the country's capabilities.
3. Bank loans. In recent years, against the background of falling inflation, interest rates on investment loans have decreased to 15-16 %. But the financial base of the Belrussian banks is limited and there is a risk of an increase in the level of problem loans against the background of the economic crisis caused by the coronavirus epidemic.
4. Funds of the population. The population has a significant amount of financial resources, but the main form of investment is bank deposits. In the conditions of lowering interest rates on deposits, it is necessary to offer the population the opportunity to invest in the economy both directly in the share capital of Belarusian enterprises and through investment funds.
5. Foreign investments could become a serious source of financing for the development of the economy of the Republic of Belarus, but for a long time they remain at the level of about $ 1.5 billion.

Investments in any economy lead to an increase in GDP. But the degree of influence varies.

The Republic of Belarus faces very serious tasks, having solved which we will enter the period of sustainable development [3]:

1. Uneven development of the country's regions. For sustainable development, it is necessary to create opportunities for self-realization for a person living in any locality of the country.
2. Logistics. The economy of the Republic of Belarus has the opportunity to make even better use of the geographical location of the country to increase the export of logistics services.
3. Export. In order to stimulate the economy of the Republic of Belarus, it is necessary to achieve a positive balance of payments and the development of exports is the main direction.
4. Innovation. Only an innovative way of developing the economy of the Republic of Belarus is able to bring the country's GDP and household incomes to a new level.

Conclusion

COVID-19 as a catalyst for the virtual economy: 2020 will be a deeply transformational year, and the shock of COVID-19 has become a catalyst for the digitalization and virtualization of the economy.

From a macro point of view, this means an asset-based economy in which technology replaces capital and labor. Understanding how companies will adapt their business models is key to assessing their ability to generate free cash flow on a sustainable basis. In light of this, the question is "What is your business strategy in the digital age?" it has become one of the most important issues for management teams.

References

1. The United Nations [Electronic resource]. – Access mode: https://unctad.org/system/files/official-document/wir2020_overview_ru.-pdf. – Date of access: 25.07.2021.
2. National Statistical Committee of the Republic of Belarus [Electronic resource]. – Access mode: http://belstat.gov.by/. – Access date: 25.07.2021.
3. Actual problems of modern economic systems – 2020: collection of scientific papers / Ministry of Education of the Republic of Belarus, Brest State Technical University ; editorial board: A. G. Prorovskiy [et al.]. – Brest: BrSTU, 2020. – 244 p.

Accepted 26.10.2021

UDK 339.9(476)

SPATIAL DEVELOPMENT OF TERRITORIES: CROSS-BORDER ASPECT

V. V. Zazerskaya

PhD in Economics, Associate Professor, Dean of Faculty of Economics,
Brest State Technical University, Brest, Belarus, e-mail: zazerskaya@mail.ru

Abstract

The work assesses innovative processes as the basis of spatial development of territories. Activating innovative processes that contribute to the development of regions. The characteristics of forms and factors of cross-border cooperation are given.

The transport industry and construction have been identified as the defining elements of regional infrastructure and have organized national and global trends in their development. The systematic approach to innovation shows that the effect of innovation extends to related industries and generates interaction between all actors in the region.

It is shown that the spatial organization of economic activity in the cross-border territory requires interaction between regional innovation complexes. This article highlights the forms of integration processes.

Keywords: cross-bordercooperation, innovation, infrastructure, economic integration, cross-border region, spatial development of.

ПРОСТРАНСТВЕННОЕ РАЗВИТИЕ ТЕРРИТОРИЙ: ТРАНСГРАНИЧНЫЙ АСПЕКТ

В. В. Зазерская

Реферат

В работе оцениваются инновационные процессы как основа пространственного развития территорий, активизация инновационных процессов, способствующих развитию регионов. Дана характеристика форм и факторов приграничного сотрудничества.

Транспортная отрасль и строительство были определены как определяющие элементы региональной инфраструктуры и определили национальные и глобальные тенденции их развития. Системный подход к инновациям показывает, что эффект от инноваций распространяется на смежные отрасли и порождает взаимодействие между всеми участниками в регионе. Показано, что пространственная организация экономической деятельности на приграничной территории требует взаимодействия региональных инновационных комплексов. В этой статье освещаются формы интеграционных процессов.

Ключевые слова: приграничное сотрудничество, инновации, инфраструктура, экономическая интеграция, приграничный регион, пространственное развитие.

Introduction

The goal of the state's socio-economic development is to ensure high living standards of the population and conditions, which is determined by the transition to a highly efficient economy based on innovation. The level of technology development causes structural restructuring of the economy and is one of the main factors of competitiveness. The activation of innovative processes that contribute to the development of regions necessitates a comprehensive in-depth theoretical and practical study of infrastructure development tools.

Cross-border cooperation as one of the forms of cross-border interaction (including also industrial cooperation, trade, tourism, diplomatic relations, interaction on security issues) is a set of bilateral and multilateral relations between authorities, business entities, public organizations and the population of border regions two or more countries. The ties that emerge and develop in the course of cross-border cooperation contribute to the deepening of other forms of cross-border interaction. A distinctive feature of cross-border cooperation is the regional nature of this process, in contrast to the traditional system of external relations, implemented in order to ensure national interests at the highest state level, cross-border cooperation is carried out at the level of regions and even local communities of neighboring territories, separated state border.

Cross-border cooperation is implemented in the framework of such forms as local border contacts, bilateral contractual relations between neighboring territories, the creation of stable network formations in the form of associations, forums, euro-regions, etc., as well as in the form of ongoing activities in various areas in framework of joint projects.

The typology of foreign neighboring countries obliges to develop and implement different variants of regional policy. These options include the following:

1. The first method is traditional - by attracting foreign investment from companies from neighboring countries. Such companies usually aim to reduce various types of costs for further re-export of products. By large enterprises with foreign participation, one can judge the development of cross-border cooperation of the regions. The volume of direct foreign investments on a net basis in the real and banking sectors of the economy of the Republic of Belarus, as well as in the sale of real estate in the territory of the republic at the end of 2020 amounted to 1,337.6 million US dollars. The share of the Gomel region - 7.7%, Mogilev region - 7.4%, Grodno region - 7.3%, Brest region - 5.3%, Vitebsk region - 3.0% [1].
2. The second way is through countertrade in various types of products. This method gives a positive economic effect when the cross-border territories have the same level of economic development. In case of unequal conditions, the weaker party will receive less economic efficiency from cooperation.

When developing joint measures to increase the competitiveness of border areas, enhance the movement of goods, services and production factors, factors should be taken into account [2]:

1) geographical location, endowment of natural resources and quality of the environment;
2) the degree of involvement in interregional and international economic relations, investment flows;
3) the presence of a developed transport infrastructure;
4) availability of market infrastructure;
6) the qualitative and quantitative composition of labor resources, its educational potential, cultural traditions;
7) scientific and technological potential and scientific information environment.

A special role in ensuring the sustainable development of the economy of individual regions with cross-border economic cooperation based on an innovative approach is assigned to transport infrastructure and construction.

The studies of international economic integration are devoted to the works of foreign (D. Peng, M. Spindler, E. Vinokurov, R. Evstigneev, A. Libman, P. Minakir, B. Kheifets) [3] and domestic scientists (A. V Belsky, T. B. Bibik, A. A. Vasilenko, E. S. Danilyuk, L. N. Davydenko, E. A. Semak) [4–7].

conomists paid attention to the innovative development of investment and construction activities: A. N. and V. V. Asaul, V. V. Buzyrev, I. N. Geraskina, Yu. M. Yasinsky and others [8-10].

Innovation is the driver of economic growth. Thus, in developed countries, innovations provide about 75% of the growth in gross domestic product. For example, in Germany this indicator reaches almost 100% of GDP. Small and medium businesses provide 78% of employment and 45% of Taiwan's GDP. The introduction of new technologies, the results of scientific research into industrial production makes it possible to make a qualitative breakthrough in the market of goods and services [11]. In many states, in the development of models of economic growth, the innovation vector is assigned a leading role. In the strategies of innovative development, the following directions can be spelled out: innovative entrepreneurship; improving the management efficiency of national innovation systems; commercialization of results and formation of a market for scientific and technical products; stimulating high-tech exports, developing infrastructure in the fields of scientific, technical and innovation activities. Thus, in Belarus, the National Academy of Sciences has developed a strategy "Science and Technology: 2018–2040". The main goal is to form the basis for the deployment of the fourth industrial revolution and the processes of new industrialization, The basis is digital production technologies, including artificial intelligence systems, quantum computers, the Internet of things and the industrial Internet, smart materials, machines and their systems for the real sector, in energy, construction and ecology are also a priority [12].

Infrastructure of the region: state and development

Construction is one of the key, fund-forming industries that largely determine the rate of development of the country's economy and the solution of the most important socio-economic problems (Table 1). The integrated development of territories depends on the construction complex, when it is necessary to interconnect the renewal of fixed assets, the modernization of enterprises, and housing construction. This not only contributes to the development of other industries, economic growth, but also improves the social situation in society.

Table 1 – Key indicators of the activities of construction organizations

Indicators	2011	2015	2016	2017	2018	2019
The number of construction organizations,						
units	9 548	10 173	9 515	8 718	8 514	8 332
The volume of contract work in the actual prices; billion rubles.	40 101,0	92 255,8	8 107,8	8 600,0	10 074,3	12 191,3
at comparable prices; percentage of the previous year	106,7	88,7	85,2	96,3	105,2	105,1

Source: [13]

The number of organizations in this area is declining, so in 2011 there were 9,548 units, and in 2019, 8,332 units of contracting were declining until 2015, due to the global trend in the industry, but from 2017 began to grow and averaged 7%.

The industry occupies the most important place in the economic system of the state: it is the largest industry in the economy of the Republic of Belarus (4.5% of the total cost output for 2019).

However, the effects of COVID-19 have affected the industry as well. Revenue from sales decreased by 5.5%, net profit of organizations by 19.7%. The number of loss-making organizations increased by 36%. However, construction remains a significant industry for other industries that are suppliers of products for construction work. The industry's share in intermediate consumption is also very high. In the structure of intermediate demand, the share of the industry is much lower, as the industry mainly produces the final products [14]

As for the transport infrastructure, the functioning checkpoints on the border of the Republic are distributed as follows: automobile - 26; railway - 15; air - 7; river - 3. In accordance with Belarus in 2019, the main share of freight turnover fell on rail transport, the annual freight turnover through railway checkpoints amounted to about 82.6 million tons, while a slight decrease by 2.5% in railway freight turnover in relation to by 2018 - 84.76 74 million tons. Freight turnover through road passes of the Republic of Belarus in 2019 amounted to about 30.1 million tons, with a wide increase of 11.9% in cargo turnover through road passes of the Republic of Belarus in relation to 2018 - 26.02 million tons. Freight turnover through the air traffic areas of the Republic of Belarus is minimal, the annual cargo turnover in 2019 amounted to no more than 0.0121 million tons, slightly decreasing compared to 2018 - 0.0125 million tons. The total cargo turnover of goods imported through all passes of the Republic of Belarus (85.03 million tons) in 2019 was 3.3 times higher than the turnover of exported goods through all checkpoints of the Republic of Belarus (25.7499 million tons) [15]. On the part of highways, many international transport routes pass through the territory of the republic, which can be divided into Trans-European routes: one European route and the International Highways of the Commonwealth of Independent States. Two international railway transport corridors pass through the territory of the Republic of Belarus: No. II Berlin - Warsaw, Minsk - Moscow - Nizhny Novgorod (within the republic, the railway section Brest - Minsk - Orsha - Osinovka); № IX - Helsinki - St. Petersburg - Kiev - Chisinau - Bucharest - Dmitrovgrad - Alexandroupolis (within the republic, the railway sections Ezerishche - Vitebsk - Mogilev - Zhlobin - Gomel - Teryukha and branch IXB - Zhlobin - Minsk - Gudogai) [16].

In order to assess infrastructure in terms of the priority of its development, the world has analysed the main trends in the world economy in the medium and long term. According to a World Bank study [17], global economic growth is projected at 4.0% in 2021 and 3.8% in 2022. The regional economies of Europe and Central Asia will grow by 3.3% in 2021. In most countries of the world, the load on infrastructure will significantly increase, therefore, to ensure sustainable economic development and growth of trade in the world, its timely modernization is necessary. According to OECD estimates, the volume of passenger air traffic by 2035 will increase 2.5 times, air cargo traffic will grow 3 times, and container traffic - 4 times. The existing transport corridors between Europe and Asia have a capacity that allows an increase in freight turnover by about 50%. However, this potential will be exhausted in the next 6-8 years. In this regard, it is already now necessary to engage in the design, construction and expansion of large infrastructure facilities.

The growth rate of the construction industry in the world is expected at the level of 3.9% per year, which is higher than the rate of global economic growth by almost 1% and by 2030 the industry will grow by 85% to 17.5 trillion. dollars. According to international experts from the organizations Global Construction Perspectives and Oxford Economics [18], the world market of construction services is characterized by the following trends in its development in the long term:

- enlargement of single-industry regional construction organizations to large multi-profile holdings that will perform construction and installation work in all segments of the construction market at objects of any complexity around the world;
- the share of design and construction corporations in the total volume of contracts for the construction of large and unique infrastructure facilities will increase;
- the number of "corporations for the economic development of territories" will increase, creating special financial funds at the expense of equity participation of companies located in this territory. Their funds will be directed to the construction of objects necessary for the full functioning of this territorial-administrative unit - residential and business complexes with shops, restaurants, cafes, hotels, sports facilities, educational and health care facilities;
- the emergence of specialized research centers for construction;
- use of environmentally friendly building materials and technologies;
- an increase in the volume of production of composite and new types of heat-insulating materials, plastics;
- strengthening the role of public-private partnership models such as build-operate-transfer - BOT (construction - operation - transfer of an object to the customer), build-own-operate - BOO (design - ownership - operation), etc.

The trends in the development of the transport aspect of infrastructure are as follows:

- active development of transit potential in the EAEU. The EAEU railways retain a dominant role in transit traffic across the Union;
- The transit potential of the EAEU in the future has opportunities for reorientation from the sea container traffic between the West and the East, a share of 5-10%.

doi.org/10.36773/1818-1112-2021-126-3-115-118

- innovative ways to raise funds for the construction of transport infrastructure without using the resources of the government (state). In particular, financing models will evolve: user charges / electronic toll systems, private sector borrowing and participation, PPP programs, land tax and many other initiatives;
- simplification of border crossing procedures;
- development along the corridors of intermodal mega-terminals, which, either as possible or as necessary, would have their own specialization.

Based on global trends in economic growth, which will cause technological modernization of promising industrial sectors and an increase in urbanization, as well as the contribution of construction and transport to GDP, it can be concluded that the need for infrastructure development, industrial and housing construction will increase.

Innovative processes as the basis for spatial development of territories

A systematic approach to innovation shows that the effect of innovation extends to related industries and generates the interaction of all subjects of the region. Such complex processes change the economic system of the construction complex as a whole.

The spatial organization of economic activity that has developed in the Republic of Belarus on a cross-border territory requires interaction between regional innovation complexes, which is achieved through the free movement of all components of the innovation process to maintain sustainable economic growth [19]. The subjects of the construction complex include research and development, design organizations, construction industry enterprises, contractor operating organizations, etc. The level of integration in the innovation sphere of their main industries determines the innovative potential. It is implemented through purposeful activities to improve the quality of economic development of the territory, taking into account the specifics of the specific characteristics of the region.

Consider the organization of innovative processes in the construction industry in cross-border areas. In this case, the specificity of the region is determined by the geographic location. The implementation of the innovative potential must take into account the innovative processes in the adjacent territory of a foreign state.

There are two models for organizing innovation processes: taking into account such activities of a foreign territorial entity and without it. In the second case, the development model is the most costly.

The presented diagram shows the features of innovation processes in cross-border regions, consisting in the coordination and systematization of managerial decisions, taking into account the socio-economic development of the neighboring border area (Figure 1). The successful implementation of unified approaches to innovative development causes diffusion of innovations in the border areas. Cross-border diffusion of innovations - processes of diffusion of innovations in socio-economic, scientific and technical activities. Diffuse processes across the border contribute to the inflow of new knowledge, management approaches and capital into the organization of economic activity and public life in general.

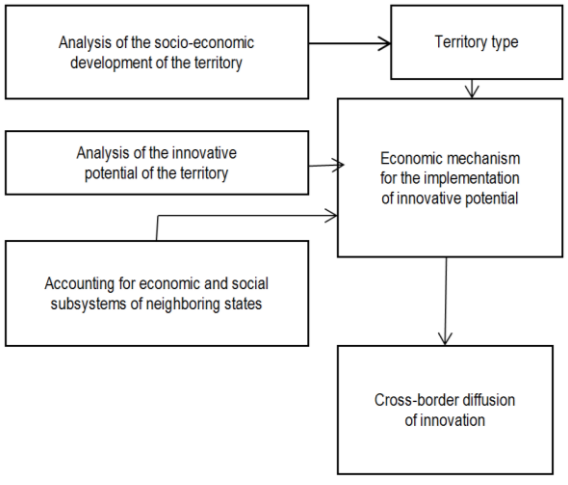

Figure 1 – Innovation processes in cross-border regions (developed by the author)

The type of territory development will determine which territory is the donor and which is the recipient of innovations. The course of innovation processes depends on the speed of movement of economic and technological innovations and on the ability to overcome the barrier environment in the form of a border.

The scientific and technical development of the region determines which state will be the resource center. The key condition for the formation of a cross-border innovation system is that the resource center for it are states that have a monopoly on managerial decision-making.

An example of successful cross-border cooperation was the implementation of a part of the project "Improving the road infrastructure of the border region by ensuring sustainable access to the border region (modernization and construction of the R-16 highway)", implemented under the cross-border cooperation program for 2014–2020. [twenty]. As part of this project, road safety has increased, the illumination of the roadway has improved 3 times, the road section with a length of 13.4 km has been brought to the parameters of the III technical category. The innovation was the concrete pavement, which increased the durability of the road surface.

Cross-border cooperation is developing within the framework of Belarus' activities in integration associations and international organizations. The purpose of creating integrated structures in the innovation sphere in the regional construction complex is to ensure the coordinated development of all technological links in the production of a construction product.

Integration processes are currently taking place in the following forms:

1) special and special economic zones created in order to attract investments, create and develop industries, create favorable conditions for the development of regions, and implement joint interstate programs and projects. In accordance with Article 7 of the Convention on Interregional Cooperation of the CIS Member States and national legislation, the States Parties to the Convention are taking measures aimed at simplifying procedures for border, customs, immigration (migration) and other types of control in order to increase the efficiency of cross-border cooperation [20].
2) the construction cluster, as an innovative form of integration aimed at the balanced use of innovative potential, voluntarily unites the participants in the construction complex who are bound by obligations throughout all stages of the construction cycle. In this case, mechanisms of sectoral, state and market coordination and regulation of high-tech products and technologies, concentrated on a certain period of time and in a certain economic space, are involved. Diffusion of innovations in the cross-border space increases the efficiency of the entire regional construction complex.

According to D.V. Arutyunova: "the organization of the innovation process is a sequential chain of events during which an innovation is implemented from an idea to a specific product, service technology and spreads in economic practice" [21]. Figure 2 shows the organization of the innovation process in construction in cross-border areas. Innovation starts at the level of subjects - participants in the construction complex.

The innovation process consists of two stages: formation and functioning. At the stage of formation of the innovation process, two functions are implemented. Regulation affects the instruments of purposeful action by the authorities on the part of the state, industry, cross-border cooperation (interregional), region. Incentives are implemented through state and market mechanisms for enhancing innovation activity from intra-firm to inter-firm (commodity) innovation. At the same time, market mechanisms are aimed at increasing the competitiveness of enterprises of the regional construction complex in cross-border interaction, and state mechanisms stimulate activities within the framework of the priorities and goals of innovation policy.

The result of the innovation process is an increase in the efficiency of the construction complex, namely: reduction of design time, saving energy resources, material and labor resources, reducing the cost and construction time, etc.

Regulation and stimulation through scientific, technological and organizational transformations affect the actors of the construction complex, who create, implement and use innovations in the process of economic relations. Subjects include investors, customers, contractors, design and research organizations, research institutes, enterprises of the construction materials industry, products and structures, enterprises related to the construction industries.

New technologies in the design of objects, innovative building materials, structures, methods of organizing production, new methods of organizing and managing construction production, new forms of financing and managing construction objects are considered as innovations.

A building cluster is a holistic economic system consisting of many interconnected elements (sub-sectors) that complement each other and enhance the competitive advantages of individual companies and the cluster as a whole.

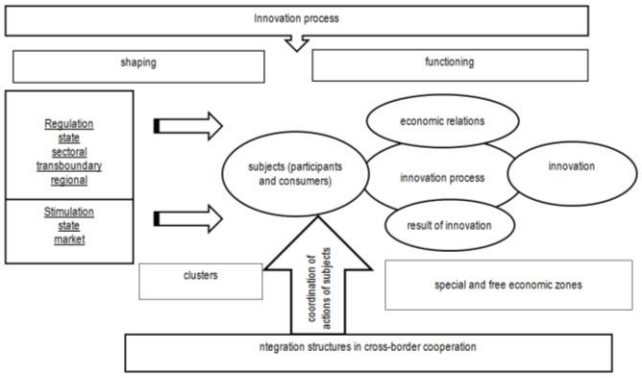

Figure 2 – Diagram of the organization of the innovation process in construction

In our case, the construction cluster is innovative and aims to introduce new innovative products in the field of construction, increase the competitiveness of products and enter new markets.

A special economic zone is a limited area with a special customs, registration and tax regime for national or foreign entrepreneurs. The main purpose of creating such zones is to solve the problems of socio-economic development by creating and developing production facilities based on new and advanced technologies, increasing the number of jobs, exporting certain regions or industries, i.e. creating high-tech enterprises in the construction industry.

Conclusion

The main goal of organizing innovation processes in cross-border cooperation is the integration of infrastructure elements that interconnect all participants in a single innovation-technological chain, thereby ensuring a high continuity of innovations.

Integration processes will allow:

- to optimize relations between companies of border regions of neighboring countries;
- develop a real manufacturing sector;
- to create common projects within the cross-border region to improve territorial and productive infrastructure;
- introduce new architectural and planning solutions, materials, technologies and other innovations.

References

1. Results of investment policy [Electronic resource]. – Access mode: http://www.economy.gov.by/ru/pezultat-ru/. – Date of access: 18.04.2021.
2. Zazerskaya, V. V. Cross-border integration as a factor in increasing the competitiveness of border regions / V. V. Zazerskaya // Engineering and management: from theory to practice: collection of materials of the XVIII International Scientific and Practical Conference, April 15, 2021 / Belarusian National Technical University ; editorial board: S. Yu. Solodovnikov (head of the editorial board) [et al.]. – Minsk : BNTU, 2021. – P. 185–186.
3. Ryzhkova, N. P. The effects of international economic integration at the regional level (on the example of Russia and China): author. dis. doct. economics of sciences. – Khabarovsk, 2013. – 47 p.
4. Belsky, A.V. Cross-border cooperation of regions of the European Union: financing and results / A. V. Belsky, E. S. Danilyuk // Problems of modern economy: global, national and regional context: collection of scientific articles: in 2 parts / Grodno State University named after Ya. Kupala. – Grodno, 2012. – Part 2. – P. 9–14.
5. Bibik, T.B. Cross-border interaction as an important factor in the development of cooperation between the Republic of Belarus and the European Union / T. B. Bibik, A. A. Vasilenko // Integration of the Republic of Belarus into international economic and political processes: analysis of cooperation in the economic and political spheres of the Republic of Belarus and the European Union: collection of scientific papers / edited by S. A. Kizim. – Minsk, 2019. – P. 17–27.
6. Davydenko, L. N. Institutional aspects of cross-border cooperation of the Republic of Belarus with the countries of the European Union / L. N. Davydenko // European Union and the Republic of Belarus: prospects for cooperation: a collection of abstracts of the II International Conference, Minsk, June 2, 2016 / editorial board: V. G. Shadurskiy [et al.]. – Minsk, 2017. – P. 123–127.
7. Semak, E. A. International economic integration: a course of lectures / E. A. Semak. – Minsk : Belarusian State University, 2009. – 194, [1] p.
8. Introduction to innovation: textbook / A. N. Asaul [et al.] ; editor: A. N. Asaul. – SPb. : IERP, 2010. – 280 p.
9. Construction economics: a textbook for the specialty "Economics and management at a construction enterprise" / V. V. Buzyrev [et al.]. – 3rd ed., Stereotyped. – Moscow : Academy, 2010. – 335 p.
10. Yasinsky, Yu. M. Analysis of the effectiveness of the use of innovations in construction / Yu. M. Yasinsky. – Minsk : BelNIINTI, 1983. – 53 p.
11. Commitment to innovation strategy. – URL: http://195.50.4.140/-notes/stati/priverzhennost-innovatsionnoy-strategii/. – Date of access: 21.04.2021.
12. Strategy "Science and Technology: 2018–2040": Resolution of the Presidium of the National Academy of Sciences of Belarus No. 17 dated February 26, 2018. – URL: https://nasb.gov.by/congress2/-strategy_2018-2040.pdf. – Date of access: 17.04.2021.
13. Construction and investment in fixed assets. – URL: https://www.belstat.gov.by/ofitsialnaya-statistika/realny-sector-ekonomiki/investitsii-i-stroitelstvo//. – Date of access: 04.17.2021.
14. Review of the construction industry in the member states of the Eurasian Economic Union and proposals for its development in order to use the integration potential of the Union. – 2013. – 34 p.
15. Analysis of the state, dynamics and development trends of the customs infrastructure in the places of movement of goods across the customs border of the countries of the Eurasian Economic Union [Electronic resource]. – Access mode: http://www.eurasiancommission.org/ru/act/tam_sotr/dep_tamoj_infr/SiteAssets/CIDD3_-DevCI/CIDD4_analysis_DCI_2020.pdf. – Date of access: 10.04.2021.
16. Musin, A. K. Analysis of existing international transport corridors passing through the territories of the member states. Analytical report. – Department of Transport and Infrastructure EEK [Electronic resource]. – Access mode: https://index1520.com/analytics/analiz-sushchestvuyushchikh-mezhdunarodnykh-transportnykh-koridorov-prokhodyashchikh-cherez-territor/. – Date of access: 10.04.2021.
17. Global Economic Prospects. – Access mode: https://www.worldbank.org/en/publication/global-economic-prospects/. – Date of access: 20.04.2021.
18. Review of the development of the world construction market. – https://budexport.by/world_market.php/. – Date of access: 10.04.2021.
19. Zazerskaya, V. V. Economic growth in conditions of sustainable development / V. V. Zazerskaya // Innovations: from theory to practice: collective monograph / scientific editor: A. M. Omelyanyuk [et al.]. – Brest : BrSTU, 2019. – P. 254–262.
20. Convention on Interregional Cooperation of the Member States of the Commonwealth of Independent States [Electronic resource]: concluded in Bishkek on September 16, 2016 // ConsultantPlus. Belarus / YurSpektr, National Center for Legal Information of the Republic of Belarus. – Minsk, 2021.
21. Arutyunov, D. V. Innovation management: textbook. allowance / D. V. Arutyunov. – Rostov on Don : SFedU, 2014. – 152 p.

Accepted 25.10.2021

doi.org/10.36773/1818-1112-2021-126-3-115-118

Scientific publication

VESTNIK OF BREST STATE TECHNICAL UNIVERSITY

TECHNICAL SCIENCE (CIVIL AND ENVIRONMENTAL ENGINEERING, MECHANICAL ENGINEERING, GEOECOLOGY); ECONOMICS

No. 3 (126). 2021

COMPOSITION OF THE EDITORIAL TEAM

Chief Editor	**Bakhanovich A. G.**
Deputy editor-in-chief	**Shalobyta N. N.**
Executive Secretary	**Kovalchuk E. N.**

TECHNICAL SCIENCE

Responsible editor for the section «Civil and Environmental Engineering»	**Tur V. V.**
Deputy executive editor by section «Civil and Environmental Engineering»	**Poita P. S.**
Responsible editor for the section «Mechanical Engineering»	**Neroda M. V.**
Deputy executive editor by section «Mechanical Engineering»	**Poddubko S. N.**
Responsible editor for the section «Information Technology»	**Golovko V. A.**
Deputy executive editor by section «Information Technology»	**Lebed S. F.**
Responsible editor for the section «Geoecology»	**Volchak A. A.**
Deputy executive editor by section «Geoecology»	**Meshyk A. P.**

ECONOMICS

Responsible editor for the section «Economics»	**Zazerskaya V. V.**
Deputy executive editor by section «Economics»	**Medvedeva G. B.**
Technical editor	**Sokolyuk A. P.**
Design by	**Kolb K. S.**
Proofreader	**Dudaruk S. A.**

License No. 02330/463 from 27.03.2014. It is passed for the press 29.11.2021. Format 60×84 $^{1}/_{8}$. Paper writing No. 1. Font of Arial Narrow. Condish. print. page 13,95. Ed. edit. 15,0. Order No. 1302. Circulation 100 copies. Printed on a risograph "Brest State Technical University". Editorial office address: 224017, Brest, Moskovskaya st., 267, Brest State Technical University. Telephone: 32 17 40, e-mail: rio_nikand@mail.ru, site: http://journal.bstu.by